UNIVERSITÀ DEGLI STUDI FIRENZE

DOTTORATO DI RICERCA IN SCIENZE CHIMICHE
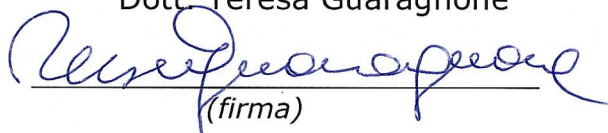
CICLO XXXIII

COORDINATORE Prof. PIERO BAGLIONI

NOVEL FORMULATIONS OF POLYVINYL ALCOHOL-BASED PEELABLE SYSTEMS FOR THE CLEANING OF METAL ARTEFACTS

(Nuove formulazioni di sistemi peelable a base di polivinil alcol per la pulitura di manufatti metallici)

Settore Scientifico Disciplinare CHIM/12

<table>
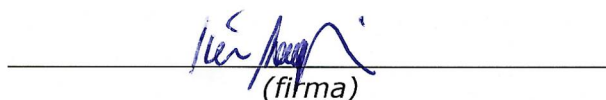<tr><td>Dottorando
Dott. Teresa Guaragnone</td><td>Tutore
Prof. Rodorico Giorgi</td></tr>
<tr><td>_____
(firma)</td><td>_____
(firma)</td></tr>
</table>

Coordinatore
Prof. Piero Baglioni

_____
(firma)

Anni 2017/2020 *(di inizio e fine corso)*

To my family

Abstract

The presence of dirt, soil, aged polymers or corrosion patinas can hinder the readability of artworks; in these cases, non-invasive and controlled removal is essential. Nanostructured fluids (NSFs) - such as micellar solutions and microemulsions- allowed achieving this purpose, decreasing, at the same time, the drawbacks related to the use of solvents. In the last decades, several cleaning fluids have been developed; surfactants, in particular, have a crucial role in the NSFs' formulations. For this reason, the research of innovative and highly performing amphiphiles represents one of the main goals in modern conservation science, in order to develop safer and greener systems. Two different NSFs were prepared with MPD surfactant and their interaction with soil and polymeric layers was evaluated through several techniques (CLSM, photographic observation, contact angle and surface tension measurements). Moreover, a comparison with a conventional nonionic surfactant (PDE) was made. MPD-based NSFs were found to be more effective in cleaning surfaces, also without mechanical action. Confining cleaning fluids in retentive matrices like gels represents one of the most powerful strategies to obtain greater control of the cleaning action. Two different pHEMA-based semi-IPNs were used as scaffold for a high selective agent (i.e., TEPA) able to remove corrosion products without affecting the protective cuprite layers. Changes in gels' structure were evaluated by means DSC, TGA and SEM analysis before and after the interaction with the copper alloys; Cu(II) ion adsorption kinetics were used to assess the effect of the gels' structure on the adsorption process. The pHEMA-based gels, classified as "rigid systems", are not suitable for the treatment of bronze sculpture characterized by deep cavities and high reliefs. To overcome these limitations, TEPA was confined into a PVA-based film (HVPD) forming system. Thanks to its viscoelastic properties and its ability to combine a chemical action with a mechanical one, the HVPD represents a good option in these cases. The physico-chemical characterization was carried out to evaluate the effect of TEPA-addition on (1) the kinetics of the film formation, quantified through gravimetric and rheological measurements, and on (2) the final films' properties, determined by DSC, ATR-FTIR and SEM analysis. 2D FTIR FPA Imaging confirmed the complete removal of corrosion products, the preservation of cuprite layers and the absence of residues on the mock-up surfaces after the treatment with both semi-IPNs and HVPDs. Finally, tests on real cases study are presented.

Table of contents

List of abbreviations

2-MPD = 2-methyl-1,3-propanediol

AIBN = Azoisobutyronitrile

CLSM = Confocal Laser Scanner Microscopy

CMC = Critical Micellar Concentration

DC = Degree of crystallinity

DH = Degree of hydrolysis

DPG = Dipropylene glycol

DSC = Differential Scanning Calorimetry

EDTA= Ethylenediaminetetraacetic acid disodium salt

EtAc = Ethyl Acetate

EtOH = Ethanol

EWC = Equilibrium Water Content

FPA = Focal Plane Array

FWI = Free Water Index

GLY = Glycerol

HCl = Hydrochloric acid

HEMA = 2-Hydroxyethyl methacrylate

HVPDs = Highly viscous polymeric dispersion

MBA= N,N-methylene-bis(acrylamide)

MEK = 2-butanone

MPD = methoxy-pentadeca(oxyethylene) dodecanoate

NaOH = Sodium hydroxide

NSFs = Nanostructured Fluids

PAA = Poly(acrylic acid)

PC = Propylene carbonate

PDE = Pentadeca(oxyethylene) dodecyl ether

PEG = Polyethylene glycol

pHEMA = Poly(2-hydroxyethyl methacrylate)

PS = Polystyrene

PVA= Poly(vinyl alcohol)

PVAc = Poly(vinyl acetate)

PVP = Polyvinyl pyrrolidone

RS = Rochelle's salts

Semi-IPNs = Semi-interpenetrated networks

TEPA = Tetraethylenepentamine

TGA = Thermogravimetric analysis

General background and aims

Cleaning is considered one of the most common actions performed on cultural heritage artefacts, aimed at removing "unwanted layers" (dirt, soil, aged polymers – such as adhesives, varnishes or protective used in past restorations – or corrosion patinas). This operation is necessary since such unwanted layers can hinder the readability and accessibility of artworks, enhance their degradation processes, or be the results of no more efficient restoration or vandalism [1], [2].

In the theoretical debate of modern restoration, cleaning represents a fundamental topic. Over the years, artists and conservators have given various assessments of the relationship between the artwork and time [3]. During the seventeenth century, for example, the visible sign of time on the artwork was not only a guarantee of authenticity but also had a precise aesthetic value. The time, considered on a par with the artist, was able to dampen the colours' violence by giving greater homogeneity and harmony to the paintings. Some painters even used varnishes or appropriate mixtures to achieve this effect [4]. In the eighteenth century, on the other hand, the action of the time takes on a negative meaning as it obscures the original splendour of the works and makes them "more fragile". These different considerations have given rise to a controversy – known as the "cleaning controversy" – about the preservation of the patina, defined "a layer of aged or corrosion products that can be granted aesthetic or historical value" [5]. Regardless of the different opinions about patina removal, the cleaning operation, due to its intrinsic irreversibility, must be carried out with a selective, non-invasive and controlled approach. In this way, it is possible to tune the removal of layers without affecting original or precious components of the artefact, according to the ethics of conservation.

The methods used for the removal of unwanted layers are closely related to the nature of what should be removed, as well as to the material and conservation state of the surface. Cleaning methods must meet three fundamental requirements: (1) selectivity and efficiency in the removal, (2) chemical-physical compatibility with the original layers, (3) safety for the operator and the environment [6].

Mechanical methods (micro-sandblasting, laser ablation and use of scalpels or chisels) involve direct removal of unwanted layers, without any preliminary solubilization or softening action. These systems, in addition to being strongly linked to the manual skill of the operator, usually require longer times, they are poorly selective and involve risks for the substrate [7][8].

Traditional chemical methods use substances, more or less reactive, which dissolve the materials to be removed by acting on their chemical bonds. Over centuries, cleaning was performed – with a very empirical approach – through the use of a great variety of natural materials, mainly alimentary products (wine, vinegar, lemon juice), biological fluids (saliva, urine or bile) or even ash and soaps [5], [9].

Later, restorers and conservators began to replace these natural materials with organic solvents, which today are still considered as the most comfortable solutions, thanks to their apparent ease of handling, predictability of their solving power, and their low cost [10].

The effectiveness of solvent cleaning depends on the ability of solvents to dissolve a specific material while leaving unaltered all the others. In this regard, the knowledge of several parameters – such as evaporation speed, viscosity and polarity of solvents – is crucial. In order to choose the most appropriate solvent (or solvent mixture) for a specific cleaning case, conservators typically match the solubility parameters of solvents with those of the varnish/soil to be removed; solubility parameters have been defined by Hildebrand [11] and Hansen [12] and graphically represented in a triangular chart by Teas [13].

However, the use of organic solvents does not allow sufficient control of the removal process as it involves spreading of the solubilized materials inside the pores of the treated artefact. Other undesirable effects that may occur as a result of the use of free solvents include swelling of the underlying layers and the binding agents, alteration of pigments and opacification of surfaces. Moreover, the use of solvents poses problems due to their toxicity and eco-compatibility [14].

Aqueous cleaning systems – free or confined inside retentive matrices like gels – represent a valid alternative to solvents and the starting point for the formulation of green cleaning systems. The use of aqueous methods permits greater control over the cleaning process thanks to the possibility of tuning

the systems' properties. For example, the modulation of several parameters such as the solutions pH, the conductivity and the ionic strength allow limiting swelling of acrylic paint films [15]. The addition of several compounds (acids and alkalis, solvents, chelating agents or enzymes) to water increases its cleaning effectiveness and allows the aqueous systems to become able to interact also with water-insoluble materials [16][17].

The development of nanostructured fluids (NSFs), defined as "water-based systems in which the solvents are present in limited quantities both in the dispersed (as nanometric droplets stabilized by the surfactants) and in the continuous phase of the fluids" [18], made a considerable contribution to aqueous cleaning methods' use. The NSFs, such as micellar solutions and microemulsions, provide several advantages over traditional cleaning methods [19]–[21].

The small amount of solvent necessary to formulate the aqueous NSFs allows to decrease the solvent evaporation rate and the system toxicity; thus, it is possible to obtain a more controlled and safer cleaning operation, without decreasing its effectiveness. The large surface area developed by the nano-sized droplets and the synergistic action of solvents and surfactants are responsible for enhanced cleaning power. Furthermore, the aqueous phase – principal component (75-99%) of a nanostructured fluid – acts like a hydrophilic-barrier and prevents the re-deposition of the dispersed hydrophobic materials [14].

Following the first application, in the late 1980s, of a nanostructured fluid for the removal of wax stains from Masolino and Masaccio's frescoes in the Brancacci's Chapel (Florence), several cleaning fluids have been formulated, suitable to the removal of different types of soil and polymeric layers [22]. The interaction between NSFs and these unwanted layers involves several physicochemical processes, ranging from classic detergency to selective swelling and dewetting of polymer films [23]–[26]. The understanding of interaction mechanisms is crucial, since it allows to predict what the effects of the cleaning operation will be and provides hints to design safer and more efficient products. In this regard, it is necessary to know the role of each component of the system on the final cleaning effect.

Starting from this point, this thesis work reports on two different surfactants in two different NSFs – the use of which is new in cultural heritage – in the

soil and polymeric layers removal. Their effectiveness was compared to the conventional non-ionic amphiphiles used in conservation practice through several investigation techniques such as confocal laser scanning microscopy, fluorescence correlation spectroscopy, photographic observation, contact angle, surface tension measurements, and small-angle X-ray scattering. Particular attention has been given to the description of the mechanisms and the kinetics involved in the NSFs cleaning process.

Over the knowledge of the interaction mechanism with the polymeric layers and soil, it is crucial to improve the control of NSFs' cleaning action through confinement in matrices like gels. These materials allow having better control in the cleaning process thanks to high retention and limited penetration by capillarity of the NSFs. Moreover, the use of a gelled system permits cleaning operation even on vertical and in otherwise prohibitive conditions [27]. This need arises when the NSFs and microemulsions, initially designed for the removal of unwanted materials from wall paintings [28], have also been used on water-sensitive substrates (canvas, paper artworks, watercolours, gypsum, and wood). Confining aqueous systems (i.e., in a gelled or thickened form) allows to overcome the problems related to the absorption of water, that can lead the swelling and the detachment of the paint layers and the solubilization of water-soluble components.

Frequently, in conservation and restoration field, polymers are added to solvents and aqueous solutions to increase their viscosity; in this way it is possible to limit the diffusion of the liquid within the treated matrix and confine its action at the interface, maximizing the control over the cleaning action.

Cellulose derivatives, such as Klucel®, Tylose and hydroxy-propyl-cellulose, are commonly used to thicken water and some alcohols; the use of polyacrylic acid (PAA) was introduced by Richard Wolbers in the development of the so-called "solvent gels". Both cellulose derivatives and PAA form viscous polymer dispersions with a jam-like appearance; they are easy to prepare and apply on the surface to be treated with swabs or spatulas [9], [29], [30]. The low cohesion forces that characterize these physical gel-like networks (i.e., held by secondary bonds) make them incline to leave residues on the surfaces on which they have been applied. The removal of these residues is necessary to avoid the possibility of microbial proliferation or a general alteration of the

paint's chemistry [14], [31], [32] but it is not easy due to the adhesiveness of the materials.

Polysaccharide materials such as agar and gellan are used to prepare cleaning systems loadable with aqueous solutions, chelating agents, enzymes or surfactants. These formulations can be applied on the surfaces either as highly viscous solutions or "rigid gels" [33], [34]. Their use as "rigid gels" can overcome the drawbacks related to the residues on the surfaces [35]; however, in some cases, their water retention is not sufficient, especially on water- or solvent- sensitives dyes [36]. Furthermore, the strong cohesion forces of their networks make them scarcely adhesive and adaptable on rough and clotted surfaces [37], resulting in an inhomogeneous cleaning.

The development of chemical (i.e. held by covalent cross-links) hydrogels led to the production of confining networks with improved mechanical properties and retentiveness. In particular, semi-interpenetrated networks (semi-IPNs) obtained by incorporating polyvinyl pyrrolidone (PVP) in a poly(2-hydroxyethyl methacrylate) (pHEMA) network exhibit appealing characteristics for cleaning tasks: they are easy to handle and use, with good mechanical strength, and their high hydrophilicity allows the confinement of water, water/solvent blends and several cleaning fluids, like microemulsions, enzymes and chelating solutions [36], [38].

The semi-IPNs gels can be applied repeatedly without uncontrolled spreading of the loaded fluids and are easily removed in one piece without mechanical stress on the treated surface or removal/leaching of original components. These features make them suitable to the cleaning of water-sensitive artefacts and artistic surfaces that are poorly cohered and adhered. Such delicate materials can be paintings with a low cohesive paint layer, or with a low amount of water-sensitive binding agents [36], and mechanically brittle surfaces, like some stone materials or archaeological metals.

In this thesis work, semi-IPNs systems were used as confining matrices for cleaning solutions able to remove corrosion products without affecting the brittle mechanical surfaces. In particular, pHEMA/PVP and pHEMA/PAA gels were chose owing to the capacity of PVP [39] to form complexes with metal ions and the ability of PAA to give strong coordination bonds at alkaline pH, thanks to the presence of carboxylate groups [40]. Moreover, these semi-IPNs were used as confining matrices for tetraethylenepentamine (TEPA), a

chelating agent whose copper (II) complex has a stability constant four orders of magnitude higher [41] than that of other traditional chelators used by conservators, such as ethylenediaminetetraacetic acid disodium salt (EDTA) [42]. Despite the good stability of EDTA-copper(II) complexes, it is not uncommon to find stubborn corrosion layers that are resistant to treatments with EDTA; TEPA represents a valid alternative in this sense.

Generally, metallic artworks are characterized by pronounced cavities and reliefs that are hardly accessible with the aforementioned formulations. Based on their mechanical properties, semi-IPNs are classified as rigid gels; they are usually prepared as sheets with a thickness of a few millimetres and they have a fixed shape. Rigid gels have scarce adhesiveness and do not adhere homogenously on rough surfaces, indeed with these systems it is possible to treat only flat surfaces.

In case of metallic surfaces that exhibit highly textured surfaces with pronounced cavities and reliefs, a valid alternative to semi-IPNs systems is represented by the PVA-based highly viscous polymeric dispersions (HVPDs) [43]. The initial consistency of the system, that can be applied with a spatula or a hard brush, allows a perfect contact with any kind of substrates, such as non-horizontal, rough and irregular surfaces. After the complete evaporation of the solvent a film is formed, which can be easily removed in one piece thanks to its viscoelasticity.

To improve the cleaning capability of the formulation and make it able to eliminate also harder corrosion products, was evaluated the possibility of uploading TEPA in the HVPD, originally used as confining matrix for EDTA [43]. In addition to its greater chelating capacity for Cu(II) ions, TEPA is more soluble than the EDTA in the hydro-alcoholic network that forms the HVPDs [44]. Therefore, it is possible to upload larger quantities of chelating agent in the dispersion, boosting the removal of corrosion products and improving the cleaning efficacy with unprecedented results.

In summary, this thesis work focused on two main topics:

- analysis of the interaction mechanisms between different cleaning fluids and unwanted layers, with particular attention to the kinetics of the processes involved in the polymer films dewetting and artificial soil removal;

- development and characterization of different retentive systems for the treatment of bronze corroded artefacts (i.e., pHEMA-based gels and PVA-based HVPDs suitable for archaeological remains with fragile patinas or highly textured surfaces, respectively)

The aim of research in this field can open up new perspectives to develop new cleaning formulations, ever more suitable and safer. The design of performant systems plays a crucial role in the preservation and conservation of that "evidence with civilization values", as are defined the cultural objects by the Code of Cultural Heritage and Landscape, that must be offered to the collective knowledge and the future generations.

Chapter 1. Cleaning Unwanted Layers

1.1. Introduction

Starting from the early 1990s, nanostructured fluids have been suggested as innovative cleaning systems in the field of cultural heritage conservation [22]. Over the years, different formulations of nanofluids have been developed and applied on several materials with excellent results [19], [23], [45], [46]. Nowadays, micellar solutions and microemulsions are becoming part of the palette of solutions that conservators can adopt in the cleaning of works of art, as they overcome the limitations of classic solvent blends typically adopted in the restoration practice.

The use of NSFs in art conservation is mostly related to two main cleaning issues: the removal of polymeric coatings (protective and consolidating agents, fixatives, adhesives, aged or fresh varnishes, graffiti and overpaintings, etc.) [2], [21], [38], [45], [47] and the removal of soil (dust, particulate matter, grime, oily substances, sebum, wax stains, etc.) [22], [48], [49], which represents the most common of the interventions on artworks.

In both cases, the use of NSFs provides significant enhancements over the use of traditional cleaning techniques, i.e., the use of non-confined organic solvents, water or aqueous solutions. The synergistic action of organic solvents and surfactants results in excellent cleaning performance, combined with a safer and more controlled action. In fact, in a generic NSF, water is by far the most abundant component (about 80% w/w), the surfactant can be various, while the solvent quantity is reduced to a few percent. Being water-based systems, NSFs drastically reduce both the environmental impact of the methodology and the health risk for operators.

Compared to unconfined organic solvents, NSFs are more effective in the removal of hydrophobic polymeric coatings mainly because they interact with the polymer films through different physicochemical mechanisms. In contrast to organic solvents, which are selected to dissolve a given polymer, NSFs are

usually chosen to swell the film and pull it away from the substrate surface through, depending on the nature of the polymer, a dewetting process.

Dewetting is a "spontaneous phenomenon where a thin film on a surface rearranges itself into an ensemble of separated objects" [50] and results from the balance of attractive intermolecular forces inside the film and unfavourable interactions between the same film and the solid substrate. Dewetting of polymeric coatings from artistic surfaces induced by NSFs grants that the polymer macromolecules be effectively removed from the substrate and are not spread into the porosity of the work of art, as it would happen with unconfined organic solvents. Organic solvents in the NSFs play a major role in the dewetting of polymeric layers, as they are fundamental to increase the mobility of polymer chains by swelling the film. The surfactant nature is also crucial to promote kinetically this process thanks to its ability to lower both liquid/polymer and the liquid/solid interfacial tensions and to favour the film detachment, which is the first step of dewetting processes.

In many cases, the artworks' readability is jeopardized by the presence of dirt on the surface. Soil is usually composed of low molecular weight substances that can be accumulated on the artworks as the result of ageing, unsuitable storage, or detrimental practices. Depending on the specific needs of conservation case, grime and dirt are removed with several cleaning methods, ranging from the use of pure water to purely physical methods, to the use of aqueous solutions of pH buffers, chelating agents or surfactants. These formulations can be applied with brushes, cotton swabs, compresses, thickeners, physical gels or more technologically advanced solutions, such as highly retentive or semi-interpenetrated chemical gels, which provide the safest and most controllable cleaning action. In the formulation of the fluids used for dirt removal, surfactants have a crucial role, especially because the inclusion of organic solvents may be unnecessary. Thus, again, NSFs (mostly represented by micellar solutions) are among the most effective tools available to conservators.

It is worth noting that the use of some mechanical action to clear the soil off the treated surface is a common step to all these cleaning approaches. Therefore, this poses some significant issues when operating on delicate and fragile artworks, where further mechanical action must be avoided. In this sense, a very efficient surfactant can minimize this risk thanks to its capability

to interact with the unwanted layers, promoting their removal. Thus, nature and properties of surfactants are extraordinarily important to boost the effectiveness of NSFs in both these applicative contexts, and the search for innovative and highly performing amphiphiles is one of the main goals in the field of Cultural Heritage conservation.

The First Chapter of this PhD thesis reports on the use of a relatively innovative surfactant, a methoxy-pentadeca(oxyethylene) dodecanoate (MPD), which is present in commercial detergents, but its cleaning mechanism is poorly understood and its utilization in the conservation of cultural heritage is completely new. Despite their similar molecular architecture, MPD and the corresponding conventional alcohol ethoxylate (C12EO15, pentadeca(oxyethylene) dodecyl ether, PDE) have different phase behaviour in water and different interaction of the polar head with hydration water molecules [51]. This leads to a different excluded volume for the micelles and different effective micellar volume fraction for the two systems. These findings partly explain the experimental evidence that MPD possesses high detergent properties and significantly better cleaning efficiency than PDE, especially in low mechanical conditions.

The action mechanism and the effectiveness of MPD-based NSFs was studied and compared to the commonly employed PDE-based NSFs in the two aforementioned conservative challenges: (1) polymeric layers removal and (2) soil removal.

In the first case, the interaction between nanostructured fluids and polymeric films deposited on glass slides (model systems) was characterized trough Confocal Laser Scanner Microscopy (CLSM), which allowed to observe the processes' dynamics and the morphological modifications incurred by the polymer after the deposition of nanofluids. The results obtained at the microscale were compared with those acquired through gravimetric and surface tension measurements.

For what concerns soil removal, surfactant solutions were tested on laboratory samples (glass and plastic slides) coated with an artificial soil prepared following standard procedures available in the published literature. The results of these experiments were characterized by means of visual and photographic observation, CLSM investigation, contact angle and surface tension measurements. Also in this case, besides testing the effectiveness of NSFs, an

insight on the soil/cleaning fluid interaction was here provided, which represent, one of the first attempts to unveil the mechanism of soil removal in the context of conservation of cultural heritage.

1.2. Fundamentals

The theoretical fundamentals of the materials and systems employed in this thesis work are briefly discussed in the following paragraph. Particular attention is dedicated to the nanofluids composition and the dewetting phenomenon.

1.2.1. Nanostructured fluids

Water-based nanostructured fluids (NSFs), such micellar solutions and oil in water (o/w) microemulsions, are systems made up of several compounds: (1) water -that represents the most abundant phase-, (2) one or more solvents and (3) one or more surfactant.

The systems covered by this study are to be considered nanostructured fluids (or nanofluids) and not microemulsions because the organic solvents used, due to their miscibility in water, are located purely in the bulk phase and not within the micelle.

1.2.1.1. Solvents

Solvents used in a polymer removal process may be classified as "good" or "bad". When a "good" solvent is used, polymer chains move apart because of the repulsion forces. Simultaneously, the polymer gyration radius increases, and the swelling phenomenon occurs. The attractive forces between polymer chains, which occurs when a "bad" solvent is used, involve the shrinking of the polymer. In this last case, the polymer gyration radius decreases.

In the present work, propylene carbonate (PC) and 2-butanone (MEK) are used as solvents.

PC (4-methyl-1,3-dioxolan-2-one) is a polar aprotic solvent, partially miscible in water (~ 20% at 20 °C), with a high dipole moment (4.9 Debye), a high

boiling point (242 °C) and a very low vapor pressure. Moreover, PC has a low toxicity and high eco-compatibility.

MEK (2-butanone) is a polar aprotic solvent, partially miscible in water (~24% at 20 °C), with a boiling point equal to 79,6 °C and a dipole moment equal to 2.76 Debye.
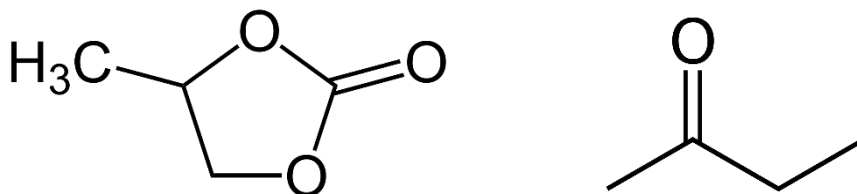
Figure 1. PC (left) and MEK (right) chemical structures.

These solvents have been chosen thanks to their high solubility in water, that allows increasing their concentration without a separation phase occurs, despite the removal of surfactant. This property makes it possible to formulate several systems, stable in all combinations. Moreover, PC and MEK are "good" solvents for Paraloid B72 and they have been tested with excellent results in the removal of different acrylic polymer [52], [53].

1.2.1.2.   Surfactants

Surfactants are amphiphilic molecules consisting of hydrophilic regions - called heads - and hydrophobic portions – called tails. Thanks to their structure, surfactants can modify the surfaces (or interfaces) properties by lowering the surface tension of a liquid, increasing the surface wetting or the miscibility between different liquids.

Numerous variations are possible within the structure of both the head and the tail groups of surfactants. The head group can be charged or neutral, small and compact in size, or a polymeric chain. The tail group is usually a single or double, straight or branched hydrocarbon chain, but it may also be a fluorocarbon or a siloxane, or contain aromatic groups [54]. The

characteristics of the head are fundamentals regarding the affinity with aqueous phases; the size of the apolar tail, on the other hand, defines the compatibility with organic phases. Depending on their molecular structure, surfactants are usually classified in: anionic, cationic, zwitterionic and non-ionic.

Non-ionic surfactants, like those used in the present work, have polar head groups that are not electrically charged. The polarity of molecule is given by the presence of atoms, such as oxygen and nitrogen, in the surfactant structure.

One of the most interesting properties of surfactants is their capability of self-assembly to form supramolecular aggregates. Depending on chemical properties, concentration and several other parameters, surfactant molecules can form small oligomers or much complex structures [55]. These aggregates are generally defined "micelles" and they only form when surfactant concentration in a liquid is above a critical value, called "critical micellar concentration" or CMC. If more surfactant is added to a solution at the CMC, the monomer concentration in solution remains almost constant, while the number of micelles increases, without appreciable changes in their size, at least until surfactant concentration is about ten times the CMC [56].

In this dissertation, the different effectiveness of two kinds of non-ionic surfactants were evaluated in the removal of soil and polymeric layers. In particular, a pentadeca(oxyethylene) dodecyl ether ($C_{12}E_{15}$) – PDE - and a methoxy-pentadeca(oxyethylene) dodecanoate – MPD - were used.
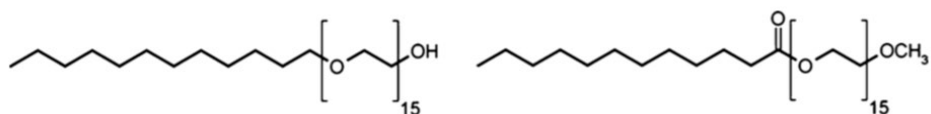
Figure 2. Molecular structure of PDE (left) and MPD (right). PDE possesses -OH as a terminal group in its hydrophilic chain, while MPD has a methoxy terminal group (-OCH3).

1.2.2. Dewetting

Dewetting is a spontaneous process where a thin film on a surface rearranges itself into an ensemble of separated objects likes holes or droplets. This phenomenon originates from the balance between unfavourable surface interactions and attractive intermolecular forces [50], and it is closely related to the wetting definition.

The wetting can be defined as the ability of a liquid to be in contact with a solid surface and it is determined by the intermolecular interactions that occur when solid and liquid come into contact: liquid-solid adhesion forces and solid-solid and liquid-liquid cohesion forces.

Contact angle between liquid and surface arises from the consideration of a thermodynamic equilibrium between three interfacial energies: (1) solid–vapor interfacial energy γ_{SG}, (2) solid–liquid interfacial energy γ_{SL}, (3) liquid–vapor interfacial energy (i.e., the surface tension) γ_{LG} (Figure 3).

The equilibrium contact angle θ_c is determined from these quantities by the Young equation:

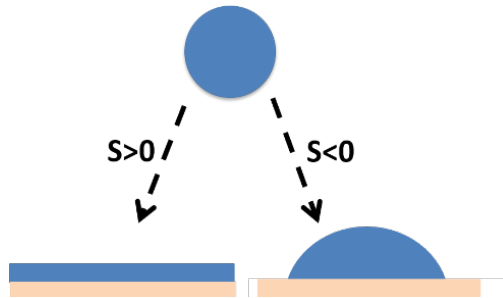$$\gamma_{SG} = \gamma_{SL} + \gamma_{LG}\, cos\theta \qquad (1)$$
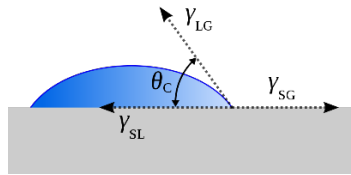
Figure 3. Schematic of a liquid drop showing the quantities in the Young equation.

A parameter for measuring wetting is the spreading parameter S:

$$S = \gamma_{SG} - (\gamma_{SL} + \gamma_{LG}) \qquad (2)$$

When S > 0, the liquid wets the surface completely (complete wetting); when S < 0, partial wetting (or dewetting) occurs.


Figure 4. Liquid behaviour as a function of the spreading parameter

In case of polymeric layers, the definition of the spreading parameter alone is not sufficient to determine the occurrence of dewetting. If the polymeric film is in a metastable state (e.g., it is below its glass transition Tg), it may not dewet despite a negative spreading parameter. Bringing the polymer to a temperature higher than the Tg, dewetting takes place as it increases the chains' mobility [57].

Film thickness plays a crucial role in the dewetting process, which occurs when the polymeric layer is below a critical thickness h_c [50]. In this condition, two mechanisms for the dewetting of a film can be distinguished:

- for homogeneous films thicker than about 100 nm, dewetting begins randomly in areas with chemical irregularities, charge thickening, discontinuity points, etc. These gaps grow over time until they coalescence and destroy the continuity of the film giving rise to filaments consisting of polymer left on the surface that can also break into droplets. This mechanism has been referred to as the *nucleation and growth regime* [58], [59];

- for homogeneous films less than about 100 nm thick, the most likely process is called "*spinoidal decomposition*"; the process of gap formation begins at all points in the polymer and nucleation patterns are formed [60], [61].

In this PhD dissertation, the dewetting process was studied at the microscale with CLSM technique. To simplify the understanding of the images in Section 1.4, following cartoon schematises the dewetting process observed and described below. The dewetting process can be divided into the following steps: (1) the flat homogeneous polymer film is exposed to the liquid system; (2) at the glass/polymer interface, the film starts losing adhesion to the glass in small areas having a round shape; (3) the area of these detachment regions increases, and they tend to coalesce decreasing the contact points between the polymer and the glass; (4) when the detachment areas reach a critical size, the film breaks and actual holes are created, which tend to expand, minimizing the contact between polymer and glass; (5) finally, the polymer reorganizes in the form of globular droplets distributed over the glass surface. Polymer droplets have a diameter which is significantly higher than the thickness of the original polymer film.
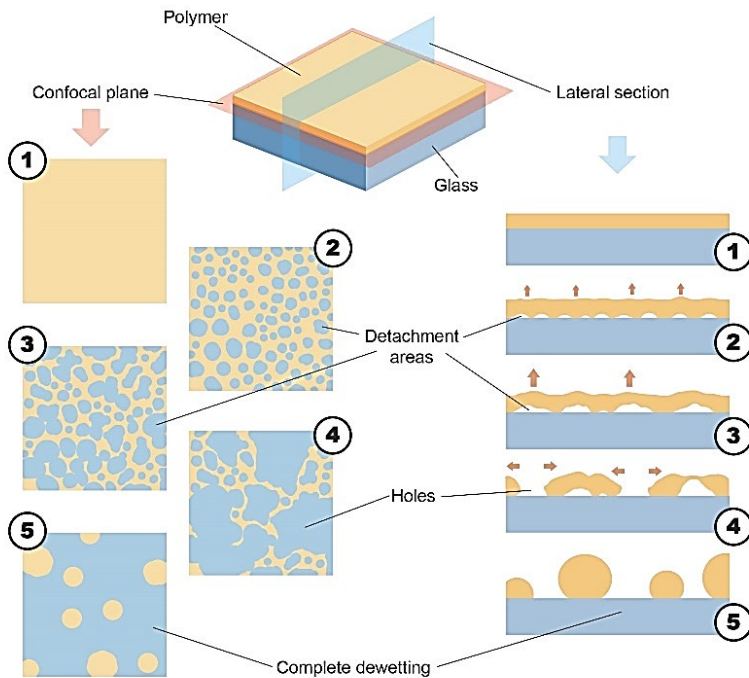
Figure 5. The cartoon describes the dewetting process observed in CLSM experiments. On the left the confocal plane view is shown, while on the right, a view of the lateral section of the system is schematized. The drawing is not in scale, i.e., the thickness of the polymer film was enhanced for the sake of clarity.

1.3. Experimental Section

1.3.1. Materials

$C_{11}(C=O)EO_{15}-CH_3$, MPD (Nikko Chemicals, assay 99%), $C_{12}EO_{15}$, PDE (Nikko Chemicals, assay +99%), dodecyl dimethyl amine oxide (DDAO, Sigma-Aldrich, 30% aqueous solution), sodium dodecyl sulfate (SDS, Sigma-Aldrich, assay 99%), propylene carbonate (PC, Sigma-Aldrich, assay 99%), 2-butanone (MEK, Sigma-Aldrich, purity 99%), , ethyl acetate (EtAc, Sigma-Aldrich, ACS Reagents, assay ≥99.5%), nonane (Sigma-Aldrich, assay 99%) and the fluorescent probes used for CLSM experiments, i.e., rhodamine 110 chloride, Nile red, and coumarin 6 (Sigma-Aldrich, purity >98−99%), were used without further purification. Water was purified with a Millipore Milli-Q gradient system (resistivity >18 MΩ cm). Carbon black, iron oxide (ochre), silica, kaolin, gelatin powder, Japanese paper (9.6 g/m2), poly(ethyl methacrylate/methyl acrylate) [p(EMA/MA)], Paraloid B72, pellets, and cellulose powder (Arbocel BC200, J. Rettenmaier & Sohne, Gmbh) were purchased from Zecchi, Florence. Soluble starch, cement, olive oil, and mineral oil commercially available and thus purchased in non-specialized stores.

1.3.2. Samples preparation

1.3.2.1.   Nanostructured fluids

For the CLSM experiments on polymer (Paraloid B72) removal, six different formulations (reported in Table 1) were prepared. The concentration of PC in the water/PC mixture was chosen taking account the PC solubility limit (16% w/w) in water [62]; water/MEK solution was formulated to be equimolar. For polymer removal tests on glass slides, four different NSFs with the same composition (apart from surfactant) were used (see Table 2). Besides MPD and PDE, an anionic (SDS) and a zwitterionic/cationic (DDAO)

surfactant were used as reference amphiphile [2]. Surfactants' concentration was changes in order to compare their effectiveness in the same conditions. For soil removal experiments, micellar solutions of MPD and PDE were used, at two different surfactant concentrations, that is, 1 and 5% w/w.

Systems	Amounts (% w/w)
H2O/MEK	88-12
H2O/PC	84-16
H2O/MEK/MPD	83.8-11.2-5
H2O/MEK/PDE	83.8-11.2-5
H2O/PC/MPD	79.9-15.1-5
H2O/PC/PDE	79.9-15.1-5

Table 1. NSFs used in CLSM experiments on polymer removal.

Components	Amounts (% w/w)
Water	60
Surfactant	~3
BuOH	10
PC	8
EtAc	8
MEK	11

Table 2. Composition of NSFs used in polymer removal tests on glass slides. Each of the 4 NSFs tested included a different surfactant selected from this list: MPD, PDE, SDS, DDAO. The amount of surfactant was calculated according to each molecular weight, in order to have the same moles of each amphiphile in the different systems.

1.3.2.2.   Artificial soil

The artificial soil mixture was formulate according to the recipe available in the literature [49] and reported in Table 3. The amounts reported in the Table

below are relative to 1L of dispersion in nonane. The solid components were weighed and mixed together. Then, olive oil and mineral oil were added to obtain a viscous paste, which was diluted with nonane.

Soil component	Amounts
Carbon black	2.0 g
Iron oxide	0.5 g
Silica	1.7 g
Kaolin	20.0 g
Gelatin powder	10.0 g
Soluble starch	10.0
Cement	17.5
Olive Oil	10.0 ml
Mineral oil	20.0 ml

Table 3. Artificial soil composition. The amounts here reported are relative to 1 L of dispersion in nonane.

1.3.2.3. Soil and polymeric layers

CLSM investigations on PB72/NSFs interaction were performed on polymeric layers of about 2 μm thickness. The films were prepared by spin-coating (2000 rpm, 120 s) 200 μL of a 10% w/w p(EMA/MA) solution in ethyl acetate, to which Coumarin 6 (10 mg L) was added, on cover glasses.

For CLSM experiments on soil/NSF interaction, glass slides were coated by drop-casting 150 μL of the artificial soil dispersion stained with Nile red 10^{-6} M, previously dissolved in nonane. The samples were let completely drying for at least a week and then used for the experiments.

Polymer removal tests were achieved on 5 x 5 cm^2 glass slides coated by drop-casting a 10% w/w PB72 solution in EtAc; for soil removal tests, 1 ml of the artificial soil dispersion was used to cover 5 x 5 cm^2 glass and PS slides. The

samples were let drying until constant weight was reached, and the final "dry" weight was about 80 mg (for PB72 samples) and 2-3 mg/cm^2 (for soil samples).

1.3.3. CLSM Experiments

Confocal Microscopy experiments were performed on a Leica TCS SP8 confocal microscope (Leica Microsystems GmbH, Wetzlar, Germany) equipped with a 63X water immersion objective. Rhodamine 110 chloride and Coumarin 6 were excited with the 488 nm laser line of an Argon laser, while Nile red was excited with a DPSS solid state laser at 561 nm. The emission of the dyes was acquired with two PMTs in the range 498-530 nm and 571-630 nm, respectively. CLSM experiments were performed to monitor the interaction of the polymer films or soil with different NSFs, as detailed in section 1.3.2.1.

200 μl of the unlabelled (or labelled with rhodamine 110 chloride) liquid phase were put in contact with the polymeric (or soil) layers. The morphological variations of the coatings were monitored over time, up to several minutes (for details, see section 1.4)

1.3.4. Removal Tests

Polymer removal tests were performed on glass slides, prepared as reported in section 1.3.2.3, using cellulose pulp poultices imbibed with the NSFs. The cellulose compress, wrapped in sheets of Japanese paper, were put in contact with the polymer film and were left interacting for 1.5 hours. After their removal, the surface was gently rinsed with water to remove possible surfactant residues. After complete drying of the samples, the treated glass slides were weighed again, and the % of removed polymer was calculated.

Soiled glass and plastic slides were immersed for 24 hours in 40 ml of the following aqueous micellar solutions: MPD 1%, MPD 5%, PDE 1%, PDE 5% (w/w). During the experiments, the samples were not moved and the

solution was not stirred. At t = 0 h, 3 h, 6 h, 24 h the NSFs were photographed. After 24 hours, the samples were taken out of the NSFs and tilted with care, in order to check for the residual adhesion of the soil coating to the glass/plastic surface.

1.3.5.　Contact Angle Measurements

The contact angle of 5 µl droplets of Milli-Q water on soiled glass slides was measured with a Rame-Hart Model 190 CA Goniometer; the obtained values were used to indirectly evaluate the surfactant adsorption. Three samples were analysed, i.e., pristine soil-coated glass slide, and two soil-coated glass slides immersed for 1 minute in a 1 % w/w solution of MPD and PDE, respectively. The equilibrium contact angle was measured in at least five different areas, and the average value and standard deviation was evaluated.

1.3.6.　Surface Tension Measurements

Surface tension values of MPD and PDE aqueous solutions were determined with K100 Tensiometer (Krüss, GmbH, Hamburg, Germany). The surface tension was measured at different concentrations by adding a concentrated stock solution of surfactant in water to a bowl containing a known volume of water (40 mL). Surface tension measurements were carried out with a platinum plate and for each concentration the average of ten readings was taken after attaining the equilibrium of solution.

1.4. Results and discussions

1.4.1. Polymer film removal

The interaction process between the polymeric layer and the NSFs (see Table 1 for the compositions) was monitored at the polymer/glass interface through CLSM.

At the beginning of the process, the Coumarin 6 dye appears as homogeneously distributed on the microscopic length scale. At first, it was monitored the interaction of the polymer film with the binary systems, i.e., the H2O/MEK and H2O/PC mixtures. As is shown in Figure 6, the system containing PC is the most efficient, since it is effective to dewet the polymer also in absence of surfactant. In contrast, water/MEK mixture cause only a partial film layer detachment. This behaviour suggests that PC has a higher affinity for pEMA/MA (PB72).
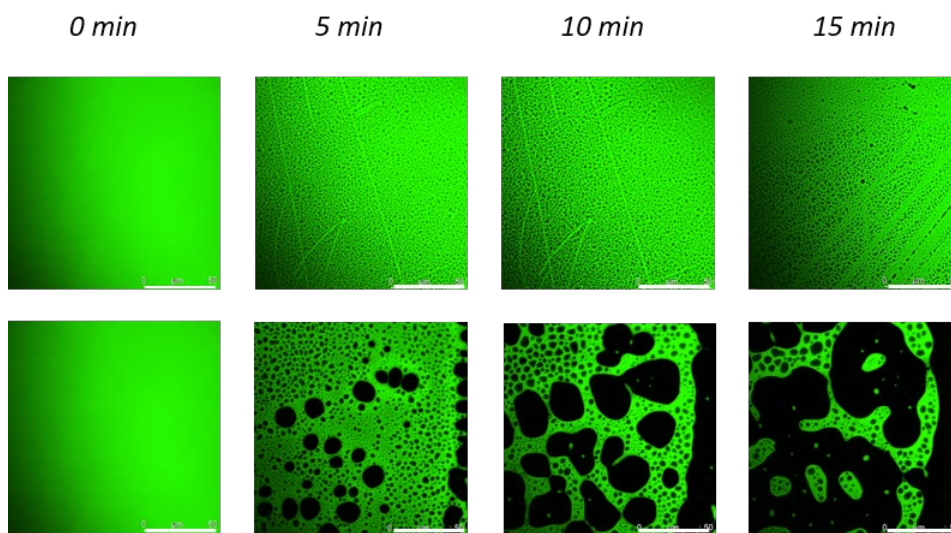
Figure 6. CLSM results on p(EMA/MA) interacting with H2O/MEK (top) and H2O/PC (bottom). Scale bars correspond to 50 µm length.

When the films are exposed to the ternary systems, different structural variations can be observed. Figure 7 shows the time evolution of the polymeric layer, taken at the glass-polymer interface. After the interaction with NSFs, some dark regions appear as a consequence of polymer detachments in those areas. These detachments slowly increase in size, and their growth and film dewetting are highly dependent on the composition of the liquid phase. The PC-based NSFs are able to dewet the polymer from the glass (Figure 7 A-B), while in the case of systems containing MEK, no complete dewetting was observed after 20 minutes of interaction (Figure 7 C-D).

As is visible in Figure 7, the surfactants differ in promoting the polymer detachment: MPD is faster and more effective than PDE and accelerates dewetting with respect to the binary water/solvent mixtures (see Figure 6). After only 5 minutes, the film interacting with the water/PC/MPD system is almost entirely dewetted (Figure 7B), while at the same time the polymer interacting with water/PC/PDE formulation showed few large holes (20-30 μm) in a continuous network (Figure 7A). The same behaviour can be observed for the MEK-based formulations; the presence of MPD accelerates the interaction process (compare Figure 7 C-D).

The 3D reconstruction highlights the film conformation before (Figure 7E) and after the interaction with the four different NSFs. The synergistic effect of PC and MPD is clearly (Figure 7 A^1-B^1-C^1-D^1).

To better understand the information provided by this complex figure, the role of the solvent and of the surfactant must be separately addressed. Despite both PC and MEK are good solvents for acrylic polymers such PB72 [63], it is clearly that PC promotes the dewetting process. The decrease of Tg value, obtained by DSC analysis, and the values of the gyration radii, obtained by the fitting of SANS data [64], also confirmed that polymer chains are more swollen in PC than MEK. These results confirm the higher affinity of PC for PB72, which represents a major driving force for dewetting.

The role of surfactant can be understood considering the thermodynamic and kinetic aspects related to the dewetting process. When a polymer is detached from a glass surface, some regions of the polymer/glass interface are partially "destroyed" and substituted by new interfacial regions (liquid/polymer and liquid/glass) (see Figure 8 for more details).
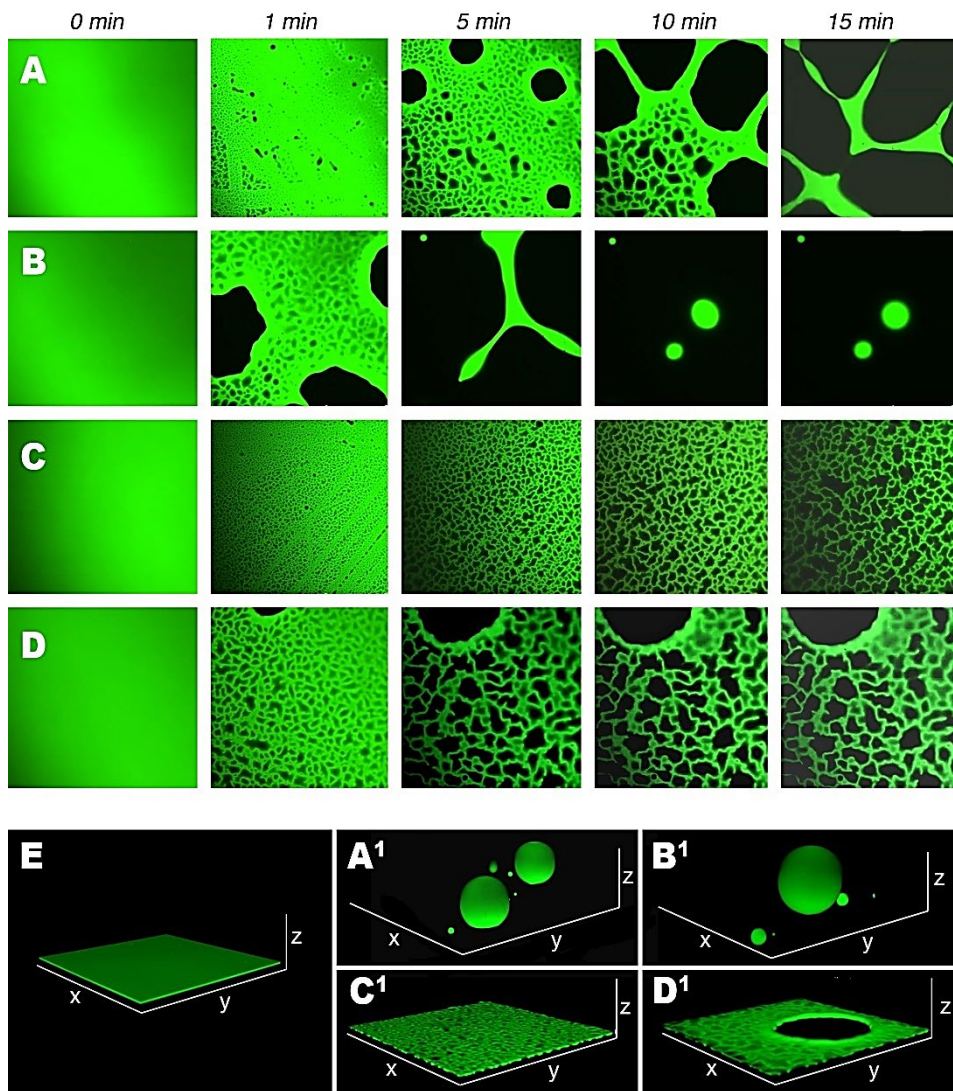
Figure 7. CLSM results on p(EMA/MA) interacting with (A) $H_2O/PC/PDE$, (B) $H_2O/PC/MPD$, (C) $H_2O/MEK/PDE$, and (D) $H_2O/MEK/MPD$. (E) 3D reconstruction of the polymer film before the interaction with NSFs, (A1−D1) 3D reconstructions of the polymer after 20 min of interaction with (A1) $H_2O/PC/PDE$, (B1) $H_2O/PC/MPD$, (C1) $H_2O/MEK/PDE$, and (D1) $H_2O/MEK/MPD$, which clarify the morphology of the film at the end of the experiments. The bottom side of each CLSM frame is 150 μm long.

The partial detachments promoted by the NSFs led to an overall increase of the total interfacial area of the system. It was found that the surfactants,

lowering both the liquid/polymer and liquid/solid interfacial tensions, reduce the energy cost related to the formation of this intermediate state, which represents the first step of dewetting [64]. In other word, surfactants with lower surface tension better promote the detachment from glass.
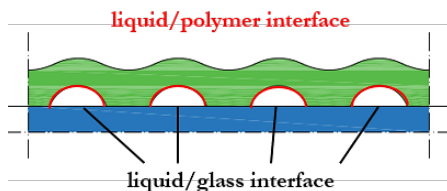
Figure 8. The cartoon shows the partial detachment of the polymeric layer from the glass slides. Liquid/polymer interfaces are coloured in red; the liquid/glass interfaces are indicated by the black lines.

Thus, the interfacial tension of the two surfactants was measured over a wide concentration range from well above the CMC of the surfactants to more than 100 times lower. The surface tension of the MPD micellar solution, $\gamma_{MPD} \approx 34.5$ N/m, is lower than that of PDE $\gamma_{MPD} \approx 37.5$ N/m (Figure 9). These values agree with a kinetically boosted dewetting process for this surfactant. Moreover, the methyl capping of MPD confers to this surfactant a higher hydrophobicity [51] and thus a higher capability of penetrating into the p(EMA/MA) film, with a consequent enhancement of polymer chains mobility.
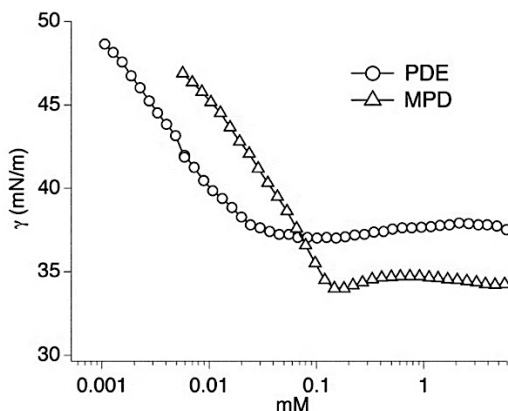
Figure 9. Surface tension of MPD and PDE aqueous solutions, as a function of surfactant concentration.

During the interaction with the polymer, the different NSFs show different mechanisms that depend not only on the organic solvent but also on the surfactant. The effectiveness of MPD was evaluated and compared to the one of PDE and other previously used amphiphiles, by formulating four systems differing only in the surfactant composition (see Table 2). Gravimetrical measurements were performed to evaluate the effects of the different NSFs on the removal of Paraloid B72 films to real cases, that is, thickness of several µm. All the cleaning fluids prove to be very effective, yielding an average removal of about 75% of the polymer after a single application of 1.5 h. Some slight differences could be spotted among different NSFs, for example, DDAO is the less effective of the tested surfactants, with a removal of 69 ± 3%.
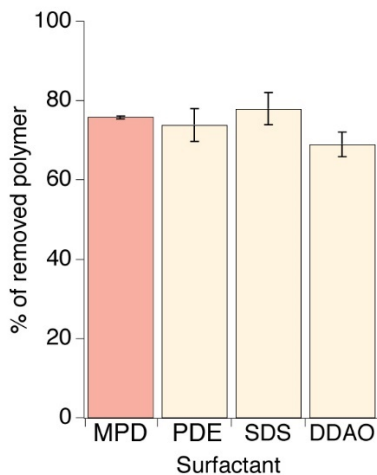
Figure 10. Histogram showing the results of polymer tests performed on glass slides with 4 NSFs differing from each other only in the surfactant.

1.4.2. Soil removal

The evolution of the samples' morphology was monitored through CLSM. Both NSFs and artificial soil were labelled with fluorescents dyes (rhodamine 110 and Nile red respectively) to better follow their interaction during the cleaning process. At the beginning, the Nile red (whose fluorescence is seen as red) appears as irregularly distributed on the glass slide because of the

complex composition of the artificial dirt. The appearance of the soil layer at the glass interface at t = 0 s shows the presence of several noncontact areas (dark zones), meaning that the adhesion (or wetting) of the soil to glass is not particularly favoured. Only 10 seconds after pouring the NSFs, the rhodamine 110 (whose fluorescence is seen as green) mixes with the Nile red, and yellow areas appear. These regions, indicating the co-presence of both fluorescent dyes, increase very fast in the first 30 s to 1 min; after this initial interaction, the soil morphology continues to evolve at slower rate (see Figure 11). The dark brown areas visible at the end of the process are associated with the depletion of the oily phase in the fluorophore.
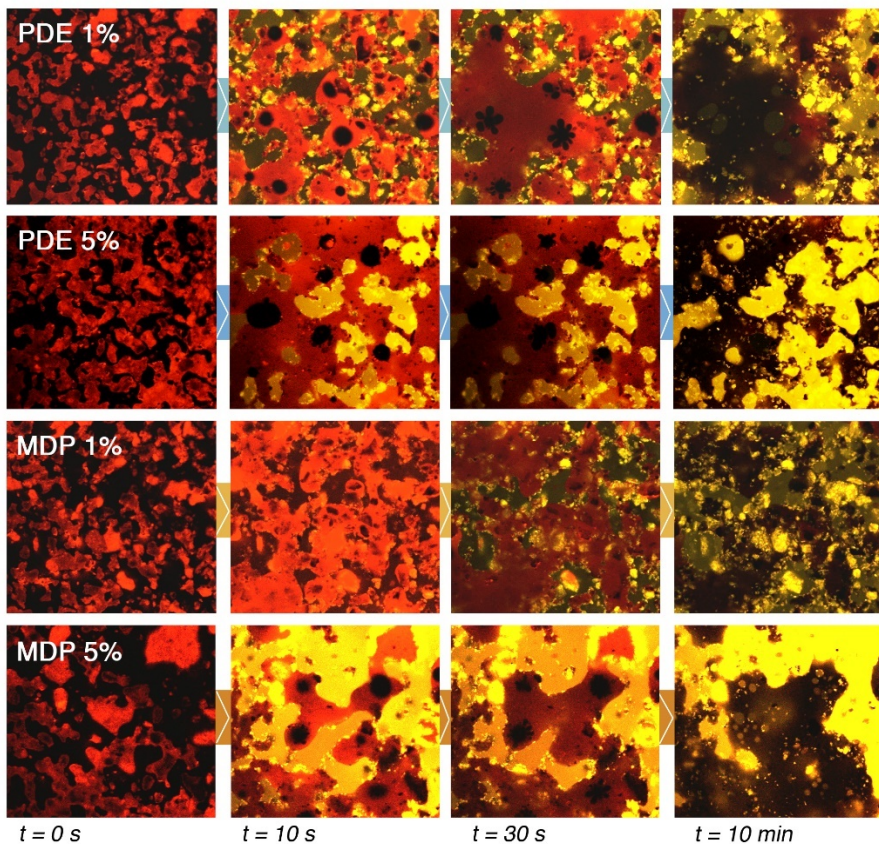

Figure 11. CLSM experiments on soil/NSF interaction. Nile red fluorescence is seen as red; rhodamine 110 chloride fluorescence is seen as green; yellow areas indicate the co-presence of both fluorescent dyes. The bottom side of each CLSM frame is 150 μm long.

When NSFs with 1% of surfactants are poured on the dirty layer, the micellar solution rapidly make the oily phase coalesce and rearrange itself in big droplets, recalling a dewetting like process. In these cases, surfactant concentration is not high enough to promote a further detachment of the soil from the glass slide.

Where NSFs with 5% of surfactants have been used, larger yellow areas are visible; this confirms that the surfactant concentration is crucial in determining a displacement and a detaching of the soil from the glass slides i.e., the first key step of the removal process. The mechanism observed for MPD 5% and PDE 5% is similar; however, on average, larger and more continuous soil detachment areas were evidenced in samples incubated with 5% MPD.

To evaluate the effectiveness in the soil removal of MPD-based NSFs, gravimetric measurements were performed on both glass and PS slides. The samples were submerged in 40 mL of the same NSFs used in CLSM experiments and were monitored at 0, 3, 6, and 24 h. As it is clearly visible in Figure 12, the samples treated with NSFs having PDE 1% and MPD 1% concentration remain almost unchanged even after 24 h.
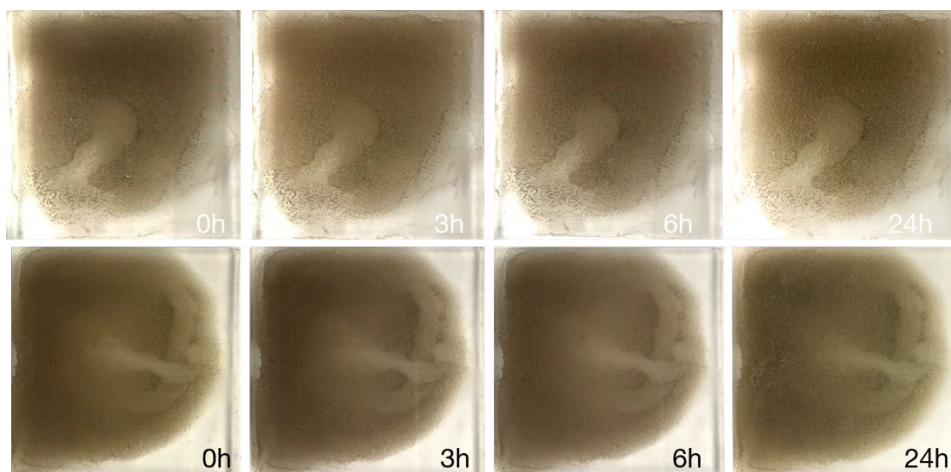
Figure 12. Sequence of zoomed picture taken during the 24 h of immersion of a soiled glass slide in the PDE 1% (top) and MPD 1% (bottom) micellar solutions.

The cracks and holes ascribable to a dewetting-like process, already observed during CLSM experiments, were also visible in the macroscopic scale only for MPD 5% concentration (Figure 13).
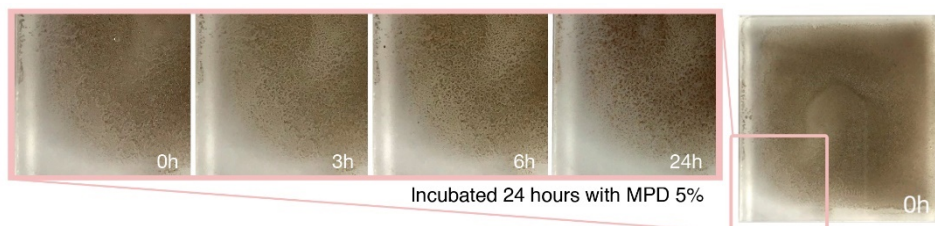
Figure 13. Sequence of zoomed picture taken during the 24 h of immersion of a soiled glass slide in the MPD 5% micellar solution. The dewetting-like process, with the formation of cracks and holes, is clearly visible.

After 24 h, the samples were extracted from the liquids and carefully tilted, in order to check for residual soil adhesion to the surfaces. Soil coatings on plastic slides was much more strongly adhered to the surface, and only in the case of the sample treated with MPD 5%, a significant, yet small (about 40% - see Figure 14-bottom) soil removal was observed. On the other hand, as observed in CLSM experiments, artificial soil is less affine to glass and, thus, after the interaction with NSFs, glass slides behaved very differently from plastic ones. Already 1% micellar solutions were able to detach and remove appreciable soil amounts, while 5% systems were able to provide even better cleaning, removing up to almost 100% in the case of MPD, which again proved to be more efficient than PDE, in the absence of any mechanical action. From the comparison of the image sequences reported in Figure 14-bottom-middle, this difference is clearly noticeable, even if both surfactants possess excellent cleaning power towards common soil. This means that, in principle, MPD-based formulations should need less mechanical action to remove soil from artistic surfaces, resulting in less stressful cleaning interventions. This feature is very important in the conservation field in view of soil removal from the delicate and fragile works of art.

To clarify the different surfactants' performances, the contact angle of water on the soil was measured ($52° \pm 8°$). After the immersion of the artificial soil

for 1 minute in the two 1% micellar solutions, the contact angle was 29° ± 1° and < 10° for sample incubated with MPD and PDE, respectively. A decrease in contact angle is predictable for the artificial soil exposed to the surfactant solutions; however, a significant difference exists in between the two surfactants.
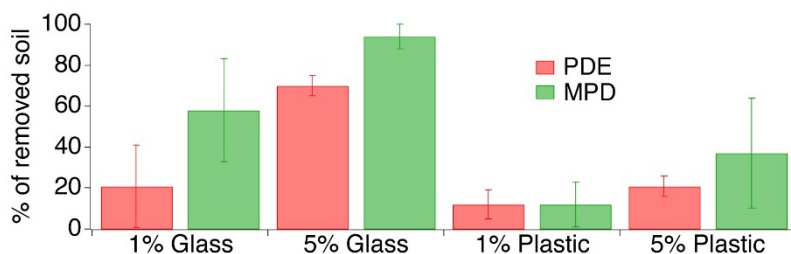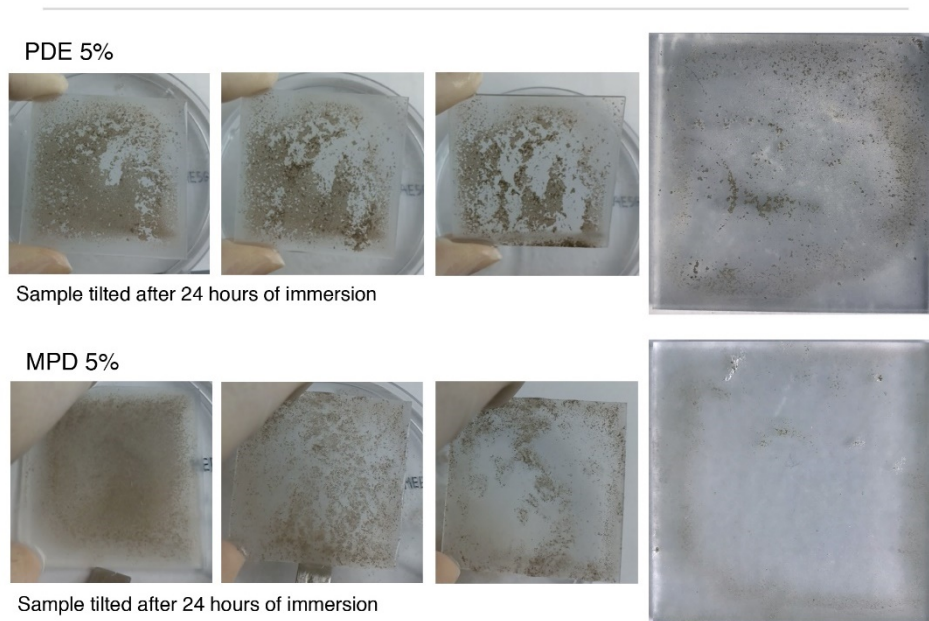
Figure 14. (Top) Glass slides incubated respectively with PDE 5% and MPD 5% micellar solutions were tilted, in order to check for residual soil adhesion to the glass surface. The soil was partially (PDE) or completely (MPD) detached from the glass; the final appearance of treated glass slides is reported. (Bottom) The histogram shows the % of soil removal achieved with the different NSFs on the two different substrates, i.e., glass and plastic. It is evident that soil removal from plastic is much harder.

These values -suggesting a higher effectiveness for MPD- are ascribable indeed to a different action mechanism of the two surfactants, as confirmed by the fitting of SAXS data. Results obtained from SAXS measurements clearly account for the higher effectiveness of MPD in removing the soil from glass surfaces, even in the absence of any mechanical action (see Paper 2 for details).

1.5. Final remarks

In the conservation field, selective and non-invasive removal of unwanted layers is a fundamental requirement. To pursue this purpose, in the last decades several nanostructured systems have been formulated using different organic solvents and surfactants. These last components, in particular, have a crucial role in the nanofluids' formulation.

Two NSFs with different composition have been prepared and the role of the two different surfactants (MPD and PDE) on the final cleaning effect have been investigated. In particular, MPD- and PDE-NSFs were tested in the removal of polymeric layers from glass and PS surfaces, while micellar solutions of the two surfactants used for the cleaning of artificially soiled surfaces. The overall results highlighted the better performance of MPD, if compared to PDE, both in inducing polymer removal and in detaching the soil from the coated surfaces. The interaction mechanism of the NSFs with the p(EMA/MA) polymer, which is observed at the micro-scale through CLSM imaging, involves dewetting-like processes, as already observed in previous works. Here, the polymer is detached from the surface and coalesces into separated droplets as the liquid phase/solid surface interfacial area increases. Explanations for these results can be found in the different surface tension and, possibly, in the different adsorption/penetration mechanism of MPD onto/into the polymer film, with respect to ordinary non-ionic surfactants. This is likely due to the methyl capping of the polar head chain and to the presence of the ester group between the hydrophilic and hydrophobic parts of the surfactant molecule. Moreover, CLSM experiments highlighted better performances of MPD, if compared to PDE, also in soil removal. The mechanism, which again is observed at the micro-scale, involves a dewetting-like process, where the oily phase is detached from the glass and coalesces into bigger droplets as the micellar aqueous phase/glass interfacial area increases. Surfactant concentration was found to be crucial to boost the interaction, as 1% surfactant solutions are less effective than 5%, even if micelles are present in both cases.

Contact angle and SAXS measurements provided an interesting explanation for the observed results. It has been hypothesized that MPD micelles tend to solubilize soil molecules inside their hydrophobic core, rather than adsorbing

on the soil layer surface, as PDE does. This different behaviour could account for the different effectiveness in soil removal of the two surfactants. MPD-based cleaning fluids are more efficient in weakening and detaching the soil from solid surfaces than PDE-based, allowing for an eased soil and grime removal with minimum mechanical action needed.

This can be key in the case of fragile and delicate works of art, which hardly tolerate mechanical stresses during cleaning operations. Overall, the features of MPD open up to new possibilities for the formulation of better-performing and safer cleaning systems to be used by restorers for the conservation of our cultural heritage.

Chapter 2. Cleaning Metals

2.1. Introduction

Metals have always had a crucial role in the process of civilization. Progress, indeed, has grown simultaneously with the increase in skills about the exploitation in the use of metals. With the improvement of the technical competencies required for the metalworking and specialization of manufacturing, men created tools, weapons and objects more and more advanced [65].

Gold, silver, iron, copper and their alloys have been used for artefacts' creation, which constitute a vast part of the artistic and architectural production spanning over millennia. The possibility of modulating its properties based on copper and tin content, made bronze one of the most used materials for the production of several artistic objects, from ornaments and jewels to statues and coins [66].

Metals are found in nature mainly in form of oxides, carbonates, sulfates, sulfurs, silicates, etc. and rarely in their native state. The melting process converts these compounds into the metallic state, which is however less stable than the natural starting one. The spontaneous reactions that occur between metals and environment cause the total or partial alteration of the artefact's original conformation and composition.

Corrosion processes that cause the degradation of metal artefacts depend on the different environmental context where these objects are located. Several parameters lead to the formation of different corrosion products, which can be classified according to their chemical structure (for more information, see Copper corrosion pro). Outdoor, buried or underwater artefacts degrade due to the presence of water, oxygen and salts, the variation of temperature and the exposition to the atmospheric agents and pollutants (CO_2, SO_2, SO_3, N_yO_x, Cl). The combined interaction of humidity, presence of visitors and use of not suitable cleaning products, may trigger or worsen corrosive processes also for indoor monuments.

Copper-based artefacts, in particular, react with the environment to form several corrosion products such as CuCl (cuprous chloride- nantokite), $CuCl_2$ (cupric chloride), Cu_2O (cuprous oxide- cuprite) and the cupric carbonates $[Cu_2(OH)_2CO_3]$ (malachite), and $[Cu_3(OH)_2(CO3)_2]$ (azurite) [67].

Among the corrosion products, chlorides are the most dangerous agents from a conservative point of view. Chlorine (Cl^-) coming from water, atmosphere and soil, induces the formation of a cuprous chloride layer, which reacts in presence of moisture and oxygen to form hydrochloric acid and basic cupric chloride. The hydrochloric acid, in turn, attacks the uncorroded metal to form more cuprous chloride and the reactions continue cyclically. This degradative process, known as "bronze disease", can consume the objects up to the complete disgregation [68]. On other hand, cuprite (a Cu(I) oxide) represents a protective layer against further corrosion because isolates the metallic surfaces from the surrounding environment (for more information, see 2.2.1.2).

The alteration products of Cu-based alloys cause the formation of overlapping structures, characterized by the presence of cuprite layer at the interface with the metal, and by an external layer of copper salts. Based on the different formation conditions, these superimposed networks, known as "patinas", have different morphologies and micro-chemical nature (see 2.2.1.1). Even if, in some cases, the patina due to the corrosion process is considered aesthetically pleasing, in most cases causes irreversible damages resulting in the loss of artistic and historical values of the object.

The cleaning intervention must be preceded by detailed diagnostic analysis and historical-artistic research to identify the most appropriate, effective and less aggressive cleaning methodology. Based on the protective role of the patina and its historical-artistic value, it is necessary to define the desired level at which the cleaning action must be interrupted. A careful distinction must also be made between a natural patina and an artificial one, intentionally created by the artist to obtain a particular aesthetic effect and which must not be removed [69]. Regarding the Italian concept of restoration, nowadays is generally accepted that the patina has not to be completely removed to respect the age and the historical information of the artwork [4].

The preservation of metal artefacts is an open challenge in conservation science as it requires a deep awareness on the characteristics of the treated

alloys and on the ongoing alteration processes, especially in case of outdoor, buried and underwater artefacts. An adequate cleaning procedure represents a fundamental operation in metals' conservation practice since it is aimed at the complete removal of the dangerous corrosion products while preserving the protective cuprite layer.

The removal of corrosion patinas from bronze is risky and time-consuming when carried out with traditional methods. Mechanical cleaning is usually performed by means brushes, scalpels, chisels, vibrating or abrasive tools, micro-peening with vegetal granulates, ultra-high-pressure water [70], and laser [71]. These techniques are invasive and scarcely controllable, potentially causing damage to the artefact; laser ablation can grant fast cleaning action but can lead to heating processes on the surface if it is not properly used (correct laser's wavelength or fluency) [72]. Chemical treatment generally involves the use of solvents such as formic acid, alkaline glycerol, sulphuric acid, ammonia and ammonium salts [73]–[75]. These reagents, when applied to the surfaces in a non-confined way (compresses or total immersion of the objects), present several issues related to the scarce selectivity of the cleaning process: (1) attack of the cuprite layer, (2) leaching out of some alloying metals, (3) precipitation and redeposition of copper salts onto the surface. Furthermore, if these chemicals are not removed completely after treatment, they continue to react with the metal, causing further deterioration.

A partial solution to these drawbacks is represented by the use of highly selective chelating agents such as Rochelle salts or ethylenediaminetetraacetic acid disodium salt (Na_2EDTA) solutions. Using chelators allows solubilizing only the corrosion products almost without any structural risk. These molecules, indeed, act only against the metallic ions of the patina because their speed of extraction on the atoms of the metal core can be considered nothing.

The confinement of chelating solutions inside gels or HVPDs involves a further reduction of risks not only for artworks but also for conservators. Use of a retentive matrix allows to gradually release the cleaning fluids also on vertical surfaces, and reduces solvent's volatility, decreasing considerably the health issues related to the chemicals' use.

In last decades, chemical gels have proved to be optimal confining matrices for cleaning fluids [20], [76]–[78]. Polymer such as pHEMA, PVP and PVA

have been employed to formulate systems with good physico-chemical and mechanical properties [48], [79].

Combining pHEMA and PVP in a semi-IPN network, for example, allows to obtain a system with the optimal features of the two homopolymers, i.e. the mechanical strength of pHEMA and the hydrophilicity of PVP [36]. Moreover, the possibility of applying these systems repeatedly without mechanical stresses, makes them excellent candidates for the use on brittle corroded surfaces, where even a slight mechanical action might be risky [80].

Besides the aforementioned advantages, a pHEMA/PVP system for cleaning metallic surfaces represents a promising approach due to the ability of PVP to form complexes with metal ions; an increase of the removal of corrosion patinas is expected [39]. Another polymer considered as semi-IPN networks was PAA. The presence of carboxylate groups at alkaline pH gives strong coordination bonds [40]; also, when PAA deprotonates and unfold, associates itself with water molecules and swells extensively [81].

The compositional and structural differences of pHEMA/PVP and pHEMA/PAA gels and the properties of water entrapped in the polymeric networks at different pH (6, 8 and 12) were investigated through different characterization's techniques. To confirm the effect of the gel's structure and functional groups on the adsorption process, the Cu(II) adsorption capability of the two pHEMA-based scaffolds was evaluated as well.

The possibility to apply repeatedly and easily remove these gels without mechanical stress on the treated surfaces, makes the semi-IPNs the most suitable systems for cleaning fragile and brittle materials. pHEMA-based gels, however, are rigid systems hardly to be adapted on cavities and pronounced reliefs that, sometimes, characterize bronze sculpture.

Using HVPDs allows to overcome this drawback; their initial viscosity let these systems able to homogeneously cover highly rough surfaces, and after the application, they can be easily removed in one piece with tweezers. These formulations, known also as "peelable films", act at the interface metal-corrosion thinning the unwanted layer to be removed.

The peelable systems used in this thesis work is made up of: (1) PVA, selected for its excellent chemical stability, biocompatibility, low toxicity and cost, and good film-forming properties [82]–[85], (2) plasticizers and (3) a hydro-

alcoholic liquid fraction. In particular, ethanol was chosen thanks to its structuring effect on water, that thus increases the order of the structure of the polymeric network [27], [86]. Properly loaded with cleaning fluids, these systems combine an effective chemical action with a gently mechanical operation.

Removal of a patina from a metallic surface requires the use of a chelator capable to act selectively on the corrosion products (commonly Cu(II) salts), preserving the protective cuprite layer of Cu(I).

Different parameters can influence the choice of the most appropriate chelating agent, such as the stability constant and the pH working conditions.

Even if the EDTA-copper (II) complexes have good stability (log Kf = 18.8 at 25°C and 1 M [42]), it is not unusual to find obstinate corrosion patinas that are resistant to treatments with EDTA.

An alternative complexing agent, whose copper (II) complex has a stability constant several orders of magnitude higher than that of EDTA, is represented by TEPA (log Kf = 22.8 at 25°C [41]). TEPA was chosen thanks to its (1) high complexing selectivity to Cu(II) ions and thus in removing only the corroded layer, (2) low cost, (3) high solubility both in ethanol and water and thus also in the hydroalcoholic network that constitutes the HVPDs network [44], (4) liquid state, that permits to use it also pure in the retentive matrices.

The PVA-based HVPDs loaded with TEPA were characterized through several techniques to study how the presence of the polyamine affects the film forming process and the physico-chemical properties of the final films. In fact, diethylene amines are usually employed as crosslinking agents of PVA, and are expected to modify the interactions among the polymer chains [87].

Semi-IPNs and HVPDs were applied on artificial corroded bronze mock-ups, and their ability to solubilize and remove copper (II) salts was checked at the micro-scale with 2D Imaging FTIR using a FPA detector.

Finally, selected formulations were used to remove corrosion patinas from several metallic object, different from each other in terms of materials, morphology and storage conditions.

2.2. Fundamentals

This paragraph briefly introduces the theoretical fundamentals related to the topic discussed in this chapter, i.e., the removal of the corrosion products from copper artefacts with gels and high viscous polymeric dispersions.

The principal corrosion products are discussed, with particular attention to those which constitute the corrosion patinas and which can activate the "bronze disease" phenomenon.

2.2.1. Copper corrosion process

Almost all the metals, in natural conditions, are found as oxides, carbonates, sulphates, etc.; these products are converted, after the manufacturing and melting processes, in their native state, which is less stable respect to the initial one [88], [89]. The interaction between these compounds and the surrounding environment, known as "corrosion phenomenon", leads to the deterioration of artefacts. The aim in the metals' restoration field is to stop or slow down these exchanges, intervening on the kinetics of the process.

The effects of a corrosion process are different, depending on the different environmental conditions of the discovery or exhibition sites (i.e., burial, water, outdoor and indoor). Presence of water, oxygen, salts, microorganisms, atmospheric agents and pollutants may trigger the corrosion process, leading to the formation of different corrosion products.

In case of copper-based artefacts, the corrosion products can be classified according to their chemical structure as reported in Table 4. A more detailed discussion is given for the corrosion products that are involved in the "bronze disease" process.

Corrosion products of copper artefacts			
	Mineral Name	**Formula**	**Color**
Oxide and Hydroxide	Cuprite*	Cu_2O	Submetallic red
	Tenorite	CuO	Metallic gray-black
Basic Carbonates	Malachite	$CuCO_3 \cdot Cu(OH)_2$	Pale green
	Azurite	$2CuCO_3 \cdot Cu(OH)_2$	Vitreous blue
Chlorides	Nantokite*	$CuCl$	Pale green
	Atacamite*	$Cu_2(OH)_3Cl$	Vitreous green
	Paratacamite*	$Cu_2(OH)_3Cl$	Pale green
	Clinoatacamite*	$Cu_2(OH)_3Cl$	Pale green
	Botallackite	$Cu_2(OH)_3Cl$	Pale bluish green
Sulphates	Brochantite	$Cu_4SO_4(OH)_6$	Vitreous green
	Antlerite	$Cu_3SO_4(OH)_4$	Vitreous green
	Posnjakite	$Cu_4SO_4(OH)_6 \cdot H_2O$	Vitreous green
Sulphites	Chalcocite	Cu_2O	Metallic blackish gray
	Covellite	CuS	Submetallic blue
Nitrates	Gherardtite	$Cu2(NO)3(OH)3$	Transparent green
Phosphates	Libethenite	$Cu2(PO)4(OH)$	Light-to-dark olive green

Table 4. Main corrosion compounds of a copper artefacts. Table adapted from [90].

Cuprite (Cu_2O) is the most common oxide present on copper artefacts. It is insoluble in water, it has a Mohs hardness of 3.5-4 and it is characterized by a varied range of colours: orange-red, orange-yellow or dark red, depending on its impurities. Cuprite represents the first interface which is formed when the metal reacts with the environment or during burial; being in contact with the metal, it represents a protective layer for the metallic alloys. During the corrosion process, cuprite may expand over the corroded layers as a result of

a copper ions migration; from an observation of the metallographic sections (Figure 16), it can be seen the presence of cuprite above and below the original surface [90].

Nantokite (CuCl) is a grey-green, translucent and waxy solid product, usually visible on underwater or buried artefacts. The nantokite layer, that forms after the interaction between chloride ions and copper, can remain inactive until the excavation [91]–[94]; at this point, CuCl can react with the moisture and the oxygen, starting the slow and inexorable corrosion process known as "bronze disease" (see 2.2.1.2). It is clear that the presence of nantokite as a corrosion product can cause problems for the stability and the aesthetic values of the object. The visual effect of "bronze disease" is the formation of green and powdery spots of the three copper trihydroxychlorides: **atacamite**, **paratacamite** and **clinoatacamite** (Figure 15) [95]. The presence of atacamite, that is the most common among the three copper hydroxychlorides, is associated to an active corrosion process. Paratacamite and clinoatacamite may be found together; the first one is less common, except for zinc-rich alloys.


Figure 15. Conversion of nantokite (left) to atacamite (right) after reaction with oxygen and moisture.

2.2.1.1.   Patina

The corrosion process affecting metallic objects leads to the formation of a complex patina, characterized by different composition and morphologies, depending on the chemical structure and the conservation environment (burial, water, indoor or outdoor) of the Cu-based artefacts. Corrosion layers are defined by complex and stratified structures, very different moving from the surface to the metal interface.

Figure 16 shows two different patinas constituted by a green layer of Cu(II) salts (atacamite), an area composed by a reddish phase of cuprite (Cu_2O) and by a layer of cuprous chloride -nantokite- (CuCl). The cuprous chloride triggers the cyclic corrosion phenomenon, known as "bronze disease" (see Bronze disease2.2.1.2), that progressively deteriorates the bronze artefacts turning it in green powdery objects.
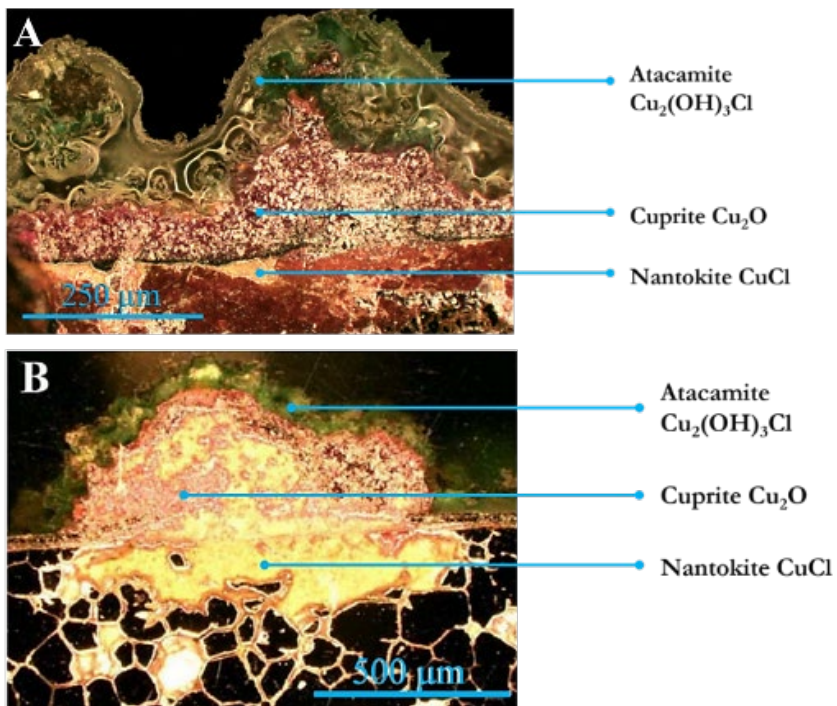

Figure 16. Example of overlapping structures on different archaeological objects (dark-field metallographic images) [96], [97]. The images show the complex nature of the corrosion products.

From a conservative point of view, the controlled and progressively removal of the Cu(II) alteration layers is crucial in order to preserve the cuprite layer and prevent the exposure of the dormant underlying copper chlorides.

2.2.1.2.   Bronze disease

The bronze disease [68], [73], [90] is the irreversible and nearly inexorable corrosion process occurring when chlorides come into contact with bronze. Primary factors that activate this phenomenon are related to the high-level humidity of environment (RH > 35%) and the presence of pollutants.

In acidic conditions copper is oxidized to the cuprous ion:

$$Cu \rightarrow Cu^+ + e^- \quad \textbf{(1)}$$
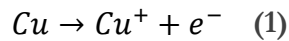
The cuprous ion combines with the chlorine to form cuprous chloride – nantokite- as a major component of the corrosion layer:

$$Cu^+ + Cl^- \rightarrow CuCl \quad \textbf{(2)}$$
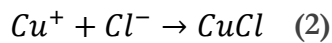
Cuprous chlorides are very unstable and in presence of moisture and oxygen are hydrolyzed to form hydrochloric acid and basic cupric chloride:

$$4CuCl + 4H_2O + O_2 \rightarrow CuCl_2 \cdot 3Cu(OH)_2 + 2\,HCl \quad \textbf{(3)}$$
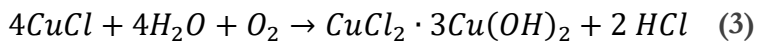
The conversion of cuprous chlorides to one of the copper-trihydroxychlorides causes a volume expansion. This situation creates physical stress, resulting in fractures and cracks.

The hydrochloric acid, in turn, attacks the uncorroded metal to form more cuprous chloride, until no metal remains:

$$2Cu + 2HCl \rightarrow 2CuCl + H_2 \quad \textbf{(4)}$$
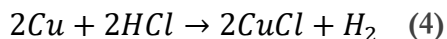
This phenomenon is manifest by green and powdery excrescences, which can disfigure the objects. During a cleaning operation, the removal of copper(II) hydroxychlorides must be done gradually and carefully, in order to preserve the cuprite layer that acts like a "protective barrier" against further corrosion processes.
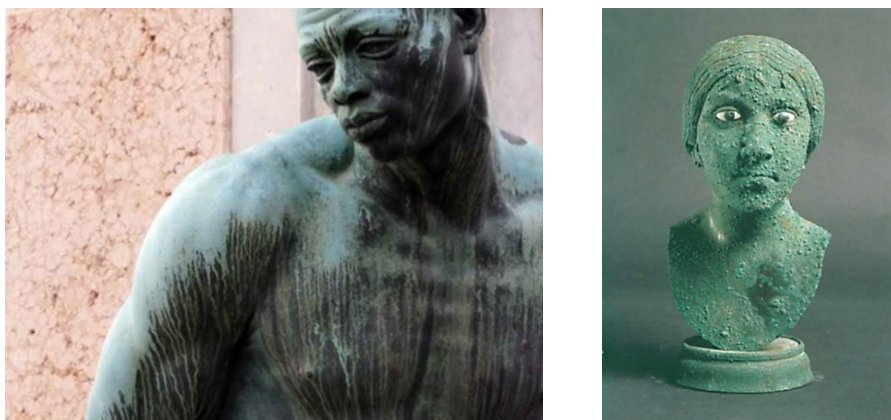
Figure 17. G. Bandini and P. Tacca, "The monument of the Four Moors", Livorno, Italy (left). Miniature Portrait Bust of a Woman, Malibu, J. Paul Getty Museum (right). In the images are clearly evident the pits and the streaked surfaces, due to corrosion processes.

2.3. Experimental Section

2.3.1. Materials

2-Hydroxyethyl methacrylate (HEMA) (purity 99%), poly(acrylic acid) (PAA) (average Mn ≈ 1200 kDa), azoisobutyronitrile (AIBN) (purity 98%), N,N-methylene-bis(acrylamide) (MBA) (purity 99%), poly(vinylpyrrolidone) (PVP) (average Mn ≈ 1300 kDa), Poly(vinyl alcohol) (PVA) (87–89% hydrolyzed, Mw 85,000–124,000, DP ≈ 2000, cps 23.0–27.0), dipropylene glycol (DPG) (99%, mixture of isomers), 2-methyl-1,3-propanediol (MPD) (99%), polyethylene glycol (PEG) (average Mn 300), glycerol (GLY) (analytical grade), tetraethylenepentamine (TEPA) (purity ≥95%), ethylenediaminetetraacetic acid disodium salt dihydrate (EDTA) (purity 98.5-101.5%), copper(II) chloride dihydrate (purity >99.0%), NH4OH solution (30–33% NH3,), hydrochloric acid (37%,), sodium chloride (purity ≥99.0%) and ethanol (EtOH) (purity ≥98%) were purchased from Sigma-Aldrich and used as received. Potassium dihydrogen phosphate (purity ≥99.0%) and dipotassium hydrogen phosphate (purity ≥98%) were purchased from Merck and used as received to prepare a pH 8 buffer. Sodium hydroxide (NaOH) (98.5%, for analysis, pellets) was used as received from Acros Organics. Water was purified by a MilliRO-6 Milli-Q gradient system (resistivity >18 MΩ·cm).

2.3.2. Semi-IPNs pHEMA synthesis

pHEMA/PVP semi-IPN was prepared by free radical polymerization of HEMA and MBA, in an aqueous solution of PVP and AIBN. All the chemicals were mixed in a beaker, which was stored in fridge overnight to decrease the eventual presence of gas bubbles incorporated during the stirring operation. Respect to the synthetic process reported elsewhere [36], some variations were adopted to obtain slightly softer and more flexible gel sheets to adapt to the rough surface of corrosion patinas. The HEMA/PVP ratio was changed from 30/70 to 27.5/72.5 (% w/w), the water content in the pre-

gel solution was 62.2% instead of 65%, while the cross-linker concentration was halved.

An aqueous solution of PAA was added to HEMA monomer and AIBN to prepare the pHEMA/PAA semi-IPN. The mass between HEMA and PAA (96.5/3.5 % w/w) was chosen to have a molar ratio between hydroxy and carboxyl groups of 16/1. This proportion proved optimal to yield gels with good mechanical properties. The obtained mixture was sonicated in pulsed mode to eliminate the last remained gas bubbles.

Each mixture (i.e., pHEMA/PVP and pHEMA/PAA) was polymerized at 60° C for 4 hours between two glass slides. After the reaction, a 2 mm thick flat hydrogel sheet was obtained; the gel was then washed and placed in a container filled with water. To remove residues of unreacted monomers and free PAA molecules, water was changed once a day for seven days. Table 5 shows the composition of the pHEMA semi-IPNs gels.

	pHEMA/PAA	pHEMA/PVP
HEMA (wt%)	52.5%	10.3
water (wt%)	45.2%	62.2
MBA (wt%)	-	0.4
AIBN (wt%)	0.4%	0.1
PAA (wt%)	1.8%	-
PVP (wt%)	-	27.0
HEMA/PAA ratio (%w/w)	96.5/3.5	-
HEMA/PVP ratio (%w/w)		27.5/72.5

Table 5. pHEMA semi-IPNs composition

2.3.2.1. Gels' swelling

After seven days, the semi-IPNs reached a stable pH of 6.3. To evaluate the influence of structural and chemical changes and the role of TEPA in the coordination of Cu (II) ions, small pieces (5 x 5 x 0.2 cm³) of each gel were cut and swollen in water at pH 8 and 12 (adjusted with a sodium hydroxide solution), and in a water solution of TEPA (20% w/w). In all cases, the gels were put in excess, as compared to the gel's mass, of NaOH or TEPA solution for at least 5 days. These conditions have been adopted to ensure a complete exchange of the semi-IPNs.

2.3.3. PVA-based HVPDs preparation

The PVA powder was dissolved into purified water at 90 °C for 2 hours, in a three-neck flask equipped with a condenser to avoid water evaporation during heating. After checking the complete solubilization of the PVA, the temperature was decrease to 70 °C. Plasticizers (PEG, DPG, MPD, GLY) were added and after about 30 minutes also ethanol. The final system was sonicated for 1 h in pulsed mode at 55 °C until a transparent polymeric dispersion was obtained. The synthesis was carried out under continuous stirring at 150 rpm with a stirring paddle, to reach and maintain the correct homogenization. The pH of the HVPD, measured with an indicator paper, was 6.5 ± 0.5. Table 6 shows the composition of the HVPDs.

2.3.3.1. Complexing agents' addition

An aqueous solution of EDTA 0.5 M was added to the solution under stir-ring, before the addition of EtOH to avoid the salt precipitation. The aqueous solution of EDTA corresponds to 3% (w/w) of the total weight of the HVPD (see Table 6). This chelator concentration is typically used in the bronze conservation field [98]. Further addition of EDTA solution to the HVPD leads to a phase separation and sedimentation of EDTA [43]. Before the use,

the pH of the dispersion has been taken to 9 ± 0.5 by addition of a concentrated (33%) ammonia solution.

An aqueous solution of TEPA 0.5 M (3% w/w) was loaded in the HVPD after the addition of EtOH (see Table 6). The final pH was 8.2 ± 0.2. Direct addition of TEPA (as received from the supplier) in the polymeric dispersion (3% w/w) was carried out for application onto stubborn corrosion patinas on the real bronze artifact. The HVPDs was stirred with a vortex at 2400 rpm to dissolve completely the amine. The final pH was strongly alkaline.

	PVA	PVA$_{ES}$	PVA$_{TS}$	PVA$_T$
PVA	20	20	20	20
H2O	57	54	54	54
EtOH	17	17	17	17
DPG	2.5	2.5	2.5	2.5
2-MPD	2.5	2.5	2.5	2.5
GLY	0.6	0.6	0.6	0.6
PEG	0.4	0.4	0.4	0.4
EDTA 0.5 M	-	3	-	-
TEPA 0.5 M	-	-	3	-
TEPA	-	-	-	3

Table 6. Composition (w/w %) of HVPDs. ES= loaded with an aqueous solution of EDTA (0.5M); TS = loaded with an aqueous solution of TEPA (0.5 M); T = loaded with TEPA

2.3.4. Physico-chemical characterization

This section reports equations and experimental conditions used for the physico-chemical characterization of the prepared systems (pHEMA-based gels and PVA-based HVPDs).

2.3.4.1.   Water states

Information on the absorption and permeation properties of the polymeric dispersions can be found from the investigation of the amount and the type of water contained in the gel network.

In particular, the equilibrium water content (EWC) and the equilibrium solvent content (ESC) can be calculated as follows (5):

$$EWC\ (ESC) = \frac{W - W_d}{W} \qquad (5)$$

where W is the weight of the hydrated sample and W_d the weight of the dry sample. The values of W_d were experimentally determined from TGA analysis, considering the weight of the sample at ca. 200 and 300°C to quantify the EWC (semi-IPNs swollen in water) and the ESC (semi-IPNs swollen in TEPA) respectively.

Thermogravimetric analysis (TGA) was carried out with an SDT Q600 (TA Instruments). The balance sensitivity is 0.1 µg. Measurements were performed in a nitrogen atmosphere with a flow rate of 100 mL/min. The samples were put in open alumina pans, and the analyses were performed with a heating rate of 10 °C/min from 25 °C to 450 °C [99].

Differential scanning calorimetry analysis (DSC) was performed with a Q2000 Calorimeter (TA Instruments). The temperature range was from -80 °C to 200 °C with a scan rate of 2 °C/min; sealed stainless steel pans were used. From the DSC curves it is possible to determine the different types of water present

in the hydrogels [100]. Water in porous systems like gels can be classified as non-freezing bound water, free or bulk water [101]. The non-freezing water forms hydrogen bonds with the functional groups of the polymer, rather than with other water molecules (as would be necessary for water to freeze); bulk water has the same properties of pure water and can bind with other water molecules to form ice crystals when temperature is around 0°C. It is possible to determine the free water index (FWI) according to the following equation (6):

$$FWI = \frac{\Delta H_{tr}}{\Delta H_f \; x \; EWC} \qquad (6)$$

where ΔH_{tr} (J/g) is the heat of transition obtained by the integral of melting peaks around 0°C in the DSC curves, and ΔH_f is the theoretical value of the specific enthalpy of fusion of water at 0 °C (333,6 J/g) [102].

2.3.4.2. Crystallinity degree and thermal properties

The crystallinity degree of the dried films was measured using differential scanning calorimetry (DSC) on a Q2000 Calorimetry (TA Instrument). 0.5 g of each formulation was applied on microscope glass slides with a spatula over an area of 2.5 x 2.5 cm^2 and let dry overnight at room temperature. The obtained films were peeled from the surface and cut into small pieces of the appropriate dimensions for the size of the steelpan. The samples were scanned in a nitrogen atmosphere with a flow rate of 50 mL/min using a heating rate of 10 °C/min. First, an annealing cycle was carried out by bringing the sample to 250°C, cooling it to 25°C and re-heated to 250 °C.

Glass transition (Tg) and melting (Tm) were obtained from the thermal curves after the second heating cycle; the enthalpy of fusion (ΔH_m) was determined integrating the melting peak area obtained from the thermal curves after the second heating cycle.

The degree of crystallinity (DC%) was calculated from equation (7) [103]:

$$DC\ (\%) = \frac{\Delta H_m}{\Delta H_{100}} \cdot 100 \quad (7)$$

Where Δ_m is the experimental melting enthalpy and Δ_{100} is the literature value for melting enthalpy of a complete crystalline PVA (Δ_{100} = 138.6 J/g) [104]. All the measurements were repeated three times.

2.3.4.3.   Evaporation kinetics

Gravimetric measurements were performed to evaluate the evaporation kinetics of the hydro-alcoholic fraction from HVPDs. To simulate the film formation process in real conditions, 0.5 g of each formulation was spread with a spatula on a microscopic glass slide over a covered area of 6.25 cm^2; after equilibration, the systems had a thickness of about 0.2 mm.

The volatile fraction loss over time, determined by weighting the glass slide until the weight became constant, was calculated as reported in the following equation (8):

$$W_{vf} = \frac{W_t - W_d}{W_i - W_d} \cdot 100 \quad (8)$$

where W_{vf} is the volatile fraction loss in function of time, W_t is the weight of the sample at the specific time t, W_d and W_i are the final dry weight and the initial weight of the sample. All the measurements were made at 25 °C and 45% RH. Five samples were prepared for each HVPD system; one of these was periodically weighted and the 4 slides were let dry in the same conditions until the film could be easily removed with tweezers from the glass without disrupting it or leaving residues. At this point in the evaporation process the films were thus deemed to be peelable. Weight measurements were repeated twice.

2.3.4.4.   Adsorption kinetics

Adsorption kinetics of Cu(II) were carried out on were carried out on 500 mL of copper chloride solutions (10^{-4} M) at two different pH values (6 and 8); the solution at pH 8 was obtained using a phosphate buffer solution. The Cu(II) adsorption at pH 12 was not evaluated owing to the precipitation of copper hydroxide. Pieces of pHEMA/PAA and pHEMA/PVP semi-IPNs were cut (5.0 x 5.0 x 0.2 cm^3), dried with blotting paper to remove any excess of surface water, and weighed. Kinetic measurements started when the gel was immersed in the copper chloride solution and, stopped after 180 minutes; this time interval was chosen as it widely covers real application times (generally no more than 2-3 hours). 1 mL aliquots were taken from the solution at set times and analyzed with a Perkin-Elmer Model AAnalyst 100 Flame Atomic Absorption Spectrometer (F-AAS) equipped with a 10 cm air–acetylene burner. The instrument was equipped with a multielement hollow cathode lamp and a deuterium lamp for background correction.

The instrument was operated under the conditions recommended by the manufacturer: lamp current of 30 mA, wavelength of 324.8 nm, slit width of 0.2 nm. The standard solutions and samples were introduced into the flame atomic absorption spectrophotometer by means of a standard nebuliser and flow spoilers. The absorbance of the samples was measured in triplicate against the blank solution and the average of the three measurements was used as the analytical signal. Standard solutions for Cu^{2+} calibration were daily prepared in polyethylene vials by diluting a Cu^{2+} stock standard solution (1000 mg L^{-1}) purchased from Merck (Darmstadt, Germany) with ultrahigh purity water (UHQ) of resistivity >18 MΩ cm (Milli-Q system by Millipore, Billerica, MA).

2.3.4.5.   Rheological behavior

Oscillatory shear measurements were performed on the different HVPDs formulation (with and without TEPA) to analyze the changes in viscoelastic behavior as a function of time during drying. The tests were carried out at 25.0

± 1 °C using a Discovery HR-3 rheometer from TA Instruments equipped with a parallel plate geometry of 20 mm diameter and a Peltier temperature control system; the gap was adapted to gain a maximum normal force of 0.9 N.

11 g of the polymeric dispersion were poured into a Petri dish and kept under manual stirring to maintain the homogeneity of the systems. Frequency sweep measurements were performed within the linear viscoelastic range (5% strain) defined by previous amplitude sweep tests. The storage (G′) and loss (G″) moduli were determined over the frequency range 0.01–100 Hz at different time (0, 30 and 60 minutes) of the drying process.

2.3.4.6.   Structural and morphological properties

SEM analysis were carried out on both semi-IPNs gels and HVPDs dried films to observe the structural and morphological properties of the systems.

To evaluate the macroporosity of the semi-IPNs, it was first necessary to subject thin slices of the hydrogels to a freeze-drying process. The obtained xerogels have a porous structure very similar to that of the swollen gels. To observe the morphological features of the HVPDs, the films were prepared as specified above (see Crystallinity degree and thermal properties). Before conducting the analysis, both semi-IPNs and HVPDs were metallized with a thin layer of gold using an Agar Scientific Auto Sputter Coater.

A Field Emission Gun Scanning Electron Microscope SIGMA (FEG-SEM, Carl Zeiss Microscopy GmbH, Germany (FEG-SEM, Carl Zeiss Microscopy GmbH, Germany) was used to acquire the images of both systems. To acquire the images was used an acceleration potential and a working distance of 2 kV and 3 mm (for the semi-IPNs gels) and of 3 kV and 3.9 mm (for HVPDs).

2.3.4.7.   Composition and chemical structure

The composition of the dry films obtained from the different HVPDs (loaded with water or loaded with TEPA 3%) was collected by ATR-FTIR analysis. A

Thermo Nicolet Nexus 870 equipped with an MCT detector (Mercury Cadmium Tellurium) was used to record the spectra between 650 cm^{-1} and 4000 cm^{-1}, with a spectral resolution of 4 cm^{-1} and 128 scans for each spectrum.

2.3.4.8.   Artificial aging

Cleaning tests were performed on artificial bronze coins provided by CNR-ISMN (Rome, Italy). The chemical composition (Cu 92.3 wt%, Sn 7.5 wt%, Pb 0.2 wt% [105]) simulates that of a typical coin related to the classical Roman period. Before artificial ageing, the coins sample was treated mechanically with sanding paper to increase its surface roughness, to favour the formation and more adhesion of degradation products. The ageing protocol was carried out as reported elsewhere [106] and produces corrosion patinas containing copper(II) chlorides that are similar in appearance and composition to those of archaeological bronze artifacts [107].

FEG-SEM images and energy dispersive X-ray (EDX) maps of elemental chlorine were collected before and after the artificial ageing process to evaluate the corrosion treatment efficacy. The X-ray counts were obtained by integrating Kα X-ray peaks using an Oxford Instruments INCA X-act microanalyzer.

2.3.4.9.   Cleaning procedure and evaluation of efficacy

The cleaning effectiveness of both systems was evaluated through application on the bronze coins, corroded as specified above (see 2.3.4.8)

Small pieces of pHEMA-PAA and pHEMA-PVP gels (1 x 1 x 0.2 cm^3) were loaded either with a 20% (w/w) TEPA or with a 9.7% (w/w) EDTA aqueous solution, both at pH 12. Two subsequent 45-minute applications were made on the coin surfaces; during the treatment the semi-IPNs were covered with parafilm to limit fluids' evaporation from the retentive matrices.

The HVPDs, loaded with chelating agents as specified in 2.3.3.1, were applied directly on bronze surfaces, lying down 0.25 g on 20 mm². After drying, a film was obtained, and it was peeled off from the surface using tweezers. The same protocol was adopted on the real bronze artefact.

During the application of both systems, a strong blue discoloration indicates the absorption of Cu(II) ions and the formation of Cu(II) complexes. After the treatment, the coin substrate was rinsed with water and air-dried.

To evaluate the cleaning effectiveness, 2D FTIR images and elemental analysis were acquired directly on the surface of the coins both before and after treatment with the gels and the HVPDs using a Cary 620-670 FTIR microscope (Agilent Technologies), equipped with Focal Plane Array (FPA) 128 x 128 detector. This set-up provides the highest spatial resolution currently available to FTIR microscopes. The spectra were acquired directly on the surface of the gels or of the Au background in reflectance mode, with open aperture and a spectral resolution of 4 cm-1, acquiring 128 scans for each spectrum. The spectral range was 4000–900 cm-1. A "single-tile" analysis results in a map of 700 x 700 µm2 (128 x 128 pixels), and the spatial resolution of each imaging map is 5.5 µm (i.e. the dimensions of each pixel are 5.5 x 5.5 µm2). Multiple tiles were acquired to form mosaics. The readability of the spectra was improved by reducing the background noise with the "smooth" tool (set at 11) of the Igor Pro software (Wavemetrics), taking care not to alter any diagnostic information considered useful to this investigation. The intensity of characteristic bands of the corrosion products was imaged in each 2D map. The increased absorbance is showed trough the follow chromatic scale: blue < green < yellow < red.

2.4. Results and Discussion

2.4.1. Characterization of pHEMA-based gels

After the synthesis, pHEMA semi-IPNs gels were swollen in water at different pH and in a TEPA solution (for more details, see 2.3.2 and 2.3.2.1).

Physico-chemical characterization of both the pHEMA-based systems was carried out to evaluate (1) the gels' behaviour at different pH and (2) the interactions between these systems and copper (II) ions.

In particular the structural differences at the micron-scale, investigated by SEM, DSC and TGA analysis, were employed to evaluate the gels' solvent content and the properties of water entrapped in the polymeric networks. The Cu (II) ion adsorption kinetics of pHEMA/PVP and pHEMA/PAA semi-IPNs at different pH values were studied and compared, highlighting the effect of the gels' structure and functional groups on the adsorption process.

2.4.1.1. Gels' behaviour at different pH

The influence of pH on the gels' microstructure was evaluated through FEG-SEM analysis (Figure 18). At pH 6, pHEMA/PAA semi-IPN shows a compact structure without any porosity at the microscale (Figure 18A), while at pH 8 has a quite homogeneous porosity in the 7-10 μm range (Figure 18B). The same gel, swollen in water at pH 12, exhibit a more heterogeneous structure, where pores have irregular shape and broad size distribution from 1 to 15 μm (Figure 18C).

All pHEMA/PVP gels show a macroporosity, with a different pores' distribution and shape. At pH 6 the pores have size between 5 and 12 μm and quite regular shape, while at pH 8, it is possible to observe three dimensions distributions (< 1 μm, 4-5 μm, and 14-20 μm). Gels' structure strongly changes in alkaline conditions (pH 12): pores exhibit elongated shapes arranged in rows and in a more ordered structure.

SAXS measurements confirm the polymer rearrangement in basic environment also at the nanoscale (for more details, see Paper 3).

At alkaline pH values (>10), the enol tautomer of PVP can lose a proton to form an enolate [108]. The partial deprotonation might lead to an enhancement of inter and intramolecular hydrogen bonds between enol and enolate groups in the PVP chains, resulting in a in a more compact structure.
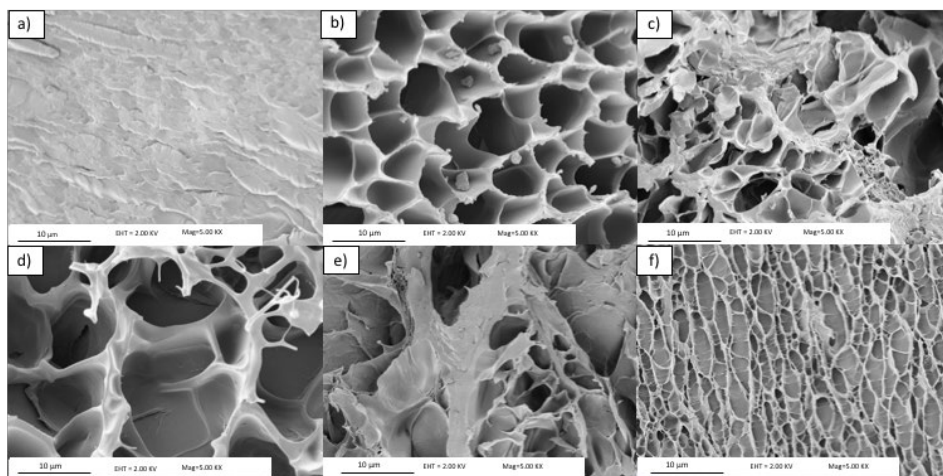
Figure 18. FEG-SEM images of pHEMA-based xerogels obtained after swelling of the corresponding hydrogels in water at pH 6 (a and d), pH 8 (b and e) and pH 12 (c and f). Scale bar is 10 µm.

From data obtained by DSC thermograms (Figure 19), it was possible to calculate the type and the amount of water uploaded in the semi-IPNs and provide information on the absorption and permeation of the hydrogels.

The EWC in pHEMA/PAA semi-IPNs, swollen at different pH, is mainly due to the gels' porosity and to the hydrophilic character of PAA. At pH 6, where the carboxylic group are completely protonated, the EWC is about 43% (see Table 7), similar of that of classical pHEMA chemical gels [109], [110], and it moves from 57% to 79 % at pH 8 and 12, owing to the ionization of the carboxyls.

The increase of the EWC, that corresponds to an increase of the mesh size observed through SAXS measurements (for more details, see Paper 3), is in

agreement with other studies [111]. This behaviour can be explained considering the electrostatic repulsion between PAA chains when the carboxyl groups are ionized, leading to the stretching of the polymer chain [112].

The FWI values increase passing from pH 6 to 12 (see Table 7), consistently with the presence of more hydrophilic moieties in the network (carboxylate groups in PAA), and with a higher macroporosity as shown by SEM measurements.
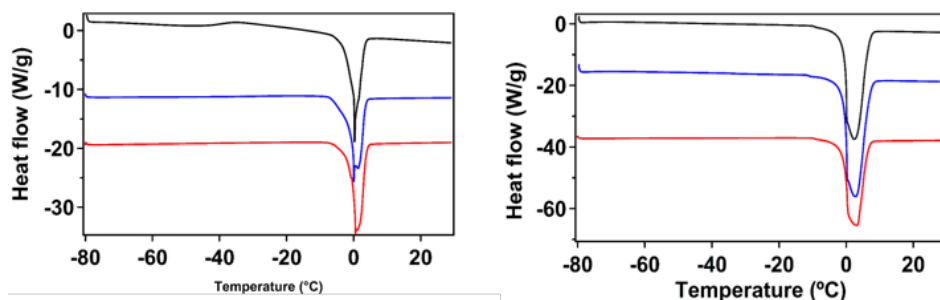
Figure 19. DSC thermograms for the pHEMA/PAA (left) and pHEMA/PVP (right) semi-IPNs gels swollen at pH 6 (black line), pH8 (blue line) and pH12 (red line). All thermograms were normalized to sample weight. The reported curves are offset along y-axis for clarity.

	ΔH_{tr} (J/g)	EWC	FWI
pH 6	76.5 ± 1.7	$42.9\% \pm 0.9\%$	0.53 ± 0.02
pH 8	154.3 ± 1.27	$56.8\% \pm 1.1\%$	0.81 ± 0.02
pH 12	293.2 ± 6.1	$79.1\% \pm 3.7\%$	1.11 ± 0.07

Table 7. Data obtained from DSC and TGA analysis of pHEMA/PAA semi-IPNs swollen in water at pH 6, 8 and 12.

Both the EWC and FWI of the pHEMA/PVP semi-IPNs remain substantially unchanged after the swelling in water at different pH (Table 8). These high values, higher than those of pHEMA/PAA semi-IPNs, can be ascribed to the high amount of PVP inside the gels, that results in a high hydrophilicity of the systems.

	ΔH_{tr} (J/g)	EWC	FWI
pH 6	296.1 ± 3.9	88.3% ± 0.5%	1.01 ± 0.02
pH 8	317.2 ± 1.1	89.1% ± 1.3%	1.07 ± 0.02
pH 12	299.5 ± 5.26	89.0% ± 2.1%	1.01 ± 0.04

Table 8. Data obtained from DSC and TGA analysis of pHEMA/PVP semi-IPNs swollen in water at pH 6, 8 and 12.

2.4.1.2. Cu(II)-gels interactions

When the pHEMA/PAA semi-IPNs are loaded with TEPA (pH 12), the solvent content is ca. 76% and it decreases to 71% after Cu(II) adsorption (Table 9). This reduction should be associated to (1) the interactions between TEPA and the carboxylic groups in PAA, and to (2) the leak of some free water and TEPA during the application of gels on the bronze coin, despite having covered the gel with parafilm. This small decrease in the ESC, in agreement with the lower mesh size observed with SAXS experiments (see Paper 3 for more information), can be also associated to the formation of complexes between Cu(II) and ionized carboxylic groups of PAA, e.g. each copper ion coordinating with two COO⁻ groups from different chains [110].
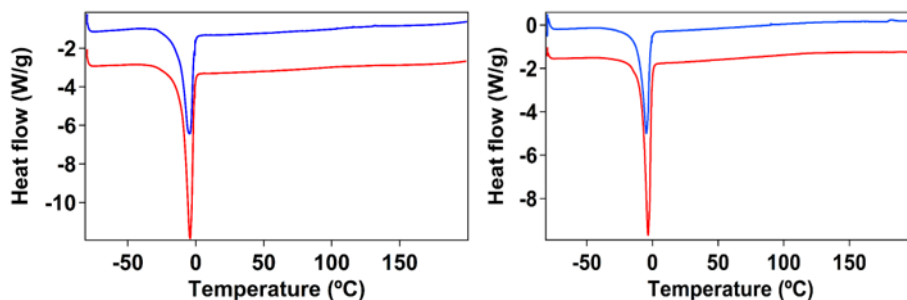
Figure 20. DSC thermograms for the pHEMA/PAA (left) and pHEMA/PVP (right) semi-IPNs gels swollen in a water solution of TEPA (20% w/w) (red line) and after the absorption of Cu(II) (blue line). Both thermograms were normalized to sample weight. The reported curves are offset along y-axis for clarity.

	ΔH$_{tr}$ (J/g)	ESC	FWI
TEPA	127.4 ± 4.1	76.3% ± 1.6%	0.50 ± 0.03
TEPA Cu	109.0 ± 3.1	71.3% ± 1.4%	0.46 ± 0.02

Table 9. Data obtained from DSC and TGA analysis of pHEMA/PAA semi-IPNs swollen in TEPA water solution before and after Cu(II) uptake.

In presence of TEPA and after the Cu(II) uptake, the ESC of the pHEMA/PVP semi-IPNs does not change significantly, demonstrating the high hydrophilicity of these systems.

	ΔH$_{tr}$ (J/g)	ESC	FWI
TEPA	154.6 ± 2.5	86.5% ± 0.01%	0.54 ± 0.01
TEPA Cu	133.5 ± 4.1	85.6% ± 0.8%	0.47 ± 0.02

Table 10. Data obtained from DSC and TGA analysis of pHEMA/PVP semi-IPNs swollen in TEPA water solution before and after Cu(II) uptake.
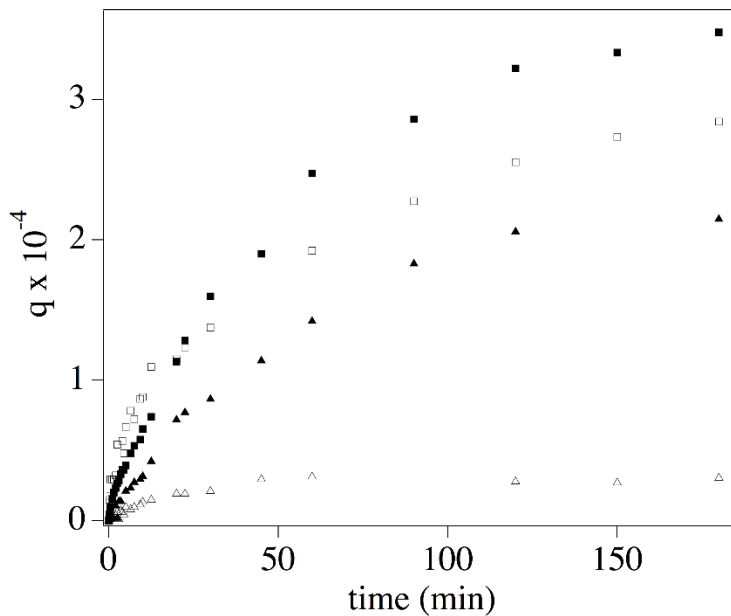
It must be noticed that for both systems there is a significant decrease in the heat of the melting transition (ΔH$_{tr}$, see Table 9 and Table 10) when Cu(II) ions are absorbed in the gels. The FWI decreases accordingly. This was explained considering that part of the bulk water molecules coordinate with the metal ions, participating in the formation of complexes.

Adsorption kinetics highlighted the specific effect of the different semi-IPNs' structures and functional groups on the uptake of Cu(II) ions. Figure 21 summarizes the trend of q (grams of solute sorbed per gram of sorbent) over time for the pHEMA/PAA and pHEMA/PVP semi-IPNs at pH 6 and 8.

The first observable feature is that the values of q moving towards the equilibrium value (qe) clearly follow the trend PAA_pH 8 > PAA_pH 6 > PVP_pH 8 > PVP_pH 6. This confirms that the presence of carboxylate (in

PAA) and enolate groups (in PVP) is a major drive to Cu(II) complexation by the semi-IPNs, and the effect of alkalinity on the increase of q is even more pronounced for PVP than PAA.

The second notable feature regards the first stages of the adsorption kinetics, where steeper curves are observed for the pHEMA/PAA semi-IPNs; namely, pHEMA/PAA at pH 6 has the steepest initial increase.

Figure 21. Plots of q (grams of solute sorbed per gram of sorbent) over time for the uptake of Cu(II) ions by the pHEMA/PAA (squares) and pHEMA/PVP (triangles) semi-IPNs at pH 6 (empty markers) and 8 (full markers).

Two types of equations are usually used for fitting the uptake curves of materials, i.e. (1) the diffusion-controlled models (intraparticle diffusion, IPD [113]–[116], diffusion-adsorption [117], adsorption dynamic intraparticle model [118]) and (2) the adsorption-controlled kinetics (generally both pseudo-first (K1) and pseudo-second order (K2) were compared). For example, Azizian derived independently, and concluded that the initial concentration of solute (C_0) determines the kinetic regime, e.g. K1 provides the best fit when C_0 is very high compared to the coverage of available sites in the sorbent (θ), while K2 fits adsorption curves better when C_0 is not too

high with respect to θ [119]. However, as reported in the literature [117]–[119], obtaining a good fit of the experimental data is not sufficient to validate the fitting model as the underlying mechanism: the literature reports several cases where significant contribution of diffusion, up to being the rate-controlling step, was recognized for data sets well fitted by K2 [117], [120]–[124].

Starting from this considerations, the adsorption curves of the two semi-IPNs at pH 6 and 8 to K1, K2, and IPD models reported in the literature [122] has been fitted. To obtain statistically relevant comparisons, we used the fitting models on the original scale (y = q(t)) rather than adopting transformed scales or linearized equations [117], [125], [126]. The models' equations, the full set of fitted curves and the fitting parameters (rate constants k, qe and chi-square values) are reported in the Appendix 1 (Table S1-4, Figure S1-4).
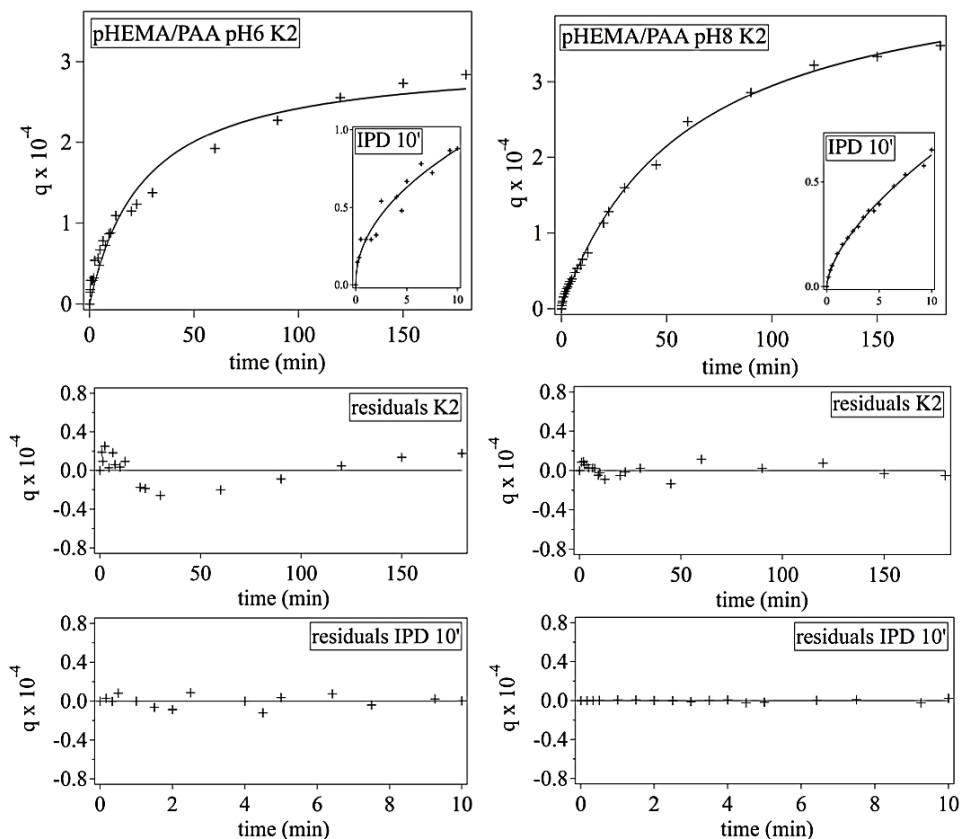
In the case of pHEMA/PAA semi-IPNs at pH 6, the pseudo-second order model provides a better fit than pseudo-first (K2>K1, see Figure S1; the K2 fit is shown in Figure 22), even though both K1 and K2 underestimate the uptake in the first part of the process. Instead, the IPD model provides a very good fit of the experimental data, but it does not account well for the uptake decrease in the final stages (see inset in Figure 22 and Figure S1).

Overall, as recently reported by Simonin, this behaviour suggests a process where a fast initial step limited by diffusion is followed by a slower second step, limited by diffusion in smaller pores or by slow adsorption [122]. This can be explained considering that initially the binding of Cu(II) at carboxylate (and to a lower extent carboxylic) sites is fast, and the rate-controlling step is the diffusion of the ions through the gel, while in the second stage diffusion in smaller pores and binding at less available sites control the process. In fact, at pH 8 the IPD equation fits only the first minutes of the uptake, and overall K2>K1>IPD (see Appendix 1-Figure S2 and inset in Figure 22), while at pH 6 the contribution of diffusion seems to be more significant; this is in good agreement with the much smaller porosity exhibited by the pHEMA/PAA gel before carboxylic groups are deprotonated.

For pHEMA/PVP semi-IPNs, in general K1>K2>IPD at pH 6 and 8 (see Figure S3 and S4; the K1 fit is shown in Figure 23). The IPD model provides significantly worse fittings of the whole curves than for pHEMA/PAA, even though the first stages are fitted reasonably well (see insets in Figure 23). In

71

this case, considering the porogen role of PVP in the semi-IPN network, the contribution of diffusion was indeed expected to be more limited.

Overall, the analysis of the curves confirmed the importance of pH control to boost the uptake of Cu(II) ions, and indicated that the ion-matrix interaction is stronger for pHEMA/PAA than pHEMA/PVP.

Figure 22. Plots of q (grams of solute sorbed per gram of sorbent) and residuals over time for the uptake of Cu(II) ions by the pHEMA/PAA semi-IPNs at pH 6 and 8. The full uptake curves (0-180 min) are fitted to the pseudo-second order kinetic model (K2), while the insets show the fitting of the first process stages (0-10 min) to the intraparticle diffusion model (IPD).
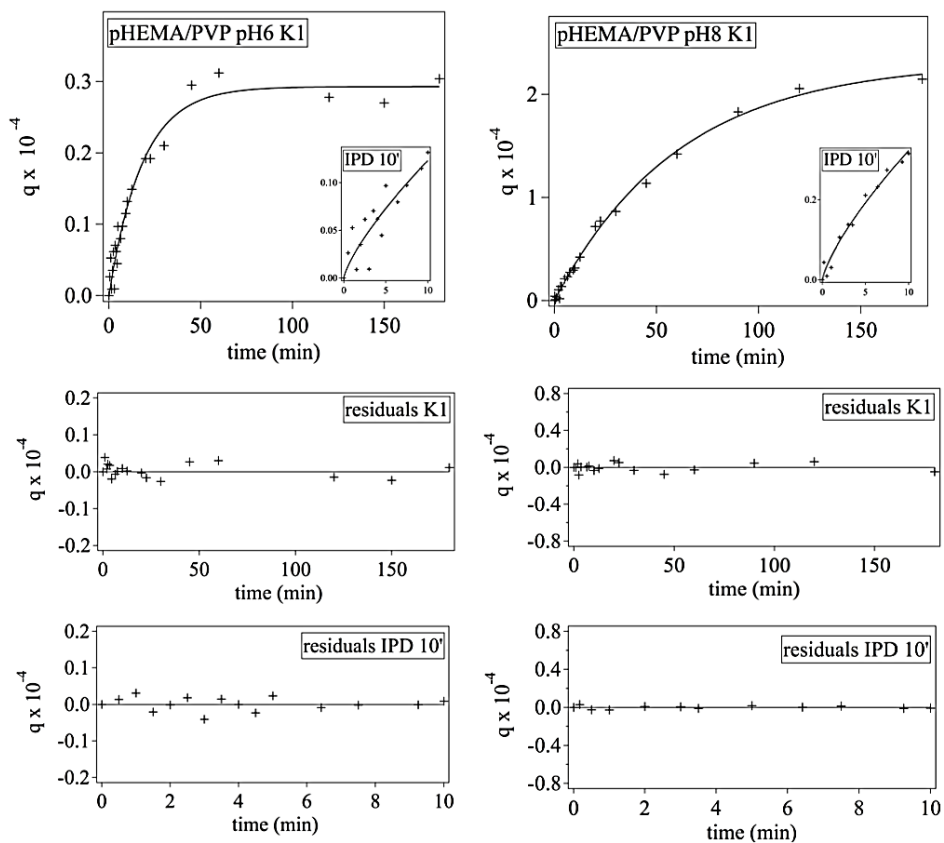
Figure 23. Plots of q (grams of solute sorbed per gram of sorbent) over time for the uptake of Cu(II) ions by the pHEMA/PVP semi-IPNs at pH 6 and 8. The full uptake curves (0-180 min) are fitted to the pseudo-first order kinetic model (K1), while the insets show the fitting of the first process stages (0-10 min) to the intraparticle diffusion model (IPD).

2.4.2. Characterization of PVA-based HVPDs

After the preparation and the addition of the TEPA complexing agent (for more details, see 2.3.3), the system appears yellowish and more viscous than the transparent dispersion loaded with water.

Physico-chemical characterization of both the PVA-based HVPDs systems, loaded and not loaded with the complexing agent, was carried out to evaluate (1) the kinetics of the film formation and (2) the properties of the final layer.

In particular, the evaporation of the liquid fraction (i.e., water and ethanol) was measured starting from the viscous dispersions toward the formation of the final layer through gravimetric and rheological measurements. The properties of the dried films were evaluated by DSC, ATR and SEM measurements.

2.4.2.1.   Kinetics of the film formation

Gravimetric and rheological measurements quantified the addiction of TEPA on the film-forming process and on the viscoelastic behaviour of the dispersions during drying. Figure 24 shows the loss of volatile fraction (i.e. water and ethanol) over time for both systems. In the plots, full markers indicate the time after which the films can be easily peeled off from the glass surfaces using tweezers (Figure 25); this can reasonably as considered as the time for the formation of the film.

Loading a solution of TEPA 0.5 M (3% w/w) in the polymeric dispersion, reduces film-forming time down to 100 minutes, i.e., half the time needed when the complexing agent is not added.

At the end of the process, the TEPA-loaded system contains 15% of volatile fraction, while the TEPA-free system is completely dry. This reduced volatility in presence of TEPA is most probably due to the faster drying of the evaporation front and to the high boiling point of the chelator (340 °C when pure).
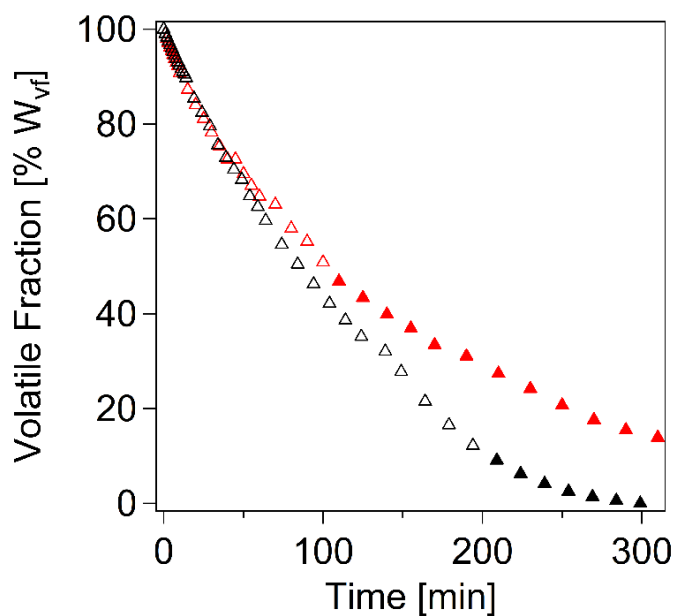
Figure 24. Loss of hydro-alcoholic fraction over time, from PVA-based HVPDs loaded with water (black) and TEPA complexing agents (red). Full markers show the points at which the system can be easily removed from the glass. The first full marker can be considered the time of the film formation.
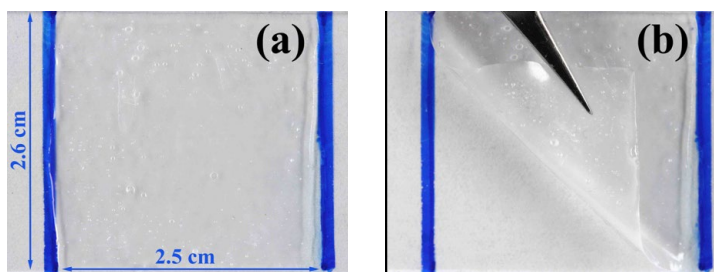
Figure 25. HVPDs on glass slide at the beginning of the process (a) and after film formation (b)

To follow the evolution of the mechanical and viscoelastic properties of the HVPDs during drying, rheological measurements (oscillatory frequency sweeps) were carried at different time out on the not-loaded and the TEPA 0.5 M (3% w/w) loaded systems.

At the beginning of the process, both systems behave as a viscous fluid, with the loss modulus (G") higher than the storage modulus (G') over whole the investigated frequencies. A cross-over point (ω_c) (i.e. the point in frequency sweeps were the two curves meet) between G' and G" is observed at high frequencies, as typical for entangled network [127], [128] (Figure 26).
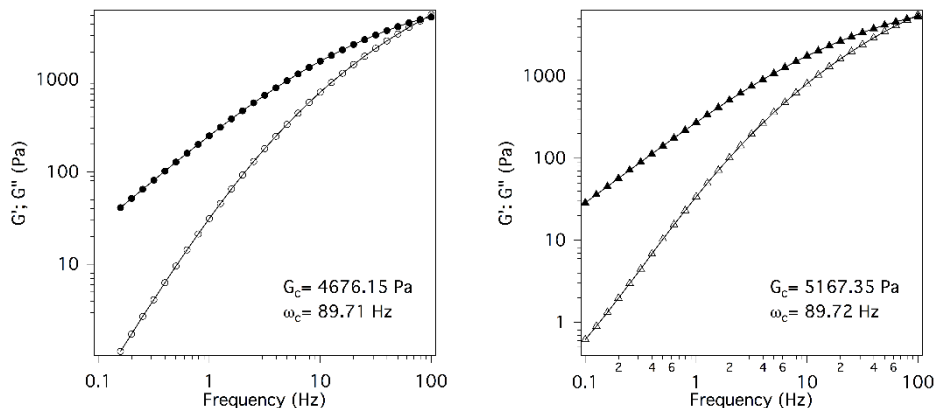
Figure 26. Frequency sweeps (strain of 5%) of the HVPDs systems not-loaded (left) and loaded with TEPA (right) measured at the beginning of the process. Empty and full markers represent G' and G" respectively.

As the hydro-alcoholic fraction evaporates, the increase of the storage modulus (G') suggest the progressive improvement of entanglement density between PVA chains, due to the formation of intra- and inter-molecular hydrogen bonds. Furthermore, the increase of the cross-over modulus (G_c) and the reduction of the cross over point (ω_c) to lower oscillation frequencies indicates that the dispersions become more "solid-like" as the film forms.

This process is faster when the complexing agent is loaded in the polymeric dispersions, in agreement with the gravimetric measurements (Figure 27).
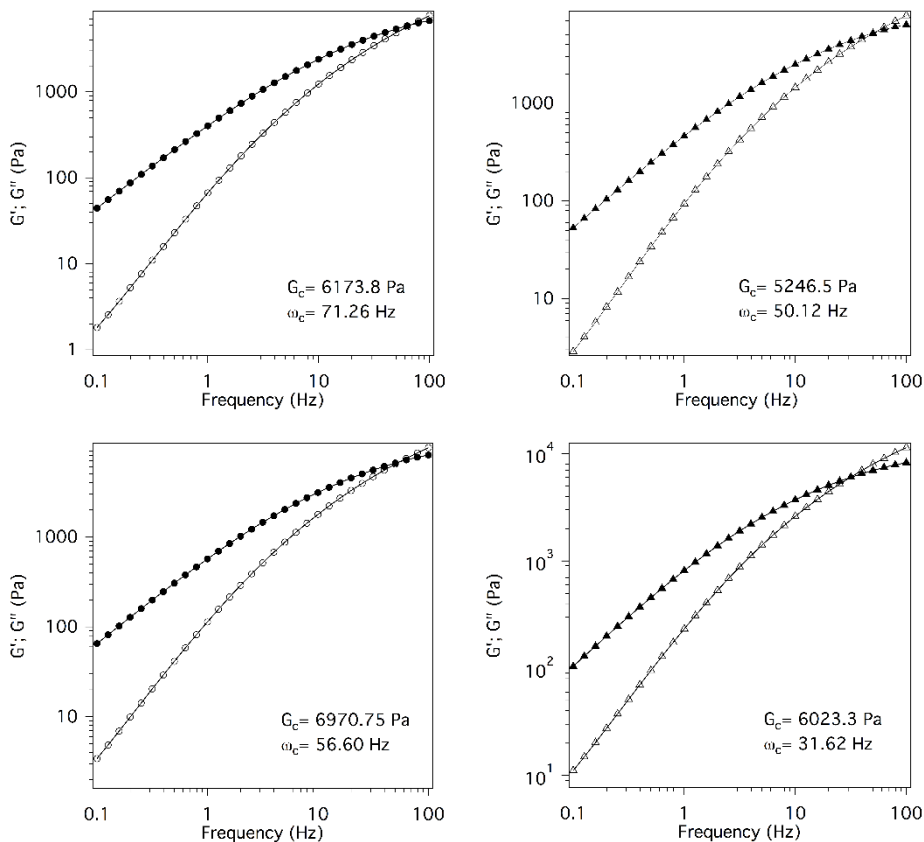
Figure 27. Frequency sweeps (strain of 5%) of the HVPDs systems not-loaded (left) and loaded with TEPA (right) measured after 30' (top) and 60' (bottom) of the process. Empty and full markers represent G' and G" respectively.

These improved interactions between PVA chains, resulting also in earlier film formation, are probably favoured by the high alkalinity environment promoted by TEPA. In fact, as known from the literature [103], sodium hydroxide solutions at high pH induce significant hydrolysis of the acetyl groups of PVA, leading to a higher intermolecular association and viscosity. Effectively, the addition of several drops of a NaOH solution (pH 14) leads to the formation of a solid-like gum already within one minute, which prevent gravimetric and rheological measurement. This irreversible transformation makes these systems unusable from an applicative point, as the gums are too rigid and retentive to be used in the conservation fields.

	HVPD loaded with water		HVPD TEPA 3%	
	G_c	ω_c	G_c	ω_c
0'	4676.15	89.71	5167.35	89.72
30'	6173.8	71.26	5246.5	50.12
60'	6970.75	56.60	6023.3	31.62

Table 11. Crossover point and cross-over modulus of HVPDs loaded with water or TEPA at different time of drying. Gc increases and ωc decreases with time for both systems because they become more "solid-like". It should also be noted that ωc values of TEPA-loaded HVPDs are higher than that of water-loaded already after 30 minutes.

In presence of TEPA, however, the increase of viscosity and the subsequent formation of the gum is much slower (e.g., 1 week), even at high pH. This behaviour is probably due to the lower diffusion of TEPA solution, that is more viscous respect to NaOH solution. In addition, TEPA is a weaker base respect to sodium hydroxide [129].

While the addition of the chelating agent significantly reduces the time required for film formation, it also decreases the shelf life of the product. This last aspect, however, can be solved adding the complexing agent at the time of use.

2.4.2.2. Films characterization

The crystallinity degree was evaluated trough DSC measurements to verify the effective reduction of the hydrolysis degree in an alkaline environment.

The degree of crystallinity (DC) of PVA depends on the degree of hydrolysis (DH), which is the percentage of acetate groups converted to hydroxyl groups during the hydrolysis of poly (vinyl acetate) (PVAc) to obtain PVA; resins with a lower DH contain more acetate groups, which disrupt the stereoregularity of the polymer chains and do not readily participate in intra- and intermolecular hydrogen bonding, decreasing thus the DC [130], [131]. The crystallinity of PVA is also affected by the presence of plasticizers, non-

volatile and low-molecular-weight compounds added to reduce brittleness, improve flow and flexibility, and increase the toughness and the impact resistance of the films [98], [132]. In PVA networks, plasticizers cause an increase in the free volume, in the macromolecular mobility and flexibility, as well as a decrease of intermolecular forces, of the glass transition temperature (Tg) and the DC [44], [133], [134].
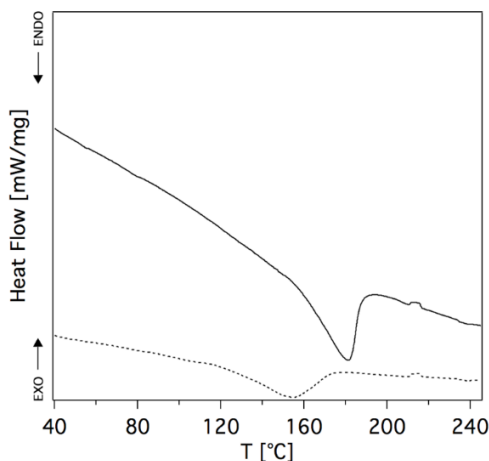
Figure 28. DSC curves of films cast from PVA-based HVPDs loaded with water (broken line) or with TEPA (3% w/w; full line).

As shown in Figure 28, the films loaded with water show a DC of 10.60% and a melting temperature of 155±2 °C in presence of plasticizers (PEG, GLY, MPD and DPG). These values are lower than that of films obtained with the same quantity of PVA simply loaded with the water (i.e. 12.80% and 161.3±0.1 °C [43]). The presence of plasticizers, as expected, reduce secondary bonds between polymer chains and, consequently, the DC. When TEPA is added to the formulation, the crystallinity degree raises to 15%. Besides, the melting peak becomes narrower and the melting temperature increases up to 177±7 °C, closer to the melting of fully hydrolyzed PVA (230.0 °C) [135].

Increase of crystallinity degree and narrowing of melting peak support the hypothesis that the alkaline environment provided by the TEPA solution favours the hydrolysis of PVA acetyl groups and the association of the polymer chains into more ordered structures.

The hydrolysis of PVA acetyl groups is also confirmed by ATR analysis shown in Figure 29. ATR spectra of films cast from water-loaded HVPDs show the typical absorption of PVA (see Table 12 for peaks assignments [136]). The alkaline environment leads to the appearance of band at 1643 cm^{-1}, associated to the N-H deformation of ammonio groups in the partially protonated TEPA molecules, and 1564 cm^{-1}, assigned to the carbonyl stretching of acetate ions formed by hydrolysis of PVAc groups, in the spectra of TEPA-containing films. At the same time, the intensity of the carbonyl peak of non hydrolyzed acetate groups (1718 cm^{-1}) decreases until it disappears moving from the TEPA-loaded film to the gum spectra. The spectrum of the gum formed ca. 1 week after the addition of TEPA (G$_{3\%}$) shows a marked increase of the protonated TEPA band (1643 cm^{-1}). Peaks assignments for TEPA-containing systems are summarized in Table 13.

Polyvinyl alcohol	
Frequency	**Assigments**
3300	-OH stretching
2934, 2914	C-H stretching
1718	C=O stretching of the acetate carbonyl group
1143, 1088	C-O stretching in PVA

Table 12. IR band assignments for water-loaded PVA film

TEPA-containing HVPDs	
Frequency	**Assigments**
1643	NH$_3^+$ deformation
1564	COO- stretching
1716	C=O stretching

**Table 13.** IR band assignments for TEPA-loaded film
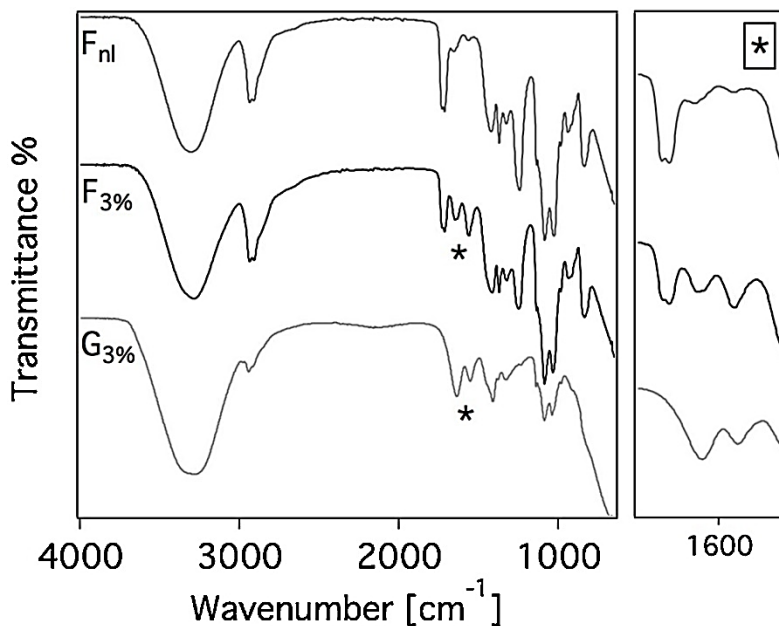
Figure 29. ATR spectra of films cast from PVA-based HVPDs loaded with water (Fnl), or loaded with TEPA 3% ($F_{3\%}$). The spectrum of the gum formed ca. 1 week after the addition of TEPA ($G_{3\%}$) is also showed. Moving from Fnl to $G_{3\%}$ it is possible to observe the appearance of bands at 1643 (N-H deformation of -NH_3^+ groups in the partially protonated TEPA) and 1564 cm^{-1} (carbonyl stretching of acetate ions formed by the alkaline hydrolysis of polyvinyl acetate groups in PVA), and the corresponding disappearance of the acetate C=O stretching peak (1716 cm^{-1}) (see also the inset).

Partly protonated polyamines are able to interact with acetate ions, and the formed ionic couples might hinder (e.g., through steric hindrance) the association of PVA chains. These interactions slow down the gum formation process, which instead is immediately observed after NaOH addition, and makes feasible the application of the TEPA-loaded HVPDs on bronze surfaces.

SEM analysis on the film loaded with water (Figure 30A) shows a pores distribution ranging from 1 to 20 μm, oriented along axes normal to the film surface. Most of the pores are placed in the lower layers, near to the base surface of the film; instead, the upper layers exhibit a more compact structure with elongated pores with a section of few microns. This morphology is probably due to the fast evaporation rate at the upper layers during the first

minutes of the process, that leads the collapse of porous structure closer to the top layers. The lower part of film is characterized by the presence of micron-sized pores, which could help the migration of dissolved corrosion products from the film-patina interface into the film's bulk.
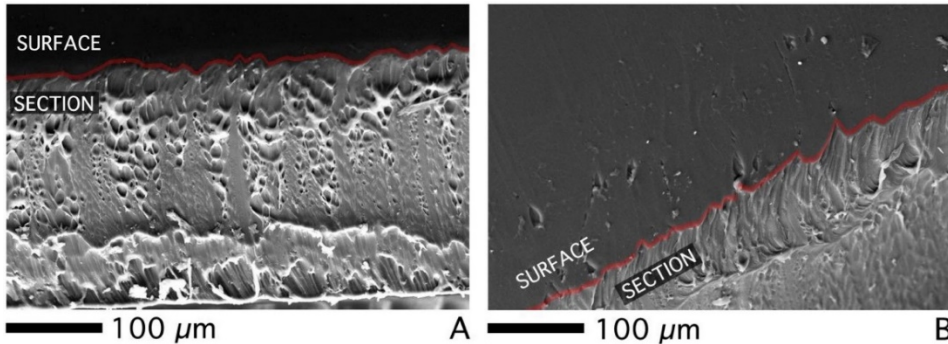
Figure 30. SEM images of films cast from PVA-based HVPDs loaded with water (A) or with TEPA 3% wt (B). Panel A shows a cross-section of a film, while panel B shows the edge between the upper surface of a film (smooth dark grey area, top left part of the image) and the underlying layers (bottom right portion of the image).

Pores structure of films obtained by drying the TEPA-loaded HVPDs don't show significant differences between bottom and upper part. As highlighted in Figure 30.B, film surface and underlying film layers are smooth, with no observable porosity.

In conclusion, based on the characterization discussed in the previous paragraphs, the TEPA-loaded systems were considered as a good candidate to the treatments of bronze surfaces.

2.4.3.   Applicative tests on artificial aged samples

2.4.3.1.   Corrosion products characterization

The TEPA-loaded HVPD and the pHEMA-based semi-IPNs were applied on artificial samples provided by CNR-ISMN (Rome, Italy). Further information about coin composition is given in section 2.3.4.8. The coin surface was characterized before and after the corrosion process, to evaluate its effectiveness and have a deep knowledge of the products to remove.

To simulate an archaeological patina, the coin mock-up was degraded by an accelerated corrosion treatment developed by Ingo et al. [106] and shown in Figure 31. The alloy sample, previously sprayed with solutions of $CuCl_2$ and NaCl, was placed over an inert grid and kept at controlled temperature (60°C) and high relative humidity (100%) for 3 days. The high humidity level was ensured with HCl solution, that also enhance the corrosion process.
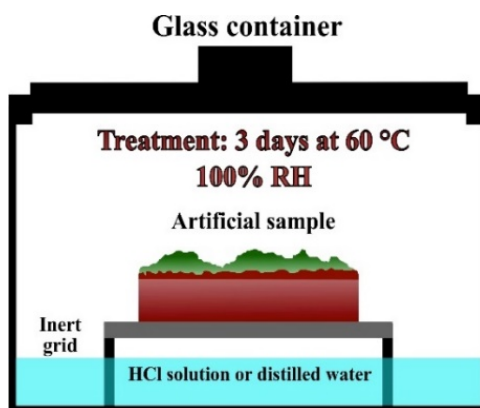
Figure 31. Sealed glass container used for the accelerated degradation methodology of Cu-base alloy samples. The corrosion procedure is reported in the main text. Image reprinted from [98].

The patina obtained following this procedure (Figure 32B) was characterized by SEM-EDX and micro-FTIR analysis. The spectra collected on the bronze mock-up after the corrosion process (Figure 33) show intense hydroxyl stretching bands of hydrated copper (II) hydroxy chlorides, such as

atacamite/clinoatacamite, at 3467, 3339, 3245, and 3154 cm^{-1} [137], [138]. These corrosion products are particularly dangerous for copper-based artifacts [139] because they are typically involved in the "bronze disease" (for more information, see 2.2.1.2). Less intense bands at 1489, 1461, 1451 and 1385 cm^{-1} are ascribable to the presence of copper carbonates (azurite and malachite) [140].
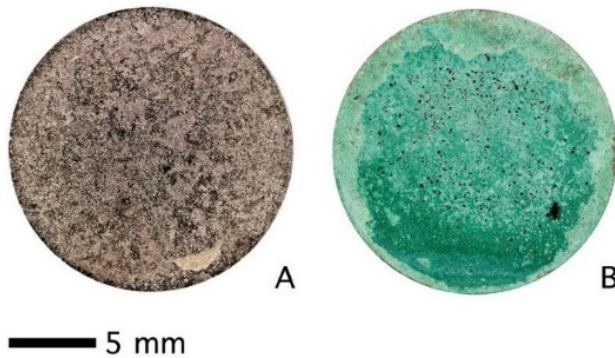
Figure 32. Macro photography of the bronze coin mock-up before artificial aging (A), after artificial aging (B).
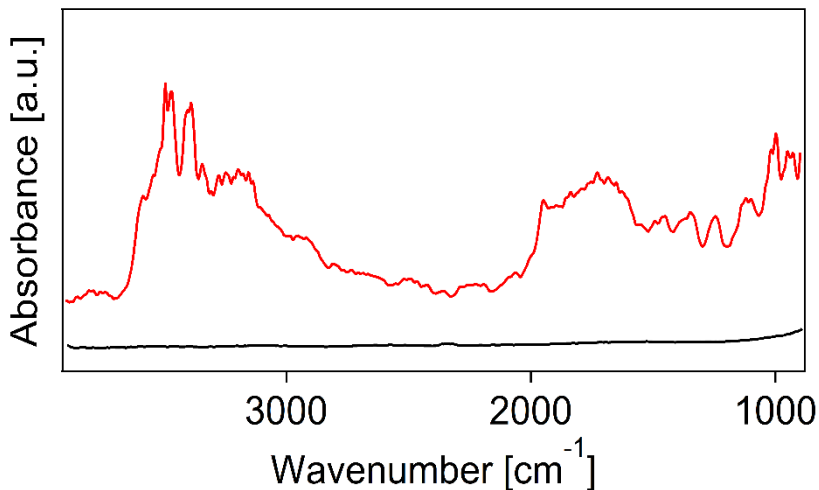
Figure 33. FTIR Reflectance spectra collected on the bronze mock-ups before (black line) and after (red line) the corrosion process. The reported spectra are offset along y-axis for clarity.

The presence of atacamite/clinoatacamite was confirmed by 2D FTIR Imaging with an FPA detector. This set-up allowed to control the presence of corrosion products down to the micron-scale, with a spatial resolution of 5.5 μm. It has been mapped the region, between 3111 and 3679 cm^{-1}, related to the presence of atacamite and clinoatacamite. As is clearly observable in Figure 34, before the corrosion process is performed, the bronze metal surface is characterized by blue pixels, which correspond to a low intensity (i.e., to a small amount) of corrosion products. After the accelerated ageing, the red pixels demonstrate the presence of a corrosion patina on the surface, as confirmed also with SEM-EDX analysis (Figure 35).
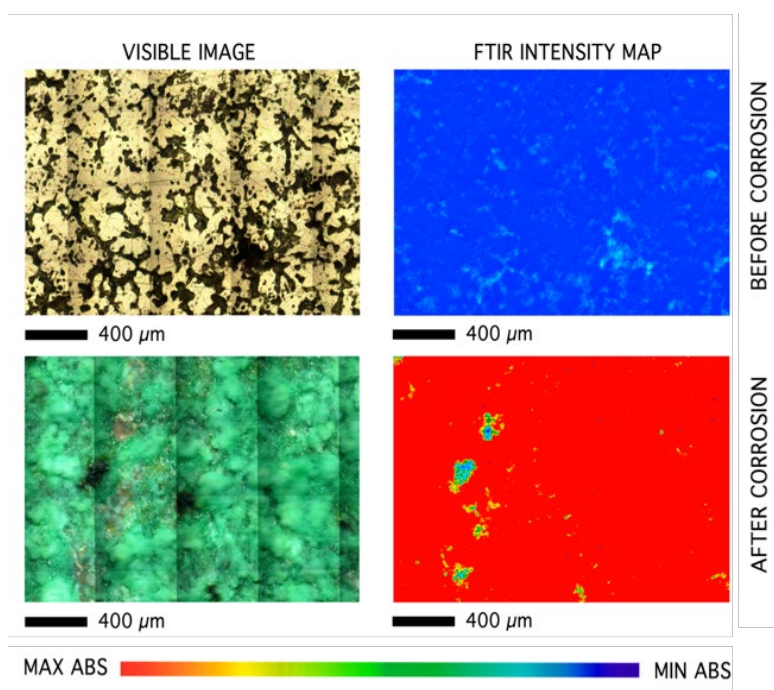
Figure 34. FTIR 2D Imaging of the coin before (top) and after (bottom) artificial aging. Beside each visible map, the corresponding 2D FTIR map shows the intensity, between 3111 and 3679 cm−1, of the hydroxyl stretching bands of hydrated copper(II) hydroxychlorides (e.g. atacamite/clinoatacamite, common copper corrosion products). All maps have dimensions of 1400 × 2100 μm².
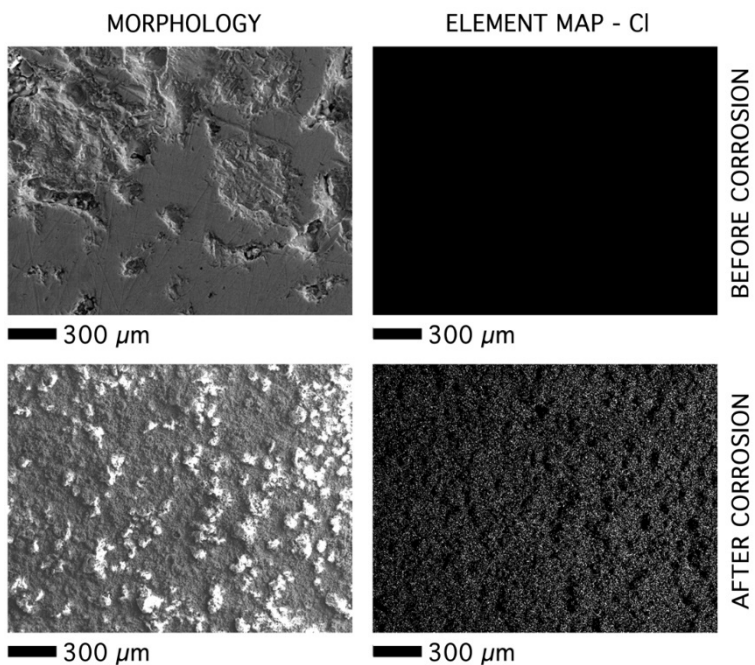
Figure 35. FEG-SEM images vs. energy dispersive X-ray (EDX) maps of elemental Cl, related with the presence of copper(II) hydroxychlorides (corrosion products). Top row: the surface of a bronze mock-up (coin) before accelerated aging. Bottom row: the coin surface after aging.

2.4.3.2.   Cleaning efficacy evaluation

The bronze coin, aged with the corrosion process described above, was treated with the HVPDs loaded with water, EDTA and TEPA Figure 36. The system loaded with water was used on mock-up to observe its peeling action on the surface, while those with EDTA and TEPA was applied on the bronze coin to evaluate the synergistic effect of the chemical and mechanical treatment.

After ten applications, the systems loaded with water and with a small concentration of chelating agents (0.5 M) did not produce an adequate removal of the stubborn corrosion patinas, even though some slight removal was carried out with the TEPA-loaded HVPD. Near to the edge of the coin, the corrosion products were less strongly cohered and adhered, so that the

mechanical action consequent to the removal of the HVPDs was enough to partially detach the patina (Figure 36).

The possibility to upload higher amount of TEPA in the HVPD system, over EDTA, represents a fundamental applicative improvement; complete removal of the patinas, indeed, was obtained using pure TEPA (3% w/w) in the polymeric dispersion.
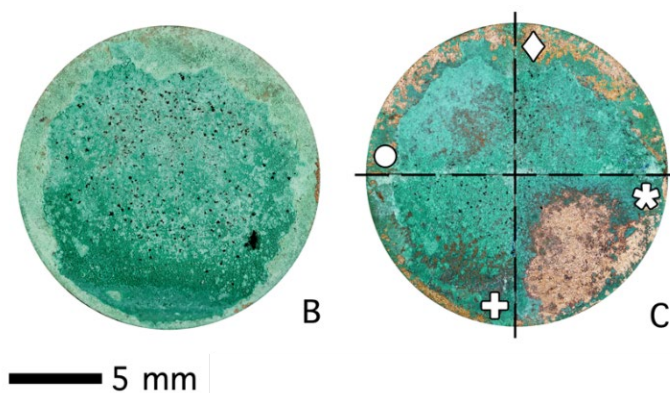
Figure 36. Macro photography of the bronze coin mock-up before (B) and after the application of PVA HVPDs (C) loaded with water (+), TEPA 0.5 M 3% wt (•), EDTA 0.5 M 3% wt (♦), and TEPA 3% wt (*).

During the application, moreover, the strong blue discoloration of the films indicates the formation of the TEPA-copper (II) complex, and such a visual change is advantageous, as it permits to macroscopically follow the solubilization and removal of the corrosion layers from the bronze surface [141].
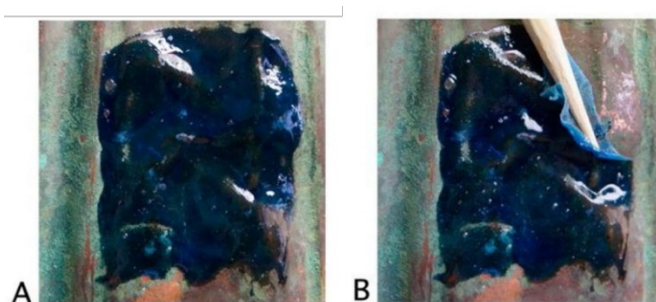
Figure 37. (A) A film of HVPD loaded with TEPA 3% wt lying on a corroded copper surface. The deep blue colour is indicative of the TEPA complexing action. (B) Detail showing the feasible peeling of the film off the surface.

The FTIR reflectance (Figure 38) and the FTIR 2D Imaging (Figure 39) spectra collected on the bronze mock-up after the cleaning procedure show that the bronze metal surface brought back. Besides, no traces of PVA were detected on the treated surface, down to the detection limit of the detector (<1 pg/pixel, 1 pixel = 30.25 μm^2).
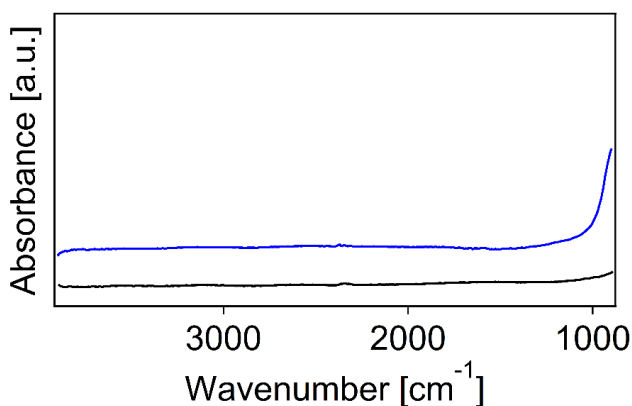
Figure 38. FTIR Reflectance spectra collected on the bronze mock-ups before (black line) and after (blue line) the cleaning process. The reported spectra are offset along y-axis for clarity.
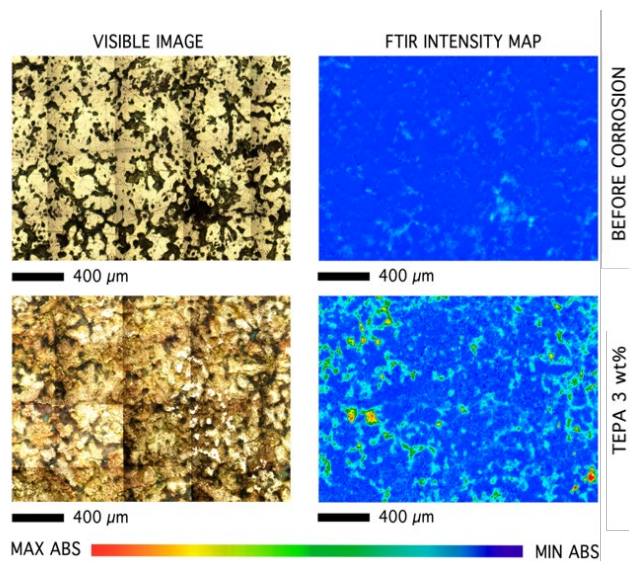
Figure 39. FTIR 2D Imaging of the coin before (top) and after (bottom) cleaning process. Beside each visible map, the corresponding 2D FTIR map shows the intensity, between 3111 and 3679 cm^{-1}, of the hydroxyl stretching bands of hydrated copper(II) hydroxychlorides. All maps have dimensions of 1400 × 2100 μm^2.

SEM-EDX confirmed that chlorine-containing patinas were efficiently removed following the application of the HVPDs loaded with the polyamine solution (Figure 40).
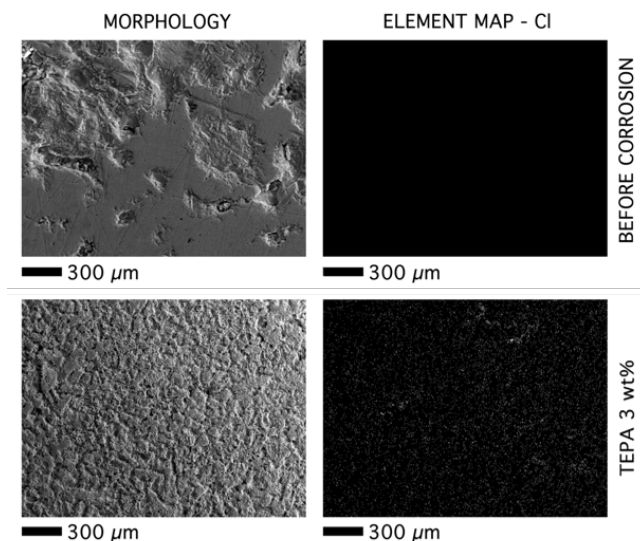
Figure 40. FEG-SEM images vs. energy dispersive X-ray (EDX) maps of elemental Cl, related with the presence of copper(II) hydroxychlorides (corrosion products). Top row: the surface of a bronze mock-up (coin) before accelerated aging. Bottom row: the coin surface after cleaning procedure.

The pHEMA-PVP gels, loaded as specified in Cleaning procedure and evaluation of efficacywere used to remove the corrosion products from the fragile and brittle surface, which was obtained with accelerated aging (see Artificial aging). The system has been chosen thanks to its high ESC and hydrophilicity, that are responsible for an effective cleaning operation [142]. These characteristics make pHEMA/PVP more effective than the pHEMA/PAA semi-IPNs despite the stronger complexing strength of carboxylate groups in PAA with respect to carbonyls in PVP.

After the aging process, a heterogeneous patina of copper oxychlorides was observable on the coin surface (Figure 41); FTIR reflectance spectra (Figure 42) show characteristic IR bands between 3550 and 3300 cm^{-1} (OH stretching) and at 950 cm^{-1} [143]. Gels' application led to the gradual removal of corrosion

products, preserving the inner red cuprite layer [144] irregularly present over the surface.

The cleaning intervention took back the bronze surface in the areas without the cuprite; the whitish patinas of calcium carbonate (characteristic IR bands at 2512, 1793 and 1463 cm^{-1} [145]) may be potentially removed using a complexing agent selective for calcium.

2D FTIR imaging confirmed that using TEPA-loaded system leads to the removal of copper oxychlorides at the micron scale (see Figure 42), down to the detection limit of the instrument (< 1 pg/pixel; 1 pixel = 5.5 x 5.5 μm^2 [64]). It further should be noted that the application of a semi-IPN loaded with EDTA did not produce any corrosion products removal, even after longer time application.
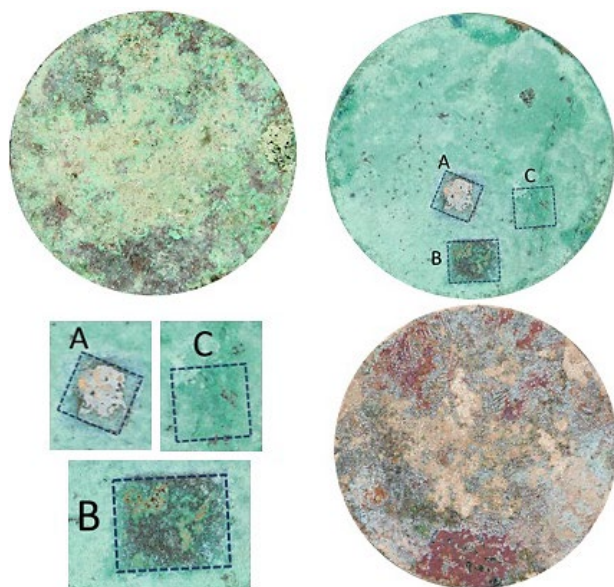
Figure 41. Artificially aged bronze coin before (top left) and after (bottom right) cleaning with semi-IPNs loaded with TEPA. The application of the gels (two cleaning rounds, 45 minutes each) led to the removal of the green corrosion products (copper oxychlorides), preserving the red cuprite layer that is irregularly present on the coin surface. In some portions, whitish patinas composed of calcium carbonate were present beneath the oxychlorides layer. (Top right, bottom left) Preliminary cleaning tests detailing the progressive removal of corrosion products after the application of

semi-IPNs loaded with TEPA for 1 hour (A) or 20 minutes (B). The application of a semi-IPN loaded with EDTA for 1 hour (C) did not remove the corrosion products.
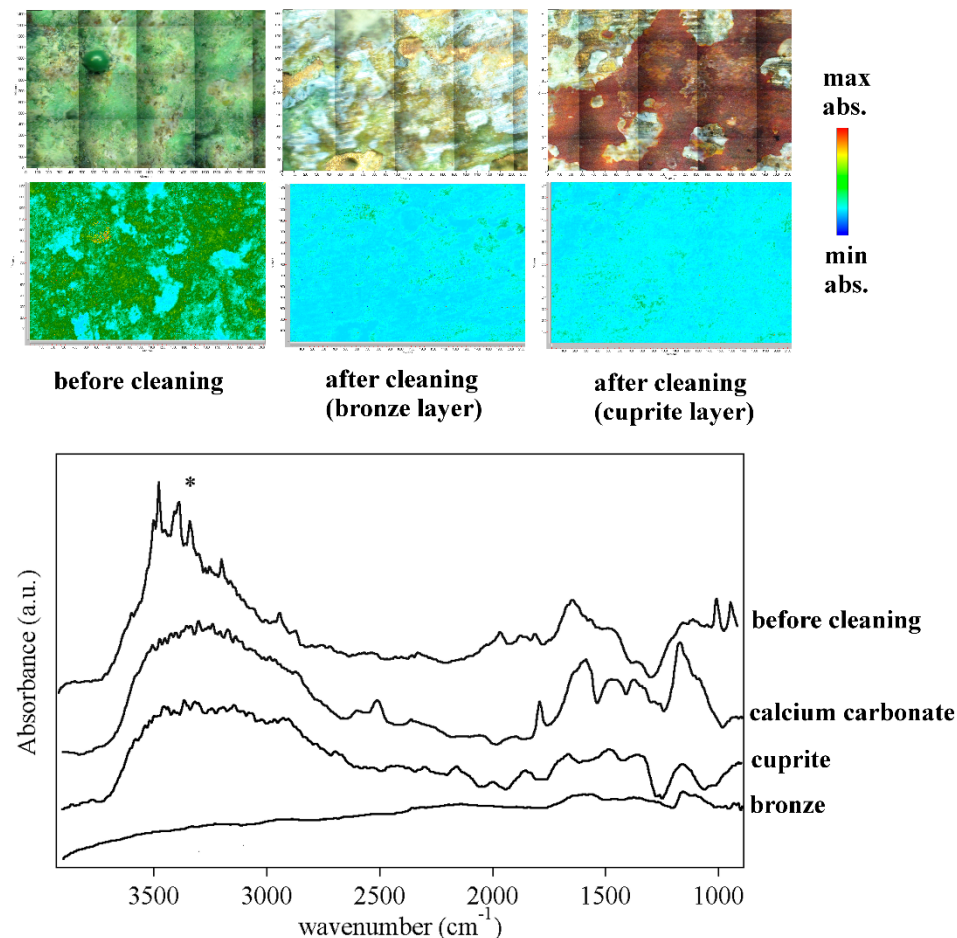
Figure 42. FTIR 2D Imaging of an artificially aged bronze coin before (top, left panel) and after (top, center and right panel) the application of a pHEMA/PVP semi-IPN loaded with TEPA. Below each visible image, the corresponding 2D FTIR Imaging map shows the intensity of the band between 3550 and 3300 cm^{-1} (stretching of OH groups in Cu(II) oxychlorides). All maps have dimensions of 1400 x 2000 μm^2, each axis tick being 50 μm. The bottom panel shows representative spectra of pixels (5.5 x 5.5 μm^2) in the corresponding 2D Imaging maps, from bottom to top: the cleaned bronze surface, the red layer of cuprite, calcium carbonate patinas, and copper oxychlorides (atacamite, paratacamite).

2.4.4.   Applicative test on real case studies

Metallic artworks have their degradation history, which is mainly influenced by the subjected corrosion processes. The effects of these alterations are very different depending on the conditions of conservation and discovery of the object and are very far from those that can be reproduced in the laboratory.

Figure 43. Perseus with the Head of Medusa

For this reason, testing new materials in real cases is extremely important to evaluate the effect of these systems in conservation and restoration practice. During this PhD course, there was the possibility to test the gels and HVPDs systems on several metallic object, different from each other in terms of materials, morphology and storage conditions.

The applicative tests, carried out with several restoration and research institutes, have shown the extreme versatility of these cleaning matrices.

2.4.4.1.   Perseo libera Andromeda by Benvenuto Cellini

HVPDs loaded with TEPA were used to remove corrosion patinas from the 16th Perseus' bronze pedestal made by Benvenuto Cellini. The bas-relief, originally located in the Piazza della Signoria in Florence (Italy) and now kept at the Bargello National Museum of Florence, represents the classic myth of Perseus rescuing Andromeda from a sea-monster (Figure 43)

The greenish bronze degradation products had accumulated through centuries all around the pronounced reliefs and the cavities of the monster's scales, skin, eyes and ears, endangering the artwork's readability (Figure 44). The patinas were stubborn and resistant to EDTA (either confined in the HVPDs or not),

and the only traditional approach left was dry mechanical cleaning, a time-consuming process that needs great care to avoid damaging the bronze layer underneath the corrosion products.

Figure 44. Benvenuto Cellini, Perseo libera Andromeda (Perseus frees Andromeda), 1545-1554, National Museum of Bargello, Florence (Italy): detail of the bas-relief surface before (left) and after (right) cleaning with HVPDs loaded with TEPA**.**

TEPA, uploaded in the HVPDs in different percentages depending on the toughness of the patinas (Figure 45), led to the feasible and controlled removal of the corrosion products, preserving the underlying reddish cuprite (Cu_2O). Usually, conservators wish to maintain the cuprite layer as it passivates the metal against further and recurring corrosion.

A crucial factor that made the intervention feasible was the ability of the HVPDs to penetrate cavities , adhering homogeneously to the surface, and filming into foils that were easily peeled off using tweezers, after solubilization and absorption of the Cu(II) degradation products.
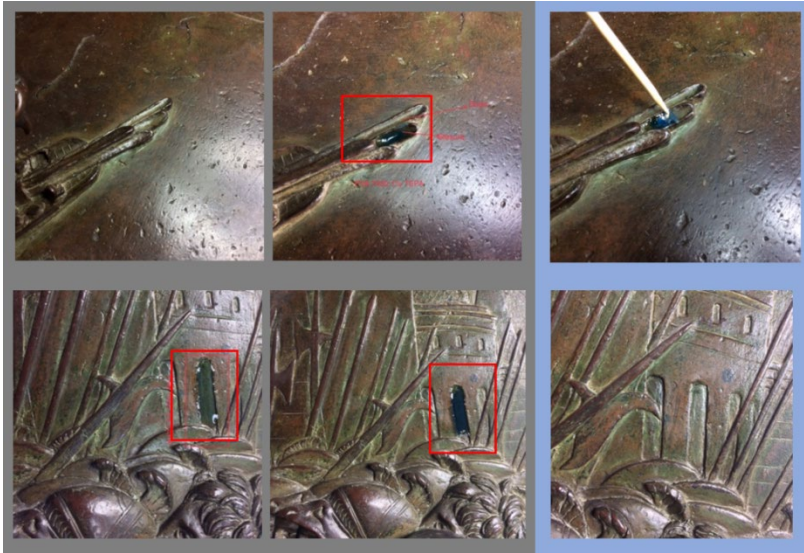
Figure 45. Benvenuto Cellini, Perseo libera Andromeda (Perseus frees Andromeda): detail of the bas-relief surface cleaning with HVPDs loaded with TEPA 1% wt (top) and TEPA 3% wt (bottom).
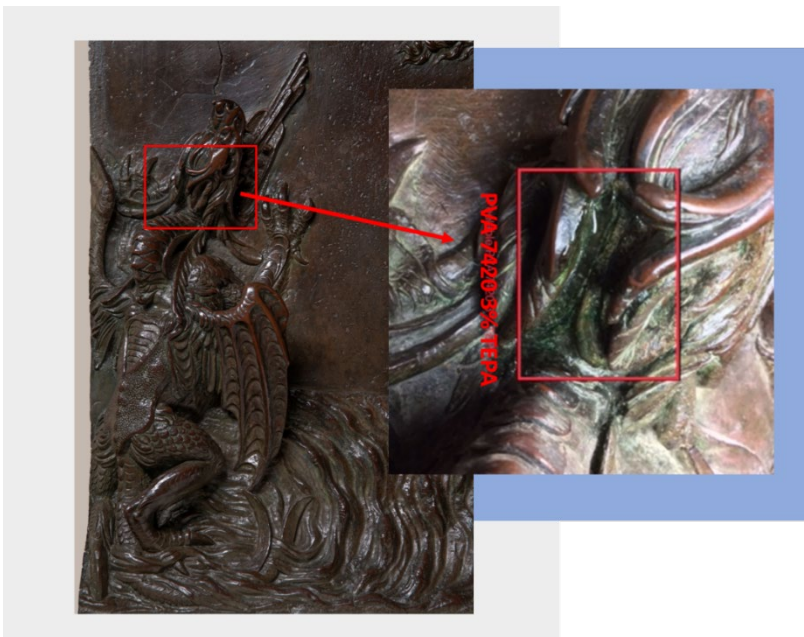
Figure 46. Benvenuto Cellini, Perseo libera Andromeda (Perseus frees Andromeda): detail of the sea monster's head treated with TEPA 3% wt. System adaptability made it possible also the application in hard-to-access cavities.

2.4.4.2.   Donna giacente by Rebeca Matte Bello de Iñiguez

Peelable systems were employed for the restoration of a small bronze statue (75x55x60 cm) portraying a female figure, known as "Donna giacente" (lying woman). This piece, made by Rebeca Matte Bello de Iñiguez in the early 1900s, is kept at Gallery of Modern Art in Pitti Palace (Florence, Italy).

On this artwork were present, as well as the corrosion products, intentional patinas created by the artist. The viscous appearance, which allows the application of the peelable only on the areas actually to be treated, has made it possible to discriminate alterations from intentional coatings [146].

HVPDs loaded with TEPA (1% and 3% w/w) and EDTA were used to treat the corrosion products (chlorine and carbonates) on the bronze surface and also on the iron in contact with copper alloy with good results.

Figure 47. Rebeca Matte Bello de Iñiguez, Militza, 1900, Gallery of Modern Art, Pitti Palece, Florence (Italy): detail of the bronze statue cleaning with HVPDs loaded with TEPA 3% (top), water (center) and EDTA (bottom)

2.4.4.3. Other applicative tests

Applicative tests were executed on several archaeological objects at the Arc'Antique Laboratories in Nantes (France). These applications allow checking the developed cleaning systems on real patina formed during long burial.

Figure 48 shows the results obtained by ten subsequent applications of the HVPDs loaded with TEPA 5% on a gilded bronze leg. It must be noticed that the corrosion layer is so stubborn to completely jeopardize the artefact's readability. In this case, however, it can be observed a thinning of the corrosion products without effects on the gold layer.
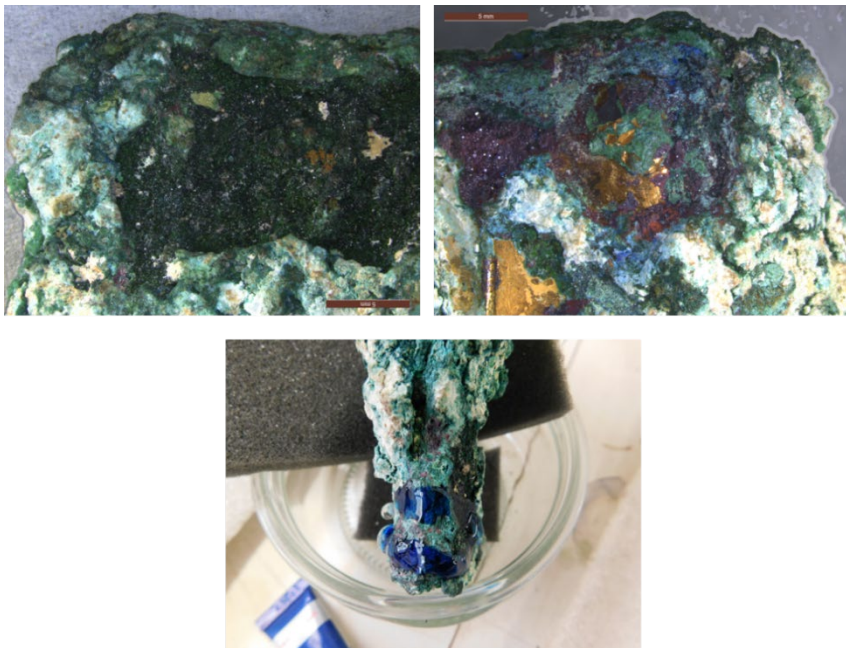
Figure 48. Gilded bronze leg before (top left) and after (top right) the cleaning process with the HVPD loaded with TEPA5%. Bottom figure shows the strong blue discoloration of the HVPD during the application.

Figure 49 shows the results obtained after chemical cleaning obtained with pHEMA/PVP semi-IPN loaded with TEPA 3% solution for one hour. The

gel's application let to the partial solubilization of the copper corrosion products; carbonate clusters, however, were still present on the coin. The corrosion products left on the surface were removed by the conservator with a micro-scalpel under a microscope. In this specific case, the peeling action promoted by the HVPDs would be excessive for the brittle and fragile material. Using the pHEMA/PVP gel loaded with TEPA allowed to thin the corrosion products, without affecting the bronze surface.
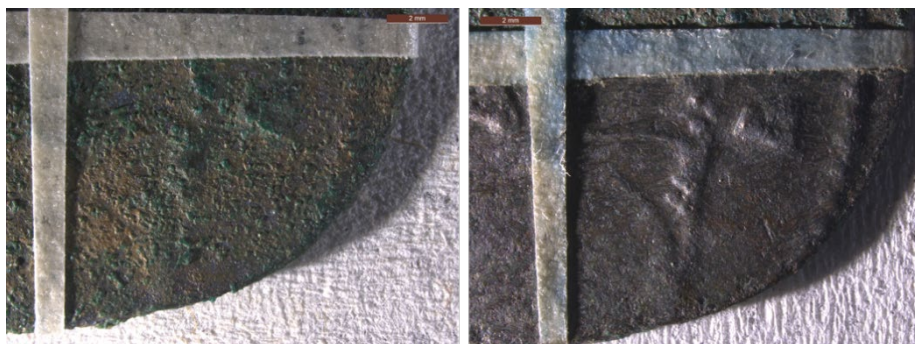
Figure 49. Bronze coin before (left) and after (right) the cleaning process. The treatment was carried out with pHEMA/PVP system loaded with TEPA 3% for one hour, followed by a mechanical cleaning (micro-microscalpel).

To remove copper corrosion products (carbonates and oxides) and $CaCO_3$ patina from a brass bucket kept at the Diocesan Museum of Nantes, HVPDs loaded with TEPA 3% (w/w) and EDTA 0.1 M were used. During the application of the TEPA-loaded HVPDs, a strong blue discoloration indicates the Cu(II) complexes formation (Figure 50 bottom). After the cleaning process the corrosion products were almost completely removed and the red cuprite layer was preserved (Figure 50).

The polymeric dispersions and the pHEMA-based gels loaded with complexing agents presented in this PhD dissertation, were devised for the specific purpose of cleaning copper-based artworks. However, they were tested also over other materials, such as steel and iron.

For the removal of corrosion patinas from iron and steel materials it is necessary to work with an acidic formulation. The high stability of the iron corrosion products (iron oxides and hydroxides) requires an extreme reaction

environment [147], which can be locally maintained through the action of the retentive systems.

Figure 50. Diocesan bucket before (top left) and after (top right) the cleaning procedure. The bottom figure shows the application of the HVPDs loaded with TEPA 3% and EDTA 0.1 M. It must be notice that the viscosity of the systems allows the application also on vertical surfaces.

Chelators used for copper-based alloys (i.e., TEPA and EDTA) have been replaced by citric acid. This chelating agent is already used in the conservation fields and it is compatible with the HVPDs and the semi-IPNs system. Moreover, it is environmentally friendly, economic and has a good effectiveness in a short time.

Before the application on the iron and steel objects, the systems (pHEMA/PVP and HVPDs) were upload with a solution of citric acid (10% w/w), adjusted to pH 2.0 using few drops of concentrated hydrochloric acid (HCl).

The effects of the cleaning process are show in Figure 51 and Figure 52. Following the application of gels and HVPDs, rust and corrosion products are completely removed. The high systems' retention keeps the object surfaces healthy, despite the acidity of the solution.

Figure 51. Iron chalice before (top left) and after (bottom left) the treatment with HVPD loaded with citric acid (10% w/w). Figure on the right shows the results obtained after the application of pHEMA/PVP semi-IPN loaded with the citric acid (10% w/w) solution.
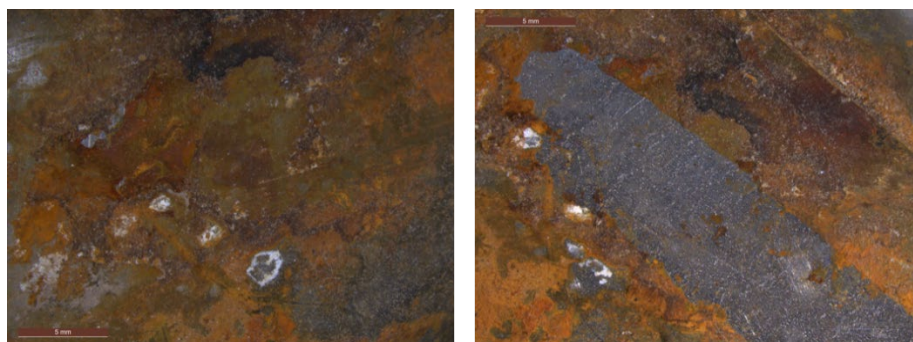
Figure 52. Steel airplane fragment before (left) and after (right) the treatment with HVPD loaded with citric acid (10% w/w).

The retentive systems have also been applied on a decorated tin box; in this case, it was mandatory to remove only the corrosion layers preserving painting colours.

As it is clear from Figure 53 (left), the peeling action of the HVPDs is too strong for an application on a delicate painted surface. The confinement of the same chelating solution inside the pHEMA/PVP semi-IPN makes it possible the gently removal of the rust layer, without damaging the colours (Figure 53 centre). The pHEMA/PVP gels was used as retentive matrix for a solution of TEPA (3% w/w); in this case, the decoration has been partially lost probably due to a varnish solubilization caused by the chelator.

Figure 53. Decorated tin box before (top) and after (bottom) the cleaning procedure. Area treated with the HVPD (left) and pHEMA/PVP semi-IPN (centre) both loaded with citric acid solution (1% w/w). Area treated with pHEMA/PVP semi-IPN loaded with TEPA (3% w/w) (yellow).

2.5. Final remarks

In case of metallic objects, cleaning requires a deep knowledge of the alteration process, especially in case of outdoor monuments, buried or underwater artefacts. The alteration of copper-based alloys cause the formation of overlapping structures, characterized by the presence of cuprite -a Cu(I) oxide- in contact with the metal and by an external layer of Cu(II) salts. Cuprite represents a protective layer against further corrosion; on other hand, the presence of Cu(II) salts is usually considered as a symptom of the so-called "bronze-disease", a particularly dangerous phenomenon occurring when chlorides come into contact with bronze. The removal of these reactive products is necessary to prevent further degradation processes and to improve the chemical-physical stability of metal objects. For this reason, an adequate cleaning procedure should aim to the complete removal of the corrosion products, while preserving the cuprite layer.

A retentive system, able to confine and gradually release a chelating agent, represents a very important innovation in this field; a gel, indeed, can act gently on the surfaces thinning the patina. In this way, it is possible to overcome the limitations imposed by traditional methods, often scarcely selective and risky for the artifacts.

In this work, the potential of pHEMA-based gels as confining tools for chelating solutions, was investigated. First of all, two different hydrogels' formulations were optimized to an application on metallic surfaces. In this regard, PAA and PVP were considered as semi-interpenetrating polymers in the pHEMA network thanks to their properties. In particular, PAA gives strong coordination bonds at high pH and PVP forms stable complexes with metal ions.

The synthetized hydrogels were swollen at different pH and the changes in gels' structure were evaluated by means SEM analysis. Increasing the pH induces changes in the gels' structure. In the case of pHEMA/PAA, gels' structure become more heterogenous, as confirmed by the increase of macroporosity and in the amount of free water uploaded in the gels. This behaviour is probably due to the electrostatic repulsion between PAA chains when carboxyls groups are progressively ionized.

For what concerns pHEMA/PVP semi-IPNs, increasing the pH progressively leads to the partial abstraction of protons from the alcohol group in the enol form of PVP. Significant changes in the macroporosity are observed at each pH variation step (6; 8; 12). Besides, the mesoporosity decreases at high pH values as the inter and intramolecular hydrogen bonds between enol and enolate groups in the PVP chains cause a decrease in the mesh size.

For the same pH values, the interaction of Cu(II) ions with the gel matrix is stronger in the case of pHEMA/PAA, leading to higher amounts of ions absorbed as compared to pHEMA/PVP. In all cases, the uptake process seems to be constituted by a fast initial adsorption step controlled by diffusion of the ions in the network, followed by a second stage controlled by diffusion in smaller pores or adsorption at less available sites. As expected, the contribution of diffusion is more significant in the case of pHEMA/PAA at pH 6, while at higher pH values the deprotonation of carboxyls increases the macro- and mesoporosity, favouring the diffusion of ions.

The removal of copper corrosion products from a real artefact requires the uploading of a chelating agent; in this dissertation TEPA was chose thanks to its high stability constant, that allow to treat also stubborn patinas.

When Cu(II) ions are absorbed in the TEPA-loaded network, ternary PAA-Cu-TEPA complexes are probably formed, where two coordination sites are covered by PAA carboxylates and two by amine groups. The interactions between chelator and carboxyl groups are confirmed by a decrease in the ESC value, which instead remains almost unchanged in the pHEMA/PVP semi-IPNs, because of the high hydrophilicity of these systems.

Even though loading with alkaline solutions of water and TEPA changes the micro- and nanostructure of the gels, it does not hinder their applicability for the removal of corrosion products from bronze surfaces.

Before application on a real artefact, semi-IPNs were tested over bronze mock-ups, provided by ISMN-CNR of Rome (Monterotondo), that reproduce coins covered by an archaeological alteration patina. The samples' surface was characterized by SEM-EDX and micro-FTIR analysis before and after the artificial ageing in order to have a thorough knowledge of the alteration products to remove.

When the TEPA-loaded gels are applied onto corroded bronze coins, they gradually release the polyamine solution on the surface, solubilizing and removing the Cu(II) oxychlorides in the corrosion layers. The dissolved copper ions migrate into the gels and form complexes, which gives the gels an intense blue colour. Despite the stronger complexing strength of carboxylate groups in PAA with respect to carbonyls in PVP, the higher ESC values and the more hydrophilicity makes the pHEMA/PVP gels a better candidate for the removal of corrosion products. This system, indeed, can upload more complexing solution.

The drawbacks related to the use of this systems can be ascribed to their scarce adhesiveness and rigidity, which make them ill-suited to the application on metallic sculptures, often characterized by pronounced cavities and reliefs hardly accessible. A valid alternative in this sense is represented by the PVA-based highly viscous polymeric dispersions (HVPDs), which can perfectly cover also very irregular surfaces thanks to their "honey-like" consistency. After the evaporation of the liquid fraction, the resulting film can be easily removed in one piece. The peeling of the polymeric film, combined with the presence of a selective complexing agent, guarantees excellent results in the cleaning field of metallic artworks.

Starting from these observations, it was decided to uploading TEPA in the HVPDs, in order to boost the removal of corrosion products and improve the cleaning efficacy. Physico-chemical characterization was carried out on the polymeric formulation non-loaded and loaded with TEPA. In particular, two main aspects were investigated: (1) the modification of the systems over time, through gravimetric and rheological measurements and (2) the evaluation of the final films' properties through differential scanning calorimetry (DSC), scanning electron microscopy (SEM) and ATR-FTIR spectroscopy experiments.

Studies on the evaporation kinetics of the volatile fraction, carried out by gravimetric and rheological measurements, showed that the presence of the chelating agent halves the time needed for the film formation and makes more viscous the TEPA-based HVPDs. The information gained by DSC and ATR-FTIR measurements on the obtained films better clarified this behaviour. Respect to the non-loaded, TEPA-loaded systems exhibit a higher crystallinity degree (DC), that can be ascribed to a PVA with a high hydrolysis degree

(DH). This result, also confirmed by the decrease of the peak related to the presence of acetate groups, support the hypothesis which means that the alkaline environment provided by TEPA favours the association of the polymer chains into more ordered structures. As a consequence, the film-forming time is reduced.

The possibility to upload higher quantities of TEPA in the HVPDs, respect to EDTA, enhances the cleaning power also on corrosion patinas, which are resistant to treatments with small concentration of chelating agents.

2D FTIR FPA Imaging confirmed the complete removal of corrosion products, the preservation of cuprite layers and the absence of residues on the surface after the treatment with both semi-IPNs and HVPDs.

During this PhD, there was the opportunity to test the systems over several typologies of metallic substrates. The possibility of adding different chelating agents ensures a chemical cleaning action that can be adjusted depending on the patina composition and morphology. In all cases, the systems allowed recovering the aesthetical look of the artworks.

Conclusions

The removal of unwanted layers - dirt, soil, aged polymers and corrosion products- is one of the most common and, at the same time, controversial action performed on cultural heritage artefacts mainly due to its intrinsic irreversibility. This operation, necessary when phenomena linked to the ageing of the material occur or when the artworks' readability is hind, must be carried out in a selective and non-invasive approach.

Nanostructured fluids (NSFs) -such as micellar solutions or microemulsions- allowed to overcome the drawbacks related to the use of non-confined organic solvents (i.e., scarce selectivity, poor control and high toxicity). In the last decades, several formulations have been developed using different organic solvents and surfactants; these last components have, also, a crucial role in the nanofluids' formulation. For this reason, the research of innovative and highly performing amphiphiles represents one of the main goals in the field of Cultural Heritage conservation, in order to develop safer and greener systems.

Starting from this consideration, the potential and the effectiveness of an innovative surfactant was investigated in comparison with a traditional one, widely used in the conservation field. In the present work, a methoxy-pentadeca(oxyethylene) dodecanoate (MPD) surfactant was used to prepare different NSFs, that have been tested on polymeric layers and soil. To better evaluate the surfactant efficacy, all the experiments were also performed replacing MPD surfactant with its alcohol etoxylate homologue, pentadeca(oxyethylene) dodecyl ether (PDE).

Removal test carried out on the removal of both Paraloid B72 (an acrylic resin, probably the most used polymer in restoration fields) and soil from glass and PS surfaces highlighted better performances of MPD-based NSFs if compared to those with PDE, despite their similar molecular structure. The different phase behaviour in water and the polar head hydration leads to a different excluded volume for the micelles and different effective micellar volume fraction for the two systems. These findings can partially explain the better cleaning action of MPD, especially in low mechanical conditions (i.e., without stirring).

Since the effectiveness of MPD-based NSFs was clearly demonstrated, it has been decided to perform a deepen study about the mechanism that rules the interaction with the unwanted layers to be removed. Also in this case, PDE-based NSFs were chosen as a term of comparison.

Confocal Laser Scanning Microscopy (CLSM) was used to investigate at the micro-scale the interaction mechanism of the NSFs with the PB72 layers. When propylene carbonate (PC) is added in the formulations, a dewetting process is observed, also without surfactant. This result can be attributed to the higher affinity of PC -respect to 2-butanone (MEK)- for the polymer. The presence of surfactants speeds up the whole mechanism; in this sense, MPD has a higher effect. Surface tension measurements clarified this behaviour: MPD shows lower surface tension values respect to PDE. This result, strictly connected to the film's greater tendency to detachment, is in agreement with a kinetically boosted dewetting process for this surfactant. Moreover, CLSM showed better performances of MPD-based micellar solutions also in soil removal. A dewetting-like process, resulting from the coalescence of the oily phase into big droplets after pouring micellar solutions, is boosted by surfactant concentration; 1% surfactant solutions are less effective than 5%, even if micelles are present in both cases. Concurrently, contact angle and SAXS measurements confirmed that MPD-based cleaning fluids are more efficient in weakening and detaching the soil from solid surfaces, without additional mechanical action.

These features make MPD surfactant a good candidate for the formulation of new systems aimed at cleaning of fragile and delicate artworks.

Confining NSFs in retentive matrices represents one of the most powerful strategies to obtain even greater control of the cleaning action; for this purpose, during last years have been developed several gels formulations, addressed to the solution of different cleaning issues on different materials.

In case of metallic objects, and in particular of copper-based metals, the alteration products cause the formation of overlapping structures, characterized by the presence of cuprite -a Cu(I) oxide- at the interface with the metal, and by an external layer of Cu(II) salts. Cuprite represents a protective coating against further corrosion and for this reason, an adequate cleaning operation should aim to preserve it, while removing the corrosion products.

Traditional cleaning procedures usually involve mechanical (vibrating or abrasive tools, ultra-high-pressure water), optical (laser) and/or chemical methods (bases, acids and complexing agents). These approaches, however, are scarcely selective, time-consuming and entail risks for the artifacts. Retentive systems, able to confine and gradually release a high selective chelating agent, represent optimal strategy to achieve controlled removal without risks for the objects.

In this work, two semi-IPNs based on pHEMA were synthetized and their effectiveness in the removal of corrosion patinas from metallic surfaces was investigated. Two different polymers -PAA and PVP- were considered as semi-interpenetrating thanks to their capacity to gives strong coordination bonds at high pH and to forms stable complexes with metal ions. Changes in the gels' structure were evaluated at different pH. The increase of pH and the consequent electrostatic repulsion between the polymeric chains, makes more heterogenous PAA gel structure. This leads to gel with a higher free water content, which is the main responsible for an effective cleaning action, as confirmed by DSC and TGA analysis. Significant changes in the macroporosity were observed also in pHEMA/PVP networks; at high pH values gel structure become more compact, as a result of the enhancement of inter- and intramolecular hydrogen bonds between enol and enolate groups in the PVP chains. The Cu(II) ion adsorption kinetics of pHEMA-based semi-IPNs at different pH values highlighted the effect of the gels' structure and functional groups on the adsorption process, and showed that PAA-based gels can uptake more ions respect to PVP-based gels.

To remove copper corrosion products from a real artefact, loading a chelating agent solution is essential; thanks to its stability constant higher than that of the traditional chelators, TEPA has been chosen as complexing agent to confine inside gel matrices.

After the interaction with copper salts, TEPA-loaded gels show a decrease in the FWI, which can be associated to the formation of complexes. This result confirms that these systems represent promising tools for an application on metallic objects.

Based on its good properties, PHEMA/PVP gel loaded with TEPA was then applied onto an artificially aged bronze coin. The controlled release of TEPA

solution allows the solubilization and removal of the corrosion products from the surface, preserving the protective cuprite layer.

The pHEMA-based gels, classified as "rigid systems", are not suitable for the treatment of bronze sculpture characterized by deep cavities and high reliefs. Thanks to its viscoelastic properties and its ability to combine a chemical action with a mechanical one, a highly viscous polymeric dispersion (HVPD) represents a good option in these cases.

The effect of uploading TEPA in the HVPDs was evaluated through several phyco-chemical investigation techniques. The alkaline environment promoted by this chelator induces the alkaline hydrolysis of acetyl groups in PVA chains; consequently, the viscoelasticity increases and the film-forming time is reduced. The process advances to the formation of a gum in one week, while strongly alkaline solutions of hydroxides yield similar effects in much shorter times (e.g., 1 min). The slower process with TEPA has been attributed to the presence of partially protonated polyamine molecules interacting with acetate ions formed by the alkaline hydrolysis of acetate groups in PVA, which could hinder the association of PVA chains.

Both semi-IPNs and HVPDs loaded with TEPA showed a complete removal of patinas and the preservation of the cuprite layers and from mock-ups and real artefacts. 2D FTIR FPA Imaging confirmed that these systems exhibit an excellent cleaning efficacy, without leaving any residues on the surfaces.

Overall, pHEMA/PAA and pHEMA/PVP semi-IPNs proved to be promising tools for the preservation of archaeological and historical bronze artifacts, while HVPDs are particularly suitable for the treatment of very three-dimensional sculptures.

The different mechanical and viscoelastic properties of the semi-IPNs and HVPDs, combined with the possibility of loading different chelating agents, makes the systems developed during this PhD as effective and reliable materials for the cleaning of metal sculptures.

Future directions might include the use of these systems to remove thick and disfiguring encrustations from archaeological works of art (e.g., ceramics and glazed surfaces), while preserving the so-called "noble" patina, i.e. the compact passive protective layer that forms upon long-term exposure to the environment.

Acknowledgements

List of publications

- Guaragnone T., Poggi G., Chelazzi D., Giorgi R., Baglioni P., **Understanding the Effect of Hydrolysis Degree and Plasticizers Concentration on Drying PVA-systems**, manuscript in preparation

- Guaragnone T., Rossi M., Chelazzi D., Mastrangelo R., Severi M., Fratini E., Baglioni P., **pHEMA/PAA and pHEMA/PVP semi-IPNs: effect of pH and loading with tetraethylenepentamine for the removal of bronze corrosion products**, submitted to Applied Materials and Interfaces, (I.F. 8.758)

- Guaragnone T., Casini A., Chelazzi D., Giorgi R., **PVA-Based peelable systems loaded with tetraethylenepentamine for the removal of corrosion products from bronze**, published on Applied Materials Today, 2020 (IF 8.352) https:// doi.org/10.1016/j.apmt.2019.100549

- Baglioni M., Guaragnone T., Mastrangelo R., Hidetomo Sekine F., Ogura T., Baglioni P., **Nonionic surfactants for the cleaning of works of art- insights on acrylic polymer films dewetting and artificial soil removal**, published on Applied Materials and Interfaces, 2020 (I.F. 8.758) https://doi.org/10.1021/ acsami.0c06425

- Baglioni M., Montis C., Brandi F., Guaragnone T., Meazzini I., Baglioni P. and Berti D**., Dewetting acrylic polymer films with water/propylene carbonate/ surfactant mixtures- Implications for cultural heritage conservation**, published on Physical Chemistry Chemical Physics, 2017 (IF 4.123) https:/ /doi.org/10.1039/C7CP02608K
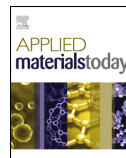
Paper 1

PVA-based peelable films loaded with tetraethylenepentamine for the removal of corrosion products from bronze

Teresa Guaragnone, Andrea Casini, David Chelazzi*, Rodorico Giorgi*

University of Florence, Department of Chemistry "Ugo Schiff" and CSGI, Via della Lastruccia 3, 50019 Sesto Fiorentino, Italy

ARTICLE INFO

ABSTRACT

The removal of corrosion products from bronze artifacts is still an open challenge, in particular when stubborn corrosion patinas are found on surfaces with pronounced cavities and reliefs. Highly viscous polymeric dispersions (HVPDs) of polyvinyl alcohol (PVA) are able to adhere to highly textured 3D surfaces, forming films that can be easily peeled off. Here, PVA-based HVPDs were loaded with tetraethylenepentamine (TEPA), whose copper(II) complex has a stability constant four orders of magnitude higher than that of EDTA tetrasodium salt, traditionally used by conservators for cleaning bronze. TEPA promotes alkaline hydrolysis of acetyl groups in PVA, leading to the association of the polymer chains into more ordered structures, reducing significantly the time needed for the formation of films as compared to HVPDs loaded with water. Besides, the solubility of TEPA in most polar solvents allows to upload higher quantities of chelating agent in the HVPD, as opposed to EDTA. The confinement of TEPA inside the PVA matrix allowed the effective and progressive removal of copper corrosion products from a 16th century Italian bronze masterpiece, preserving the natural cuprite patina of the historical bronze, in times drastically shorter than traditional cleaning methods.

1. Introduction

The preservation of metal artifacts is an open challenge in conservation science, owing to the severe degradation processes (such as the so-called "bronze disease" [1]) that affect metallic sculptures and objects belonging to different artistic productions and ages [2]. In particular, the removal of corrosion patinas from bronze is risky and time-consuming when carried out with traditional methods. Both dry mechanical (brushes, scalpels, chisels) and wet cleaning with non-confined solvents and solutions, are invasive and scarcely controllable, potentially causing damage to the artifacts [3]. Laser ablation can grant fast cleaning action, but can lead to heating processes on the surface [4]. Alternatively, wet cleaning shows enhanced efficacy and non-invasiveness when solvents or solutions are confined in retentive matrices able to gradually release the cleaning fluids on sensitive surfaces. Besides, confined fluids have reduced volatility, which strongly decreases the health issues related to the use of solvents in art conservation [3].

Chemical and physical gels have proved to be optimal confining matrices for cleaning fluids, and in the last decades polymers such as poly(2-hydroxyethyl methacrylate) (pHEMA), polyvinyl pyrrolidone (PVP) and polyvinyl alcohol (PVA) have been employed to formulate systems with ideal mechanical properties and retentiveness [5–9]. In particular, both gels and highly viscous polymeric dispersions (HVPDs) have been widely employed; the first are characterized by the presence of polymer networks physically or chemically cross-linked, with rheological properties that resemble those of solids (e.g. highly viscoelastic, with storage modulus higher than loss modulus over the whole frequency span as measured in oscillatory frequency sweeps [10]). Hydrogels are able to upload aqueous solutions and, to some extent, polar solvents, as opposed to organogels that are used to confine average- or low-polarity solvents [11]. HVPDs comprise polymer dispersions or solutions that do not exhibit the aforementioned rheological behavior and are mainly used as thickeners to limit the diffusion of cleaning fluids. Typically, hydrogels are prepared as sheets with a thickness of few millimeters, whose elasticity can be tuned changing the type of polymer and the synthetic process. These systems allowed the treatment of flat surfaces and contemporary painted layers with 3D texture [12]. However bronze sculptures usually exhibit highly textured surfaces with pronounced cavities and reliefs that are hardly accessible with the aforementioned formulations. PVA-based highly viscous polymeric dispersions (HVPDs) are able to homogeneously cover highly rough surfaces, and after application

Table 1

Composition (w/w %) of the polymer dispersion. ES = loaded with an aqueous solution of EDTA (0.5 M); TS = loaded with an aqueous solution of TEPA (0.5 M); T = loaded with TEPA.

Name	PVA	H$_2$O	EtOH	DPG	MPD	GLY	PEG	EDTA 0.5 M	TEPA 0.5 M	TEPA
PVA	20	57	17	2.5	2.5	0.6	0.4	–	–	–
PVA$_{ES}$	20	54	17	2.5	2.5	0.6	0.4	3	–	–
PVA$_{TS}$	20	54	17	2.5	2.5	0.6	0.4	–	3	–
PVA$_T$	20	54	17	2.5	2.5	0.6	0.4	–	–	3

they can be easily removed in one piece thanks to their viscoelasticity [13]. PVA has excellent chemical stability, biocompatibility, low toxicity and cost, and good film forming properties [14–16]. The characteristics of the films can be tuned by adding solvents and plasticizers to the formulation, for instance ethanol has a structuring effect on water, and thus increases the order of the structure of the polymeric network [9,13]. The adhesion of these films onto the substrate can be such that decohered and detached layers are peeled along with the film. This feature is particularly appealing when treating metal substrates, whose cohesive forces are typically much stronger than those of superficial corrosion layers [17].

Initially, HVPDs formulated for the cleaning of bronze were applied as loaded with an aqueous solution of ethylenediaminetetraacetic acid disodium salt dihydrate (Na$_2$EDTA) [17], a traditional chelating agent widely used for the removal of copper corrosion products [18]. Despite the good stability of EDTA-copper(II) complexes, it is not uncommon to find stubborn corrosion layers that are resistant to treatments with EDTA. Indeed, obtaining a safe, fast and effective removal of degradation products from bronze artifacts is still an open issue in art conservation. A valid alternative to EDTA is represented by tetraethylenepentamine (TEPA), whose copper(II) complex has a stability constant (logK$_f$ = 22.8 at 25 °C) four orders of magnitude higher than that of EDTA tetrasodium salt (Y^{4-}, logK$_f$ = 18.8 at 25 °C) [19]. The use of TEPA, properly confined in retentive matrices, is thus expected to enhance cleaning efficacy, with unprecedented results.

Moreover, EDTA is poorly soluble in ethanol, and it was shown that only limited amounts of Na$_2$EDTA can be uploaded in the water-ethanol blend contained in the PVA-based HVPDs before phase separation occurs [17]. Instead, TEPA has high solubility in most polar solvents [20], which allows the upload of larger quantities of chelating agent in the dispersion, likely boosting the removal of corrosion products.

In this contribution, we formulated PVA-based HVPDs loaded with TEPA, and studied how the presence of the polyamine affects the film forming process and the physico-chemical properties of the films. In fact, diethyleneamines are usually employed as crosslinking agents of PVA, and are expected to modify the interactions among the polymer chains [21]. The HVPDs and the filmed dispersions were characterized through differential scanning calorimetry (DSC), rheological measurements, attenuated total reflectance Fourier transform infrared spectroscopy (ATR-FTIR) and field emission gun scanning electron microscopy (FEG-SEM) coupled with energy-dispersive X-ray analysis (EDX). The HVPDs were then applied onto corroded bronze mock-ups, and the removal of corrosion patinas was checked at the micron scale with 2D Imaging FTIR, using a Focal Plane Array (FPA) detector. Finally, a selected HVPD formulation was used to remove stubborn corrosion layers from a 16th century bronze masterpiece by Benvenuto Cellini.

2. Materials and methods

2.1. Materials

Poly(vinyl alcohol) [PVA] (87–89% hydrolyzed, Mw 85,000–124,000, DP ≈ 2000, cps 23.0–27.0, Aldrich), dipropylene

glycol [DPG] (99%, mixture of isomers, Aldrich), 2-methyl-1,3-propanediol [MPD] (99%, Aldrich), glycerol [GLY] (analytical grade, Merck), polyethylene glycol [PEG] (average Mn 300), ethanol [EtOH] (purity ≥98%, Fluka), ethylenediaminetetraacetic acid disodium salt dihydrate [Na$_2$EDTA] (>99.9%, Aldrich), NH$_4$OH solution (30–33% NH$_3$, Sigma-Aldrich), tetraethylenepentamine [TEPA] (technical grade, Aldrich), hydrochloric acid (37%, Sigma), copper(II) chloride dihydrate (>99.9%, Sigma), sodium chloride (≥99.0%, Aldrich), and sodium hydroxide (98.5%, for analysis, pellets, Acros Organics), were used as purchased. Water was purified by a Millipore MilliRO-6 Milli-Q gradient system (resistivity >18 MΩ cm).

2.2. HVPDs preparation

A polymeric dispersion (20% w/w) was prepared by dissolving PVA powder into purified water at 90 °C for 2 h, in a three-neck flask equipped with a condenser to avoid water evaporation during heating. Once the polymer solubilization was completely achieved, the temperature was decreased to 70 °C and plasticizers (PEG, DPG, MPD, GLY) were added (see Table 1). After 30 min, ethanol was added (17% w/w), and the final system was sonicated for 1 h in pulsed mode at 55 °C until a transparent polymeric dispersion was obtained. The synthesis was carried out under continuous stirring at 150 rpm with a stirring paddle, to reach and maintain the correct homogenization. The pH of the HVPD, measured with an indicator paper, was 6.5 ± 0.5.

2.3. Complexing agents addition

The upload of EDTA was carried out as follows. A 0.5 M EDTA aqueous solution (pH 8.5) was added to the PVA solution under stirring, after the solubilization of PVA and the addition of plasticizers, but before the addition of ethanol, so as to avoid the precipitation of the salt. The EDTA solution corresponds to 3% (w/w) of the total weight of the HVPD (see Table 1); similar concentration values are typically used in the bronze restoration practice [17]. Adding more EDTA solution to the HVPD results in a phase separation and sedimentation of Na$_2$EDTA [17]. The pH was then adjusted to 9 ± 0.5 by addition of few droplets of a concentrated (33%) ammonia solution.

Loading with TEPA was carried out by adding a 0.5 M solution of TEPA (3% w/w) to the HVPD (see Table 1). The final pH was 8.2 ± 0.2. For application onto stubborn corrosion patinas on the real bronze artifact, the loading was carried out by direct addition of TEPA (as received from the supplier) to the polymeric dispersion (3% w/w), and subsequent stirring with a vortex at 2400 rpm, until the amine was completely dissolved. The final pH is strongly alkaline.

It is worth noticing that, even though the volatility and dispersibility (and hence the risk exposure) of fluids is decreased once they are confined in polymeric networks [11], the health and environmental issues involved in the handling and disposal of TEPA-loaded dispersions/films must be considered. The standard safety measures can be adopted for handling these systems (e.g. use of laboratory gloves and goggles), and for their disposal.

2.4. Physico-chemical characterization

Studies of the evaporation kinetics of the volatile fraction (water and ethanol) contained in the HVPDs were carried out by gravimetric measurements. To simulate the process of film formation in real conditions, 0.5 g of each formulation was applied on microscope glass slides and spread with a spatula over an area of 2.5 × 2.5 cm^2 to obtain a thickness of about 0.2 mm. Five samples were prepared for each HVPD system, and one sample for each HVPD type was periodically weighted for 5 h to control the evaporation process at 25 °C and 45% RH. The other 4 slides were let dry in the same conditions until the film could be easily removed with tweezers from the glass without disrupting it or leaving residues. At this point in the evaporation process the films were thus deemed to be peelable. The loss of volatile fraction as a function of time was calculated according to the following equation:

$$W_{vf} = \frac{W_t - W_d}{W_i - W_d} \cdot 100$$

where W_{vf} is the volatile fraction loss, W_t is the weight of the film at given time t, W_d and W_i are, respectively, the final dry weight and the initial weight of the film. Weight measurements were repeated twice.

Changes in viscoelastic behavior as a function of time during drying were investigated by means of oscillatory shear measurements performed on formulations with and without TEPA. Oscillatory tests were performed using a Discovery HR-3 rheometer from TA Instruments equipped with a parallel plate geometry of 25 mm diameter and a Peltier temperature control system (all measurements were carried out at 25.0 ± 1 °C). The gap was adjusted in order to obtain a maximum normal force of 0.9 N. Fluid samples were continuously kept under manual stirring in order to maintain the homogeneity of the systems. Film samples were prepared by pouring 11 g of the polymeric dispersion into a Petri dish, and then the dispersions were equilibrated for 2 days at 25 °C and 55% RH. Frequency sweep measurements were carried out within the linear viscoelastic range (5% strain) determined by previous amplitude sweep tests. The storage (G′) and loss (G″) moduli were measured over the frequency range 0.01–100 Hz.

The thermal properties of the dried films were determined by DSC on a TA Instruments (Q2000) apparatus. The films were cast as specified above, peeled from glass slides, and let dry overnight at room temperature. Then, the films were dried at 40 °C for 48 h in an oven. The films were placed in sealed steel pans and heated with a heating rate of 10 °C/min, under nitrogen flow (50 mL/min). First, an annealing cycle was carried out, heating the films up to 250 °C. Then, the films were cooled to 25 °C and re-heated to 250 °C. Glass transition (T_g) and melting temperatures (T_m) were obtained from the thermal curves after the second heating cycle, and the enthalpy of fusion (ΔH_m) was obtained from the integrated area of the melting peak. Each measurement was repeated 3 times. The degree of crystallinity (DC%) was determined using the equation:

$$DC\% = \frac{\Delta H_m}{\Delta H_{100}} \cdot 100$$

where ΔH_m is the measured melting enthalpy and ΔH_{100} is the melting enthalpy of a completely crystalline PVA ($\Delta H_{100} = 138.6$ J/g) [22].

Morphological features of the HVPD films and of the artificially aged bronze samples were studied by SEM analysis performed using a Field Emission Gun Scanning Electron Microscope SIGMA (FEG-SEM, Carl Zeiss Microscopy GmbH, Germany), using an acceleration potential of 3 kV and a 3.9 mm working distance. Prior to SEM analysis, films were prepared as for the DSC measurements, and metallized with gold using an Agar Scientific Auto Sputter

Coater. The bronze mock-up (coin) was analyzed without gold sputtering.

Elemental analysis was conducted with EDX associated to the SEM apparatus. The X-ray counts were obtained by integrating Kα X-ray peaks using an Oxford Instruments INCA X-act microanalyzer.

ATR-FTIR analysis was carried out on dry films using a Thermo Nicolet Nexus 870 with an MCT detector (Mercury Cadmium Tellurium). The spectra were recorded between 650 cm^{-1} and 4000 cm^{-1}, with a spectral resolution of 4 cm^{-1} and 128 scans for each spectrum.

FTIR analysis on bronze mockups was carried out using a Cary 620–670 FTIR microscope (Agilent Technologies). Measurements were performed using a Focal Plane Array (FPA) 128 × 128 detector, which allows the highest spatial resolution currently available to FTIR microscopes. The spectra were recorded directly on the surface of the samples (corroded bronze mock-ups, or the Au background) in reflectance mode, with open aperture and a spectral resolution of 8 cm^{-1}, acquiring 128 scans for each spectrum. The spectral range was 4000–900 cm^{-1}. The FPA detector was used to perform 2D FTIR imaging. A "single-tile" analysis results in a map of 700 × 700 mm^2 (128 × 128 pixels), and the spatial resolution of each imaging map is 5.5 mm (i.e. each pixel has dimensions of 5.5 × 5.5 mm^2). Multiple tiles were acquired to form mosaics.

2.5. Artificially aged samples

A bronze coin was provided by CNR-ISMN (Rome). The chemical composition mimics that of bronze coins typical of the classic Roman period and was assumed to be a standard for classic bronze artifacts. The composition of the coin is as follows: Cu 92.3 wt%, Sn 7.5 wt%, Pb 0.2 wt% [23]. The coin was treated mechanically with sanding paper to increase its surface roughness, so as to favor the formation and adhesion of degradation products during accelerated aging. The aging protocol for the production of artificial patinas containing copper(II) chlorides was carried out as reported elsewhere [24].

2.6. Cleaning procedure

The HVPDs were applied directly on bronze surfaces, lying down 0.25 g on 20 mm^2. The HVPDs were let dry and film for 1.5 h, and then were peeled off the surface using tweezers. The same application protocol was followed on a real bronze artifact (16th century bronze bas-relief by Benvenuto Cellini).

3. Results and discussion

HVPDs loaded with TEPA appear yellowish and more viscous than transparent dispersions loaded with water. Besides, films cast from TEPA-containing HVPDs seem to have a more pronounced elastic behavior. Gravimetric and rheological measurements quantified the effect of the addition of TEPA on the film-forming process and on the viscoelastic properties of dispersions and films. Fig. 1 shows the loss of volatile fraction, i.e. water and ethanol, over time from HVPDs loaded either with water or with TEPA. In the plots, we marked the points in time when the films are easily peeled off the glass slide surface. Loading with TEPA (0.5 M, 3% w/w) reduces the time needed for the formation of peelable films down to ca. 100 min, i.e. half the time needed when the HVPD is loaded with water (pH 6.5). When film formation occurs, the TEPA-containing system has the highest liquid content, and still contains a liquid fraction after 300 min, when the water-loaded system is completely dry. We ascribed the reduced volatility in the presence of TEPA both to the earlier formation of a surface film that limits evaporation, and to the high boiling point of TEPA (340 °C when pure).
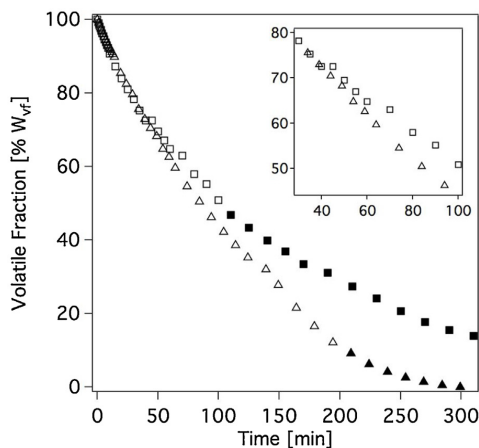
Fig. 1. Loss of volatile fraction (water, ethanol) over time, from PVA-based HVPDs loaded with water (triangles) or TEPA (3% w/w; squares). Full markers indicate the time span, up to 300 min, where films could be easily peeled off the surface in one piece; the first full marker can be thus assumed as the time of film formation. The inset highlights the first 100 min of volatile fraction loss.

Fig. 2. ATR spectra of films cast from PVA-based HVPDs loaded with water (F_{nl}), or loaded with TEPA 3% (F3%). The spectrum of the gum formed ca. 1 week after the addition of TEPA (G3%) is also showed. Moving from F_{nl} to G3% it is possible to observe the appearance of bands at 1643 (N—H deformation of -NH_3^+ groups in the partially protonated TEPA) and 1564 cm^{-1} (carbonyl stretching of acetate ions formed by the alkaline hydrolysis of polyvinyl acetate groups in PVA), and the corresponding disappearance of the acetate C=O stretching peak (1716 cm^{-1}) (see also the inset).

Overall, gravimetric measurements suggest that the high alkalinity of the TEPA solution favors the interactions between PVA chains, resulting in earlier film formation than for water-loaded HVPDs. In fact, Hebeish et al. reported that sodium hydroxide solutions at high pH cause significant hydrolysis of the acetyl groups of PVA, increasing the tendency of PVA molecules to associate, and thus enhancing the viscosity of the PVA dispersions [25]. We verified that, when the HVPDs are loaded with solutions of NaOH (pH 14), they turn into highly elastic, solid-like gums already within one minute, which prevented gravimetric and rheological measurements on those systems. The transformation is thermally irreversible. Such a fast viscosity increase prevents any practical application, as the gums are too rigid and retentive to be used for cleaning purposes. Interestingly, in the presence of TEPA the formation of the gum is much slower (e.g. 1 week) even at high pH values, making the application of TEPA-loaded HVPDs feasible. The HVPD loaded with water at pH 6.5 is stable for long time (e.g. one year) if stored in sealed vials.

The ATR spectra of the films loaded with water show the typical absorptions of poly(vinyl alcohol) at 3300 (—OH stretching), 2934 and 2914 (C—H stretching), 1718 (C=O stretching of the acetate carbonyl group), 1143 and 1088 cm^{-1} (C—O stretching in PVA) [26]. In the spectra of the TEPA-containing HVPDs, the bands at 1643

and 1564 cm^{-1} are assigned respectively to the N—H deformation of —NH_3^+ groups in the partially protonated TEPA molecules [27], and to the carbonyl stretching of acetate ions formed by the alkaline hydrolysis of polyvinyl acetate groups in PVA [28]. The intensity of the carbonyl peak of non-hydrolyzed acetate groups (1718 cm^{-1}) decreases accordingly, and the peak is no longer observable in the spectra of the gum, which show a marked increase of the band of protonated TEPA at 1643 cm^{-1}.

Partly protonated polyamines are able to interact with acetate ions, and the formed ionic couples might hinder (e.g. through steric hindrance) the association of PVA chains, slowing down the process that turns the HVPDs into gums (Fig. 2).

Morphological analysis by SEM showed that the cross-section of the films loaded with water (Fig. 3A) exhibit pores with diameters ranging from 1 to 20 µm, oriented along axes normal to the film surface. The majority of the pores are found in the lower layers, closer to the base surface of the film; instead, towards the upper surface, the film bulk becomes more compact and the pores turn into elongated channels with a section of few microns. This structure could be due to the rapid evaporation rate at the upper surface in the first minutes after the film is cast, leading to the collapse of porous structure closer to the top layers. The presence of micron-sized pores in the lower part of the film is expected to help the migration of dissolved degradation products from the film-patina interface into the
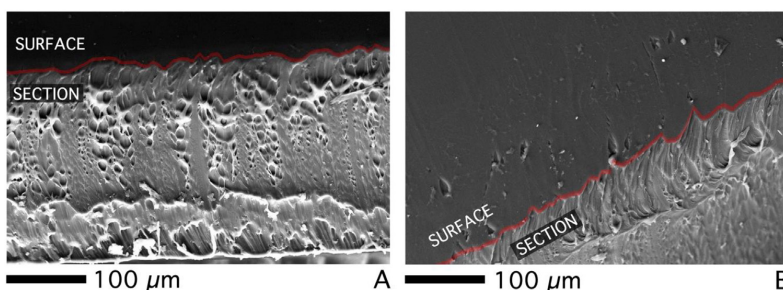
Fig. 3. SEM images of films cast from PVA-based HVPDs loaded with water (A) or with TEPA 3% wt (B). Panel A shows a cross-section of a film, while panel B shows the edge between the upper surface of a film (smooth dark grey area, top left part of the image) and the underlying layers (bottom right portion of the image).
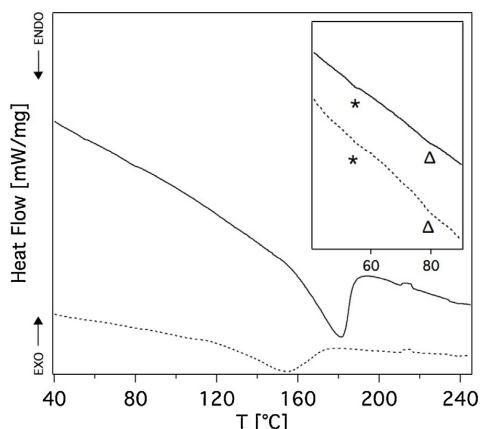
Fig. 4. DSC curves of films cast from PVA-based HVPDs loaded with water (broken line) or with TEPA (3% w/w; full line). The inset highlights the 50–90 °C region, showing the glass transition temperatures of PVA at ca. 55 °C (*) and 80 °C (Δ).

film's bulk, favoring the removal of degradation products. No significant differences were observed in the pore structure of films cast from HVPDs loaded with TEPA, as highlighted in Fig. 3B, where the bottom right portion of the image shows the underlying film layers beneath the surface. The surface of the films is smooth, with no observable porosity (see Fig. 3B, smooth dark grey area in the top left part of the image).

Further information was gained by thermal analysis. The degree of crystallinity of the films loaded with water, in the presence of plasticizers (PEG, DPG, MPD, GLY), is 10.60%, i.e. lower than that of films obtained with the same quantity of PVA (of the same type) simply loaded with water (DC% = 12.80% [29]). As expected, the presence of plasticizers weakens the secondary bonds between the PVA chains, decreasing the crystallinity. However, when TEPA is added to the formulation, the films DC% raises to ca. 15%. Besides, the melting temperature of PVA increases from 155 ± 2 °C to 177 ± 7 °C, closer to the melting of fully hydrolyzed PVA (230 °C [30]). The melting peak becomes narrower, consistently with the crystallinity increase (see Fig. 4). This behavior supports the hypothesis that the hydrolysis of PVA acetyl groups in the alkaline environment provided by the TEPA solution, favors the association of the polymer chains into more ordered structures. The amorphous regions in the films exhibit similar glass transition temperatures (T_g, see inset in Fig. 4) regardless the type of solution loaded (water or TEPA); in both cases two transitions are observed at ca. 55 °C and 80 °C. The first one is the less intense and is close to the T_g of polyvinyl acetate, while the second is assigned to PVA with a low degree of hydrolysis [31].

The rheological behavior of the HVPDs (oscillatory frequency sweeps), is shown in Fig. 5. Essentially, the dispersions initially behave as viscous fluids, with a loss modulus (G") higher than the storage modulus (G') over the whole frequency span. After the dispersions are cast, the film formation process results in an increase of both G' and G", and the cross-over point (i.e. the point in frequency sweeps where the G' and G" curves meet) recedes to lower oscillation frequencies, indicating that the dispersions become more "solid-like" as the films form. When the dispersions are loaded with TEPA, the whole process is faster, in agreement with the information obtained from the other techniques.

In conclusion, based on the physico-chemical characterization discussed in the previous paragraphs, the TEPA-loaded HVPD was deemed as a good candidate for cleaning tests on corroded bronze

mock-ups (coins), before application on a real bronze artifact. Fig. 6 shows the treatment of a bronze coin that exhibits corrosion patinas after accelerated aging. In all cases, ten applications were made for each type of HVPD (i.e. loaded with water, EDTA, or TEPA). In this case, loading the HVPD with low concentrations of chelating agents (0.5 M) did not produce satisfactory removal of the highly stubborn patinas, even though some slight removal was achieved with the TEPA-loaded HVPD as opposed to EDTA. Closer to the border of the coin, the patinas were less strongly adhered and cohered, so that peeling action upon film removal was enough to partially detach them even with the water-loaded dispersion. Complete removal of the patinas was instead obtained using the HVPD loaded with pure TEPA (3% w/w). As a matter of fact, the possibility of uploading higher quantities of chelating agent represents a fundamental applicative advantage of the TEPA-loaded HVPDs over EDTA. It must be noticed that Fig. 6 shows the final cleaning results after all the applications were carried out; however, the removal of the corrosion products was gradual and controllable, which is an important feature in real case studies where patinas need to be progressively thinned to avoid the removal of desired layers (e.g. cuprite [24]).

2D FTIR Imaging with an FPA detector allowed checking the removal of corrosion products down to the micron-scale, with a spatial resolution of 5.5 μm. Before cleaning, the spectra collected on the coin surface show intense hydroxyl stretching bands of hydrated copper(II) hydroxychlorides such as atacamite/clinoatacamite, at 3467, 3339, 3245, and 3154 cm^{-1} [32], as evidenced by the presence of red pixels in the FTIR 2D maps in Fig. 7. These corrosion products are particularly detrimental [33], as they are typically involved in the "bronze disease", a cyclic process that leads to the complete consumption of the metal layers [1]. Less intense bands at 1489, 1461, 1451 and 1385 cm^{-1} are ascribable to the presence of copper carbonates (azurite and malachite) [34]. After the application, the bronze metal surface is brought back (blue pixels in the maps). Besides, no traces of PVA were detected on the treated surface, down to the detection limit of the detector (<1 pg/pixel, 1 pixel = 30.25 μm^2). SEM-EDX confirmed that chlorine-containing patinas were efficiently removed following the application of the HVPDs loaded with the polyamine solution (see Fig. 8).

HVPDs loaded with TEPA (3% w/w) were then used to remove corrosion patinas from a 16th century bronze pedestal by Benvenuto Cellini, belonging to the Bargello National Museum of Florence (Italy). The pedestal is a bas-relief that represents the classic myth of Perseus rescuing Andromeda from a sea-monster. Greenish bronze degradation products had accumulated through centuries all around the three-dimensional figures, and in the cavities of the monster's scales, skin, eyes and ears, jeopardizing the visual aspect of the sculpture (see Fig. 9). The patinas were stubborn and resistant to EDTA (either confined in the HVPDs or not), and the only traditional approach left was dry mechanical cleaning, a time-consuming process that needs great care to avoid damaging the bronze layer underneath the corrosion products. Instead, the application of the HVPDs led to the feasible and controlled removal of the greenish corrosion layers, preserving the underlying reddish layer of cuprite (Cu_2O) [2,24,35] that conservators typically wish to maintain, as it passivates the metal against recurring corrosion. A crucial factor that made the intervention feasible was the ability of the HVPDs to penetrate cavities, adhering homogeneously to the surface, and filming into foils that were easily peeled off using tweezers, after solubilization and absorption of the Cu(II) degradation products. During the application, the strong blue discoloration of the films (see Fig. 9A,B) indicates the formation of the TEPA-copper(II) complex, and such a visual change is advantageous, as it permits to macroscopically follow the solubilization and removal of the corrosion layers from the bronze surface [36]. Overall, the use of the TEPA-loaded HVPDs allowed recovering the aestheti-
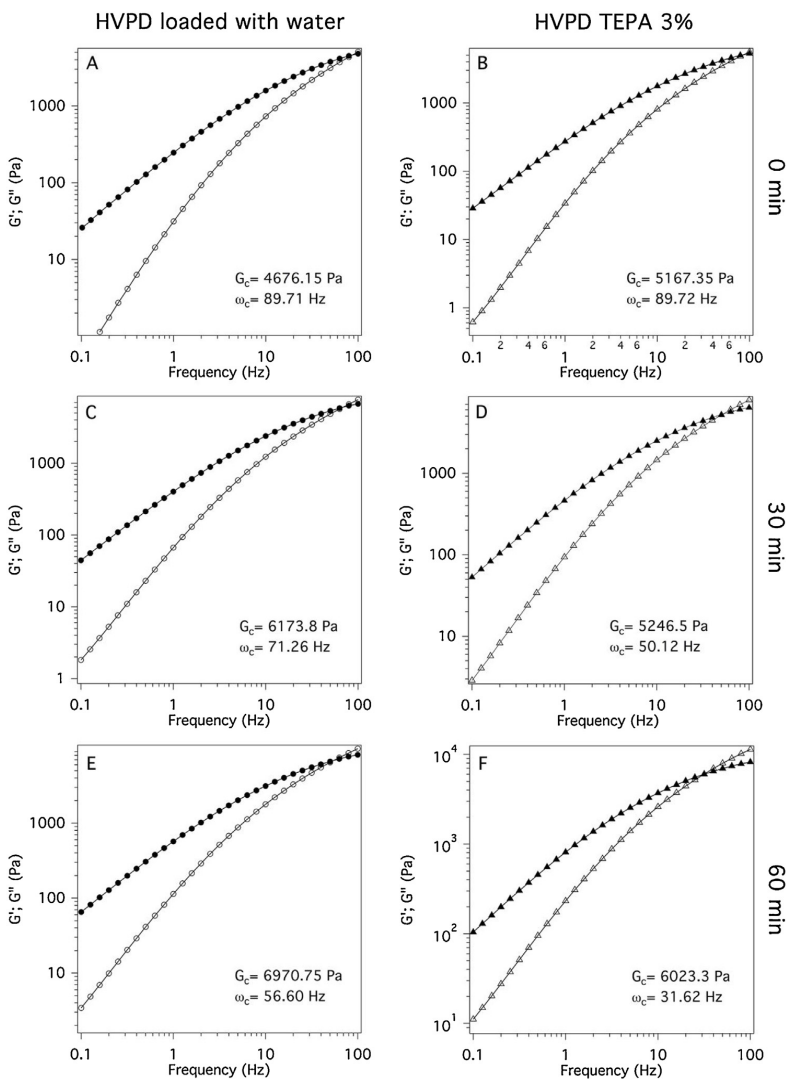
Fig. 5. Frequency sweeps (strain of 5%) of PVA-based HVPDs loaded with water and with TEPA (3 wt %), measured at different times after the films were cast. Open and closed markers represent G' and G", respectively.
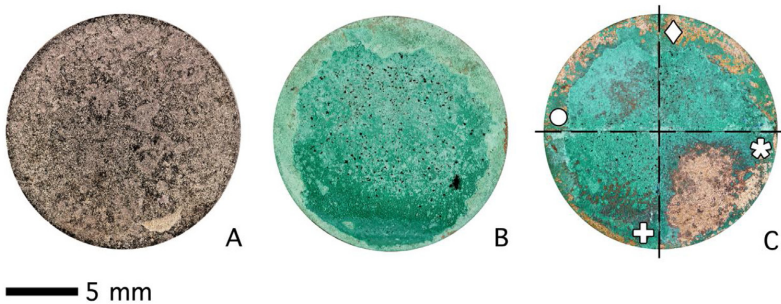
Fig. 6. Macro photography of the bronze coin mock-up before artificial aging (A), after artificial aging (B), and after the application of PVA HVPDs (C) loaded with water (+), TEPA 0.5 M 3% wt (●), EDTA 0.5 M 3% wt (♦), and TEPA 3% wt (*).
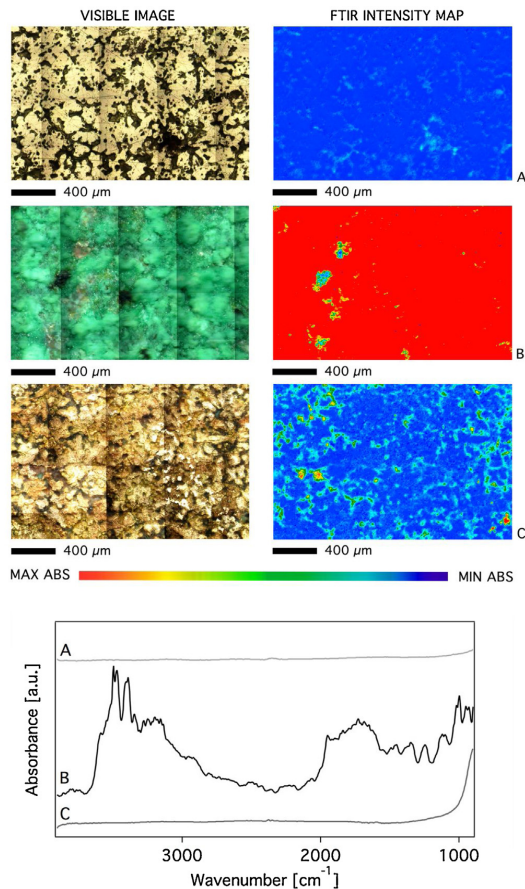
Fig. 7. FTIR 2D Imaging of a bronze mock-up (coin) before artificial aging (A), after artificial aging (B), and after cleaning with an HVPD system loaded with TEPA 3% wt (C). Beside each visible map, the corresponding 2D FTIR map shows the intensity, between 3111 and 3679 cm^{-1}, of the hydroxyl stretching bands of hydrated copper(II) hydroxychlorides (e.g. atacamite/clinoatacamite, common copper corrosion products). All maps have dimensions of 1400×2100 μm^2. The bottom panel shows the FTIR Reflectance spectra corresponding to representative pixels (5.5×5.5 μm^2) of each 2D Imaging map.

cal look of the masterpiece in times dramatically shorter than the conventional restoration practice (days vs. months).

4. Conclusions

TEPA, a strong Cu(II) chelating agent, was confined in PVA-based HVPDs to allow safe and feasible removal of corrosion products from bronze sculptures. The main effect of uploading the polyamine in the polymer network is to induce the alkaline hydrolysis of acetyl groups in PVA chains, which promotes the association of the chains into more ordered structures. As a result, the viscoelasticity of the HVPDs increases significantly, reducing the time needed for film formation, which fulfills the conservator requirements. The process proceeds up to the formation of a highly elastic gum in one week, while strongly alkaline solutions of hydroxides produced similar effects in much shorter time (e.g. 1 min). The slower process with TEPA was ascribed to the presence of polyamine molecules partially protonated and interacting with acetate ions formed by the alkaline hydrolysis of acetate groups in PVA, which might hinder the association of the PVA chains.

The TEPA-loaded HVPDs have a rheological behavior that allows their homogeneous adhesion on highly textured 3D surfaces hardly accessible by rigid gels. The dispersions were used in applications of 1–2 h, which was enough to remove stubborn degradation patinas that had proved resistant to EDTA. The confinement of the chelating agent inside the PVA matrix allowed the effective and progressive removal of the degradation layers (containing copper(II) hydroxychlorides) from a 16th century Italian bronze masterpiece, bringing back the natural cuprite patina of the historical bronze. 2D FTIR FPA Imaging showed that the removal is homogeneous down to the micron scale, and that no PVA residues are left on the surface. In conclusion, these HVPDs formulations candidate as effective and reliable materials for the cleaning of metal sculptures, overcoming the limitations and risks of traditional dry- and wet-cleaning in the restoration practice. Future perspectives might include the use of these systems to remove thick and disfiguring encrustations from archaeological artworks (potentially including also ceramics and glazed surfaces), preserving the so-called "noble" patina, i.e. the compact passive protective layer formed during the long-term exposure to the environment.

MORPHOLOGY   ELEMENT MAP - Cl
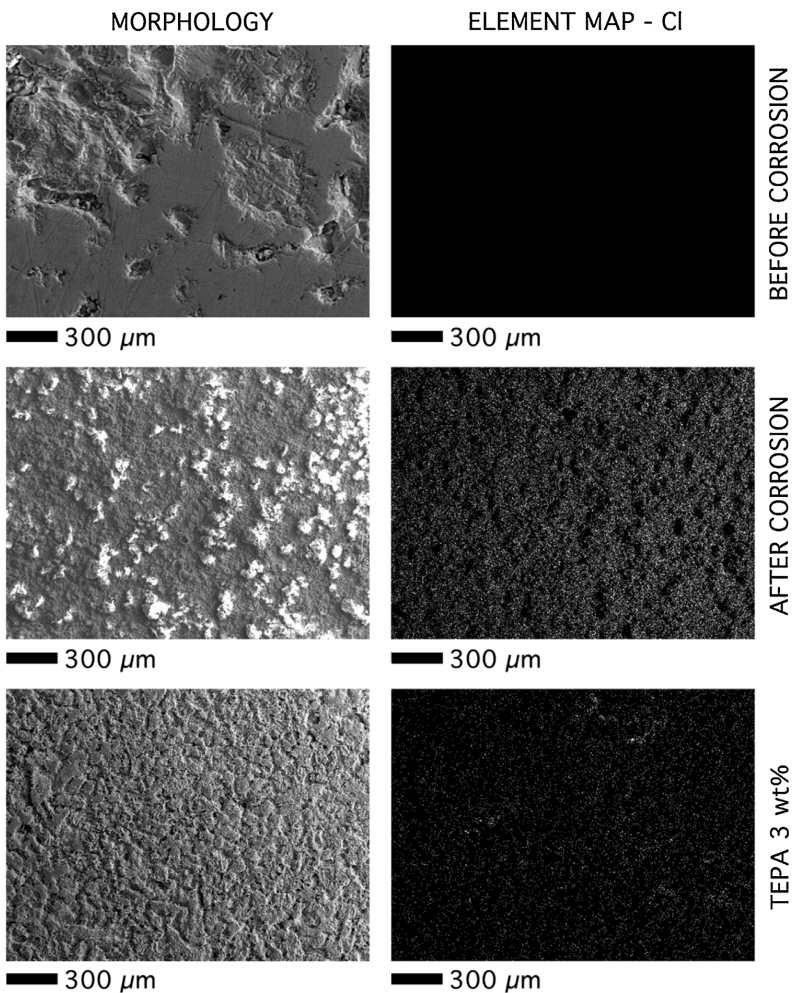
Fig. 8. FEG-SEM images vs. energy dispersive X-ray (EDX) maps of elemental Cl, related with the presence of copper(II) hydroxychlorides (corrosion products). Top row: the surface of a bronze mock-up (coin) before accelerated aging. Center row: the coin surface after aging. Bottom row: the coin surface after removal of corrosion products with an HVPD loaded with TEPA 3% wt.

Fig. 9. (Left Panel) (A) A film of HVPD loaded with TEPA 3% wt lying on a corroded copper surface. The deep blue color is indicative of the TEPA complexing action [36]. (B) Detail showing the feasible peeling of the film off the surface. (Center and Left panels). Benvenuto Cellini, *Perseo libera Andromeda (Perseus frees Andromeda),* 1545-1554, National Museum of Bargello, Florence (IT): detail of the bas-relief surface before and after cleaning with HVPDs loaded with TEPA 3% wt.

Declaration of Competing Interest

CRediT authorship contribution statement

Teresa Guaragnone: Investigation, Methodology, Writing - original draft. **Andrea Casini:** Investigation, Methodology, Writing - original draft. **David Chelazzi:** Investigation, Methodology, Writing - original draft. **Rodorico Giorgi:** Conceptualization, Methodology, Investigation, Supervision.

Acknowledgements

References

[1] D.A. Scott, Bronze disease: a review of some chemical problems and the role of relative humidity, J. Am. Inst. Conserv. 29 (1990) 193–206, http://dx.doi.org/10.1179/019713690806046064.

[2] G.M. Ingo, C. Riccucci, G. Guida, M. Albini, C. Giuliani, G. Di Carlo, Rebuilding of the burial environment from the chemical biography of archeological copper-based artifacts, ACS Omega 4 (2019) 11103–11111, http://dx.doi.org/10.1021/acsomega.9b00569.

[3] P. Baglioni, D. Chelazzi, R. Giorgi, Nanotechnologies in the Conservation of Cultural Heritage, Springer, Netherlands, 2015, http://dx.doi.org/10.1007/978-94-017-9303-2.

[4] C. Fotakis, D. Anglos, V. Zafiropulos, S. Georgiou, V. Tornari, Lasers in the Preservation of Cultural Heritage: Principles and Applications, Taylor & Francis, 2006, http://dx.doi.org/10.1155/2006/7479.

[5] J.A.L. Domingues, N. Bonelli, R. Giorgi, E. Fratini, F. Gorel, P. Baglioni, Innovative hydrogels based on semi-interpenetrating p(HEMA)/PVP networks for the cleaning of water-sensitive cultural heritage artifacts, Langmuir 29 (2013) 2746–2755, http://dx.doi.org/10.1021/la3048664.

[6] N. Bonelli, D. Chelazzi, M. Baglioni, R. Giorgi, P. Baglioni, Confined aqueous media for the cleaning of cultural heritage: innovative gels and amphiphile-based nanofluids, in: Nanosci. Cult. Herit, Atlantis Press, Paris, 2016, pp. 283–311, http://dx.doi.org/10.2991/978-94-6239-198-7.10.

[7] D. Chelazzi, R. Giorgi, P. Baglioni, Microemulsions, micelles, and functional gels: how colloids and soft matter preserve works of art, Angew. Chem. Int. Ed. 57 (2018) 7296–7303, http://dx.doi.org/10.1002/anie.201710711.

[8] P. Baglioni, E. Carretti, D. Chelazzi, Nanomaterials in art conservation, Nat. Nanotechnol. 10 (2015) 287–290, http://dx.doi.org/10.1038/nnano.2015.38.

[9] P. Baglioni, D. Berti, M. Bonini, E. Carretti, L. Dei, E. Fratini, R. Giorgi, Micelle, microemulsions, and gels for the conservation of cultural heritage, Adv. Colloid Interface Sci. 205 (2014) 361–371, http://dx.doi.org/10.1016/J.CIS.2013.09.008.

[10] R. Mastrangelo, C. Montis, N. Bonelli, P. Tempesti, P. Baglioni, Surface cleaning of artworks: structure and dynamics of nanostructured fluids confined in polymeric hydrogel networks, Phys. Chem. Chem. Phys. 19 (2017) 23762–23772, http://dx.doi.org/10.1039/C7CP02662E.

[11] P. Baglioni, N. Bonelli, D. Chelazzi, A. Chevalier, L. Dei, J. Domingues, E. Fratini, R. Giorgi, M. Martin, Organogel formulations for the cleaning of easel paintings, Appl. Phys. A Mater. Sci. Process. 121 (2015) 857–868, http://dx.doi.org/10.1007/s00339-015-9364-0.

[12] N. Bonelli, G. Poggi, D. Chelazzi, R. Giorgi, P. Baglioni, Poly(vinyl alcohol)/poly(vinyl pyrrolidone) hydrogels for the cleaning of art, J. Colloid Interface Sci. 536 (2019) 339–348, http://dx.doi.org/10.1016/J.JCIS.2018.10.025.

[13] I. Natali, E. Carretti, L. Angelova, P. Baglioni, R.G. Weiss, L. Dei, Structural and mechanical properties of "peelable" organoaqueous dispersions with partially hydrolyzed poly(vinyl acetate)-borate networks: applications to cleaning

[14] painted surfaces, Langmuir 27 (2011) 13226–13235, http://dx.doi.org/10.1021/la2015786.

[14] V. Goodship, D. Jacobs, E.O. Ogur, Polyvinyl Alcohol: Materials, Processing and Applications, Smithers Rapra Technology, Shrewsbury, 2005, https://www.worldcat.org/title/polyvinyl-alcohol-materials-processing-and-applications/oclc/765554475. (Accessed 18 September 2019).

[15] C.A. Finch (Ed.), Chemistry and Technology of Water-Soluble Polymers, Springer US, Boston, MA, 1983, http://dx.doi.org/10.1007/978-1-4757-9661-2.

[16] C.M. Hassan, N.A. Peppas, Structure and applications of poly(vinyl alcohol) hydrogels produced by conventional crosslinking or by freezing/thawing methods, in: Biopolym. PVA Hydrogels, Anionic Polym. Nanocomposites, Springer, Berlin Heidelberg, Berlin, Heidelberg, 2000, pp. 37–65, http://dx.doi.org/10.1007/3-540-46414-X.2.

[17] E.I. Parisi, N. Bonelli, R. Giorgi, G.M. Ingo, P. Baglioni, Development of an innovative film-forming cleaning system for the removal of corrosion products from copper alloy artifacts, in: ICOM-CC 18th Triennial Conference Preprints, Copenhagen, 4–8 September, 2017.

[18] H. Burgess, The use of chelating agents in conservation treatments, Pap. Conserv. 15 (1991) 36–44, http://dx.doi.org/10.1080/03094227.1991.9638395.

[19] R.M. Smith, A.E. Martell, Critical Stability Constants: Volume 2: Amines, Springer US, 1975.

[20] N.I. Sax, R.J. Lewis, Hawley's Condensed Chemical Dictionary, Van Nostrand Reinhold, 1987.

[21] M. Abasian, V. Hooshangi, P.N. Moghadam, Synthesis of polyvinyl alcohol hydrogel grafted by modified Fe$_3$O$_4$ nanoparticles: characterization and doxorubicin delivery studies, Iran. Polym. J. (English Ed.) 26 (2017) 313–322, http://dx.doi.org/10.1007/s13726-017-0521-5.

[22] N.A. Peppas, E.W. Merrill, Differential scanning calorimetry of crystallized PVA hydrogels, J. Appl. Polym. Sci. 20 (1976) 1457–1465, http://dx.doi.org/10.1002/app.1976.070200604.

[23] M.P. Casaletto, T. De Caro, G.M. Ingo, C. Riccucci, Production of reference "ancient" Cu-based alloys and their accelerated degradation methods, Appl. Phys. A 83 (2006) 617–622, http://dx.doi.org/10.1007/s00339-006-3545-9.

[24] G. Di Carlo, C. Giuliani, C. Riccucci, M. Pascucci, E. Messina, G. Fierro, M. Lavorgna, G.M. Ingo, Artificial patina formation onto copper-based alloys: chloride and sulphate induced corrosion processes, Appl. Surf. Sci. 421 (2017) 120–127, http://dx.doi.org/10.1016/J.APSUSC.2017.01.080.

[25] A. Hebeish, I.I. Abdel-Gawad, I.K. Basily, S. El-Bazza, Degradation of poly(vinyl alcohol) in strongly alkaline solutions of hydrogen peroxide, J. Appl. Polym. Sci. 30 (1985) 2321–2327, http://dx.doi.org/10.1002/app.1985.070300605.

[26] D. Dibbern-Brunelli, T.D.Z. Atvars, I. Joekes, V.C. Barbosa, Mapping phases of poly(vinyl alcohol) and poly(vinyl acetate) blends by FTIR microspectroscopy and optical fluorescence microscopy, J. Appl. Polym. Sci. 69 (1998) 645–655, http://dx.doi.org/10.1002/(SICI)1097-4628(19980725)69:4<645::AID-APP3>3.0.CO;2-J.

[27] W.C. Wilfong, C.S. Srikanth, S.S.C. Chuang, In situ ATR and DRIFTS studies of the nature of adsorbed CO2 on tetraethylenepentamine films, ACS Appl. Mater. Interfaces 6 (2014) 13617–13626, http://dx.doi.org/10.1021/am5031006.

[28] K. Ito, H.J. Bernstein, The vibrational spectra of the formate, acetate, and oxalate ions, Can. J. Chem. 34 (1956) 170–178, http://dx.doi.org/10.1139/v56-021.

[29] E.I. Parisi, N. Bonelli, E. Carretti, R. Giorgi, G.M. Ingo, P. Baglioni, Film forming PVA-based cleaning system for the removal of corrosion products from Cu-based alloys, Pure Appl. Chem. 90 (3) (2017), http://dx.doi.org/10.1515/pac-2017-0204.

[30] S.Z.D. Cheng, Handbook of Thermal Analysis and Calorimetry: Volume 3: Applications to Polymers and Plastics, Elsevier, 2002.

[31] S. Muppalaneni, H. Omidian, Polyvinyl alcohol in medicine and pharmacy: a perspective, J. Develop. Drugs 02 (2013), http://dx.doi.org/10.4172/2329-6631.1000112.

[32] W. Martens, R.L. Frost, P.A. Williams, Raman and infrared spectroscopic study of the basic copper chloride minerals – implications for the study of the copper and brass corrosion and bronze disease, Neues Jahrb. Für Mineral. - Abhandlungen. 178 (2003) 197–215, http://dx.doi.org/10.1127/0077-7757/2003/0178-0197.

[33] G.M. Ingo, G. Guida, E. Angelini, G. Di Carlo, A. Mezzi, G. Padeletti, Ancient mercury-based plating methods: combined use of surface analytical techniques for the study of manufacturing process and degradation phenomena, Acc. Chem. Res. 46 (2013) 2365–2375, http://dx.doi.org/10.1021/ar300232e.

[34] S. Vahur, A. Teearu, P. Peets, L. Joosu, I. Leito, ATR-FT-IR spectral collection of conservation materials in the extended region of 4000-80 cm^{-1}, Anal. Bioanal. Chem. 408 (2016) 3373–3379, http://dx.doi.org/10.1007/s00216-016-9411-5.

[35] G.M. Ingo, S. Balbi, T. de Caro, I. Fragalà, E. Angelini, G. Bultrini, Combined use of SEM-EDS, OM and XRD for the characterization of corrosion products grown on silver roman coins, Appl. Phys. A 83 (2006) 493–497, http://dx.doi.org/10.1007/s00339-006-3533-0.

[36] P. Pulkkinen, J. Shan, K. Leppänen, A. Känsäkoski, A. Laiho, M. Järn, H. Tenhu, Poly(ethylene imine) and Tetraethylenepentamine as protecting agents for metallic copper nanoparticles, ACS Appl. Mater. Interfaces 1 (2009) 519–525, http://dx.doi.org/10.1021/am800177d.

Paper 2

Nonionic Surfactants for the Cleaning of Works of Art: Insights on Acrylic Polymer Films Dewetting and Artificial Soil Removal

Michele Baglioni, Teresa Guaragnone, Rosangela Mastrangelo, Felipe Hidetomo Sekine, Taku Ogura, and Piero Baglioni*

ACCESS | Metrics & More | Article Recommendations | Supporting Information

ABSTRACT: The use of nanostructured fluids (NSFs), that is, micellar solutions and microemulsions, in art conservation is often associated with cleaning purposes as the removal of polymeric coatings and/or soil from artistic surfaces. In both cases, the use of NSFs grants significant improvements over the use of traditional cleaning techniques that employ neat unconfined organic solvents, water, or aqueous solutions. The study of the nature and properties of surfactants present in NSF formulations is important to boost the effectiveness of these systems in applicative contexts and in the search of innovative and highly performing amphiphiles. This work reports on the methoxy-pentadeca(oxyethylene) dodecanoate (MPD) surfactant in two different NSFs, whose utilization in conservation of cultural heritage is new. Its effectiveness is compared to the conventional nonionic amphiphiles used in conservation practice, as pentadeca(oxyethylene) dodecyl ether, for the cleaning of poly(ethyl methacrylate/methyl acrylate) 70:30, p(EMA/MA), and artificially soiled surfaces. The mechanism, through which NSFs interact with polymeric coatings or soiled surfaces, was investigated by confocal laser scanning microscopy, fluorescence correlation spectroscopy, photographic observation, contact angle, surface tension measurements, and small-angle X-ray scattering. The results highlighted the superior MPD's performance, both in inducing polymer removal and in detaching the soil from coated surfaces. At the microscale, the cleaning involves dewetting-like processes, where the polymer or the soil oily phase is detached from the surface and coalesce into separated droplets. This can be accounted by considering the different surface tensions and the different adsorption mechanisms of MPD with respect to ordinary nonionic surfactants (likely due to the methyl capping of the polar head chain and to the presence of the ester group between the hydrophilic and hydrophobic parts of the MPD surfactant molecule), showing how a tiny change in the surfactant architecture can lead to important differences in the cleaning capacity. Overall, this paper provides a detailed description of the mechanism and the kinetics involved in the NSFs cleaning process, opening new perspectives on simple formulations that are able to target at a specific substance to be removed. This is of utmost importance in the conservation of irreplaceable works of art.

KEYWORDS: methoxy-pentadeca(oxyethylene) dodecanoate, pentadeca(oxyethylene) dodecyl ether, microemulsions, cleaning, conservation of cultural heritage, confocal laser scanning microscopy, fluorescence correlation spectroscopy, small-angle X-ray scattering

POLYMER FILMS DEWETTING   SOIL REMOVAL

1. INTRODUCTION

Nanostructured fluids (NSFs), such as micellar solutions and microemulsions, have been proposed as innovative cleaning systems in the field of conservation of cultural heritage, see Chelazzi et al.,[1] Baglioni et al.,[2] and references there in. Nowadays, they are an important part of the palette of the methodologies commonly used by conservators for the cleaning of works of art.[1−8] NSFs used in art conservation are mostly related to two main cleaning issues: the removal of polymeric coatings[9−11] (protective and consolidating agents, fixatives, adhesives, aged or fresh varnishes, graffiti, over-paintings, etc.) and the removal of soil[1,2,12−14] (dust, particulate matter, grime, oily substances, sebum, wax stains, etc.). This last represents the most common of the
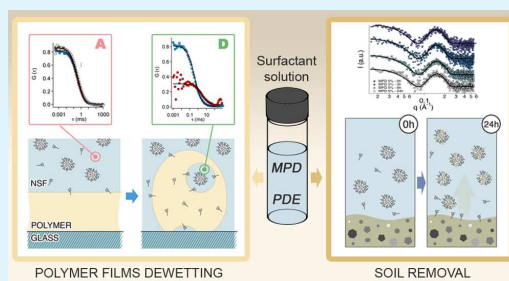
interventions on artworks. In both cases, the use of NSFs grants significant improvements over the use of traditional cleaning methods, that is, the use of neat unconfined organic solvents, water, or aqueous solutions. The synergistic action of organic solvents and surfactants allows excellent cleaning performances, combined with a safe and controlled application. In fact, in a generic NSF, the organic solvent is confined in the

water continuous phase and its amount is reduced to a few percentages, drastically lowering both the environmental impact of the methodology and the health risk for operators. Moreover, compared to unconfined organic solvents, NSFs are particularly effective for the removal of (hydrophobic) polymeric coatings. Different from organic solvents, which are chosen to dissolve a given polymer, NSFs are usually selected to be non-solvents for the polymer, in order to swell the film and detach it from the substrate surface through, depending on the polymer nature, a dewetting process.[15−18] Dewetting is a well-known physical phenomenon defined as the spontaneous withdrawal of a film of fluid (i.e., from low viscosity liquids to highly viscous swollen polymers) from a surface and subsequent rearrangement in the form of separated droplets.[19−24] The dewetting process of polymeric coatings from artistic surfaces induced by NSFs grants that polymer macromolecules are not spread into the work of art, as it would happen with neat unconfined organic solvents, resulting in an effective and controlled cleaning action. The nature of the organic solvents included in the NSF has a major role in the dewetting of polymers from solid surfaces, as they are selected to increase the mobility of polymer chains by swelling the film. Moreover, the surfactant nature is crucial to kinetically favor this process. In fact, the surfactant, lowering the polymer/solid interfacial tension, energetically favors the detachment of the film from the solid surface, and it was shown that a partial detachment of the polymer from the surface represents the first step of dewetting processes.[16−18] Thus, amphiphile-based systems having low interfacial tension may be particularly effective as dewetting agents. Most recently, it was also observed that surfactants too have a role in increasing polymer chains mobility, making them the key components in NSFs for polymer removal.[17,18]

In many cases, works of art do not present polymeric coatings, but their visual aspect is compromised by the presence of soil/grime at the surface. Soil is composed of a variety of usually low molecular weight substances that accumulate on the surface of works of art as a result of ageing, unsuitable storage, or detrimental practices, from previous conservations, and so forth. A wide choice of cleaning methodologies is employed for soil removal, according to the specific needs of the given conservation case, spanning from the use of mechanical methods, to pure water, to the use of aqueous solutions of pH buffers, chelating agents, or surfactants, which may be applied by means of brushes, cotton swabs, poultices, thickeners, physical gels,[25−28] or technologically more advanced solutions, such as highly retentive semi-interpenetrated or twin-chain polymer chemical gels, which grant the safest and most controllable cleaning action.[10,29,30] Among the chemicals used for soil removal, surfactants certainly play a major role, and in particular when they are formulated as micellar solutions or microemulsions constitute the most effective tools available to conservators. Thus, nature and properties of surfactants are important to boost the effectiveness of NSFs in applicative contexts, and the search for innovative and highly performing amphiphiles is one of the main goals in the field of conservation of Cultural Heritage and in many practical applications in cosmetics, detergency, and so forth.

This work reports on the use of a relatively innovative surfactant, a methoxy-pentadeca(oxyethylene) dodecanoate (MPD),[31−35] which is sometimes present in commercial detergents,[36−38] but its cleaning mechanism is poorly under-

stood and its utilization in conservation of cultural heritage is completely new, to the best of our knowledge. In particular, the effectiveness of MPD-based NSFs was studied and compared to the commonly employed PDE ($C_{12}EO_{15}$, pentadeca-(oxyethylene) dodecyl ether)-based NSFs. In order to quantify the mechanism of action and the effectiveness of the cleaning systems, the MPD- and PDE-based NSFs were formulated to solve two conservative challenges: (i) polymer coatings removal and (ii) soil removal. In the first case, the removal of poly(ethyl methacrylate/methyl acrylate) 70:30, p(EMA/MA), commercially known as Paraloid B72, was studied on model systems as polymer-coated glass slides. The interaction mechanism between the polymer film and the cleaning fluid was investigated by means of confocal laser scanning microscopy (CLSM), fluorescence correlation spectroscopy (FCS), dynamic light scattering (DLS), and small-angle X-ray scattering (SAXS). Paraloid B72 is one of the most used polymers in conservation of cultural heritage,[39−42] and it was widely used for a variety of different purposes and on different substrates. MPD- and PDE-based NSFs have been tested for soil removal from glass and polystyrene substrates coated with an artificial soil, prepared following standard procedures available in the literature,[43] and characterized by means of visual and photographic observation, CLSM investigation, contact angle, surface tension measurements, and SAXS. Overall, MPD-NSFs were found to be superior over NSFs based on conventional nonionic surfactants.

2. MATERIALS AND METHODS

2.1. Chemicals. $C_{11}(C=O)EO_{15}-CH_3$, MPD (Nikko Chemicals, assay 99%), $C_{12}EO_{15}$, PDE (Nikko Chemicals, assay +99%), dodecyl dimethyl amine oxide (DDAO, Sigma-Aldrich, 30% aqueous solution), sodium dodecyl sulfate (SDS, Sigma-Aldrich, assay 99%), propylene carbonate (PC, Sigma-Aldrich, assay 99%), 2-butanone (MEK, Sigma-Aldrich, purity 99%), 2-butanol (BuOH, Sigma-Aldrich, assay >99%), ethyl acetate (EtAc, Sigma-Aldrich, ACS Reagents, assay ≥99.5%), and the fluorescent probes used for CLSM experiments, i.e., rhodamine 110 chloride, Nile red, coumarin 6 (Sigma-Aldrich, purity >98−99%), and Bodipy 558/568 C12 (4,4-difluoro-5-(2- thienyl)-4-bora-3a,4a-diaza-s-indacene-3-dodecanoic acid) (Thermo Fisher) were used without further purification. Water was purified with a Millipore Milli-Q gradient system (resistivity >18 MΩ cm). Carbon black, iron oxide (ochre), silica, kaolin, gelatin powder, Japanese paper (9.6 g/m²), poly(ethyl methacrylate/methyl acrylate) [p(EMA/MA)], Paraloid B72, pellets, and cellulose powder (Arbocel BC200, J. Rettenmaier & Sohne, Gmbh) were purchased from Zecchi, Florence. Soluble starch, cement, olive oil, mineral oil, and white spirit were commercially available and thus purchased in non-specialized stores.

2.2. Nanostructured fluids. The experiments reported in this study involved different NSFs. In particular, for the experiments on polymer (Paraloid B72) removal, four different formulations were selected, by combining the two surfactants MPD and PDE with two different organic solvents, PC and MEK, both partly miscible with water, and used as reference solvents in previous studies[16,17] (see Tables S1 and S2). Besides MPD and PDE, an anionic (SDS) and a zwitterionic/cationic (DDAO) surfactant were used as reference amphiphiles.[44] For soil removal experiments, micellar solutions of MPD and PDE were used, at two different surfactant concentrations, that is, 1 and 5% w/w.

2.3. Artificial Soil. The artificial soil mixture was prepared according to the standard formulation available in the literature[43] and detailed in Supporting Information Table S3.

2.4. Sample Preparation. *2.4.1. CLSM Investigation on Polymer/NSF Interaction.* For CLSM experiments on Paraloid B72/NSFs interaction, polymer films of about 2 μm thickness were prepared by spin-coating about 200 μL of a 10% w/w p(EMA/MA)

solution in EtAc on coverglasses (2000 rpm, 120 s). The polymer films were stained with coumarin 6, co-dissolved with the polymer solution.

2.4.2. Polymer Removal Tests on Glass Slides. Weighed 5×5 cm^2 frosted glass slides were coated by drop-casting a 10% w/w p(EMA/MA), Paraloid B72, solution in EtAc, which was let drying until constant weight was reached. The average final amount of p(EMA/MA) on each glass slide was about 80 mg.

2.4.3. CLSM Investigation on Soil/NSF Interaction. For CLSM experiments on soil/NSF interaction, glass slides were coated by drop-casting 150 μL of the artificial soil dispersion stained with Nile red 10^{-6} M, previously dissolved in white spirit. The samples were let completely drying for at least a week and then used for the experiments.

2.4.4. Soil Removal Tests on Glass and Polystyrene Slides. Weighed 5×5 cm^2 frosted glass and polystyrene slides were coated by drop-casting 1 mL of the artificial soil dispersion. The samples were let drying until constant weight was reached, and the final "dry" weight of the soil coating was about 2–3 mg/cm^2, on average.

2.4.5. FCS Investigation on Polymer/NSF Interaction. Paraloid B72 films were labeled by dissolving the hydrophobic dye coumarin 6 in the 10% w/w p(EMA/MA) solution in EtAc, to a final concentration of 1 mM ca. 2 μm thick films were prepared on glass slides through the same spin-coating procedure reported for CLSM experiments. FCS allows the tracking of fluorescent-labeled species diffusing in solution. Thus, the microemulsion droplets in solution were labeled by dissolving Bodipy in the NSFs to a final concentration of 10 nM. Bodipy is an amphiphilic dye with absorption and emission spectra well separated from the ones of coumarin 6.

2.5. Paraloid B72 Removal on Glass Slides. The study of the polymer removal was performed on frosted glass slides, prepared as reported in Section 2.4.2, using cellulose pulp poultices imbibed with the NSFs, and placing a sheet of Japanese paper between the poultices and the polymer film. The poultices were left interacting for 1.5 h, removed, and then the surface was gently rinsed with water to remove possible surfactant residues. After complete drying of the samples, the treated glass slides were weighed to obtain the % of removed polymer.

2.6. Soil Removal Tests on Glass and Polystyrene Slides. Soiled glass and polystyrene slides were immersed for 24 h in 40 mL of the following aqueous micellar solutions: MPD 1%, MPD 5%, PDE 1%, PDE 5% (w/w). During the experiments, the samples were not subjected to any mechanical action. At t = 0, 3, 6, and 24 h, the immersed samples were photographed and the cleaning fluid in contact with the soil layer was sampled by taking small amounts of liquid, which was subsequently investigated by SAXS measurements, in order to follow the possible NSF structural evolution during the interaction with soil. After 24 h, samples were taken out from the NSFs and tilted with care, in order to check for the residual adhesion of the soil coating to the glass/polystyrene surface.

2.7. Confocal Laser Scanning Microscopy. Confocal Microscopy experiments were performed on a Leica TCS SP8 confocal microscope (Leica Microsystems GmbH, Wetzlar, Germany) equipped with a 63× water immersion objective. Rhodamine 110 chloride and coumarin 6 were excited with the 488 nm laser line of an argon laser, while Nile red was excited with a DPSS solid state laser at 561 nm. The emission of the dyes was acquired with two PMTs in the range 498–530 and 571–630 nm, respectively. CLSM experiments were performed to monitor the interaction of the polymer films or soil with different NSFs, as detailed in Section 2.2.

2.7.1. Paraloid B72/NSF Interaction. Unlabeled liquid phase (200 μL) were left in contact with the coumarin 6-stained Paraloid B72-coated coverglass, and the morphological variations of the polymeric film were monitored over time, up to 20 min.

2.7.2. Soil/NSFs Interaction. Liquid phase (200 μL) labeled with rhodamine 110 chloride were left in contact with the Nile red-stained soiled coverglass, and the morphological variations of the soil coating were monitored over time, up to 10 min.

2.8. Contact Angle Measurements. Surfactant adsorption was indirectly evaluated by measuring the contact angle of 5 μL of Milli-Q water droplets on soiled glass slides with a Rame-Hart model 190 CA

Goniometer. Three samples were analyzed, that is, pristine soil-coated glass slide and two soil-coated glass slides immersed for 1 min in a 1% w/w MPD and PDE solution, respectively. The equilibrium contact angle was measured in at least five different areas, and the average value and standard deviation were evaluated.

2.9. Surface Tension Measurements. Surface tension values of MPD and PDE aqueous solutions were determined with a K100 Tensiometer (Krüss, GmbH, Hamburg, Germany). The surface tension was measured at different concentrations by adding a concentrated stock solution of surfactant in water to a known volume of water (40 mL). Surface tension measurements were carried out with a platinum plate, and for each concentration, the average of ten readings was taken after attaining the equilibrium.

2.10. Small-Angle X-ray Scattering. SAXS measurements were performed with a HECUS S3-MICRO SWAXS-camera, equipped with a Hecus System 3 2D-point collimator (min divergence 0.4×0.9 mrad^2), and two position sensitive detectors (PSD-50M) consisting of 1024 channels with a width of 54 μm. The K_α radiation (λ = 1.542 Å) emitted by a Cu anode from the Oxford 50 W microfocus source with customized FOX-3D single-bounce multilayer point focusing optics (Xenocs, Grenoble) was used, while the K_β line was removed using a multilayer filter. The voltage was generated by the GeniX system (Xenocs, Grenoble). The sample-to-detector distance was 26.9 cm. The volume between the sample and the detector was kept under vacuum during the measurements to minimize the scattering from the atmosphere. The camera was calibrated in the small-angle region using silver behenate (d = 58.38 Å). Scattering curves were obtained in the q-range between 0.008 and 0.5 Å^{-1}. The temperature control was set to 25 °C. Samples were contained in 2 mm thick quartz capillary tubes sealed with hot-melting glue. Scattering curves were corrected for the empty capillary contribution considering the relative transmission factors. Desmearing of the SAXS curves was not necessary thanks to the focusing system. The fitting model adopted is described in detail in the Supporting Information file.

2.11. Fluorescence Correlation Spectroscopy. FCS measurements were performed with a Leica TCS SP8 confocal microscope (Leica Microsystems GmbH, Wetzlar, Germany) equipped with a PicoQuant FCS modulus (PicoQuant, Berlin, Germany). A water immersion objective 63×/1.2 W (Zeiss) was used. The evolution of the structure of the fluorescent-labeled film during the interaction with the NSFs was followed by confocal imaging, exciting the green dye coumarin 6 with the 488 nm laser line, and collecting the emitted signal with a PMT in the range 498–530 nm, as reported in the Confocal Laser Scanning Microscopy section. Once the polymer film structure was stabilized (i.e., no fast rearrangements were occurring) the diffusion of Bodipy, located at the microemulsion droplet interfaces, was monitored through FCS. The dye was excited with the DPSS 561 laser (561 nm), while the fluorescence intensity was acquired using a hybrid SMD detector in the 571–630 nm range. Freshly-prepared samples (water/solvents, water/surfactants and the four NSFs labeled with 10 nM Bodipy) were, at first, analyzed before the interaction with the polymer film by pouring the solutions in the appropriate sample-holder (Lab-Tek Chambered #1.0 Borosilicate Coverglass System, Nalge Nunc International, Rochester, NY, USA). Then, 200 μL of the labeled solutions were poured on the polymer-coated glass slides. During the liquid–polymer interaction, different areas were probed through FCS measurements. Depending on the sample, the diffusion of Bodipy was measured either in the liquid-filled cavities formed at the polymer/glass interface (for MEK-based NSFs), or in the cavities found inside the dewetted polymer (for PC-based NSFs), and in the bulk liquid on the top of the polymer film, after 20 min of interaction (for all the systems). Measurements were performed at 25 °C. More details on the data analysis are reported in the Supporting Information file (FCS data analysis).

2.12. Dynamic Light Scattering. DLS measurements were performed on a Brookhaven Instruments apparatus (BI 9000AT correlator and BI 200 SM goniometer) equipped with a EMI 9863B/350 photomultiplier. The 633 nm He-Ne laser was used to avoid light absorption by the Bodipy labeled systems. Measurements on the simple water-surfactant systems and on the NFSs were carried out at
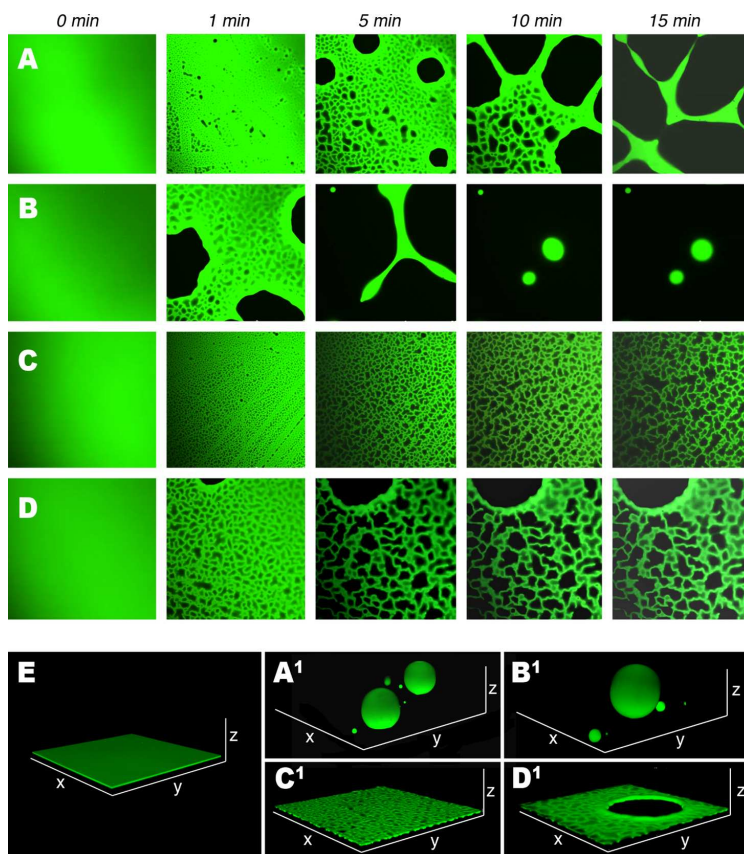
Figure 1. CLSM results on p(EMA/MA) interacting with (A) $H_2O/PC/PDE$, (B) $H_2O/PC/MPD$, (C) $H_2O/MEK/PDE$, and (D) $H_2O/MEK/MPD$. (E) 3D reconstruction of the polymer film before the interaction with NSFs, $(A^1–D^1)$ 3D reconstructions of the polymer after 20 min of interaction with (A^1) $H_2O/PC/PDE$, (B^1) $H_2O/PC/MPD$, (C^1) $H_2O/MEK/PDE$, and (D^1) $H_2O/MEK/MPD$, which clarify the morphology of the film at the end of the experiments. The bottom side of each CLSM frame is 150 μm long.

90 and 25 °C. The signal was collected performing 8 min measurements, and the diffusion coefficients were obtained either from a second-order cumulant analysis or by the weighted average of the values obtained by the CONTIN algorithm.[45] In the second case, the values of diffusion coefficients were obtained as weighted average of the most recurrent components (components accounting for less than 8% of the population were not considered). All data shown are the average of three repetitions, with relative standard deviations.

3. RESULTS AND DISCUSSION

This study focuses on the mechanism and kinetics of MPD cleaning and detergent properties in the context of cultural heritage conservation. As reported above, two main conservative issues are the scope of this study, that is, polymer removal and soil removal. Besides testing the efficacy of proposed NSFs based on MPD surfactant, our aim was to understand the interaction between this surfactant and the materials to be removed because in art conservation the value of the works of art impose very specific, controlled, and performing cleaning, without any possible damage to the original works. To this aim, all the experiments on MPD behavior and performances were compared to those obtained

replacing MPD surfactant with its alcohol ethoxylate homologue, PDE.

Recently, a thorough study by Sato et al.[46] showed that the physico-chemical behaviors of MPD and PDE are significantly different, despite their similar molecular architecture. In particular, phase behavior in water and the polar head hydration are different for the two surfactants. This leads to a different excluded volume for the micelles and different effective micellar volume fraction for the two systems. These findings partly explain the experimental evidence that MPD possesses better cleaning efficiency than PDE, especially in low mechanical conditions, that is, when micellar solutions are kept in contact with soiling materials without stirring. In particular, the removal of oleic acid from fabrics by PDE and MPD micellar solutions was studied by means of several techniques, and it was found that at the equilibrium state both surfactants have almost the same emulsification and solubilization power toward oleic acid, while, before the system is equilibrated, PDE is preferentially adsorbed onto oleic acid coatings in the form of lamellar structures. On the contrary, MPD is less efficiently
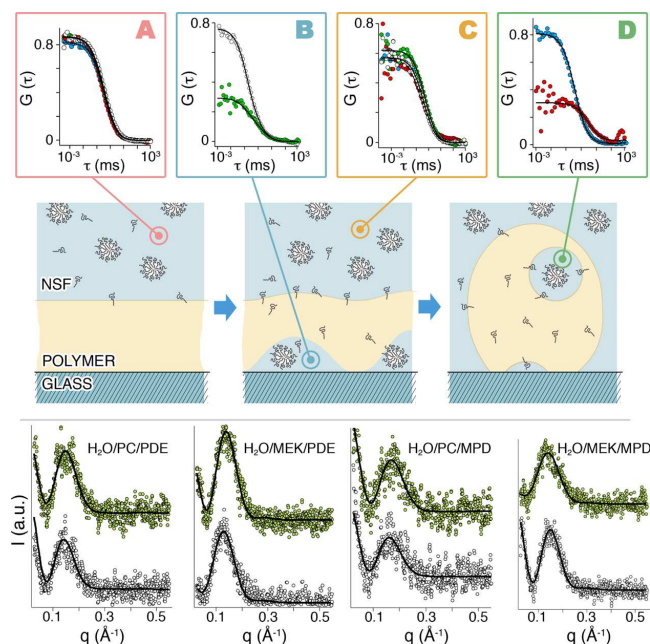
Figure 2. Cartoon illustrates the behavior of the NSFs droplets. After the local detachment of the polymer from the glass surface, the complex fluid droplets penetrate through the polymer and reach liquid-filled cavities. The top boxes report the FCS curves taken at $t = 0$ min (A), at time $t = 5-$ 15 min (B,D) and after 20 min of incubation (C) of the polymer with the four different NSFs; $H_2O/PC/PDE$ (blue circles), $H_2O/PC/MPD$ (red circles), $H_2O/MEK/PDE$ (white circles), and $H_2O/MEK/MPD$ (green circles). The best fittings are shown as solid black lines. (Bottom) SAXS profiles of the four NSFs before (white circles) and after (green circles) 20 min of incubation of interaction with the polymer. The best fittings are shown as solid black lines. The curves have been arbitrarily offset for sake of clarity.

adsorbed onto the soil surface and tends to solubilize the oil in the hydrophobic core of micelles.[47]

3.1. Polymer Film Removal. As already stated, polymer film removal with NSFs usually involves dewetting. From a thermodynamic point of view, the tendency of a film to dewet from a surface is described by the spreading coefficient, S, which accounts for the energetic balance of the system. In the case of a polymer film laid on a glass surface and immersed in a liquid, S is expressed as follows[48]

$$S = \gamma_{LG} - \gamma_{PG} - \gamma_{PL}$$

where γ_{LG} is the interfacial tension between the glass and the liquid, γ_{PG} is the interfacial tension between the glass and the polymer, and γ_{PL} is the interfacial tension between the polymer and the liquid. In total wetting regime ($S > 0$), films are always stable and dewetting does not occur. On the other hand, when a fluid (or a polymer, considered as a fluid in this context) is only partly wetting ($S < 0$), films are unstable or metastable and dewetting is thermodynamically favored below a critical thickness h_c, which for most substances is in the range of millimeters. Even in these last conditions, dewetting does not necessarily take place. In fact, it can be inhibited by a kinetic factor, that is, an energy barrier has to be overcome in order to induce the process. For thin films (thickness, $h < 100$ nm), this energy barrier is usually low and the film is unstable. This instability generates capillary waves through the film, and when their fluctuation exceeds the film thickness h, the film itself spontaneously breaks down into separated droplets according

to a mechanism termed spinodal dewetting.[19] Thick films ($h > 100$ nm), on the other hand, are metastable. A 2 μm-thick hydrophobic polymer film laid on a hydrophilic surface, such as glass, as in the case of the experiments here reported, is a good example of metastable system, where dewetting would be thermodynamically favored but kinetically inhibited because of the low mobility of entangled macromolecular chains in the film. Whenever this mobility is enhanced, the film becomes unstable and dewetting occurs. Enhanced chain mobility can be induced essentially in two distinct ways: (i) the film is heated at a temperature higher than its glass transition temperature, T_g[49] and (ii) the film is exposed to some organic solvents, which swell the polymer, lowering its T_g below room temperature.[22,50] The experiments shown in Figure 1 belong to this latter case. The figure reports the results of CLSM investigation on the interaction of 2 μm thick p(EMA/MA) films, deposited on glass slides, with four different NSFs based on two different organic solvents, PC and MEK, and the two surfactants object of this study, MPD and PDE. PC and MEK were selected as the NSF organic solvents because it was recently found that they show a different behavior in inducing p(EMA/MA) dewetting, and, in particular, PC is more efficient than MEK.[16,17]

The interaction process was monitored at the polymer/glass interface. Figure 1 shows the morphological evolution of continuous polymeric films (visible in green). Upon interacting with the NSFs, some dark areas appear in the confocal plane, meaning that the polymer is no longer present in those areas.

The observation of the film along the z-axis (here not reported) shows that the dark areas are not holes that go through the whole film thickness; instead, they are liquid-filled cavities that form as the polymer is locally detached and lifted from the solid surface. The rims of polymer remaining onto the glass surface draw a characteristic shape termed Voronoi pattern or tessellation.[19] As the cavities grow and coalesce, they become weaker and the film eventually breaks with the nucleation of holes, according to a well-known and described mechanism for the dewetting of thick films,[19] and as the glass is exposed to the bulk liquid phase, the polymer withdraws from the surface in the form of thick rims, which again describe a Voronoi pattern but on a larger scale. Complete dewetting is reached when polymer rims are also disrupted and swollen polymer globular droplets form.

It was found that the two PC-based NSFs are able to completely dewet the polymer from the glass, while in the case of MEK-based NSFs, no complete dewetting was observed after 20 min of interaction (see Figure 1). Interestingly, considering the time for the dewetting onsets for NSFs based on the same solvent (compare the series of Figure 1A,B), MPD is more efficient than PDE in inducing polymer dewetting. After only 5 min, the polymer interacting with the H$_2$O/PC/MPD system is almost completely dewetted, while at the same time, the film interacting with the H$_2$O/PC/PDE system showed just a few 20−30 μm large holes in an otherwise continuous polymer film. The same trend could be observed in the MEK-based systems. Figure 1C,D clearly shows that the interaction process is boosted by the presence of MPD. The difference in the dewetting process can be explained in view of the mechanism through which dewetting takes place in its early stages. When the polymer is locally detached from the solid surface, a portion of the polymer/glass interface is "destroyed", while new interfacial regions are formed between the polymer/liquid and the glass/liquid phases, with an overall increase of the total interfacial area of the system. It was found that the main role of surfactants in this process is reducing the energy costs related to the formation of this intermediate state, by lowering the interfacial tension.[17] Therefore, the interfacial tension of both surfactants was measured over a wide concentration range, from well above the cmc of the surfactants to more than 100 times lower (see Figure S5). It was found that the surface tension of the MPD micellar solution, $\gamma_{MPD} \approx 34.5$ N/m, is lower than that of PDE, $\gamma_{PDE} \approx 37.5$ N/m, which is in agreement with a kinetically boosted dewetting process for this surfactant. In addition, it can be hypothesized that the presence of the methyl capping at the end of the polyoxyethylene chain of MPD confers to this surfactant an increased hydrophobicity and thus a higher capability of penetrating into the p(EMA/MA) film, with a consequent enhancement of polymer chains mobility. Overall, these factors account for the better performances of MPD over PDE.

In order to get a detailed picture of the polymer dewetting process, induced by MPD- and PDE-based NSFs, the diffusion and the evolution of the droplets during the film/liquid interaction were investigated by means of FCS and SAXS measurements. The main results of these experiments are reported in Figure 2.

For confocal experiments, micellar solutions (H$_2$O/PDE 5% and H$_2$O/MPD 5%) were labeled with Bodipy, as described in the Materials and Methods section. In order to determine if the Bodipy dye addition affects the micelles, the diffusion of

micellar species in labeled and unlabeled systems was measured through DLS. The results show that micelles' diameter does not significantly change after labeling (the D values obtained by the cumulant analysis are reported in Table 1).

Table 1. Average Diffusion Coefficients, D (μm^2/s), Obtained by DLS Analysis

system	D (μm^2/s) for unlabeled sample	D (μm^2/s) for Bodipy-labeled sample
H$_2$O/PDE	85 ± 3[a]	81 ± 2[a]
H$_2$O/MPD	88 ± 6[a]	86 ± 3[a]
H$_2$O/MEK/PDE	85 ± 11[b]	87 ± 10[b]
H$_2$O/PC/PDE	72 ± 5[b]	75 ± 15[b]
H$_2$O/MEK/MPD	73 ± 5[a]	87 ± 6[b]
H$_2$O/PC/MPD	77 ± 2[a]	78 ± 2[b]

[a]Values and standard deviations obtained by cumulant analysis. [b]Weighed averages of the most recurrent D values obtained by CONTIN algorithm, with standard deviation.

PC or MEK addition to the unlabeled or labeled micellar systems produces small changes of the micellar diffusion coefficients, indicating that micelle size is only slightly affected. The diffusion coefficients reported in Table 1 were obtained as weighed average of the most recurrent D values obtained from the CONTIN analysis.

The analysis of the light scattering data by the CONTIN algorithm on labeled and unlabeled systems returns an average diffusion coefficient of 80 μm^2/s that was used as "guess value" for the FCS data analysis. SAXS measurements performed on the four NSFs before and after 20 min of interaction with the polymer were also used as an input for FCS analyses. Figure 2 (bottom) shows the fitted scattering profiles of all the investigated samples, while Table 2 reports the main fitting

Table 2. SAXS Fitting Parameters for the NSFs, Measured before and after the Interaction with the p(EMA/MA) Film[a]

system	fitting parameter	before interaction	after 20 min interaction
H$_2$O/MEK/MPD	r_c (Å)	16.2 ± 0.1	15.2 ± 1.6
	t (Å)	15.3 ± 0.4	15.6 ± 3.4
	PDI	0.12 ± 0.01	0.15 ± 0.01
H$_2$O/PC/MPD	r_c (Å)	11.5 ± 0.2	12.0 ± 3.6
	t (Å)	19.7 ± 0.7	17.0 ± 6.5
	PDI	0.15 ± 0.01	0.15 ± 0.01
H$_2$O/MEK/PDE	r_c (Å)	17.3 ± 0.1	16.8 ± 0.8
	t (Å)	16.0 ± 0.5	16.2 ± 1.6
	PDI	0.14 ± 0.01	0.12 ± 0.01
H$_2$O/PC/PDE	r_c (Å)	13.2 ± 0.1	13.8 ± 2.5
	t (Å)	22.1 ± 0.6	18.7 ± 4.7
	PDI	0.15 ± 0.01	0.15 ± 0.01

[a]PDI is the polydispersity index; r_c is the average core radius; t is the shell thickness.

parameters. SAXS analysis shows that the size, shape, and polydispersity are poorly affected by the interaction of MPD and PDE-based NSFs with the Paraloid B72 film, suggesting that up to 20 min of application, the NSFs do not solubilize the p(EMA/MA) polymer film.

The confocal analysis of the cleaning process indicated that dewetting was, as expected, the main process for the polymer

Table 3. Diffusion Coefficient Values ($\mu m^2/s$) and Percentage of D_1 Component in the Total Decay, Obtained Through the Fitting of FCS Curves of MEK-Based NSFs[a]

NSF	D_{bulk} ($t = 0$ min)	D_{cav} ($t = 5$ min)	D_{cav} ($t = 12$ min)	D_{bulk} ($t = 20$ min)
H$_2$O/MEK/PDE	$D_1 = 80$ (40%)	$D_1 = 80$ (80%)	$D_1 = 80$ (80%)	$D_1 = 80$ (40%)
	$D_2 = 17 \pm 2$	$D_2 = 0.4 \pm 0.2$	$D_2 = 6 \pm 2$	$D_2 = 16 \pm 5$
H$_2$O/MEK/MPD	$D_1 = 80$ (50%)	$D_1 = 80$ (70%)	$D_1 = 80$ (60%)	$D_1 = 80$ (50%)
	$D_2 = 17 \pm 3$	$D_2 = 7 \pm 3$	$D_2 = 6 \pm 3$	$D_2 = 6 \pm 2$

[a]FCS was performed into liquid-filled cavities trapped inside the dewetted polymer (Cav) and in the solution on the top of the film D_{bulk}. Error for D_1 component is about 10%.

removal. FCS was used to shed light on the cleaning mechanism in the "dewetting-like" polymer removal. The autocorrelation functions, $G(t)$, obtained by FCS measurements have been analyzed considering two-components decays (see Supporting Information, FCS data analysis) and using as initial guess the parameters obtained from DLS and SAXS data analysis. The diffusion of the Bodipy-labeled NSFs was measured through FCS, before and during the interaction with the polymer film, in different sample regions, as shown in Figure 2. Data on the diffusion of the droplets forming the NSFs disperse phase were collected both inside the liquid-filled cavities that form in the swollen polymer (i.e., at the polymer/glass interface for MEK-based systems, inside the dewetted polymer droplets for PC-based systems), and in the bulk liquid on top of the film, after 20 min of interaction.

The results are shown in Figure 2A−D, and the calculated diffusion coefficient, D, are reported in Tables 3 and 4.

Table 4. Diffusion Coefficient Values ($\mu m^2/s$) and Percentage of D_1 Component in the Total Decay, Obtained through Fitting of FCS Curves of PC-Based NSFs[a]

NSFs with PC	D_{bulk} ($t = 0$ min)	D_{cav} ($t = 10$ min)	D_{bulk} ($t = 20$ min)
H$_2$O/PC/PDE	$D_1 = 80$ (50%)	$D_1 = 33 \pm 2$ (99%)	$D_1 = 80$ (50%)
	$D_2 = 19 \pm 4$	$D_2 = 0.01$	$D_2 = 13 \pm 4$
H$_2$O/PC/MPD	$D_1 = 80$ (60%)	$D_1 = 5 \pm 2$ (90%)	$D_1 = 64 \pm 40$ (40%)
	$D_2 = 18 \pm 4$	$D_2 = 0.1$	$D_2 = 4$

[a]FCS was performed into liquid-filled cavities trapped inside the dewetted polymer (Cav) and in the solution on the top of the film D_{bulk}. Error for D_1 component is about 10%.

The composition and aggregates' size in the bulk MEK-based NSFs remains almost the same before and after the interaction with the polymer film, except for the slow component D_{2-bulk} in the H$_2$O/MEK/MPD system, which decreases after the interaction. However, the most remarkable features of these systems lie in the description of the diffusive behavior of labeled species in the NSF confined into the polymer cavities that form at the polymer/glass interface. The main result is that according to measured diffusion coefficients, NSF droplets are able to penetrate inside these cavities (see D_{1-cav} values in Table 3). Thus, the swollen film is somehow permeable to the passage of either micellized or monomeric surfactant. In fact, data show that the polymer film is more easily penetrated by the smaller droplets, diffusing at 80 $\mu m^2/s$.

The values of D_{2-cav} for both MEK- and PC-based NSFs suggest the presence of micelles/microemulsion droplets—polymer interactions inside the cavities formed at the polymer/glass interface. This can be explained either as diffusion coefficient of NSF droplets being slowed down by the

interaction with the polymer walls of the cavity or as droplet growth due to the solubilization of low-molecular weight polymer chains extracted from the swollen polymer. Apart from this similarity, the two surfactants show a different behavior.

In the case of the H$_2$O/MEK/PDE system, the NSF inside the confined cavities never reaches the diffusion coefficient of bulk NSF on top of the polymer film (i.e., $D_{2-cav} \neq D_{2-bulk}$), suggesting that the interaction with the NFS only slightly alters the polymer film permeability, and the polymer film acts as a sort of "molecular sieve", where only smaller aggregates, probably swollen surfactant micelles, are able to reach the liquid-filled cavities at the polymer/glass interface.

On the other hand, the H$_2$O/MEK/MPD NSF shows an evolution with time, that is, the NSF confined into the cavities at the polymer/glass interface eventually reaches the diffusion coefficient of bulk NSF located above the polymer film. The decrease of D_2 values at $t = 20$ min seems to be mainly ascribable to the extraction and solubilization of low-molecular weight polymer chains into micelles/microemulsion droplets.

The analysis of PC-based NSFs was more complicated in view of the fact that the polymer is completely and relatively quickly dewetted from the glass surface. It was not possible to perform any FCS measurements into the cavities that form at the polymer/glass interface, as they evolved too fast. Conversely, it was possible to measure the diffusion of labeled species inside the liquid-filled cavities that were found trapped into the large droplets of swollen polymer (see the right image of the cartoon in Figure 2), which remain onto the glass surface at the end of the dewetting process.

The H$_2$O/PC/PDE NSF composition before and after the interaction is almost the same. The diffusive species detected inside the cavities are, in part, strongly interacting with the polymer walls ($D_{2-cav} = 0.01$), while the D_{1-cav} value is probably an average of faster and slower diffusing species. In fact, before the rearrangement of the polymer in the form of large droplets, the NSF penetrates the film and is confined in the cavities at the glass/polymer interface, see panel D in Figure 2.

On the other side, the H$_2$O/PC/MPD NSF significantly changes during the interaction with the polymer. Slow-diffusing species can be found both in the cavities confined into dewetted polymer droplets and in the liquid on top of the film. These data confirm that, as in the case of H$_2$O/MEK/MPD, micelles/microemulsion droplets are probably able to extract and dissolve some low-molecular polymer chains present inside the polymer film, and this effect is boosted by the co-presence of both the most effective solvent, PC, and surfactant, MPD.

In conclusion, the different NSFs show different mechanisms that depend both on the organic solvent and surfactant forming the NSF. Considering the obtained results, we challenged the NSFs to the removal of Paraloid B72 polymer
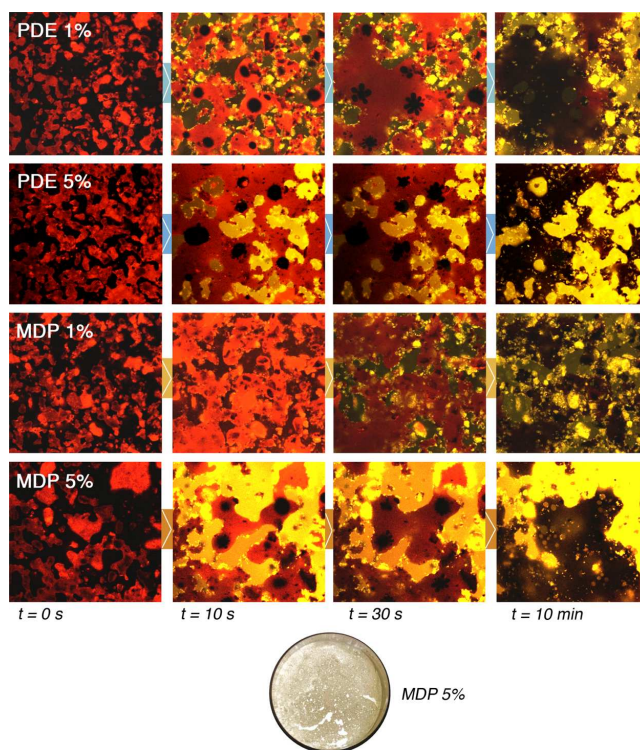
Figure 3. CLSM experiments on soil/NSF interaction. The round picture below the confocal images sequences represents the appearance of the glass incubated for 10 min with the MPD 5% micellar solution. Nile red fluorescence is seen as red; rhodamine 110 chloride fluorescence is seen as green; yellow areas indicate the co-presence of both fluorescent dyes. The bottom side of each CLSM frame is 150 μm long. In the bottom picture, cracks and holes are clearly visible as the result of the MPD 5% NSF action on the soil coating.

films to real cases, that is, thickness of several μm. We compared and quantify the performances of four different NSFs having the same composition (see Table S2, in Supporting Information) but different surfactant. Besides MPD and PDE, two additional surfactants (SDS, DDAO) were selected and used as reference.

Figure S6 in Supporting Information reports the outcome of the cleaning tests with the % of polymer removal obtained via gravimetric measurements. All the selected NSFs resulted highly effective for Paraloid B72 removal from glass slides, yielding an average removal of about 75% of the polymer after a single application of 1.5 h. Some slight differences could be spotted among different NSFs, for example, DDAO is the less effective of the tested surfactants, with a removal of 69 ± 3%, and MPD, with a removal of 78 ± 1%, was the most effective.

3.2. Soil Removal. Soil removal is a very complex subject because of the number of variables mainly linked to the heterogeneous composition of soil. The chemical nature of soiling materials and artworks constituents, the micromorphology of the surface, and possible surface/soil interactions are only some of the factors that might change from one case to another.

In the present study, glass and polystyrene slides were used as specimen for the experiments. They were coated with very thick layers (∼10−20 μm) of artificial soil; this amount of soil is not easily encountered on real artworks surfaces, where the

soil layer is usually less than 1−2 μm thick. Therefore, these experimental conditions have been chosen to amplify possible differences in the behavior of different NSFs involved with the cleaning process. Furthermore, the composition of the artificial soil used in the present work (see Table S3) is very complex, including different materials, ranging from oils (i.e., mixtures of more or less hydrophobic molecules, such as alkanes, fatty acids, fatty acid esters and triglycerides) to more hydrophilic polymeric materials (i.e., gelatin and starch) and to an inert mineral fraction composed of carbon black, iron oxide, kaolin, and silica. This makes the understanding of the interaction process between the NSFs and the soil coating more complex. Most likely, a synergistic combination of concomitant physical phenomena occurs; however, this system is closer to real cases.

Several studies dealing with artificial or real soil removal in the context of conservation of cultural heritage are reported in the literature.[14,51−56] However, to the best of our knowledge, this paper reports for the first time an insight on the interaction mechanism occurring when a surfactant-based NSF is in contact with a soiled surface.

In order to follow the evolution of sample morphology at the glass/soil interface, as reported for CLSM experiments on soil/NSFs interactions (see Section 2.7.2), both the liquid aqueous phase and the soil layer were stained with fluorescent dyes. Figure 3 summarizes the result of an extensive CLSM investigation on several soiled glasses. In the false-colors

images, soil is labeled with Nile red, whose fluorescence is seen as red, while rhodamine 110 chloride fluorescence is seen as green. The yellow areas indicate the co-presence of both fluorescent dyes and label the interaction of surfactant solution with soil. Because of the heterogeneous composition of the soil, the images reported in Figure 3 show patches with different colors, which evolve with time during the cleaning process. Four different 1 and 5% MPD and PDE solutions have been studied. As shown in Figure 3, the interaction of the surfactants with the soil is very fast in the first 30 s to 1 min. After this initial interaction, the soil morphology continues to evolve at slower rate. The appearance of the soil layer at the glass interface at $t = 0$ s shows the presence of several non-contact areas (dark zones), meaning that the adhesion (or wetting) of the soil to glass is not particularly favored, that is, the soil has a poor affinity for the glass slides surface, and in a few seconds, the oily phase present in the soil coalesces and rearranges itself in large droplets, recalling a dewetting-like process. This appears dark in the confocal images at z coordinates close to the glass slides surface. For both 5% MPD and PDE solutions, because of the presence of the dissolved rhodamine 110, the aqueous phase is initially seen as green, and turns to bright yellow when the Nile red, present in the soil layer, interacts (within 10 min of incubation) with rhodamine. At longer time of incubation, the oily phase of the soil is dark brownish because of the depletion in the fluorescent dye, which was initially dispersed in the coating. At the end of the cleaning process, the bright yellow spots unevenly distributed are related to starch and gelatin particles that remain adherent on the glass.

Even if the interpretation of the collected images is not straightforward, it is evident that surfactant concentration plays a major role in determining a displacement of the soil coating, by detaching it from the glass surface. As observed for polymer/NSF interactions, soil detachment from the surface may be regarded as the first key step of the removal process. The process observed for MPD 5% and PDE 5% is similar; however, on average, larger and more continuous soil detachment areas were evidenced in samples incubated with 5% MPD.

The effectiveness of MPD-based NSFs was also compared to PDE-based NSFs on macroscopic soil removal experiments performed on both frosted glass and polystyrene slides. Four NSFs (40 mL) used in CLSM experiments were left for 24 h in contact with the samples. The samples were monitored at 0, 3, 6, and 24 h. Figure 4-top shows that the majority of samples are unaffected by the action of the NSFs having PDE and MPD concentration below 5%. For 5% concentration, the dewetting-like process evidenced in CLSM experiments was clearly observable with the formation of cracks and holes in the originally coherent soil layer. The soil coating on polystyrene slides was adherent to the surface, and only in the case of the sample treated with PDE 5%, a significant (about 40%—see Figure 4-bottom) soil removal was observed. Figure 4-bottom shows that soil removal is proportional to surfactant concentration and that the MPD surfactant is the most efficient removing almost 100% for 5% MPD surfactant concentration in the absence of any mechanical action, see Figure 4-middle. This feature is very important in the conservation field in view of soil removal from the delicate and fragile surface of works of art.

To better clarify the MPD and PDE performances, the contact angle for pure water on soil was measured. The contact
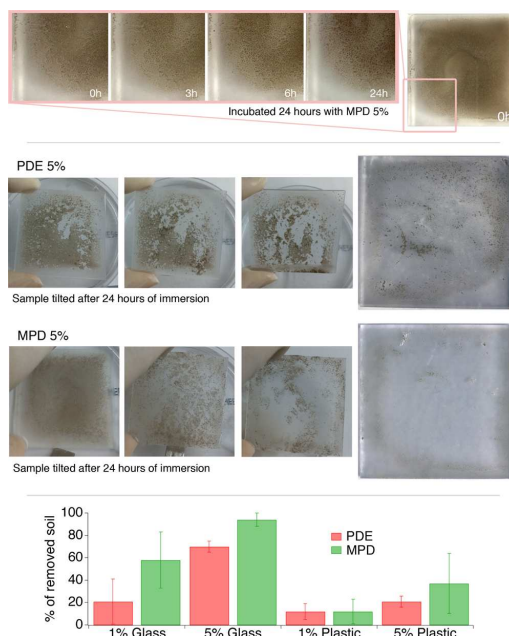
Figure 4. Soil removal experiments on glass slides. (Top) Sequence of zoomed picture taken during the 24 h of immersion of a soiled glass slide in the MPD 5% micellar solution. The dewetting-like process, with the formation of cracks and holes, is clearly visible. (Middle) Glass slides incubated respectively with PDE 5% and MPD 5% micellar solutions were tilted, in order to check for residual soil adhesion to the glass surface. The soil was partially (PDE) or completely (MPD) detached from the glass; the final appearance of treated glass slides is reported. (Bottom) The histogram shows the % of soil removal achieved with the different NSFs on the two different substrates, that is, glass and polystyrene. It is evident that soil removal from polystyrene is incomplete.

angle at the water/soil interface was $52 \pm 8°$. After the artificial soil immersion for 1 min in the two 1% surfactant solutions, the contact angle was 29 ± 1 and $<10°$ for soil incubated with MPD and PDE, respectively. This, contrarily to what can be expected, results in a lower effectiveness of MPD surfactant, when a solubilization process is involved in the cleaning mechanism. SAXS measurements performed on the cleaning fluids samples at 0, 3, 6, and 24 h on glass and polystyrene slides, shed light on the different cleaning mechanism for the two surfactants.

Figure 5 reports the scattering curves of 5% MPD and PDE solutions in contact with soiled glass slides for 24 h. The main fitting results are listed in Table 5, where the volume fraction and the micelles core radius and shell thickness are reported (the description of the fitting model is reported in Supporting Information). According to published data on the effective volume fraction of these two surfactants in water,[46] it was assumed that the volume fraction of both MPD and PDE 5% w/w (at $t = 0$ h) is 0.2 with a 10% uncertainty on this value.

The geometrical parameters obtained from the fitting are in good agreement with previously published SAXS data on these surfactants, where a model-free Fourier-transform approach was used.[46] It is worth noting that the shell thickness is
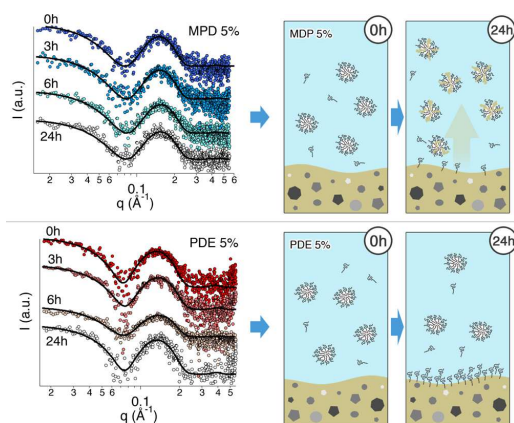
Figure 5. SAXS curves of the MPD 5% and PDE 5% systems, interacting with soiled glass slides. The measurements were performed on samples taken at different times, that is, 0, 3, 6, and 24 h. Solid black lines represent the best fitting curves for experimental data. The curves have been offset for sake of clarity.

significantly high for both surfactants, having MPD micelles a smaller shell, in agreement with literature data,[46] that report a lower hydration number for the polar head of MPD because of the methyl capping at the end of the polyoxyethylene chain. The results obtained for MPD and PDE micellar solutions in contact with the soil layer show a different behavior for the two surfactants. For both surfactants, micelles' size is almost constant, while the volume fraction significantly changes. For the 5% MPD solution, the volume fraction of scattering particles starts to increase after 6 h of interaction with the soil layer, and after 24 h, it is about 80% larger than its original value. SAXS data show that micelles do not grow indicating that the solubilization into the micelles of hydrophobic components from the soil layer occurs with a subsequent reorganization of the micellar structure. In other words, the solubilization of soil leads to a higher number of micelles with oil molecules replacing the surfactant, with the resulting effect of the presence of aggregates with similar size of the original micelles but with a different number (see the top cartoon in Figure 5).

Considering the composition of the artificial soil, see Table S3, it can be assumed that main soil components solubilized in the micelles come from mineral oil and olive oil. The mineral oil present in the artificial soil is mainly composed of saturated linear $C_{15}-C_{50}$ hydrocarbons, while the main component of olive oil is glyceryl trioleate[57] or triolein, a bulky and high molecular weight triglyceride. Several studies in the literature, about the solubilization of hydrophobic substances by nonionic surfactants' micelles,[57−61] are consistent with the interaction mechanism between MPD micelles and the soil. In particular, Kralchevsky et al. proposed a mechanism for the solubilization of triolein into nonionic micelles, where a direct interaction of the surfactant micelles with the interface, accompanied by an uptake of oil, occurs.[61] Interestingly, they found that after triolein solubilization, the rod-like micelles did not swell but rather they split into several smaller micelles, undergoing a structural reorganization,[61] similarly to the SAXS results of the present study. Interestingly, 5% PDE solution shows the opposite trend for the volume fraction of scattering objects. In fact, after an initial slight size increase, the volume fraction decreases and after 24 h is about 25% less than its original value. Therefore, at the end of the process, a number of micelles had disappeared because of surfactant depletion from the aqueous phase as a consequence of significant PDE adsorption on the soil surface (see the bottom cartoon in Figure 5). These results clearly account for the higher effectiveness of MPD in removing the soil from glass surfaces, even in the absence of any mechanical action.

SAXS from 5% MPD and PDE aqueous solutions interacting with soil layers on polystyrene slides shows a different behavior with respect to glass slides, which is mainly due to the different hydrophilic character of the two materials. Figure 6 reports the SAXS curves, together with their best fitting. The main results are listed in the second half of Table 5. Micelles' size is almost unaltered after the surfactant interaction with soil, and the volume fraction decreases for both surfactants, similarly to PDE interacting with the soiled glass slide. This is related to the higher affinity between polystyrene and the soil layer that inhibits the solubilization of its oily fraction into the micellar core. Thus, because of the adsorption of surfactant at the soil surface, a fraction of micelles is disrupted, with a subsequent decrease in the volume fraction of scattering objects. Figure 7 shows the trend of the volume fraction in the different cases,

Table 5. SAXS Fitting Results[a]

	system	fitting parameter	sampling time			
			0 h	3 h	6 h	24 h
soiled glass	MPD 5%	ϕ	0.20 ± 0.02	0.20 ± 0.02	0.33 ± 0.03	0.36 ± 0.02
		r_c (Å)	14.6 ± 1.2	14.5 ± 0.1	13.9 ± 0.9	13.9 ± 0.9
		t (Å)	19.0 ± 1.7	19.0 ± 0.3	19.0 ± 1.6	19.2 ± 1.6
	PDE 5%	ϕ	0.20 ± 0.02	0.25 ± 0.03	0.17 ± 0.02	0.15 ± 0.01
		r_c (Å)	15.6 ± 0.1	15.1 ± 0.1	15.2 ± 0.1	15.3 ± 0.2
		t (Å)	23.5 ± 0.2	22.4 ± 0.2	21.7 ± 0.2	23.4 ± 0.3
soiled polystyrene	MPD 5%	Φ	0.20 ± 0.02	0.13 ± 0.02	0.15 ± 0.02	0.14 ± 0.01
		r_c (Å)	14.6 ± 1.2	15.7 ± 0.1	15.7 ± 0.1	14.7 ± 0.5
		t (Å)	19.0 ± 1.7	22.0 ± 1.4	22.0 ± 0.3	20.0 ± 1.2
	PDE 5%	ϕ	0.20 ± 0.02	0.17 ± 0.01	0.14 ± 0.01	0.13 ± 0.01
		r_c (Å)	15.6 ± 0.1	15.3 ± 0.2	15.5 ± 0.4	15.7 ± 0.7
		t (Å)	23.5 ± 0.2	22.0 ± 0.3	23.0 ± 0.2	23.0 ± 1.1

[a]ϕ is the volume fraction of the scattering objects, with respect to the whole volume system; r_c is the average core radius; t is the shell thickness.
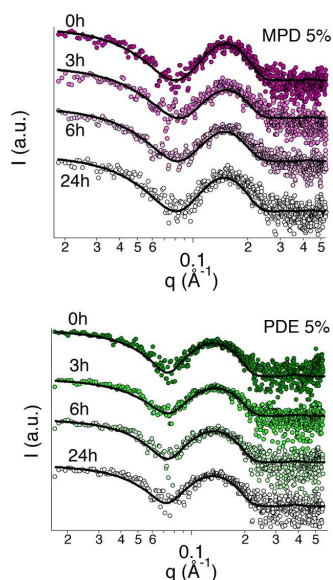
Figure 6. SAXS curves of the MPD 5% and PDE 5% systems, interacting with soiled polystyrene slides. The measurements were performed on samples taken at different times, that is, 0, 3, 6, and 24 h. Solid black lines represent the best fitting curves for experimental data. The curves have been arbitrarily stacked for sake of clarity.

highlighting that the oil solubilization occurs only in the case of MPD 5% interacting with soiled glass.
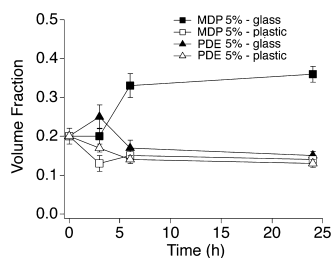
Figure 7. Trend of the volume fraction of the scattering objects for the 5% surfactant systems interacting with glass and polystyrene slides for 24 h, as obtained by the analysis of SAXS data.

The above results report a detailed picture on the surfactant interactions with two different "coatings" commonly found in classic and contemporary/modern art. Overall, it is shown that a tiny change in the molecular structure of the PDE leads to consistent changes in the mechanisms of action, the kinetics, and the cleaning efficacy of the surfactant.

4. CONCLUSIONS

Complex systems composed by MPD have been investigated, and its effectiveness was compared to PDE, a conventional nonionic amphiphile, for the cleaning of two common materials disfiguring the aesthetical aspects of works of art. In particular, MPD- and PDE-NSFs were challenged for the removal of poly(ethyl methacrylate/methyl acrylate) 70:30,

p(EMA/MA), commercially known as Paraloid B72 from glass and polystyrene surfaces, while aqueous micellar solutions of the two surfactants were used for the cleaning of artificially soiled surfaces. The overall results highlighted the better performance of MPD both for the polymer and the soil removal from coated surfaces. The interaction mechanism of NSFs for the removal of p(EMA/MA) polymer, observed at the micro-scale through CLSM imaging, involves a dewetting-like process. The polymer is detached from the surface and coalesces into separated droplets as the liquid phase/solid surface interfacial area increases. The PDE- and MPD-NSFs exhibit different mechanisms that depend both on the organic solvent and surfactant because of the different surface tensions and to the different adsorption/penetration of MPD onto/into the polymer film, with respect to PDE. This is likely due to the methyl capping of the surfactant polar head and to the presence of the ester group between the hydrophilic and hydrophobic moiety of the surfactant molecule (PDE). FCS provided a more detailed picture of the cleaning process showing that the surfactants present in the NSFs are able to penetrate through the Paraloid B72 film, that acts as a sort of "sieve", and reach the polymer/solid surface interface, where liquid-filled cavities are formed. Moreover, CLSM experiments highlighted better performances of MPD, if compared to PDE, also in soil removal. The mechanism involves a dewetting-like process, where the oily phase is detached from the glass or polystyrene substrates and coalesces into large droplets. Surfactant concentration was found to be crucial to boost the interaction with the heterogeneous soil. 1% surfactant solutions are less effective than 5%, even if micelles are present in both cases. Differently to PDE that adsorb on the soil layer surface it was found, for both glass and polystyrene substrates, that MPD micellar solutions solubilize soil. Both surfactants allow the removal of soil and grime with different efficacy, no mechanical action, and with different times. The time necessary to perform the cleaning and the mechanical action in conservation are of uppermost importance because long application times and mechanical action should be avoided particularly in the case of fragile and delicate surfaces as those of works of art, which hardly tolerate mechanical stresses during the cleaning operations. Overall, the results reported in the present work open up to new formulations for better-performing and safer cleaning systems to be used by restorers for the conservation of cultural heritage or in other applications as detergency, cosmetics, and so forth.

■ ASSOCIATED CONTENT

Ⓢ Supporting Information

The Supporting Information is available free of charge at https://pubs.acs.org/doi/10.1021/acsami.0c06425.

> Details on materials and methods and additional figures of all FCS curves, cleaning tests, and surface tension measurements (PDF)

■ AUTHOR INFORMATION

Corresponding Author

Piero Baglioni − *Department of Chemistry and CSGI, University of Florence, 50019 Sesto Fiorentino, Florence, Italy;* ⓞ orcid.org/0000-0003-1312-8700; Email: baglioni@csgi.unifi.it

Authors

Michele Baglioni − *Department of Chemistry and CSGI, University of Florence, 50019 Sesto Fiorentino, Florence, Italy*

Teresa Guaragnone − *Department of Chemistry and CSGI, University of Florence, 50019 Sesto Fiorentino, Florence, Italy;* orcid.org/0000-0002-7226-0958

Rosangela Mastrangelo − *Department of Chemistry and CSGI, University of Florence, 50019 Sesto Fiorentino, Florence, Italy;* orcid.org/0000-0003-0420-947X

Felipe Hidetomo Sekine − *NIKKOL GROUP Nikko Chemicals Co., Ltd., 103-0002 Tokyo, Japan*

Taku Ogura − *NIKKOL GROUP Nikko Chemicals Co., Ltd., 103-0002 Tokyo, Japan; NIKKOL GROUP Cosmos Technical Center Co., Ltd., 174-0046 Tokyo, Japan; Research Institute for Science & Technology, Tokyo University of Science, Chiba 278-8510, Japan;* orcid.org/0000-0003-4205-2477

Complete contact information is available at:
https://pubs.acs.org/10.1021/acsami.0c06425

■ REFERENCES

(1) Chelazzi, D.; Bordes, R.; Giorgi, R.; Holmberg, K.; Baglioni, P. The Use Of Surfactants In The Cleaning Of Works Of Art. *Curr. Opin. Colloid Interface Sci.* **2020**, *45*, 108−123.

(2) Baglioni, P.; Carretti, E.; Chelazzi, D. Nanomaterials In Art Conservation. *Nat. Nanotechnol.* **2015**, *10*, 287−290.

(3) Baglioni, M.; Rengstl, D.; Berti, D.; Bonini, M.; Giorgi, R.; Baglioni, P. Removal of Acrylic Coatings from Works of Art by Means of Nanofluids: Understanding the Mechanism at the Nanoscale. *Nanoscale* **2010**, *2*, 1723.

(4) Giorgi, R.; Baglioni, M.; Berti, D.; Baglioni, P. New Methodologies for the Conservation of Cultural Heritage: Micellar Solutions, Microemulsions, and Hydroxide Nanoparticles. *Acc. Chem. Res.* **2010**, *43*, 695−704.

(5) Baglioni, P.; Giorgi, R.; Berti, D.; Baglioni, P. Smart Cleaning of Cultural Heritage: A New Challenge for Soft Nanoscience. *Nanoscale* **2012**, *4*, 42−53.

(6) Baglioni, M.; Jàidar Benavides, Y.; Berti, D.; Giorgi, R.; Keiderling, U.; Baglioni, P. An Amine-Oxide Surfactant-Based Microemulsion for the Cleaning of Works of Art. *J. Colloid Interface Sci.* **2015**, *440*, 204−210.

(7) Baglioni, M.; Berti, D.; Teixeira, J.; Giorgi, R.; Baglioni, P. Nanostructured Surfactant-Based Systems for the Removal of Polymers from Wall Paintings: A Small-Angle Neutron Scattering Study. *Langmuir* **2012**, *28*, 15193−15202.

(8) Baglioni, M.; Raudino, M.; Berti, D.; Keiderling, U.; Bordes, R.; Holmberg, K.; Baglioni, P. Nanostructured Fluids from Degradable Nonionic Surfactants for the Cleaning of Works of Art from Polymer Contaminants. *Soft Matter* **2014**, *10*, 6798−6809.

(9) Baglioni, P.; Chelazzi, D.; Giorgi, R.; Poggi, G. Colloid and Materials Science for the Conservation of Cultural Heritage: Cleaning, Consolidation, and Deacidification. *Langmuir* **2013**, *29*, 5110−5122.

(10) Baglioni, M.; Domingues, J. A. L.; Carretti, E.; Fratini, E.; Chelazzi, D.; Giorgi, R.; Baglioni, P. Complex Fluids Confined into Semi-Interpenetrated Chemical Hydrogels for the Cleaning of Classic Art: A Rheological and SAXS Study. *ACS Appl. Mater. Interfaces* **2018**, *10*, 19162.

(11) Giorgi, R.; Baglioni, M.; Baglioni, P. Nanofluids and Chemical Highly Retentive Hydrogels for Controlled and Selective Removal of Overpaintings and Undesired Graffiti from Street Art. *Anal. Bioanal. Chem.* **2017**, *409*, 3707.

(12) Baglioni, M.; Poggi, G.; Ciolli, G.; Fratini, E.; Giorgi, R.; Baglioni, P. A Triton X-100-Based Microemulsion for the Removal of Hydrophobic Materials from Works of Art: SAXS Characterization and Application. *Materials* **2018**, *11*, 1144.

(13) Mastrangelo, R.; Montis, C.; Bonelli, N.; Tempesti, P.; Baglioni, P. Surface Cleaning of Artworks: Structure and Dynamics of Nanostructured Fluids Confined in Polymeric Hydrogel Networks. *Phys. Chem. Chem. Phys.* **2017**, *19*, 23762−23772.

(14) Ormsby, B.; Keefe, M.; Phenix, A.; von Aderkas, E.; Learner, T.; Tucker, C.; Kozak, C. Mineral Spirits-Based Microemulsions: A Novel Cleaning System for Painted Surfaces. *J. Am. Inst. Conserv.* **2016**, *55*, 12−31.

(15) Raudino, M.; Selvolini, G.; Montis, C.; Baglioni, M.; Bonini, M.; Berti, D.; Baglioni, P. Polymer Films Removed from Solid Surfaces by Nanostructured Fluids: Microscopic Mechanism and Implications for the Conservation of Cultural Heritage. *ACS Appl. Mater. Interfaces* **2015**, *7*, 6244−6253.

(16) Baglioni, M.; Montis, C.; Brandi, F.; Guaragnone, T.; Meazzini, I.; Baglioni, P.; Berti, D. Dewetting Acrylic Polymer Films with Water/Propylene Carbonate/Surfactant Mixtures − Implications for Cultural Heritage Conservation. *Phys. Chem. Chem. Phys.* **2017**, *19*, 23723−23732.

(17) Baglioni, M.; Montis, C.; Chelazzi, D.; Giorgi, R.; Berti, D.; Baglioni, P. Polymer Film Dewetting by Water/Surfactant/Good-Solvent Mixtures: A Mechanistic Insight and Its Implications for the Conservation of Cultural Heritage. *Angew. Chem., Int. Ed.* **2018**, *57*, 7355−7359.

(18) Montis, C.; Koynov, K.; Best, A.; Baglioni, M.; Butt, H.-J.; Berti, D.; Baglioni, P. Surfactants Mediate the Dewetting of Acrylic Polymer Films Commonly Applied to Works of Art. *ACS Appl. Mater. Interfaces* **2019**, *11*, 27288−27296.

(19) Gentili, D.; Foschi, G.; Valle, F.; Cavallini, M.; Biscarini, F. Applications of Dewetting in Micro and Nanotechnology. *Chem. Soc. Rev.* **2012**, *41*, 4430−4443.

(20) Reiter, G. Unstable Thin Polymer Films: Rupture and Dewetting Processes. *Langmuir* **1993**, *9*, 1344−1351.

(21) Reiter, G. n.; Khanna, R.; Sharma, A. Self-Destruction and Dewetting of Thin Polymer Films: The Role of Interfacial Tensions. *J. Phys. Condens. Matter* **2003**, *15*, S331.

(22) Xu, L.; Sharma, A.; Joo, S. W. Dewetting of Stable Thin Polymer Films Induced by a Poor Solvent: Role of Polar Interactions. *Macromolecules* **2012**, *45*, 6628−6633.

(23) Xu, L.; Shi, T.; An, L. Nonsolvent-Induced Dewetting of Thin Polymer Films. *Langmuir* **2007**, *23*, 9282−9286.

(24) Tomasetti, E.; Rouxhet, P. G.; Legras, R. Viscoelastic Behavior of Polymer Surface during Wetting and Dewetting Processes. *Langmuir* **1998**, *14*, 3435−3439.

(25) Khandekar, N. A Survey of the Conservation Literature Relating to the Development of Aqueous Gel Cleaning on Painted and Varnished Surfaces. *Stud. Conserv.* **2000**, *45*, 10−20.

(26) Stulik, D.; Miller, D.; Khandekar, N.; Wolbers, R.; Carlson, J.; Petersen, W. C. *Solvent Gels for the Cleaning of Works of Art: The Residue Question*; Getty Publications: Los Angeles, 2004.

(27) Angelova, L. V.; Ormsby, B.; Townsend, J.; Wolbers, R. *Gels in the Conservation of Art*; Archetype Publications, 2017.

(28) Carretti, E.; Dei, L. Gels as Cleaning Agents in Cultural Heritage Conservation. In *Molecular Gels*; Weiss, R. G., Terech, P., Eds.; Springer: Netherlands, 2006; pp 929−938.

(29) Mastrangelo, R.; Chelazzi, D.; Poggi, G.; Fratini, E.; Pensabene Buemi, L.; Petruzzellis, M. L.; Baglioni, P. Twin-Chain Polymer Hydrogels Based On Poly(Vinylalcohol) As New Advanced Tool For The Cleaning Of Modern And Contemporary Art. *Proc. Natl. Acad. Sci. U.S.A.* **2020**, *117*, 7011−7020.

(30) Bonelli, N.; Poggi, G.; Chelazzi, D.; Giorgi, R.; Baglioni, P. Poly(Vinyl Alcohol)/Poly(Vinyl Pyrrolidone) Hydrogels for the Cleaning of Art. *J. Colloid Interface Sci.* **2019**, *536*, 339−348.

(31) Hama, I.; Okamoto, T.; Nakamura, H. Preparation and Properties of Ethoxylated Fatty Methyl Ester Nonionics. *J. Am. Oil Chem. Soc.* **1995**, *72*, 781−784.

(32) Hama, I.; Sasamoto, H.; Okamoto, T. Influence of Catalyst Structure on Direct Ethoxylation of Fatty Methyl Esters over Al-Mg Composite Oxide Catalyst. *J. Am. Oil Chem. Soc.* **1997**, *74*, 817−822.

(33) Hama, I.; Sakaki, M.; Sasamoto, H. Effects of Ethoxylate Structure on Surfactant Properties of Ethoxylated Fatty Methyl Esters. *J. Am. Oil Chem. Soc.* **1997**, *74*, 823−827.

(34) Hama, I.; Sakaki, M.; Sasamoto, H. Nonionic Surfactant Properties of Methoxypolyoxyethylene Dodecanoate Compared with Polyoxyethylene Dodecylether. *J. Am. Oil Chem. Soc.* **1997**, *74*, 829−835.

(35) Cox, M. F.; Weerasooriya, U. Impact of Molecular Structure on the Performance of Methyl Ester Ethoxylates. *J. Surfactants Deterg.* **1998**, *1*, 11−22.

(36) Nagai, Y.; Togawa, N.; Tagawa, Y.; Gotoh, K. Comparison of Cleaning Power Between Alcohol Ethoxylates or Methyl Ester Ethoxylates Having Different EO Chain Lengths and a Common Anionic Surfactant. *Tenside Surfactants Deterg.* **2014**, *51*, 113−118.

(37) Renkin, M.; Fleurackers, S.; Szwach, I.; Hreczuch, W. Rapeseed Methyl Ester Ethoxylates: A New Class of Surfactants of Environmental and Commercial Interest. *Tenside Surfactants Deterg.* **2005**, *42*, 280−287.

(38) Yu, Y.; Zhao, J.; Bayly, A. E. Development of Surfactants and Builders in Detergent Formulations. *Chin. J. Chem. Eng.* **2008**, *16*, 517−527.

(39) Chiantore, O.; Lazzari, M. Photo-Oxidative Stability of Paraloid Acrylic Protective Polymers. *Polymer* **2001**, *42*, 17−27.

(40) Bracci, S.; Melo, M. J. Correlating Natural Ageing and Xenon Irradiation of Paraloid B72 Applied on Stone. *Polym. Degrad. Stab.* **2003**, *80*, 533−541.

(41) Borgia, G. C.; Bortolotti, V.; Camaiti, M.; Cerri, F.; Fantazzini, P.; Piacenti, F. Performance Evolution of Hydrophobic Treatments for Stone Conservation Investigated by MRI. *Magn. Reson. Imag.* **2001**, *19*, 513−516.

(42) Crisci, G. M.; La Russa, M. F.; Malagodi, M.; Ruffolo, S. A. Consolidating Properties of Regalrez 1126 and Paraloid B72 Applied to Wood. *J. Cult. Herit.* **2010**, *11*, 304−308.

(43) Ormsby, B.; Keefe, M.; Phenix, A.; Learner, T. *A Summary of Recent Developments in Wet Surface Cleaning Systems: Unvarnished Modern and Contemporary Painted Surfaces*; Archetype Publications, 2015.

(44) Baglioni, M.; Poggi, G.; Jaidar Benavides, Y.; Martínez Camacho, F.; Giorgi, R.; Baglioni, P. Nanostructured Fluids for the Removal of Graffiti − A Survey on 17 Commercial Spray-Can Paints. *J. Cult. Herit.* **2018**, *34*, 218.

(45) Provencher, S. W. CONTIN: A General Purpose Constrained Regularization Program for Inverting Noisy Linear Algebraic and Integral Equations. *Comput. Phys. Commun.* **1982**, *27*, 229−242.

(46) Sato, T.; Akahane, T.; Amano, K.; Hyodo, R.; Yanase, K.; Ogura, T. Scattering and Spectroscopic Study on the Hydration and Phase Behavior of Aqueous Alcohol Ethoxylate and Methyl Ester Ethoxylate: Effects of Terminal Groups in Hydrophilic Chains. *J. Phys. Chem. B* **2016**, *120*, 5444−5454.

(47) Ogura, T.; Kaneko, Y.; Suekuni, T.; Tobori, N.; Glatter, O. *Dynamics of Spontaneously-Generated Solubilization of Oleic Acid by the Plant-Based Ingredient MEE (Methyl Ester Ethoxylate)*, 2012.

(48) Butt, H.-J.; Graf, K.; Kappl, M. Contact Angle Phenomena and Wetting. In *Physics and Chemistry of Interfaces*; Wiley-VCH Verlag GmbH & Co. KGaA, 2003; pp 118−144.

(49) Castro, L. B. R.; Almeida, A. T.; Petri, D. F. S. The Effect of Water or Salt Solution on Thin Hydrophobic Films. *Langmuir* **2004**, *20*, 7610−7615.

(50) Verma, A.; Sharma, A. Submicrometer Pattern Fabrication by Intensification of Instability in Ultrathin Polymer Films under a Water−Solvent Mix. *Macromolecules* **2011**, *44*, 4928−4935.

(51) Wolbers, R. *Cleaning Painted Surfaces: Aqueous Methods*; Archetype Publications, 2000.

(52) Phenix, A.; Burnstock, A. *The Deposition of Dirt: A Review of the Literature with Scanning Electron Microscope Studies of Dirt on Selected Paintings*; UKIC, 1990.

(53) Murray, A.; Berenfeld, C. C. d.; Chang, S. Y. S.; Jablonski, E.; Klein, T.; Riggs, M. C.; Robertson, E. C.; Tse, W. M. A. The Condition and Cleaning of Acrylic Emulsion Paintings. *MRS Online Proc. Libr.* **2002**, *712*, 1−8.

(54) Morrison, R.; Bagley-Young, A.; Burnstock, A.; van den Berg, K. J.; van Keulen, H. An Investigation of Parameters for the Use of Citrate Solutions for Surface Cleaning Unvarnished Paintings. *Stud. Conserv.* **2007**, *52*, 255−270.

(55) Phenix, A.; Burnstock, A. The Removal of Surface Dirt on Paintings with Chelating Agents. *The Conservator* **1992**, *16*, 28−38.

(56) Stulik, D. *Solvent Gels for the Cleaning of Works of Art: The Residue Question*; Getty Publications, 2004.

(57) Tongcumpou, C.; Acosta, E. J.; Scamehorn, J. F.; Sabatini, D. A.; Yanumet, N.; Chavadej, S. Enhanced Triolein Removal Using Microemulsions Formulated with Mixed Surfactants. *J. Surfactants Deterg.* **2006**, *9*, 181−189.

(58) Chen, B.-H.; Miller, C. A.; Garrett, P. R. Rates of Solubilization of Triolein into Nonionic Surfactant Solutions. *Colloids Surf., A* **1997**, *128*, 129−143.

(59) Cox, M. F.; Weerasooriya, U. Methyl Ester Ethoxylates. *J. Am. Oil Chem. Soc.* **1997**, *74*, 847−859.

(60) Christov, N. C.; Denkov, N. D.; Kralchevsky, P. A.; Broze, G.; Mehreteab, A. Kinetics of Triglyceride Solubilization by Micellar Solutions of Nonionic Surfactant and Triblock Copolymer. 1. Empty and Swollen Micelles. *Langmuir* **2002**, *18*, 7880−7886.

(61) Kralchevsky, P. A.; Denkov, N. D.; Todorov, P. D.; Marinov, G. S.; Broze, G.; Mehreteab, A. Kinetics of Triglyceride Solubilization by Micellar Solutions of Nonionic Surfactant and Triblock Copolymer. 2. Theoretical Model. *Langmuir* **2002**, *18*, 7887−7895.

Paper 3

pHEMA/PAA and pHEMA/PVP semi-IPNs: effect of pH and loading with tetraethylenepentamine for the removal of bronze corrosion products

Teresa Guaragnone‡, Marta Rossi‡, David Chelazzi, Rosangela Mastrangelo, Mirko Severi, Emiliano Fratini, Piero Baglioni

Department of Chemistry "Ugo Schiff" and CSGI, University of Florence, via della Lastruccia 3-Sesto Fiorentino, I-50019, Florence, Italy.

*email: piero.baglioni@unifi.it;

‡ These authors contributed equally

KEYWORDS: semi-IPN; hydrogel; pHEMA; PAA; PVP; TEPA; copper ions; cleaning; corroded bronze.

Abstract

Bronze artifacts constitute a fundamental portion of cultural heritage, but there is a lack of effective methodologies for the removal of corrosion layers, such as those produced by the "bronze disease". We propose for the first time networks of poly(2-hydroxyethyl methacrylate) (pHEMA) semi-interpenetrated (semi-IPN) with polyacrylic acid (PAA) or polyvinylpyrrolidone (PVP), loaded with tetraethylenepentamine (TEPA) for the removal of copper corrosion products. Alkaline pH causes the ionization of carboxyls in PAA increasing the swelling and the porosity of the pHEMA/PAA semi-IPN. In pHEMA/PVP, increasing the pH leads to the co-presence of the enol and enolate forms of PVP, along with significant changes in the macroporosity and a decrease in the mesh size. 2D FTIR imaging indicates that TEPA interacts with carboxylates in PAA, and with polar or charged CO groups in PVP. The kinetics of Cu(II) ions uptake by the semi-IPNs showed that the ion-matrix interaction is stronger for pHEMA/PAA. The process likely follows two stages, i.e. an initial diffusion-controlled step followed by diffusion in smaller pores or adsorption at less available sites.

Upon application of the TEPA-loaded gels onto corroded bronze, copper oxychlorides dissolve and migrate inside the gels. Cu(II) ions probably form ternary complexes with TEPA and carboxylates in PAA or CO in PVP. The

application of the semi-IPNs allowed the gradual and effective removal of oxychlorides, leaving unaltered patinas of cuprite that are needed to passivate bronze against corrosion. Loading the semi-IPNs with TEPA provides a much higher cleaning efficacy than traditional EDTA, opening new perspectives in the restoration of bronze works of art.

INTRODUCTION

The conservation of cultural heritage has deep societal and economic implications, because well preserved and accessible works of art constitute both a drive for social inclusion and an important resource to promote tourism and job creation [1]. Metallic objects and artifacts constitute a vast part of the artistic and architectural production spanning over millennia, however they are typically affected by several degradation processes that can significantly alter their appearance and integrity. In particular, copper-based artifacts are affected by corrosion phenomena that induce the formation of a complex patina on their surface, usually characterized by the presence of copper oxychlorides (atacamite and its polymorphs) responsible of the so called "bronze disease", a cyclic degradative process able to consume the objects up to their complete disgregation [2, 3]. The removal of corrosion products is thus a fundamental operation in conservation practice, but still an open challenge that needs feasible solutions. Traditionally, cleaning is performed by mechanical (vibrating or abrasive tools, ultra-high-pressure water) [4], optical (laser ablation), or chemical wet methods (bases, acids and complexing agents)[5]. However, these approaches involve several risks for the artifacts, unless time consuming protocols are adopted: mechanical treatments and non-confined cleaning fluids are invasive and scarcely selective, while laser ablation can trigger heating processes on the artifacts' surfaces [5, 6]. The confinement of cleaning fluids is an optimal strategy to achieve controlled removal without risks for the objects, but traditional thickeners used in restoration (e.g. cellulose derivatives, viscous dispersions of polyacrylic acid) are either not enough retentive or exhibit poor mechanical properties and tend to leave residues on the treated surfaces [7]. In the last decade, chemical hydrogels have been proposed as optimal matrices to confine fluids for the safe cleaning of works of art [8–11]. In particular, polymeric networks of poly(2-hydroxyethyl methacrylate) (pHEMA) semi-interpenetrated (semi-IPN) with polyvinylpyrrolidone (PVP) have advantageous properties similar to the average of the two homopolymers characteristics, i.e. the mechanical strength of pHEMA and the hydrophilicity of PVP, resulting in ideal mechanical properties and

retentiveness. The pHEMA/PVP gels can be applied repeatedly without uncontrolled spreading of the loaded fluids, and simply removed in one piece without mechanical stress on the treated surface or removal/leaching of original components [8]–[14]. These features are particularly advantageous on brittle and mechanically weak corroded surfaces, where mechanical removal or peeling of surface layers (e.g. using film-forming polymeric dispersions [15]) might be risky.

In this contribution, pHEMA/PVP semi-IPNs were used as confining matrices for cleaning solutions, based on the aforementioned advantages and on the ability of PVP to form complexes with metal ions [16], which is expected to enhance the removal of corrosion patinas. Besides PVP, we also considered polyacryilic acid (PAA) as semi-interpenetrating polymer in the pHEMA network, owing to its ability to give strong coordination bonds at alkaline pH, thanks to the presence of carboxylate groups [17]; the latter also account for the ability of PAA to associate with water molecules and swell extensively at alkaline pH when the polymer deprotonates and unfolds [18]. We used tetraethylenpentamine (TEPA) as a cleaning fluid to upload in the semi-IPNS owing to its high complexing selectivity to Cu(II) ions, which are typically found in detrimental and defacing corrosion products (Cu(II) oxides and carbonates, copper oxychlorides). The complex formed by Cu(II) and TEPA has a stability constant ($logK_f$ = 22.8 at 25°C [19]) four orders of magnitude higher than that of the complex formed with the tetrasodium salt of ethylenediaminetetraacetic acid (EDTA, Y^{4+}) ($logK_f$ = 18.8 at 25°C and 1 M [20]), the chelating agent traditionally employed by conservators in the removal of copper corrosion products [4, 18].

The pHEMA/PVP and pHEMA/PAA semi-IPNS were swollen in water at different pH values (6, 8, 12), and in a water solution of TEPA (pH 12), and analyzed by small angle X-ray scattering (SAXS) and scanning electron microscopy (SEM), to investigate structural differences at the micron- and nano-scale. Differential scanning calorimetry (DSC) and thermogravimetric analysis (TGA) were employed to evaluate the gels' solvent content and the properties of water entrapped in the polymeric networks. Fourier Transform Infrared Spectroscopy (FTIR) measurements were performed, using a Focal Plane Array (FPA) detector, to gain information on the composition and structure of the polymers in the semi-IPNS, and on their interaction with TEPA and copper(II) ions. The Cu(II) ion adsorption kinetics of pHEMA/PVP and pHEMA/PAA semi-IPNs at different pH values were studied and compared, highlighting the effect of the gels' structure and functional groups on the adsorption process.

Finally, the semi-IPNs were applied on corroded bronze mock-ups, and their ability to solubilize and remove copper oxychlorides was inquired with FTIR-FPA chemical mapping with spatial resolution at the micron-scale.

EXPERIMENTAL SECTION

Materials 2-Hydroxyethyl methacrylate (HEMA) (purity 99%), poly(acrylic acid) (PAA) (average Mn ≈ 1200 kDa), azoisobutyronitrile (AIBN) (purity 98%), N,N-methylene-bis(acrylamide) (MBA) (purity 99%), poly(vinylpyrrolidone) (PVP) (average Mn ≈ 1300 kDa), tetraethylenepentamine (TEPA) (purity ≥95%), sodium hydroxide pellets (purity 97%), ethylenediaminetetraacetic acid disodium salt dihydrate (EDTA) (purity 98.5-101.5%), and copper(II) chloride dihydrate (purity >99.0 %) were purchased from Sigma-Aldrich and used as received. Potassium dihydrogen phosphate (purity ≥99.0%) and dipotassium hydrogen phosphate (purity ≥98%) were purchased from Merck and used as received to prepare a pH 8 buffer. Water was purified by a Millipore Milli-Q gradient system (resistivity >18 MΩ·cm).

Hydrogels synthesis The pHEMA/PVP semi-IPN was prepared by radical polymerization as reported by Domingues et al [22]. Some variations in the synthetic process were adopted: the HEMA/PVP ratio was changed from 30/70 to 27.5/72.5 (% w/w), the water content in the pre-gel solution was 62.2% instead of 65%, while the cross-linker concentration was halved; these changes were due to the necessity of having slightly softer and more flexible gel sheets to adapt the rough surface of corrosion patinas.
The pHEMA/PAA semi-IPN was synthesized adding an aqueous solution of PAA to HEMA monomer and AIBN. The ratio between the mass of pHEMA and PAA (96.5/3.5 % w/w) was chosen in order to have a molar ratio between -OH and -COOH groups of 16/1, which proved to be an optimal condition to favor the synthetic process, yielding gels with good mechanical properties. After sonication and degassing, the mixture was transferred between two glassy covers and polymerized at 60°C for 4 hours. After the reaction, a 2 mm thick flat hydrogel sheet was obtained; the gel was then washed by renewing water once a day for 7 days to remove residues of unreacted monomers and free PAA molecules. Table 1 shows the composition of the two hydrogels.
The semi-IPNs were swollen in water, reaching a stable pH of 6.3. Small pieces (5 x 5 x 0.2 cm³) were cut and swollen with water at pH 8 and 12 (adjusted with a sodium hydroxide solution), and in a water solution of

TEPA (20% w/w). In all cases, the gels were placed in the NaOH or TEPA solutions for at least 5 days, using an excess of solution as compared to the gel's mass, to make sure that the semi-IPNs exchanged completely.

Semi-IPN	pHEMA/PAA	Semi-IPN	pHEMA/PVP
HEMA (wt%)	52.5%	HEMA (wt%)	10.3
water (wt%)	45.2%	Water (wt%)	62.2
MBA (wt%)	-	MBA (wt%)	0.4
AIBN (wt%)	0.4%	AIBN (wt%)	0.1
PAA (wt%)	1.8%	PVP (wt%)	27.0
HEMA/PAA ratio (%w/w)	96.5/3.5	HEMA/PVP ratio (%w/w)	27.5/72.5

Table 1. Composition of pHEMA/PAA and pHEMA/PVP semi-IPNs.

Thermal analyses Thermogravimetric analysis (TGA) was carried out with an SDT Q600 (TA Instruments). The balance sensitivity is 0.1 µg. Measurements were performed in a nitrogen atmosphere with a flow rate of 100 mL/min. The samples were put in open alumina pans, and the analyses were performed with a heating rate of 10 °C/min from 25 °C to 450 °C [23].

The equilibrium water content (EWC) and the equilibrium solvent content (ESC) were calculated as follows (Eq. 1):

$$EWC\ (ESC) = \frac{W-W_d}{W} \tag{1}$$

where W is the weight of the hydrated sample and W_d the weight of the dry sample. The values of W_d were experimentally determined from TGA analysis, considering the weight of the sample at ca. 200 and 300°C to quantify the EWC (semi-IPNs swollen in water) and the ESC (semi-IPNs swollen in TEPA) respectively.

Differential scanning calorimetry analysis (DSC) was performed with a Q2000 Calorimeter (TA Instruments). The temperature range was from -80 °C to 200 °C with a scan rate of 2 °C/min; sealed stainless steel pans were used. From the DSC curves it is possible to determine the different types of water present in the hydrogels [24]. Water in porous systems like gels can be classified as non-freezing bound water, free or bulk water [25]. The non-freezing water forms hydrogen bonds with the functional groups of the polymer, rather than with other water molecules (as would be necessary for water to freeze); bulk water has the same properties of pure water and can bind with other water molecules to form ice crystals when temperature is

around 0°C. It is possible to determine the free water index (FWI) according to the following equation (Eq. 2):

$$FWI = \frac{\Delta H_{tr}}{\Delta H_f \times EWC} \tag{2}$$

where ΔH_{tr} (J/g) is the heat of transition obtained by the integral of melting peaks around 0˚C in the DSC curves, and ΔH_f is the theoretical value of the specific enthalpy of fusion of water at 0 °C (333,6 J/g [26]).

Scanning electron microscopy SEM investigation was performed on the xerogels, obtained by freeze-drying thin slices of the hydrogels. A FEG-SEM ΣIGMA (Carl Zeiss, Germany) was used to acquire the images using an acceleration potential of 2 kV and a working distance of 3 mm. Before carrying out the analysis, the samples were coated with a thin layer of gold using an Agar Scientific Auto Sputter Coater.

2D image analysis. SEM images were analyzed through the chord length distribution approach, in order to obtain the average dimension of gels' pores and walls. More specifically, the MATLAB® algorithm developed by M. Ryan MacIver [27] was used. Each chosen SEM micrograph was transformed in a grey-scale image, then contrast-enhanced and finally binarized; the resulting black and white (b/w) image is simplified with respect to the original SEM picture, having lost its tridimensionality. At this point, the MATLAB® algorithm drew a set of 10000 randomly-oriented lines on the 2D, b/w image. Segments, called chords, form when lines cross phase-boundaries (i.e. when lines pass from black to white areas, or *viceversa*). The frequency of chords of a certain length, f(R), is plotted against the length of the chords themselves, R (μm). The minimum detectable chord length was set to 2 pixels (0.18 μm) for gels with smaller pores (pHEMA/PAA at pH 8 and 12, pHEMA/PVP at pH 12) and to 5 pixels (0.3 μm), to reduce noise, for pHEMA/PVP at pH 6 and pHEMA/PVP at pH 8; the data trend was, in fact, independent on the minimum chord value. The final datasets were smoothed through the Igor Pro® built-in function to improve readability. For the gels' pores and walls, the decay in the frequency of the most abundant chords evolves according to exponential functions [28]:

$$f_{Pores}(R) \propto \exp\left(-\frac{R}{\lambda_{Pores}}\right) \tag{3}$$

$$f_{Walls}(R) \propto \exp\left(-\frac{R}{\lambda_{Walls}}\right) \qquad\qquad (4)$$

In both equations, $1/\lambda$ represents the slope of the function in a semi-log graph. λ is called persistence length, and represents a characteristic length scale of the gel domains. For the analysis of chord lengths, frontal SEM pictures were considered, so as to avoid artifacts in the length distributions.

Small angle x-ray scattering Small angle x-ray scattering analysis (SAXS) were carried out with a HECUS S3-MICRO SWAXS camera, equipped with a Hecus System3 2D-point collimator and two position-sensitive detectors (PSD-50M) containing 1024 channels with a width of 54 microns. The copper anode from the Oxford 50 W microfocus source emits radiation with the wavelength of the Kα-line given by $\lambda = 1.542$ Å. The Kβ-line is removed by FOX-3D single-bounce multilayer point focussing optics (Xenocs, Grenoble). The voltage is generated by the GeniX X-ray generator (Xenocs, Grenoble). The sample-to-detector distance was 281 mm. The volume between sample and detector was kept under vacuum in order to minimize the scattering from the air. This camera was calibrated in the small angle region using silver behenate, which is known to have a well-defined lamellar structure (d = 58.38 Å)[29]. Scattering curves were acquired in the q-range between 0.01 and 0.55 Å^{-1}. Samples were placed into demountable cells, with kapton film used as windows. The temperature control was set to 25°C by a Peltier element, with an accuracy of $\pm$ 0.1 °C. All the scattering curves were corrected for the empty cell and water contribution considering the relative transmission factors.

2D FTIR imaging 2D FTIR imaging analysis was carried out on xerogels and bronze mock-ups, using a Cary 620-670 FTIR microscope, equipped with an FPA 128 x 128 detector (Agilent Technologies). This set up allows the highest spatial resolution currently available to FTIR microscopes. The spectra were recorded directly on the surface of the samples (gels, corroded bronze coins, or the Au background) in reflectance mode, with open aperture and a spectral resolution of 4 cm^{-1}, acquiring 128 scans for each spectrum. A "single-tile" analysis results in a map of 700 x 700 μm^2 (128 x 128 pixels), and the spatial resolution of each imaging map is 5.5 μm (i.e. each pixel has dimensions of 5.5 x 5.5 μm^2). Multiple tiles can be acquired to form mosaics. In order to improve the readability of the spectra, the background noise was reduced using the "smooth" tool (set at 11) of the Igor Pro software (Wavemetrics), taking care not to alter any diagnostic information deemed useful to this investigation. In each 2D map, the

intensity of characteristic bands of the gels, or of bronze corrosion products, was imaged. The chromatic scale of the maps shows increasing absorbance of the bands as follows: blue < green < yellow < red.

Cu(II) adsorption kinetics of the semi-IPNs were carried out on 500 mL of copper chloride solutions (10^{-4} M) at two different pH values (6 and 8); the solution at pH 8 was obtained using a phosphate buffer solution. The Cu(II) adsorption at pH 12 was not evaluated owing to the precipitation of copper hydroxide. Pieces of pHEMA/PAA and pHEMA/PVP semi-IPNs were cut (5.0 x 5.0 x 0.2 cm³), dried with blotting paper to remove any excess of surface water, and weighed. Kinetic measurements started when the gel was immersed in the copper chloride solution and, stopped after 180 minutes; this time interval was chosen as it widely covers real application times (generally no more than 2-3 hours). 1 mL aliquots were taken from the solution at set times and analyzed with a Perkin-Elmer Model AAnalyst 100 Flame Atomic Absorption Spectrometer (F-AAS) equipped with a 10 cm air–acetylene burner. The instrument was equipped with a multielement hollow cathode lamp and a deuterium lamp for background correction.

The instrument was operated under the conditions recommended by the manufacturer: lamp current of 30 mA, wavelength of 324.8 nm, slit width of 0.2 nm. The standard solutions and samples were introduced into the flame atomic absorption spectrophotometer by means of a standard nebuliser and flow spoilers. The absorbance of the samples was measured in triplicate against the blank solution and the average of the three measurements was used as the analytical signal. Standard solutions for Cu^{2+} calibration were daily prepared in polyethylene vials by diluting a Cu^{2+} stock standard solution (1000 mg L^{-1}) purchased from Merck (Darmstadt, Germany) with ultrahigh purity water (UHQ) of resistivity >18 MΩ cm (Milli-Q system by Millipore, Billerica, MA).

Bronze mock-ups and cleaning procedure To evaluate the gels' effectiveness, cleaning tests were carried out on an artificially aged bronze coin, which was provided by CNR-ISMN (Rome, Italy). The artificial aging procedure, developed by Ingo et al., produces corrosion patinas that are similar in appearance and composition to those of archeological bronze artifacts [30]. Small sheets of the two gels (1 x 1 x 0.02 cm³) were loaded either with a 20% (w/w) TEPA or with a 9.7% (w/w) EDTA aqueous solution, both at pH 12. EDTA was considered as a reference complexing agent in the restoration practice; 9.7% is the maximum concentration of the compound at pH 12. The gels were applied twice on the coin surface for 45

minutes, covered with parafilm to limit evaporation of fluids from the polymer network. During the application, the strong blue color of the gels indicates the absorption of Cu(II) ions and the formation of Cu(II) complexes. After the treatment, the coin substrate was rinsed with water and air-dried. 2D FTIR Imaging was carried out on the coin surface before and after the application of the gels, checking the presence of corrosion products and gel residues.

RESULTS AND DISCUSSION

FEG-SEM images were acquired to understand how the pH influences the gels' microstructure. At pH 6, pHEMA/PAA semi-IPN has a compact structure and does not exhibit any porosity at the microscale (Figure 1a), while at pH 8 it shows a quite homogeneous porosity in the 7-10 μm range (Figure 1b). A more heterogeneous structure is noted at pH=12, where pores have irregular shape and a broader size distribution (Figure 1c). The pHEMA/PVP semi-IPNs exhibit a macroporosity at pH 6-12 (Figure 1d-f); at pH 12 the pores have elongated shapes and are arranged in rows in a more ordered pattern (Figure 1f). When the gels are loaded with TEPA, the polyethylene amine completely fills the pores, and a plain smooth surface is observed, with no relevant features.
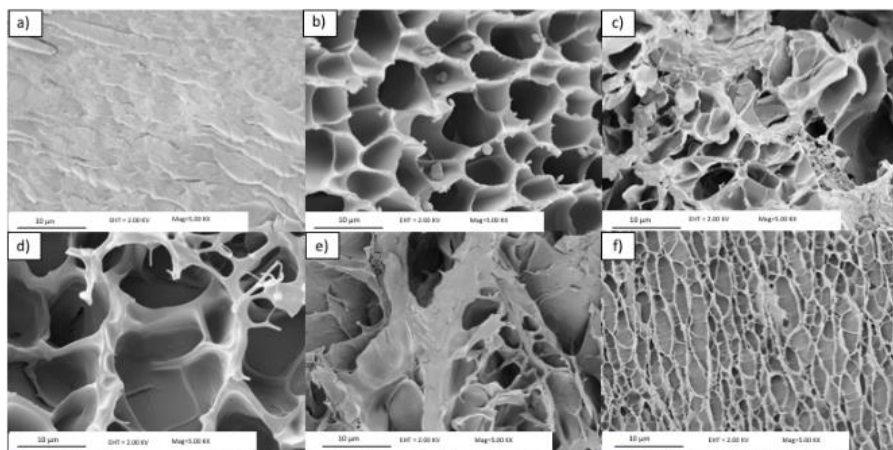
Figure 1. SEM images of pHEMA/PAA and pHEMA/PVP xerogels obtained from the corresponding hydrogels swollen in water at pH 6 (1a, 1d), 8 (1b, 1e), and 12 (1c, 1f). Bar is 10 μm.

Quantitative information about the average pores and walls dimensions were obtained by implementing the chord length distribution analysis. This

method [31] allows to measure the characteristic length scales, λ, of biphasic media. Such measurement is obtained by drawing a set of randomly oriented lines on binarized, frontal SEM micrographs (Figure S1). Chords are defined when a line crosses phase boundaries. The frequency of occurrence of chords of a certain length, f(R), plotted against the chord dimension, R, gives information on the sample morphology and characteristic dimensions. The distributions of the gels' pores and walls for pHEMA/PAA and pHEMA/PVP gels, equilibrated at pH 6, 8 and 12, are shown in Figure 2a-d (pHEMA/PAA gel at pH 6 was not included, being non-porous at the investigated length scales, see Figure 1a). General information about maximum and minimum pore size of each sample can be obtained by observing the intersection of the distributions with the x axis (Figure 2a-d): in pHEMA/PAA gels, chords describing pores extend up to 8 μm ca. at pH 8, and to 9 μm ca. at pH 12; pHEMA/PVP pores, on the other hand, are described by chords whose dimension varies largely with pH: at pH 6 the maximum pores size is 9 μm ca., at pH 8 it increases to 19 μm ca, while at pH 12 it drastically reduces, to 5 μm ca. In pHEMA/PAA gels, the largest walls thickness is 4 μm at pH 8 and 10 μm at pH 12. In pHEMA/PVP, chords describing walls are almost superimposed at pH 6 and 8 (in Figure 2d, data of the sample at pH 6 have been shifted to the right for the sake of clarity), their maximum being around 18 μm at pH 8 and 20 μm at pH 6. pHEMA/PVP at pH 12 has thinner walls, being their maximum dimension around 5 μm.

For all the investigated samples, f(R) of both pores and walls displays a slight initial increase at the first 2-3 points of the curves, followed by one or more exponential decays (Figures 2a-d). Each portion of the curves that showed a clearly observable trend was fitted to equations 3 and 4, focusing in general on the most abundant chord lengths. The variation with pH of the persistence length of pores and walls (λ_{Pores} and λ_{Walls}, obtained from the fittings) is shown for all the investigated samples in Figure 2e and 2f; the values of λ are listed in Table S1-2.

Regarding pore distributions, the pHEMA/PAA gels clearly show two different slopes, describing the trend of smaller and larger pores (Figure 2a and 2e). pH affects only the smaller pores dimension, which is larger at pH 12: the deprotonation of carboxyl groups in PAA is probably leading to an increased electrostatic repulsion and enhanced swelling of the gels' structure. However, the larger pores dimensions are unaffected by the pH increase from 8 to 12. The pHEMA/PVP gels have, in general, larger pores than pHEMA/PAA networks, except at pH 12 (see Figure 2c and 2e); λ increases passing from pH 6 to 8, and decreases at pH 12. The latter behavior could be

explained considering that, at highly alkaline pH values (>> 10), the enol tautomer of PVP is predominant and can lose a proton to form an enolate [32]; the enol and enolate forms are likely to interact tightly, leading to a more shrunk pore network.
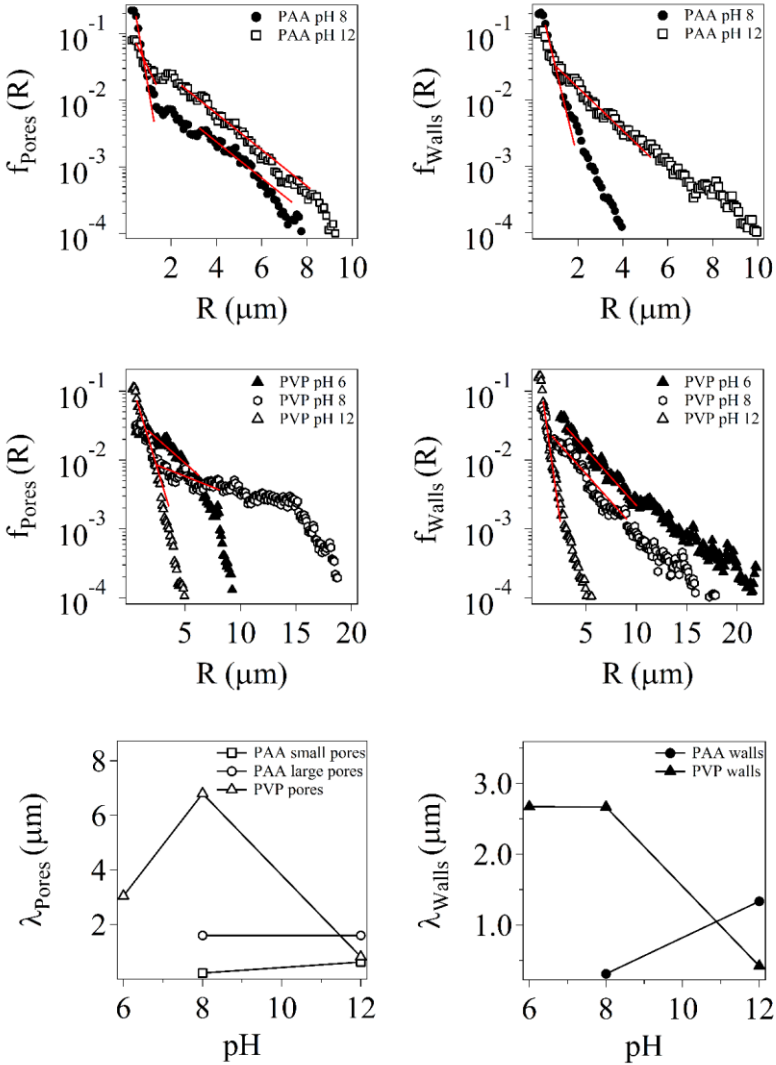
Figure 2. Chord length distributions, f(R), for the pores and the walls of the pHEMA/PAA and pHEMA/PVP gels (panels a-d), and plots of relative persistence lengths (λ, calculated from the curves slopes, see Table S1-2) vs. pH. a,b) pHEMA/PAA gels at pH 8 and 12; c,d) pHEMA/PVP gels at pH 6, 8 and 12; in panel d, the curve of pHEMA/PVP walls at pH 6 is shifted rightwards to improve readability; its x-axis intercept still falls at 20 μm. e,f) Trends of λ (for pores and walls) vs. pH.

Regarding walls size distributions, λ_{Walls} is larger for pHEMA/PVP gels than pHEMA/PAA, again with the exception of the gels at pH 12 (figure 2f). Noticeably, the chord distributions of both pores and walls for pHEMA/PVP gel at pH 12 are characterized by a steep slope: this indicates that pores are elongated, and walls are thin and threadlike, in agreement with the morphology of the porous networks directly observed in the SEM images.

While chord analysis provided quantitative details about the micron-sized porosity of the gels, SAXS experiments were carried out to investigate changes in the nanostructure of the semi-IPNs. In this case, changes could be induced by pH variations, the presence of TEPA, and the co-presence of TEPA and Cu(II) ions (following the application of the gels onto corroded bronze coins). Figure 3 and 4 show respectively the SAXS curves of pHEMA/PAA and pHEMA/PVP hydrogels at pH 6, 8 and 12, and loaded with TEPA or with TEPA and Cu(II) ions, after subtraction of cell contribution. All the SAXS curves were modelled using a generalized version of the Debye-Bueche approach [33], with two q-dependent contributions and an instrumental flat background [34] (Eq.5):

$$I(q) = I_{sol}(q) + I_{ex}(q) + bkg \qquad (5)$$

The first contribution $I_{sol}(q)$ is a generalized version of the Ornstein-Zernicke equation (Eq.6)

$$I_{sol}(q) = \frac{I_{lor}(0)}{[1+(\zeta q)^m]} \qquad (6)$$

where $I_{lor}(0)$ is the scattering intensity at q = 0, dependent from the contrast between the polymer and the solvent and from the volume fraction of the polymer in the gel, ζ is the characteristic average mesh size (or correlation length) of the network, and m is the Porod exponent associated with the solvation term. The second contribution $I_{ex}(q)$ is related to the excess of scattering at low q caused by the solid-like inhomogeneities of the polymeric network (Eq.7):

$$I_{ex}(q) = \frac{I_{ex}(0)}{(1+a^2q^2)^2} \qquad (7)$$

where $I_{ex}(0)$ represents the excess intensity at q = 0 and a is the length scale that characterizes gel inhomogeneities.

The fitting parameters of the SAXS curves of pHEMA/PAA semi-IPNs swollen in water are reported in Table 2. The average mesh size increases moving from pH 6 to pH 12, confirming that the electrostatic repulsion between PAA chains when the carboxyl groups are ionized leads to the stretching of the polymer chains [35]. Consistently, an increase of EWC is observed with increasing pH values, in agreement with other studies where the mesh dimension is strongly related to the equilibrium water content [36]. The Porod exponent has a value of ca. 3.8 for the hydrogel at pH 6, suggesting that the polymer network is collapsed, while at pH 8 and 12 the exponent is around 2.3 for both systems, indicating that the hydrogels are in a theta solvent. The dimension of spatial inhomogeneities increases from 1.7 nm at pH 6 to 7.3 nm at pH 8, and ca. 5 at pH 12, suggesting that the increase in water content (higher EWC) leads to a less homogeneous semi-IPN at the nanoscale [22].

When pHEMA/PAA is loaded with an aqueous solution of TEPA (20%, pH=12) the mesh size and the dimension of solid-like inhomogeneities are smaller than those of gels simply loaded with water at the same pH, while the Porod exponent is slightly higher. These changes are ascribable to interactions between TEPA and the carboxylic groups in PAA, where molecules of TEPA might interpose between chains of PAA, screening the repulsion between carboxylate groups, and making the semi-IPN tighter. A further decrease of the mesh and inhomogeneities size is observed in the presence of copper II ions. Cheng et al. reported a decrease of the radius of gyration (R_g) for a poly(N-isopropylacrylamide) copolymer hydrogel that adsorbed Cu(II), and such change was ascribed to the formation of complexes between the ions and chelating groups in the polymer chains [37]. In our case, the lower mesh is likely due to the formation of complexes between Cu(II) and ionized carboxylic groups of PAA, e.g. each copper ion coordinating with two -COO$^-$ groups from different chains [38]. Besides, a small decrease in the EWC (about 6%) is observed, in agreement with the lower mesh size value [36]. Finally, the increase in the Porod exponent (see Table 2) indicates a transition to a denser aggregate structure.
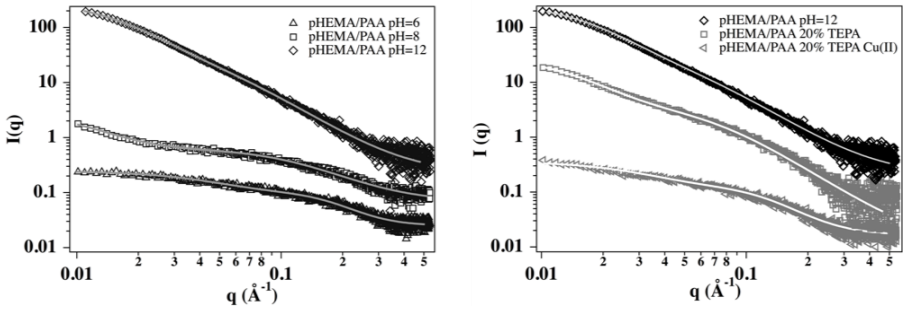
Figure 3. SAXS curves and fitting (grey and white lines) of pHEMA/PAA semi-IPNs swollen in water (left) at pH 6 (triangles), 8 (squares), and 12 (diamonds), and loaded with TEPA (right, grey squares) or TEPA and copper II ions (right, grey triangles).

	pH=6	pH=8	pH=12	20%TEPA	20%TEPA Cu(II)
I_0	1.37 ± 0.05	2.77 ± 0.05	11.15 ± 0.58	9.48 ± 0.19	3.36 ± 0.09
ζ (nm)	0.60 ± 0.01	0.83 ± 0.01	1.82 ± 0.06	1.14 ± 0.02	0.78 ± 0.01
m	3.75 ± 0.16	2.29 ± 0.05	2.34 ± 0.04	2.43 ±0.03	3.33 ± 0.07
I_{ex}	2.67 ± 0.05	13.35 ± 0.96	144.33 ± 0.99	79.30 ± 0.89	7.86 ± 0.17
a (nm)	1.67 ± 0.06	7.28 ± 0.03	4.96 ± 0.05	5.54 ± 0.05	2.52 ± 0.07
bkg	0.44 ± 0.01	0.34 ± 0.01	0.11 ± 0.01	0.03 ± 0.01	0.54 ± 0.01

Table 2. Fitting parameters obtained from SAXS curves of pHEMA/PAA semi-IPNs

Regarding pHEMA/PVP semi-IPNs (see Table 3 and Figure 4), the average mesh size at pH=6 is in agreement with previous studies [22], and remains unchanged at pH=8, while at pH 12 it decreases of about 1 nm, in

agreement with the decrease of the persistence length of pores and walls highlighted by the chord analysis.

As stated above,the formation of enolates in PVP, induced by the high pH, might lead to an enhancement of inter and intramolecular hydrogen bonds with the residual enol groups, resulting in a smaller mesh size and in a more compact structure, as also suggested by the slight increase of the Porod exponent. The gel swollen in a water solution of TEPA (pH=12) exhibits the smallest value of ζ (ca. 2 nm) and the highest value of m (2.7) (see Table 3). When Cu(II) is absorbed in the hydrogel, similarly low values are found. This behavior can be explained considering that enolate groups are able to interact with TEPA molecules and Cu(II) ions, closing together in the formation of complex structures.

Figure 4. SAXS curves and fitting (grey and white lines) of pHEMA/PVP semi-IPNs swollen in water (left) at pH 6 (triangles), 8 (squares), and 12 (diamonds), and loaded with TEPA (right, grey squares) or TEPA and copper II ions (right, grey triangles).
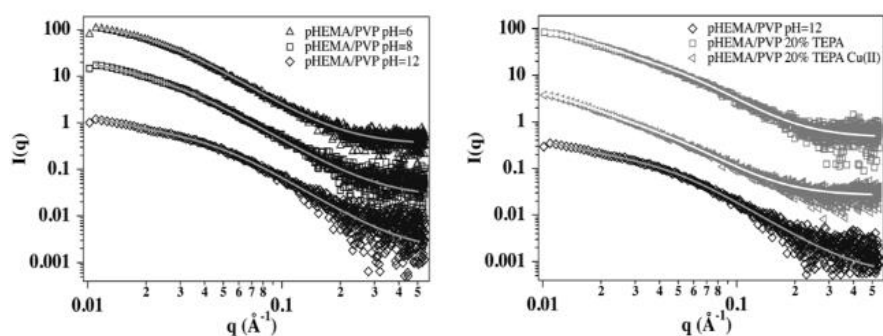
	pH=6		pH=8		pH=12		20%TEPA	20%TEPA Cu(II)
I_0	25.26	±	37.70	±	15.46	±	7.31 ± 0.41	10.78 ± 0.54
	11.3		5.39		0.63			
ζ (nm)	3.43	±	3.81	±	2.34	±	1.94 ± 0.06	2.28 ± 0.07
	0.54		0.23		0.06			
m	2.49	±	2.44	±	2.58	±	2.69 ±0.05	2.61 ± 0.05
	0.03		0.02		0.03			
I_{ex}	68.48	±	62.19	±	34.90	±	46.35	±	89.08 ± 0.98
	8.84		2.92		2.03		0.62	

a (nm)	4.93 ± 0.57	6.85 ± 0.83	6.50 ± 0.37	5.05 ± 0.10	6.15 ± 0.09
bkg	0.20 ± 0.01	0.09 ± 0.01	0.04 ± 0.01	0.20 ± 0.01	0.38 ± 0.01

Table 3. Fitting parameters obtained from SAXS curves of pHEMA/PVP semi-IPNs.

The study of the amount and type of water loaded in the hydrogels provided information on the absorption and permeation properties of these systems. The DSC curves of all the gels are reported in the SI (Figure S2-5). The EWC in pHEMA/PAA semi-IPNs, swollen at different pH, is mainly due to the gels' porosity and the hydrophilic character of PAA. At pH 6, where the carboxylic group are completely protonated, the EWC is about 43% (see Table 4), similar to that of classical pHEMA chemical gels [33, 34], and it increases up to 57 and 79% at pH 8 and 12, owing to the ionization of the carboxyls and to the pores enlargement. When the semi-IPN is loaded with TEPA (pH 12), the solvent content is ca. 76%. After the absorption of Cu(II) this value decreases to 71%, indicating that some free water and TEPA are lost through evaporation during the application of the gel on the bronze coin, despite having covered the gel with parafilm. The FWI values increase in passing from pH 6 to 12 (see Table 4), consistently with the presence of more hydrophilic moieties in the network (carboxylate groups in PAA), and with a higher meso- and macroporosity as shown by SAXS measurements and by the chord analysis implemented on SEM images.

Both the EWC and FWI of the pHEMA/PVP semi-IPNs remain unchanged when the gels are swollen in water at different pH (Table 5). In any case, these parameters have higher values than those of pHEMA/PAA gels, which is explained considering the high relative content of PVP, a highly hydrophilic polymer. The EWC does not change significantly in the presence of TEPA and Cu(II) ions, demonstrating the high hydrophilicity of these systems.

It must be noticed that for both systems there is a significant decrease in the heat of the melting transition (ΔH_{tr}, see Table 4 and 5) when Cu(II) ions are absorbed in the gels. The FWI decreases accordingly. This was explained considering that part of the bulk water molecules coordinate with the metal ions, participating in the formation of complexes.

	pH 6	pH 8	pH 12	TEPA	TEPA Cu
ΔH_{tr} (J/g)	76.5 ± 1.7	154.3 ± 1.27	293.2 ± 6.1	127.4 ± 4.1	109.0 ± 3.1
EWC	42.9% ± 0.9%	56.8% ± 1.1%	79.1 % ± 3.7%	76.3% ± 1.6%	71.3% ± 1.4%
FWI	0.53 ± 0.02	0.81 ± 0.02	1.11 ± 0.07	0.50 ± 0.03	0.46 ± 0.02

Table 4. Data obtained from DSC and TGA analysis of pHEMA/PAA semi-IPNs swollen in water at pH 6, 8, and 12 and in TEPA water solution before and after Cu(II) uptake.

|	pH 6	pH 8	pH 12	TEPA	TEPA Cu
ΔH_{tr} (J/g)	296.1 ± 3.9	317.2 ± 1.1	299.5 ± 5.26	154.6 ± 2.5	133.5 ± 4.1
EWC	88.3% ± 0.5%	89.1% ± 1.3%	89.0% ± 2.1%	86.5% ± 0.01%	85.6% ± 0.8%
FWI	1.01 ± 0.02	1.07 ± 0.02	1.01 ± 0.04	0.54 ± 0.01	0.47 ± 0.02

Table 5. Data obtained from DSC and TGA analysis of pHEMA/PVP semi-IPNs swollen in water at pH 6, 8, and 12 and in TEPA water solution before and after Cu(II) uptake.

Further information on the chemical changes of the semi-IPNs at different pH, and upon loading of TEPA and Cu(II) ions, were provided by FTIR 2D Imaging. At pH 6, the spectra of the pHEMA/PAA semi-IPN exhibit features typical of reflective surfaces, with derivative-shaped peaks and distorsions (see Figure 5). In particular, the OH stretching and CH stretching bands of pHEMA and PAA are not observable, and the main peaks are those of C=O stretching (derivative shape, maximum at 1745 cm^{-1}), CH$_2$ bending (1496 cm^{-1}), C-O stretching (1294 cm^{-1}), and C-O-C stretching

(derivative shape, maximum at 1197 cm⁻¹, and 1092 cm⁻¹)[35, 36]. At alkaline pH values the spectra change significantly, and their aspect resemble much more closely that of standard transmission spectra. This indicates that a change in the refractive index of the gel has occurred, following the neutralization of the carboxyl groups in PAA and the rearrangement of the polymer chains. Both the OH and CH stretching bands are clearly observable, and the C=O stretching peak shows two components around 1740 (pHEMA) and 1715 (PAA) cm⁻¹ [35, 36]. The spectra show a new peak at 1578 cm⁻¹, assigned to the antysimmetric stretching of the –COO⁻ groups in PAA, whose intensity increases passing from pH 8 to pH 12 (as shown in the FTIR maps in Figure 5). Besides, while at pH 8 the carboxylate groups concentrate in domains ranging from tens to hundreds of microns, at pH 12 they are homogeneously distributed across the gel matrix.
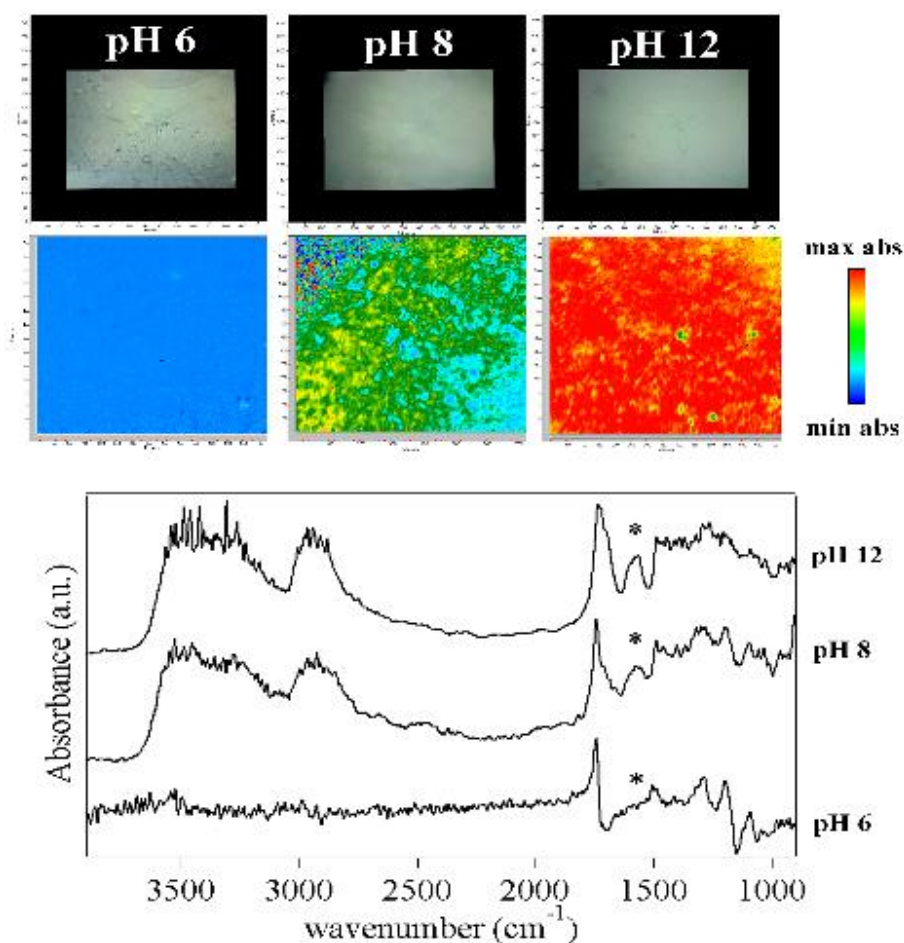
Figure 5 FTIR 2D Imaging of pHEMA/PAA xerogels obtained from hydrogels that were swollen with water at different pH values. Below each

visible image, the corresponding 2D FTIR Imaging map shows the intensity of the band at 1578 cm^{-1} (-COO$^-$ antysimmetric stretching of carboxylate groups in PAA). All maps have dimensions of 700 x 700 μm^2, each axis tick being 50 μm. The bottom panel shows representative spectra of pixels (5.5 x 5.5 μm^2) in the corresponding 2D Imaging map.

Figure 6 shows the FTIR 2D imaging of pHEMA/PAA xerogels obtained from semi-IPNs loaded with TEPA. Loading with the polyethylene amine changes the refractive index of the gels, which show again strongly derivative-shaped C=O and C-O-C stretching bands. The most relevant feature is a composite band that shows two maxima at 1660 and 1610 cm^{-1}. The latter is ascribed to the NH deformation of primary amine in TEPA [43], while the first component can be assigned to the stretching vibration of the carboxylic groups in PAA, when they are neutralized by a polyethylene amine [44]. Namely, the amine group of TEPA interacts with the acid sites of PAA, interfering with the interchain hydrogen bonds; the H atom of the carboxylic group is included in the amine groups, and the carboxylate vibration is shifted to a higher wavenumber with respect to the gels swollen in water solutions at the same pH. As shown by the 2D Imaging maps, in the presence of Cu(II) ions, the peak is no longer clearly observable, all across the gel's surface. Our hypothesis is that the carboxylate vibration is either shifted back to lower wavenumbers (convoluting with the TEPA NH deformation band), or its intensity is decreased, following the formation of a ternary polymer-metal complex by both PAA and TEPA with the copper ions. In fact, Kabanov et al. [45] reported the formation of mixed Cu(II) complexes formed by PAA and polyethylene imines (PEI), where two coordination sites are covered by PAA carboxylates, and two by amine groups. A similar behavior might occur in the case of the PAA-Cu-TEPA complex.
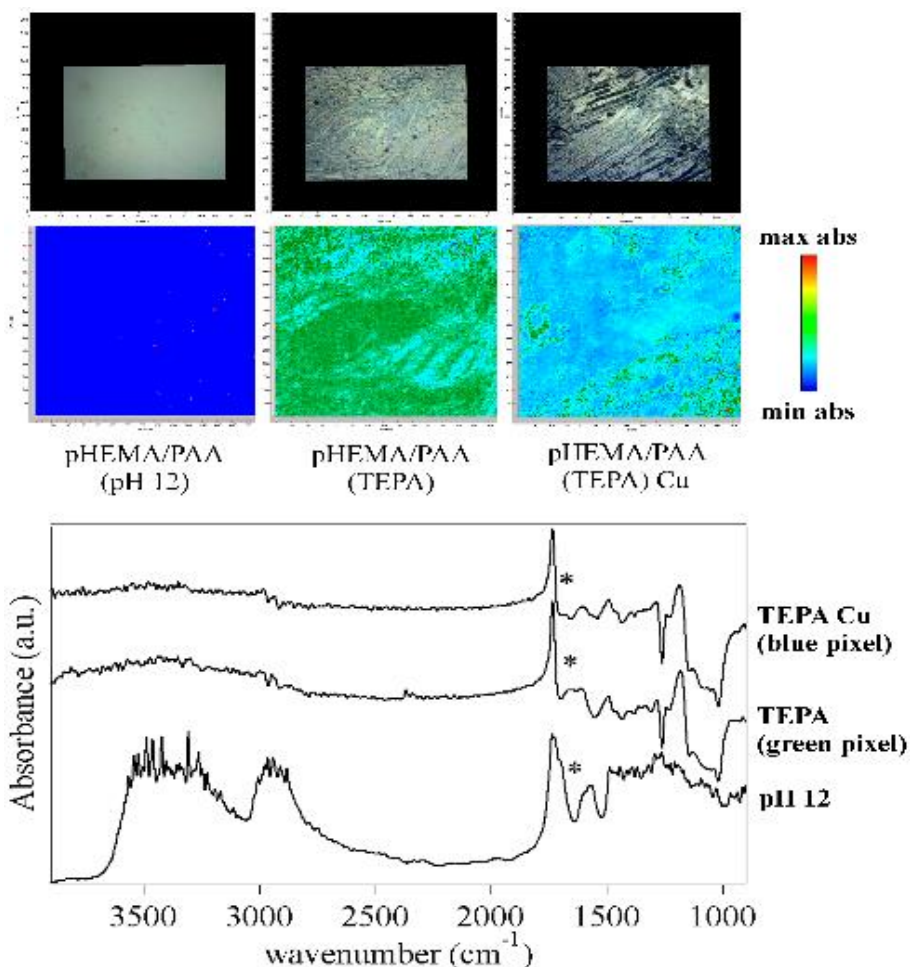
Figure 6. (Top) FTIR 2D Imaging of xerogels obtained from pHEMA/PAA hydrogels: (top left) swollen with water at pH 12; (top center) xerogels obtained from gels swollen with a TEPA solution (20%); (top right) xerogels obtained from gels that were swollen with the TEPA solution and then placed on a bronze coin mock-up containing Cu(II) corrosion products. Below each visible image, the corresponding 2D FTIR Imaging map shows the intensity of the band at 1660 cm^{-1} (assigned to the $-COO^-$ antysimmetric stretching of carboxylate groups in PAA). All maps have dimensions of 700 x 700 μm^2, each axis tick being 50 μm. The bottom panel shows representative spectra of pixels (5.5 x 5.5 μm^2) in the corresponding 2D Imaging map.

Figure 7 shows the FTIR 2D imaging of pHEMA/PVP xerogels obtained from gels swollen in water at different pH values. All the main absorptions of the two polymers are clearly observable [35, 40], however a band at 1578

cm^{-1} progressively emerges when pH passes from 6 to 8 and 12, as evidenced in the 2D Imaging maps. This band could be assigned either to a combination of O-H and C-H bending [47], or to the presence of an enolate ion, even if the latter would be expected at slightly higher wavenumbers. In fact, as previously reported, the enolate form of the enol structure of PVP becomes more stable at pH >> 10 [32]. It must be noticed that the carbonyl band of the lactam form of PVP is also observable at 1655 cm^{-1}.
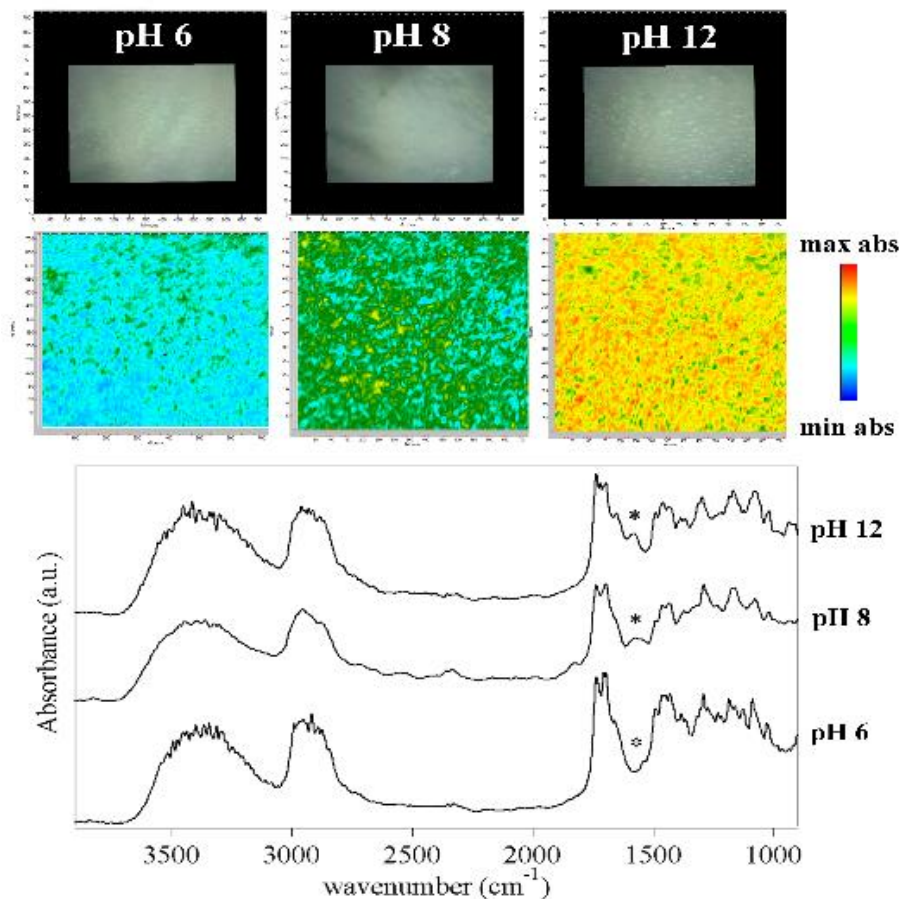
Figure 7. FTIR 2D Imaging of pHEMA/PVP xerogels obtained from hydrogels that were swollen with water at different pH values. Below each visible image, the corresponding 2D FTIR Imaging map shows the intensity of the band at 1578 cm^{-1} (assigned to the stretching of enolate ions in PVP). All maps have dimensions of 700 x 700 μm², each axis tick being 50 μm. The bottom panel shows representative spectra of pixels (5.5 x 5.5 μm²) in the corresponding 2D Imaging map.

When TEPA is uploaded in the pHEMA/PVP gels, an inhomogeneous pattern is observed in the FTIR 2D Imaging maps of the absorbance intensity in the 1615-1535 cm^{-1} region (see Figure 8). In the main portion of the maps (yellow-red pixels), the NH deformation band of TEPA at 1600 cm^{-1} is clearly observable, as part of a derivative peak whose flexus falls at ca. 1580 cm^{-1}. This band likely includes the contribution from enolate groups in PVP. In some portions (green pixels), no band around 1600 cm^{-1} is detected; instead, a shoulder to the PVP carbonyl peak is observed at ca. 1620 cm^{-1}, along with a derivative band with a maximum at 1500 cm^{-1} and a flexus at ca. 1485 cm^{-1}. We assigned the shoulder to the TEPA NH band (shifted upwards), and the derivative band to the enolate (shifted downwards) and CH$_2$ vibrations. The bands shifts were ascribed to interactions between the amine groups in TEPA and polar or charged CO groups in PVP. When Cu(II) ions are uploaded in the gel, the shifts are observed in significantly larger portions of the maps, which show a majority of green pixels. It is known that PVP is able to coordinate with copper through the O atom rather than N [48]. Therefore, we hypothesized that the interactions between PVP and TEPA are favored by the coordination of Cu(II) with CO groups and amines, which come close together while binding to the ions.
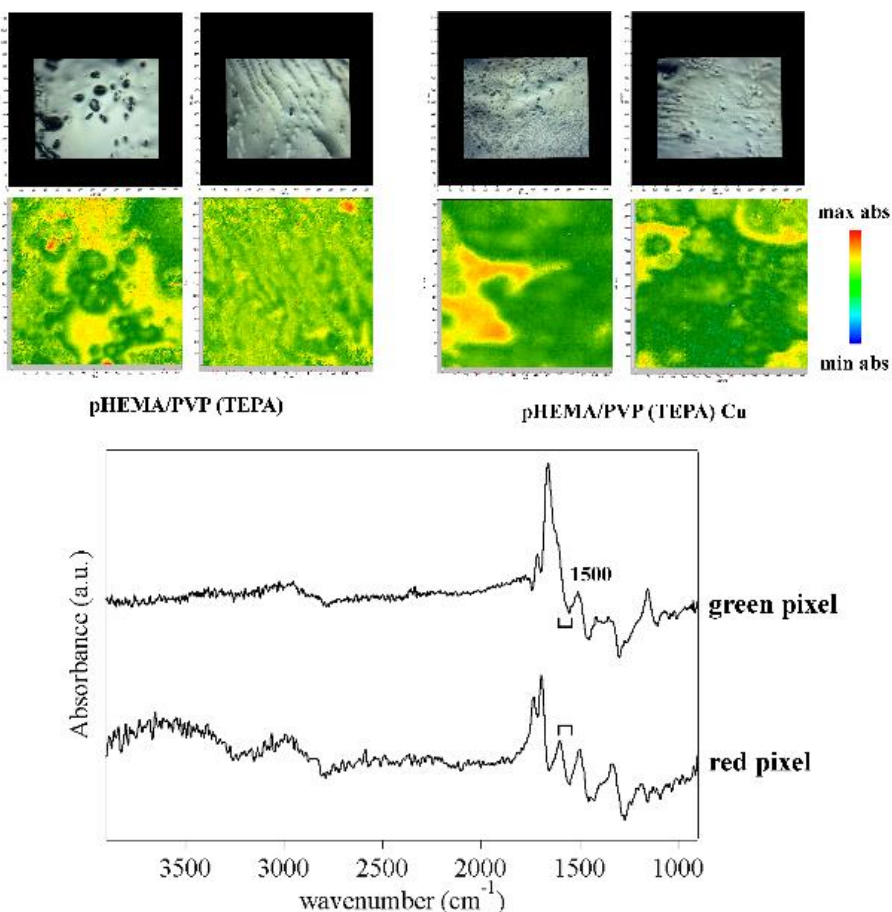
Figure 8. (Top, left panels) FTIR 2D Imaging of xerogels obtained from pHEMA/PVP hydrogels swollen with a TEPA solution (20%); (Top, right panels) xerogels obtained from gels that were swollen with the TEPA solution and then placed on a bronze coin mock-up containing Cu(II) corrosion products. Below each visible image, the corresponding 2D FTIR Imaging map shows the intensity of the 1615-1535 cm^{-1} region. All maps have dimensions of 700 x 700 μm², each axis tick being 50 μm. The bottom panel shows representative spectra of high (red) or low (green) intensity pixels (5.5 x 5.5 μm²) in the corresponding 2D Imaging map.

Adsorption kinetics highlighted the specific effect of the different semi-IPNs' structures and functional groups on the uptake of Cu(II) ions. Figure 9 summarizes the trend of q (grams of solute sorbed per gram of sorbent) over time for the pHEMA/PAA and pHEMA/PVP semi-IPNs at pH 6 and 8. The first observable feature is that the values of q moving towards the equilibrium value (q_e) clearly follow the trend PAA_pH 8 > PAA_pH 6 >

PVP_pH 8 > PVP_pH 6. This confirms that the presence of carboxylate (in PAA) and enolate groups (in PVP) is a major drive to Cu(II) complexation by the semi-IPNs, and the effect of alkalinity on the increase of q is even more pronounced for PVP than PAA. The second notable feature regards the first stages of the adsorption kinetics, where steeper curves are observed for the pHEMA/PAA semi-IPNs; namely, pHEMA/PAA at pH 6 has the steepest initial increase.

Figure 9. Plots of q (grams of solute sorbed per gram of sorbent) over time for the uptake of Cu(II) ions by the pHEMA/PAA (squares) and pHEMA/PVP (triangles) semi-IPNs at pH 6 (empty markers) and 8 (full markers).

The uptake curves of materials are traditionally fitted to two types of equations, i.e. diffusion-controlled models (intraparticle diffusion, IPD [43–46], diffusion-adsorption [53], adsorption dynamic intraparticle model [54]) and adsorption-controlled kinetics. In the latter case, both pseudo-first (K1) and pseudo-second order (K2) kinetics are generally proposed and critically compared. For instance, Azizian derived both K1 and K2 equations independently, and concluded that the initial concentration of solute (C_0) determines the kinetic regime, e.g. K1 provides the best fit when C_0 is very high compared to the coverage of available sites in the sorbent (θ), while K2 fits adsorption curves better when C_0 is not too high with respect to θ [55]. However, as reported in the literature [50–52], obtaining a good fit of the

experimental data is not sufficient to validate the fitting model as the underlying mechanism: the literature reports several cases where significant contribution of diffusion, up to being the rate-controlling step, was recognized for data sets well fitted by K2 [47, 48, 50, 53–55].

Taking into account these considerations, we fitted the adsorption curves of the two semi-IPNs at pH 6 and 8 to K1, K2, and IPD models reported in the literature [56]. In order to obtain statistically relevant comparisons, we used the fitting models on the original scale ($y = q(t)$) rather than adopting transformed scales or linearized equations [50, 56, 57]. The models equations, the full set of fitted curves and the fitting parameters (rate constants k, q_e and chi-square values) are reported in the SI file (TableS3-6, FigureS6-9).

In the case of pHEMA/PAA semi-IPNs at pH 6, the pseudo-second order model provides a better fit than pseudo-first (K2>K1, see Figure S6; the K2 fit is shown in Figure 10), even though both K1 and K2 underestimate the uptake in the first part of the process. Instead, the IPD model provides a very good fit of the experimental data, but it does not account well for the uptake decrease in the final stages (see Figure S6 and inset in Figure 10). Overall, as recently reported by Simonin, this behavior suggests a process where a fast initial step limited by diffusion is followed by a slower second step, limited by diffusion in smaller pores or by slow adsorption [56]. This can be explained considering that initially the binding of Cu(II) at carboxylate (and to a lower extent carboxylic) sites is fast, and the rate-controlling step is the diffusion of the ions through the gel, while in the second stage diffusion in smaller pores and binding at less available sites control the process. In fact, at pH 8 the IPD equation fits only the first minutes of the uptake, and overall K2>K1>IPD (see Figure S7 and inset in Figure 10), while at pH 6 the contribution of diffusion seems to be more significant; this is in good agreement with the much smaller porosity exhibited by the pHEMA/PAA gel before carboxylic groups are deprotonated.
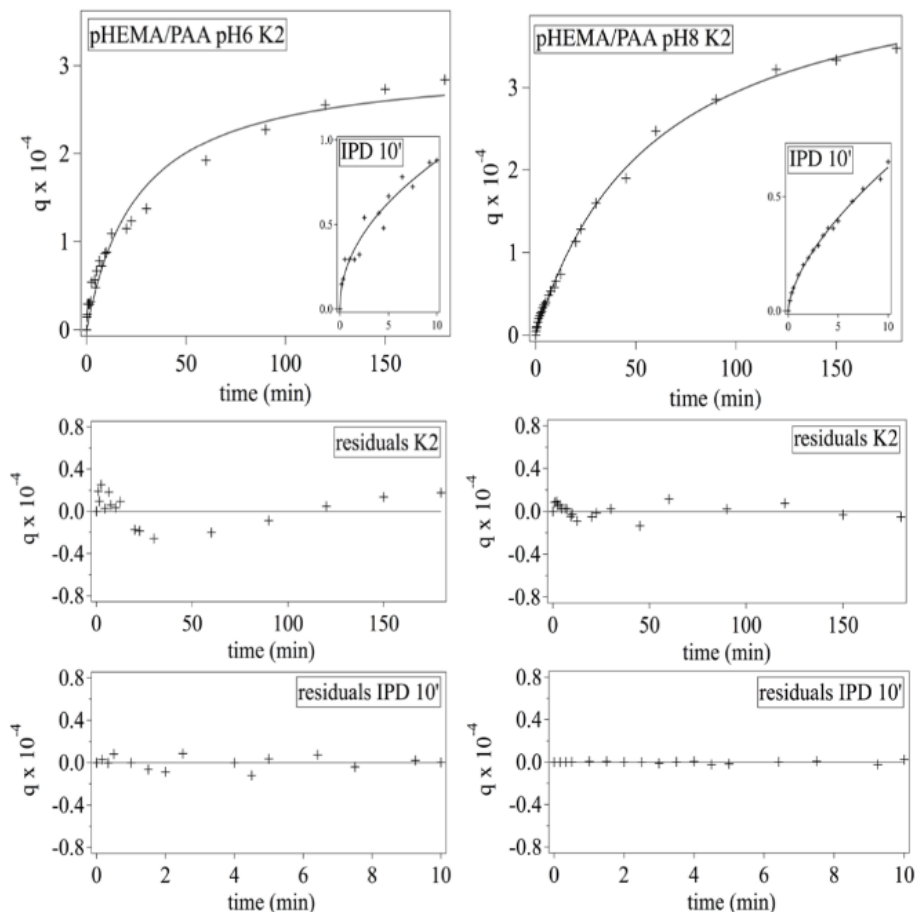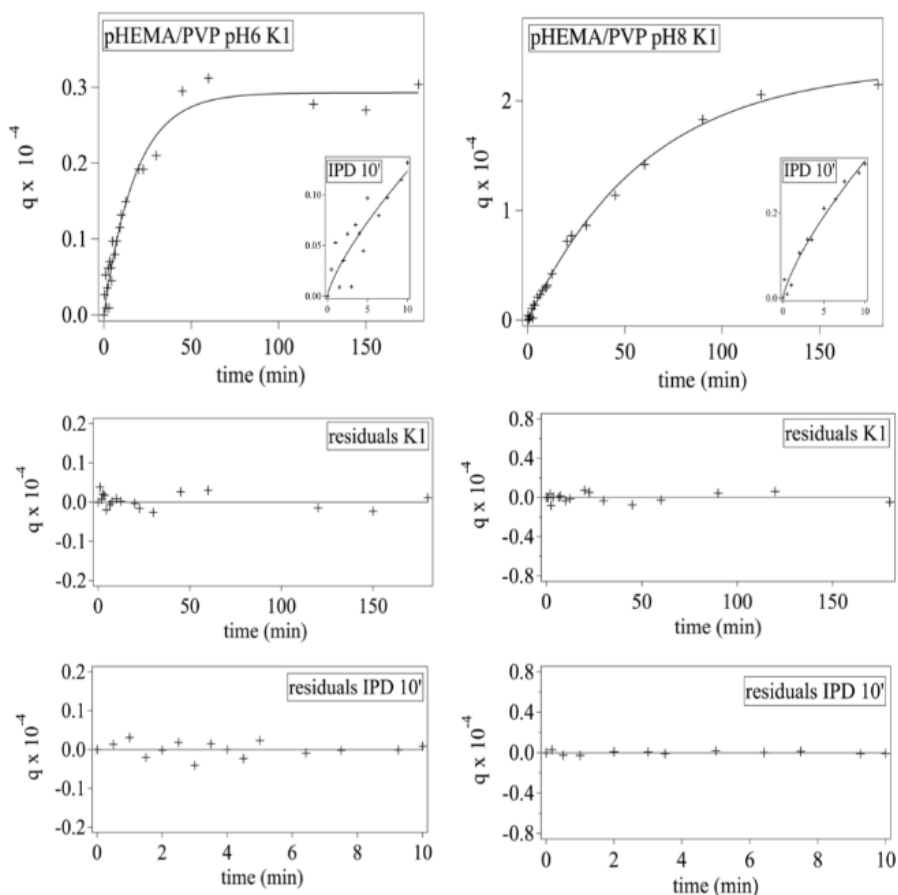
Figure 10. Plots of q (grams of solute sorbed per gram of sorbent) and residuals over time for the uptake of Cu(II) ions by the pHEMA/PAA semi-IPNs at pH 6 and 8. The full uptake curves (0-180 min) are fitted to the pseudo-second order kinetic model (K2), while the insets show the fitting of the first process stages (0-10 min) to the intraparticle diffusion model (IPD).

For pHEMA/PVP semi-IPNs, in general K1>K2>IPD at pH 6 and 8 (see Figure S8 and S9; the K1 fit is shown in Figure 11). The IPD model provides significantly worse fittings of the whole curves than for pHEMA/PAA, even though the first stages are fitted reasonably well (see insets in Figure 11). In this case, considering the porogen role of PVP in the semi-IPN network, the contribution of diffusion was indeed expected to be more limited.

Figure 11. Plots of q (grams of solute sorbed per gram of sorbent) over time for the uptake of Cu(II) ions by the pHEMA/PVP semi-IPNs at pH 6 and 8. The full uptake curves (0-180 min) are fitted to the pseudo-first order kinetic model (K1), while the insets show the fitting of the first process stages (0-10 min) to the intraparticle diffusion model (IPD).

Overall, the analysis of the curves confirmed the importance of pH control to boost the uptake of Cu(II) ions, and indicated that the ion-matrix interaction is stronger for pHEMA/PAA than pHEMA/PVP.

Figures 12 and 13 show the results of the application of semi-IPNs loaded with TEPA on the surface of a bronze coin that was artificially aged to mimic archaeological bronze artifacts. After aging, the coin surface is covered with a thick and heterogeneous green patina of copper oxychlorides, which show characteristic IR bands between 3550 and 3300 cm-1 (OH stretching) and at 950 cm-1 [64]. The application of the gels led to the progressive removal of the oxychlorides, preserving the inner red layer

(whose color is indicative of cuprite, Cu_2O [65]) inhomogeneously present over the surface. The possibility of controlling the cleaning action, thanks to the use of retentive semi-IPNs, is advantageous from an applicative standpoint; in fact, cuprite can be considered as a protective layer against further corrosion, as it passivates the surface. Where cuprite was not present, the cleaning intervention brought back the bronze surface, and whitish patinas of calcium carbonate (identified thanks to characteristic IR bands at 2512, 1793 and 1463 cm^{-1} [66]) that can eventually be removed using a complexing agent selective for calcium. 2D FTIR imaging confirmed the removal of copper oxychlorides at the micron scale (see Figure 10), down to the detection limit of the instrument (< 1 pg/pixel; 1 pixel = 5.5 x 5.5 µm² [67]). It must be noticed that semi-IPNs of pHEMA/PVP and pHEMA/PAA loaded with TEPA were equally effective in terms of cleaning power and duration of the intervention. In principle, pHEMA/PAA might be expected to remove copper corrosion products more efficiently, owing to the stronger complexing strength of carboxylate groups in PAA as compared to carbonyls in PVP. However, pHEMA/PVP gels have higher ESC, thanks to the hydrophilicity of PVP. Both formulations performed better than semi-IPNs loaded with EDTA (see Figure 12), as expected given the much higher stability constant of TEPA-Cu(II) complexes than those with EDTA.
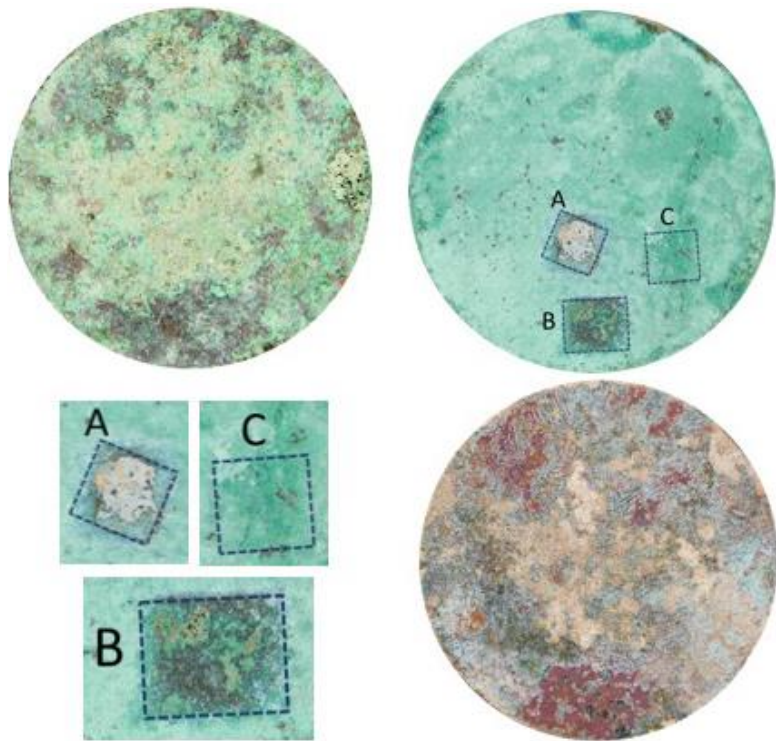
Figure 12. Artificially aged bronze coin before (top left) and after (bottom right) cleaning with semi-IPNs loaded with TEPA. The application of the gels (two cleaning rounds, 45 minutes each) led to the removal of the green corrosion products (copper oxychlorides), preserving the red cuprite layer that is inhomogeneously present on the coin surface. In some portions, whitish patinas composed of calcium carbonate were present beneath the oxychlorides layer. (Top right, bottom left) Preliminary cleaning tests detailing the progressive removal of corrosion products after the application of semi-IPNs loaded with TEPA for 1 hour (A) or 20 minutes (B). The application of a semi-IPN loaded with EDTA for 1 hour (C) did not remove the corrosion products.
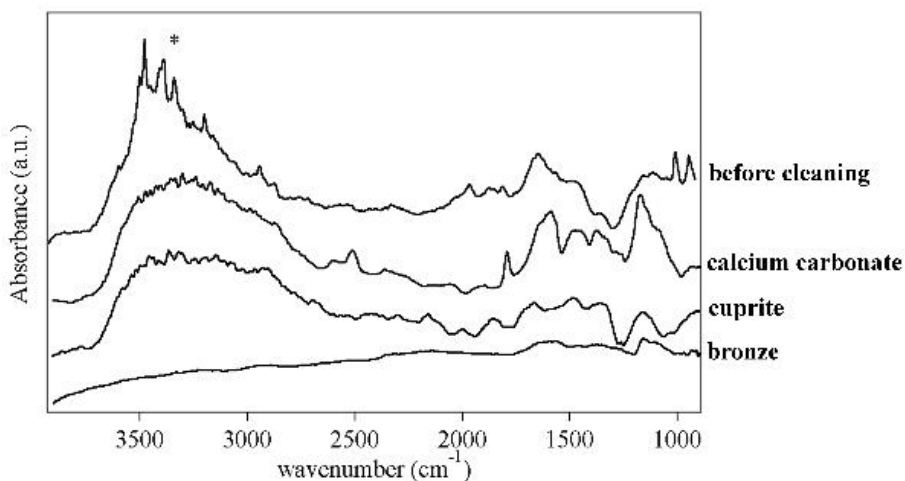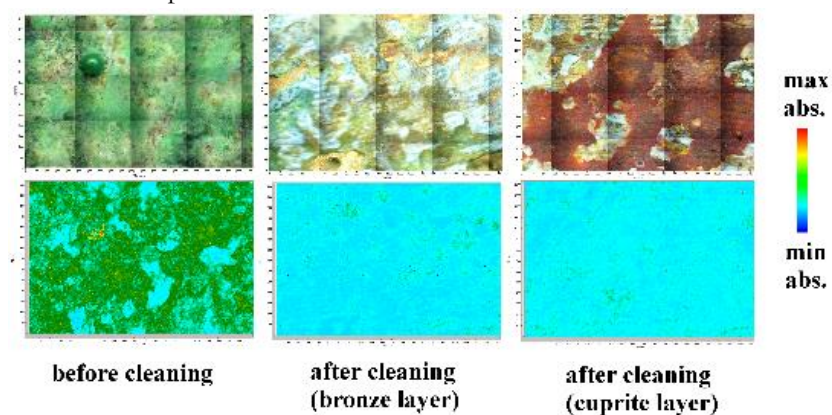
Figure 13. FTIR 2D Imaging of an artificially aged bronze coin before (top, left panel) and after (top, center and right panel) the application of a pHEMA/PVP semi-IPN loaded with TEPA. Below each visible image, the corresponding 2D FTIR Imaging map shows the intensity of the band between 3550 and 3300 cm^{-1} (stretching of OH groups in Cu(II)

oxychlorides). All maps have dimensions of 1400 x 2000 μm^2, each axis tick being 50 μm. The bottom panel shows representative spectra of pixels (5.5 x 5.5 μm^2) in the corresponding 2D Imaging maps, from bottom to top: the cleaned bronze surface, the red layer of cuprite, calcium carbonate patinas, and copper oxychlorides (atacamite, paratacamite).

CONCLUSIONS

A pHEMA/PAA semi-IPN was formulated for the first time uploading aqueous solutions at different pH values, and was compared with a pHEMA/PVP semi-IPN. Solutions of TEPA were uploaded in the two semi-IPNs to remove corrosion products from aged bronze coins.

Increasing the pH induces changes in the gels' structure. In the case of pHEMA/PAA, carboxyls in the PAA chains are progressively ionized, as confirmed by 2D FTIR imaging. This results in the swelling of the polymer network, evidenced by an increase in the meso- and macroporosity, and in the amount of free water uploaded in the gels. TEPA molecules interact with carboxyls in PAA, making the semi-IPN tighter (lower mesh size) by screening the repulsion between carboxylate groups. When Cu(II) ions are absorbed in the TEPA-loaded network, ternary PAA-Cu-TEPA complexes are probably formed, where two coordination sites are covered by PAA carboxylates, and two by amine groups. For what concerns pHEMA/PVP semi-IPNs, increasing the pH progressively leads to the partial abstraction of protons from the alcohol group in the enol form of PVP. Significant changes in the macroporosity are observed at each pH variation step (6; 8; 12), with a neat decrease in pores size when pH 12 is reached.. Also the mesoporosity decreases at high pH values, as the inter and intramolecular hydrogen bonds between enol and enolate groups in the PVP chains likely cause a decrease in the mesh size. FTIR 2D Imaging let us hypothesize that the interactions between polar or charged CO groups of PVP and TEPA are favored by the formation of ternary complexes with Cu(II) ions, where CO and amine groups come close together while binding to the metal.

For the same pH values, the interaction of Cu(II) ions with the gel matrix is stronger in the case of pHEMA/PAA, leading to higher amounts of ions sorbed as compared to pHEMA/PVP. In all cases, the uptake process seems to be constituted by a fast initial adsorption step controlled by diffusion of the ions in the network, followed by a second stage controlled by diffusion in smaller pores or adsorption at less available sites. As

expected, the contribution of diffusion is more significant in the case of pHEMA/PAA at pH 6, while at higher pH values the deprotonation of carboxyls increases the macro- and mesoporosity, favoring the diffusion of ions.

Even though loading with alkaline solutions of water and TEPA changes the micro- and nanostructure of the gels, it does not hinder their applicability for the removal of corrosion products from bronze surfaces. When the TEPA-loaded gels are applied onto corroded bronze coins, they gradually release the polyamine solution on the surface, solubilizing and removing the Cu(II) oxychlorides in the corrosion layers. The dissolved copper ions migrate into the gels and form complexes, which gives the gels an intense blue color. Both pHEMA/PAA and pHEMA/PVP allowed an effective and controlled removal of corrosion products, while preserving the inner red corrosion layer (cuprite) that is normally left on bronze artifacts as a passivation layer against recurring corrosion. Loading with TEPA dramatically enhanced the cleaning power of the gels as opposed to EDTA, strongly decreasing the time needed for the intervention.

Overall, TEPA-loaded semi-IPNs of pHEMA/PAA and pHEMA/PVP proved to be promising tools for the preservation of archaeological and historical bronze artifacts, overcoming the limitations of traditional restoration practice based on the use of EDTA solutions and mechanical cleaning.

Author contributions

The manuscript was written through contributions of all authors. All authors have given approval to the final version of the manuscript. Teresa Guaragnone and Marta Rossi contributed equally to this work.

Notes

The authors declare no competing financial interest.

REFERENCES

[1]   C. Dümcke and M. Gnedovsky, "The Social and Economic Value of Cultural Heritage: literature review," *Eur. Expert Netw. Cult.*, 2013.

[2]   D. A. Scott, "A review of copper chlorides and related salts in bronze corrosion and as painting pigments," *Studies in Conservation*. 2000, doi: 10.1179/sic.2000.45.1.39.

[3]   G. M. Ingo, S. Balbi, T. De Caro, I. Fragalà, E. Angelini, and G. Bultrini, "Combined use of SEM-EDS, OM and XRD for the characterization of corrosion products grown on silver roman coins," *Appl. Phys. A Mater. Sci. Process.*, 2006, doi: 10.1007/s00339-006-3533-0.

[4]   C. Degrigny, "Survey of European Experience on Cleaning Procedures," in *Monumenti in bronzo all'aperto. Esperienze a confronto.*, 2004.

[5]   D. A. Scott, *Copper and bronze in art*. The Getty Conservation Institute, 2002.

[6]   S. Siano *et al.*, "Laser cleaning in conservation of stone, metal, and painted artifacts: State of the art and new insights on the use of the Nd:YAG lasers," *Appl. Phys. A Mater. Sci. Process.*, 2012, doi: 10.1007/s00339-011-6690-8.

[7]   P. Baglioni, D. Chelazzi, and R. Giorgi, *Nanotechnologies in the Conservation of Cultural Heritage*. 2015.

[8]   D. Chelazzi, R. Giorgi, and P. Baglioni, "Microemulsions, Micelles, and Functional Gels: How Colloids and Soft Matter Preserve Works of Art," *Angewandte Chemie - International Edition*. 2018, doi: 10.1002/anie.201710711.

[9]   P. Baglioni, D. Chelazzi, R. Giorgi, and G. Poggi, "Colloid and materials science for the conservation of cultural heritage: Cleaning, consolidation, and deacidification," *Langmuir*, 2013, doi: 10.1021/la304456n.

[10]   P. Baglioni, E. Carretti, and D. Chelazzi, "Nanomaterials in art conservation," *Nature Nanotechnology*. 2015, doi: 10.1038/nnano.2015.38.

[11]   E. Carretti *et al.*, "New frontiers in materials science for art conservation: Responsive gels and beyond," *Acc. Chem. Res.*, 2010, doi: 10.1021/ar900282h.

[12]   N. Bonelli, C. Montis, A. Mirabile, D. Berti, and P. Baglioni, "Restoration of paper artworks with microemulsions confined in hydrogels for safe and efficient removal of adhesive tapes," *Proc. Natl. Acad. Sci.*, vol. 115, no. 3, pp. 5932–5937, 2018.

[13]   M. Baglioni *et al.*, "Complex Fluids Confined into Semi-interpenetrated Chemical Hydrogels for the Cleaning of Classic Art: A Rheological and SAXS Study," *ACS Appl. Mater. Interfaces*, vol. 10, pp. 19162–19172, 2018.

[14]   M. Baglioni *et al.*, "Nanomaterials for the cleaning and pH adjustment of vegetable-tanned leather," *Appl. Phys. A Mater. Sci. Process.*, vol. 122, no. 114, 2016.

[15]   T. Guaragnone, A. Casini, D. Chelazzi, and R. Giorgi, "PVA-based peelable films loaded with tetraethylenepentamine for the removal of corrosion products from bronze," *Appl. Mater. Today*, 2020, doi: 10.1016/j.apmt.2019.100549.

[16]   E. Díaz, R. B. Valenciano, and I. A. Katime, "Study of complexes of poly(vinyl pyrrolidone) with copper and cobalt on solid state," *J. Appl. Polym. Sci.*, 2004, doi: 10.1002/app.20620.

[17]   N. Sebastian, B. George, and B. Mathew, "Metal complexes of poly(acrylic acid): Synthesis, characterization and thermogravimetric studies," *Polym. Degrad. Stab.*, 1998, doi: 10.1016/s0141-3910(97)00095-5.

[18]   J. E. Elliott, M. MacDonald, J. Nie, and C. N. Bowman, "Structure and swelling of poly(acrylic acid) hydrogels: Effect of pH, ionic strength, and dilution on the crosslinked polymer structure," *Polymer (Guildf).*, 2004, doi: 10.1016/j.polymer.2003.12.040.

[19]   A. Martell, Ed., *Critical Stability Constant - Vol. 2: Amines*. Springer US, 1975.

[20]   A. E. Comyns, "Handbook of Copper Compounds and Applications. H.W. Richardson (ed.) Marcel Dekker, New York, 1997 viii?+?432 pages $175 ISBN 0-8247-8998-9," *Appl. Organomet. Chem.*, 2000, doi: 10.1002/(sici)1099-0739(200003)14:3<174::aid-aoc940>3.0.co;2-g.

[21]   J. L. Schrenk, *Ancient & Historic Metals. Conservation and Scientific Research.* 1993.

[22]   J. A. L. Domingues, N. Bonelli, R. Giorgi, E. Fratini, F. Gorel, and P. Baglioni, "Innovative hydrogels based on semi-interpenetrating p(HEMA)/PVP networks for the cleaning of water-sensitive cultural heritage artifacts," *Langmuir*, 2013, doi: 10.1021/la3048664.

[23]   B. D. Fecchio, S. R. Valandro, M. G. Neumann, and C. C. S. Cavalheiro, "Thermal decomposition of polymer/montmorillonite nanocomposites synthesized in situ on a clay surface," *J. Braz. Chem. Soc.*, 2016, doi: 10.5935/0103-5053.20150216.

[24]   F. Müller-Plathe, "Different states of water in hydrogels?," *Macromolecules*, 1998, doi: 10.1021/ma980685b.

[25]   A. K. Lele, M. M. Hirve, M. V. Badiger, and R. A. Mashelkar, "Predictions of bound water content in poly(N-isopropylacrylamide) gel," *Macromolecules*, 1997, doi: 10.1021/ma950894l.

[26]   P. A. Bhagwan, *A Handbook of Thermodynamics*. Mittal Publications.

[27]   M. R. MacIver and M. Pawlik, "Analysis of In Situ Microscopy Images of Flocculated Sediment Volumes," *Chem. Eng. Technol.*, 2017, doi: 10.1002/ceat.201600523.

[28]   P. Levitz, "Toolbox for 3D imaging and modeling of porous media: Relationship with transport properties," *Cem. Concr. Res.*, 2007, doi: 10.1016/j.cemconres.2006.08.004.

[29]   T. Blanton *et al.*, "JCPDS-International Centre for Diffraction Data Low-Angle Powder Diffraction Study of Silver Behenate," *Adv. X-ray Anal.*, 1994, doi: 10.1154/s0376030800017699.

[30]   G. M. Ingo, C. Riccucci, G. Guida, M. Albini, C. Giuliani, and G. Di Carlo, "Rebuilding of the Burial Environment from the Chemical Biography of Archeological Copper-Based Artifacts," *ACS Omega*, 2019, doi: 10.1021/acsomega.9b00569.

[31]   P. Levitz and D. Tchoubar, "Disordered porous solids : from chord distributions to small angle scattering," *J. Phys. I*, 1992, doi: 10.1051/jp1:1992174.

[32]   T. E. Nikiforova, V. A. Kozlov, and M. K. Islyaikin, "Acid-base interactions and complex formation while recovering copper(II) ions from aqueous solutions using cellulose adsorbent in the presence of polyvinylpyrrolidone," *Russ. J. Phys. Chem. A*, 2012, doi: 10.1134/S0036024412120199.

[33]   P. Debye and A. M. Bueche, "Scattering by an inhomogeneous solid," *J. Appl. Phys.*, 1949, doi: 10.1063/1.1698419.

[34]   F. Horkay and B. Hammouda, "Small-angle neutron scattering from typical synthetic and biopolymer solutions," *Colloid and Polymer Science*. 2008, doi: 10.1007/s00396-008-1849-3.

[35]   W. Wang *et al.*, "Interactions among spherical poly(acrylic acid) brushes: Observation by rheology and small angle X-ray scattering," *J. Polym. Sci. Part B Polym. Phys.*, 2016, doi: 10.1002/polb.23901.

[36]   T. Canal and N. A. Peppas, "Correlation between mesh size and equilibrium degree of swelling of polymeric networks," *J. Biomed. Mater. Res.*, 1989, doi: 10.1002/jbm.820231007.

[37]   J. Cheng, G. Shan, and P. Pan, "Temperature and pH-dependent swelling and copper(ii) adsorption of poly(N-isopropylacrylamide) copolymer hydrogel," *RSC Adv.*, 2015, doi: 10.1039/c5ra09965j.

[38]   K. Hara, M. Sugiyama, M. Annaka, and Y. Soejima, "Nanostructural characterization of the dehydrated (NIPA/SA + additive ion) gels," in *Colloids and Surfaces B: Biointerfaces*, 2004, doi: 10.1016/j.colsurfb.2004.04.012.

[39]   D. Noferini, A. Faraone, M. Rossi, E. Mamontov, E. Fratini, and P. Baglioni, "Disentangling polymer network and hydration water dynamics in polyhydroxyethyl methacrylate physical and chemical hydrogels," *J. Phys. Chem. C*, 2019, doi: 10.1021/acs.jpcc.9b04212.

[40]   O. Okay, "Macroporous copolymer networks," *Progress in Polymer Science (Oxford)*. 2000, doi: 10.1016/S0079-6700(00)00015-0.

[41]   T. S. Perova, J. K. Vij, and H. Xu, "Fourier transform infrared study

of poly (2-hydroxyethyl methacrylate) PHEMA," *Colloid Polym. Sci.*, 1997, doi: 10.1007/s003960050089.

[42] J. Dong, Y. Ozaki, and K. Nakashima, "FTIR studies of conformational energies of poly (acrylic acid) in cast films," *J. Polym. Sci. Part B Polym. Phys.*, 1997, doi: 10.1002/(SICI)1099-0488(199702)35:3<507::AID-POLB9>3.0.CO;2-O.

[43] C. S. Srikanth and S. S. C. Chuang, "Spectroscopic investigation into oxidative degradation of silica-supported amine sorbents for CO2 capture," *ChemSusChem*, 2012, doi: 10.1002/cssc.201100662.

[44] M. Todica, R. Stefan, C. V. Pop, and L. Olar, "IR and Raman investigation of some poly(acrylic) acid gels in aqueous and neutralized state," *Acta Phys. Pol. A*, 2015, doi: 10.12693/APhysPolA.128.128.

[45] N. M. Kabanov, N. A. Kozhevnikova, A. I. Kokorin, V. B. Rogacheva, A. B. Zezin, and V. A. Kabanov, "Study of the structure of a polyacrylic acid-Cu (II)-poly-4-vinylpyridine ternary polymeric metal complex," *Polym. Sci. U.S.S.R.*, 1979, doi: 10.1016/0032-3950(79)90121-7.

[46] K. M. Koczkur, S. Mourdikoudis, L. Polavarapu, and S. E. Skrabalak, "Polyvinylpyrrolidone (PVP) in nanoparticle synthesis," *Dalt. Trans.*, 2015, doi: 10.1039/c5dt02964c.

[47] A. Mondal and B. Mandal, "CO2 separation using thermally stable crosslinked poly(vinyl alcohol) membrane blended with polyvinylpyrrolidone/polyethyleneimine/tetraethylenepentamine," *J. Memb. Sci.*, 2014, doi: 10.1016/j.memsci.2014.02.040.

[48] M. Shahmiri, N. A. Ibrahim, F. Shayesteh, N. Asim, and N. Motallebi, "Preparation of PVP-coated copper oxide nanosheets as antibacterial and antifungal agents," *J. Mater. Res.*, 2013, doi: 10.1557/jmr.2013.316.

[49] G. E. Boyd, A. W. Adamson, and L. S. Myers, "The Exchange Adsorption of Ions from Aqueous Solutions by Organic Zeolites. II. Kinetics," *J. Am. Chem. Soc.*, 1947, doi: 10.1021/ja01203a066.

[50] W. Weber, "Kinetics of Adsorption on Carbon from Solution," *J. Sanit. Eng. Div.*, 1963.

[51]   W. Rudzinski and W. Plazinski, "Theoretical description of the kinetics of solute adsorption at heterogeneous solid/solution interfaces," *Appl. Surf. Sci.*, 2007, doi: 10.1016/j.apsusc.2006.12.038.

[52]   A. Chatterjee and S. Schiewer, "Multi-resistance kinetic models for biosorption of Cd by raw and immobilized citrus peels in batch and packed-bed columns," *Chem. Eng. J.*, 2014, doi: 10.1016/j.cej.2013.12.017.

[53]   J. P. Simonin and J. Bouté, "Intraparticle diffusion-adsorption model to describe liquid/solid adsorption kinetics," *Rev. Mex. Ing. Quim.*, 2016.

[54]   V. Russo, R. Tesser, E. Santacesaria, and M. Di Serio, "Chemical and technical aspects of propene oxide production via hydrogen peroxide (HPPO process)," *Industrial and Engineering Chemistry Research*. 2013, doi: 10.1021/ie3023862.

[55]   S. Azizian, "Kinetic models of sorption: A theoretical analysis," *J. Colloid Interface Sci.*, 2004, doi: 10.1016/j.jcis.2004.03.048.

[56]   J. P. Simonin, "On the comparison of pseudo-first order and pseudo-second order rate laws in the modeling of adsorption kinetics," *Chem. Eng. J.*, 2016, doi: 10.1016/j.cej.2016.04.079.

[57]   H. Qiu, L. Lv, B. C. Pan, Q. J. Zhang, W. M. Zhang, and Q. X. Zhang, "Critical review in adsorption kinetic models," *Journal of Zhejiang University: Science A*. 2009, doi: 10.1631/jzus.A0820524.

[58]   J. J. Pignatello and B. Xing, "Mechanisms of slow sorption of organic chemicals to natural particles," *Environ. Sci. Technol.*, 1996, doi: 10.1021/es940683g.

[59]   S. He *et al.*, "Uptake of arsenic(V) using alumina functionalized highly ordered mesoporous SBA-15 (Alx-SBA-15) as an effective adsorbent," *J. Chem. Eng. Data*, 2015, doi: 10.1021/je500978k.

[60]   "Theories of occlusion; and the sorption of iodine by carbon," *Trans. Faraday Soc.*, 1919, doi: 10.1039/tf9191400202.

[61]   D. D. Do, *Adsorption Analysis: Equilibria and Kinetics*. 1998.

[62]   A. Scott and C. Wild, "Transformations and r2," *Am. Stat.*, 1991, doi: 10.1080/00031305.1991.10475785.

[63]   R. Anderson-Sprecher, "Model comparisons and r2," *Am. Stat.*, 1994, doi: 10.1080/00031305.1994.10476036.

[64]   W. Martens, R. L. Frost, and P. A. Williams, "Raman and infrared spectroscopic study of the basic copper chloride minerals - Implications for the study of the copper and brass corrosion and 'bronze disease,'" *Neues Jahrb. fur Mineral. Abhandlungen*, 2002, doi: 10.1127/0077-7757/2003/0178-0197.

[65]   G. Di Carlo *et al.*, "Artificial patina formation onto copper-based alloys: Chloride and sulphate induced corrosion processes," *Appl. Surf. Sci.*, 2017, doi: 10.1016/j.apsusc.2017.01.080.

[66]   C. Ricci, C. Miliani, B. G. Brunetti, and A. Sgamellotti, "Non-invasive identification of surface materials on marble artifacts with fiber optic mid-FTIR reflectance spectroscopy," *Talanta*, 2006, doi: 10.1016/j.talanta.2005.12.054.

[67]   R. Mastrangelo *et al.*, "Twin-chain polymer hydrogels based on poly(vinyl alcohol) as new advanced tool for the cleaning of modern and contemporary art," *Proc. Natl. Acad. Sci.*, vol. 117, no. 13, pp. 7011–7020, 2020.

Appendix 1

Kinetic Models

Pseudo-first order rate law, K1

The pseudo-first order kinetic equation, initially introduced by Lagergren [148], is generally used in the form proposed by Ho and McKay [149]:

$$\ln[q_e - q(t)] = \ln q_e - k_1 t$$

where q is the amount of adsorbed solute, q_e its value at equilibrium, k_1 is the pseudo-first order rate constant, and t is the time.

For fitting the experimental data, we used the alternative expression:

$$q(t) = q_e [1 - \exp(-k_1 t)].$$

Pseudo-second order rate law, K2

The pseudo-second order kinetics equation is normally used as indicated by Ho and McKay [149]:

$$\frac{t}{q(t)} = \frac{t}{q_e} + \frac{1}{k_2 q_e^2}$$

where k_2 is the pseudo-second order kinetic rate constant.

In order to compare K1 and K2 models for fitting the experimental data, we used the following expression that considers the original scale (y = q(t)):

$$q(t) = q_e \frac{k_2^* t}{1 + k_2^* t}$$

Intraparticle diffusion model, IPD

The intraparticle diffusion model employs a power law where $q \propto t^{1/2}$ [150]:

$$q(t) = k_{ipd} \cdot t^{1/2} + c$$

In our case, c was constrained at 0 because there is no adsorption at the beginning of the uptake process (t = 0). Instead, we let the t exponent vary during the fittings:

$$q(t) = k_{ipd} \cdot t^{pow}$$

Fitting parameters and chi square (chi-sq) values for K1, K2 and IPD equations applied to the uptake of Cu(II) ions by the pHEMA semi-IPNs.

	pHEMA/PAA pH 6 (Table S1)			
	K2	**K1**	**IPD**	**IPD 10'**
q_e	$3.04 \times 10^{-4} \pm$ 1.5×10^{-5}	$2.57 \times 10^{-4} \pm$ 1.1×10^{-5}	-	-
$k_2{}^*$	$3.87 \times 10^{-2} \pm$ 4.8×10^{-3}	-	-	-
k_1	-	$3.50 \times 10^{-2} \pm$ 4.2×10^{-3}	-	-
k_{ipd}	-	-	$3.29 \times 10^{-5} \pm 1.3$ $\times 10^{-6}$	$2.93 \times 10^{-5} \pm$ 2.3×10^{-6}
pow	-	-	0.423 ± 0.009	0.48 ± 0.04
chi-sq	5.66×10^{-9}	9.77×10^{-9}	1.04×10^{-9}	4.95×10^{-10}

pHEMA/PAA pH 8 (Table S2)			
	K2	**K1**	**IPD**	**IPD'**
q_e	$4.68 \times 10^{-4} \pm 1.0 \times 10^{-5}$	$3.52 \times 10^{-4} \pm 6.0 \times 10^{-5}$	-	-
$k_2{}^*$	$1.70 \times 10^{-2} \pm 8.1 \times 10^{-3}$	-	-	-
k_1	-	$1.97 \times 10^{-2} \pm 7.6 \times 10^{-3}$	-	-
k_{ipd}	-	-	$2.07 \times 10^{-5} \pm 2.1 \times 10^{-6}$	$1.48 \times 10^{-5} \pm 0.4 \times 10^{-6}$
pow	-	-	0.562 ± 0.022	0.627 ± 0.014
chi-sq	9.93×10^{-10}	1.25×10^{-9}	6.16×10^{-9}	2.12×10^{-11}

pHEMA/PVP pH 6 (Table S3)			
	K2	**K1**	**IPD**	**IPD 10'**
q_e	$3.37 \times 10^{-5} \pm 1.6 \times 10^{-6}$	$2.93 \times 10^{-5} \pm 1.0 \times 10^{-6}$	-	-
$k_2{}^*$	$6.16 \times 10^{-2} \pm 8.4 \times 10^{-3}$	-	-	-
k_1		$5.50 \times 10^{-2} \pm 4.9 \times 10^{-3}$		
k_{ipd}			$5.11 \times 10^{-6} \pm 8.2 \times 10^{-7}$	$2.16 \times 10^{-6} \pm 6.1 \times 10^{-7}$
pow			0.367 ± 0.038	0.757 ± 0.149
chi-sq	1.16×10^{-10}	8.78×10^{-11}	3.47×10^{-10}	4.98×10^{-11}

pHEMA/PVP pH 8 (Table S4)			
	K2	**K1**	**IPD**	**IPD 10'**
q_e	$3.21 \times 10^{-4} \pm 1.2 \times 10^{-5}$	$2.31 \times 10^{-4} \pm 0.5 \times 10^{-5}$	-	-
k_2*	$6.16 \times 10^{-2} \pm 8.4 \times 10^{-3}$	-	-	-
k_1		$5.50 \times 10^{-2} \pm 4.9 \times 10^{-3}$		
k_{ipd}			$5.11 \times 10^{-6} \pm 8.2 \times 10^{-7}$	$2.16 \times 10^{-6} \pm 6.1 \times 10^{-7}$
pow			0.367 ± 0.038	0.757 ± 0.149
chi-sq	1.16×10^{-10}	8.78×10^{-11}	3.47×10^{-10}	4.98×10^{-11}

Figure S1. Fitting of *q* (grams of solute sorbed per gram of sorbent) and residuals over time for the uptake of Cu(II) ions by the pHEMA/PAA semi-IPNs at pH 6 using K2, IPD and K1 equation.
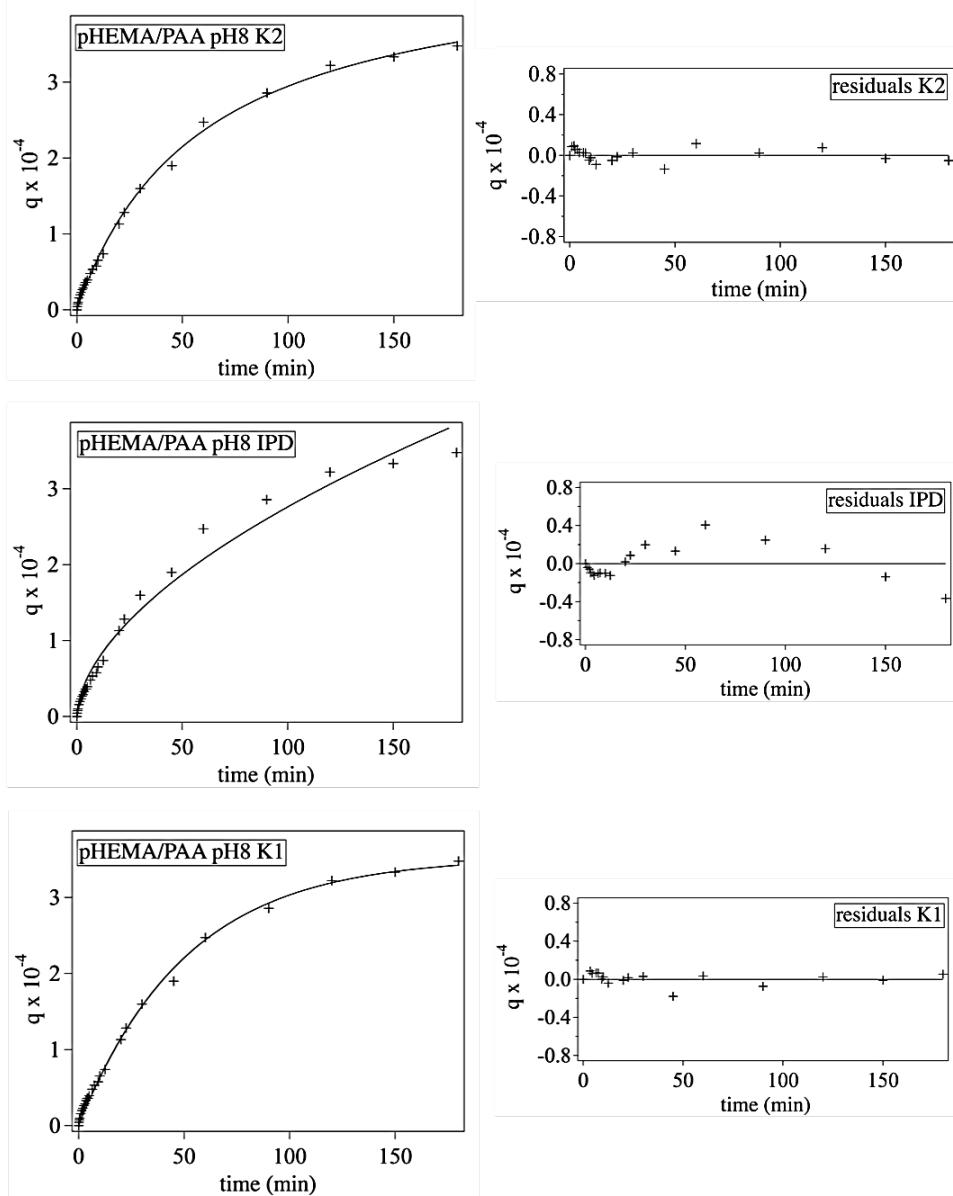
Figure S2. Fitting of *q* (grams of solute sorbed per gram of sorbent) and residuals over time for the uptake of Cu(II) ions by the pHEMA/PAA semi-IPNs at pH 8 using K2, IPD and K1 equation.
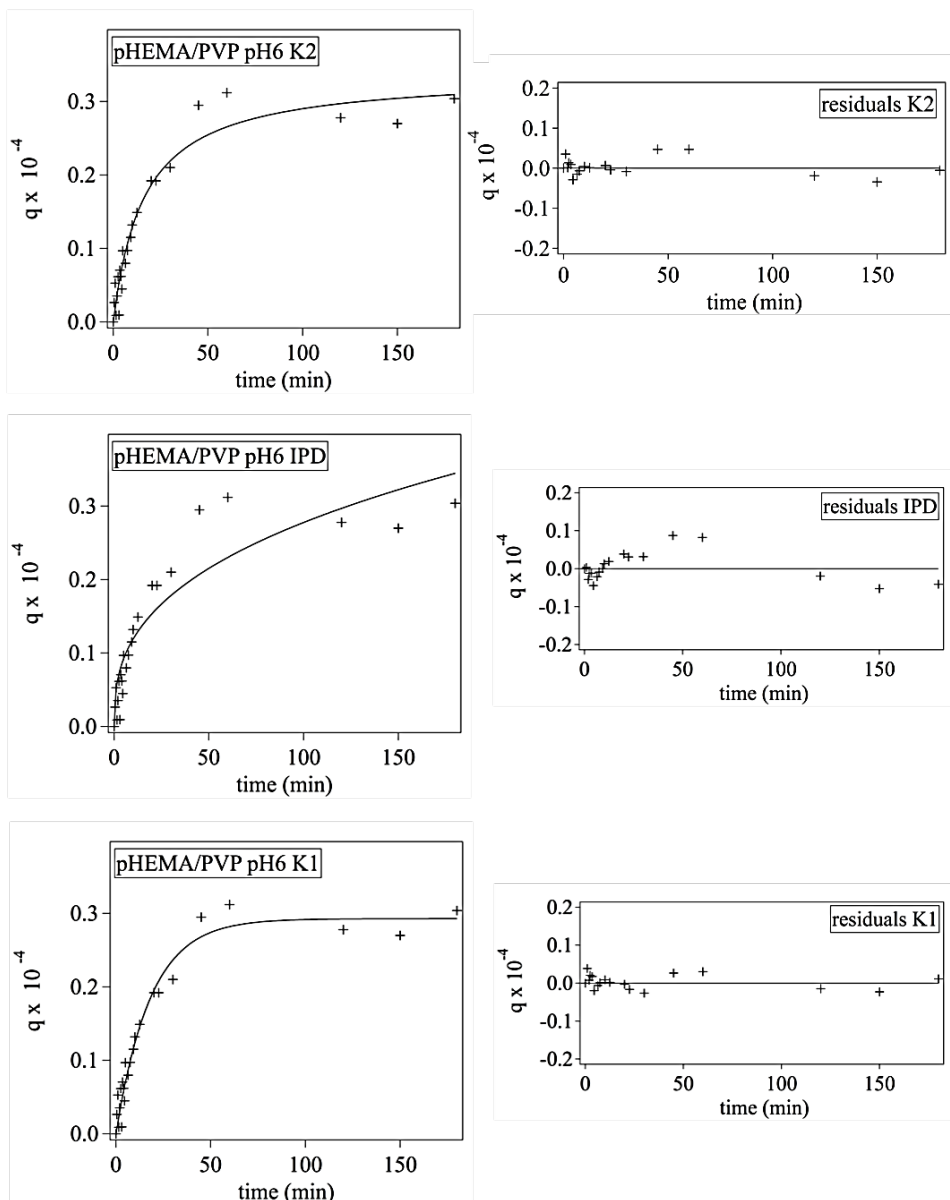
Figure S3. Fitting of *q* (grams of solute sorbed per gram of sorbent) over time for the uptake of Cu(II) ions by the pHEMA/PVP semi-IPNs at pH 6 using K2, IPD and K1 equation.

Figure S4. Fitting of *q* (grams of solute sorbed per gram of sorbent) over time for the uptake of Cu(II) ions by the pHEMA/PVP semi-IPNs at pH 8 using K2, IPD and K1 equation.

Bibliography
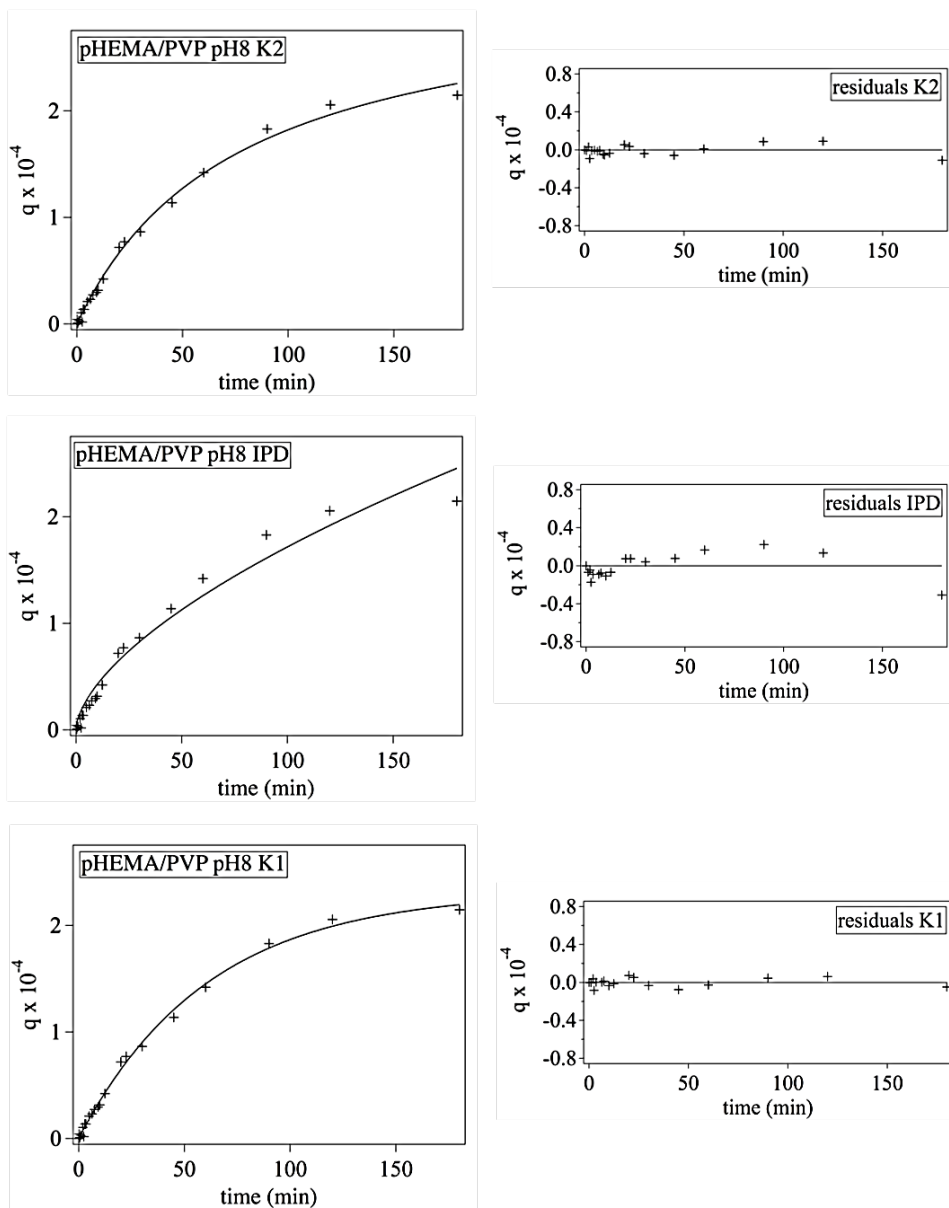
[1]   P. Baglioni, E. Carretti, and D. Chelazzi, "Nanomaterials in art conservation," *Nature Nanotechnology*. 2015, doi: 10.1038/nnano.2015.38.

[2]   M. Baglioni, G. Poggi, Y. Jaidar Benavides, F. Martínez Camacho, R. Giorgi, and P. Baglioni, "Nanostructured fluids for the removal of graffiti – A survey on 17 commercial spray-can paints," *J. Cult. Herit.*, 2018, doi: 10.1016/j.culher.2018.04.016.

[3]   G. Perusini, "Il dibattito sulla pulitura dei dipinti della National Gallery e del Louvre alla metà dell'Ottocento: alcune considerazioni generali," in *La cultura del restauro. Modelli di ricezione per la museologia e la storia dell'arte*, 2013, pp. 335–349.

[4]   M. Ciatti, *Appunti per un manuale di storia e teoria del restauro. Dispense per gli studenti.* 2004.

[5]   Bomford D., "Picture cleaning: positivism and metaphysics," in *The conservation of easel paintings*, H. S. J and Rushfield R, Eds. New York, 2012, pp. 481–491.

[6]   L. Dei, "CHAPTER 3. Conservation Treatments: Cleaning, Consolidation and Protection," in *Nanoscience for the Conservation of Works of Art*, 2013, pp. 77–92.

[7]   C. Fotakis, D. Anglos, V. Zafiropulos, S. Georgiou, and V. Tornari, *Lasers in the Preservation of Cultural Heritage: Principles and Applications.* 2007.

[8]   C. Degrigny, "Survey of European Experience on Cleaning Procedures," in *Monumenti in bronzo all'aperto. Esperienze a confronto.*, 2004.

[9]   R. Wolbers and C. Stavroudis, "Aqueous methods for the cleaning of paintings," in *Conservation of Easel Paintings*, 2012.

[10]   P. Cremonesi, *L' uso dei solventi organici nella pulitura di opere policrome.* 2004.

[11]   J. H. Hildebrand and R. L. Scott, "Solutions of Nonelectrolytes," *Annu. Rev. Phys. Chem.*, 1950, doi: 10.1146/annurev.pc.01.100150.000451.

[12]   C. M. Hansen and K. Skaarup, "Three-dimensional solubility parameter-key to paint component affinities. III. Independent

calculation of the parameter components," *J. Paint Technol.*, 1967.

[13]   J. P. Teas, "Graphic analysis of resin solubilities," *J. Paint Technol.*, 1968.

[14]   P. Baglioni, D. Chelazzi, and R. Giorgi, *Nanotechnologies in the Conservation of Cultural Heritage*. 2015.

[15]   C. E. Dillon, A. F. Lagalante, and R. C. Wolbers, "Acrylic emulsion paint films: The effect of solution pH, conductivity, and ionic strength on film swelling and surfactant removal," *Stud. Conserv.*, 2014, doi: 10.1179/2047058412Y.0000000076.

[16]   A. Burnstock and R. Wolbers, "Cleaning Painted Surfaces: Aqueous Methods," *Stud. Conserv.*, 2001, doi: 10.2307/1506812.

[17]   E. Balliana, G. Ricci, C. Pesce, and E. Zendri, "Assessing the value of green conservation for cultural heritage: Positive and critical aspects of already available methodologies," *Int. J. Conserv. Sci.*, 2016.

[18]   M. Baglioni, M. Alterini, D. Chelazzi, R. Giorgi, and P. Baglioni, "Removing Polymeric Coatings With Nanostructured Fluids: Influence of Substrate, Nature of the Film, and Application Methodology," *Front. Mater.*, 2019, doi: 10.3389/fmats.2019.00311.

[19]   E. Carretti, L. Dei, and P. Baglioni, "Solubilization of acrylic and vinyl polymers in nanocontainer solutions. Application of microemulsions and micelles to cultural heritage conservation," *Langmuir*, 2003, doi: 10.1021/la034757q.

[20]   E. Carretti *et al.*, "New frontiers in materials science for art conservation: Responsive gels and beyond," *Acc. Chem. Res.*, 2010, doi: 10.1021/ar900282h.

[21]   E. Carretti, R. Giorgi, D. Berti, and P. Baglioni, "Oil-in-water nanocontainers as low environmental impact cleaning tools for works of art: Two case studies," *Langmuir*, 2007, doi: 10.1021/la700487s.

[22]   L. Borgioli, G. Caminati, G. Gabrielli, and E. Ferroni, "Removal of hydrophobic impurities from pictorial surfaces by means of heterogeneous systems," *Sci. Technol. Cult. Herit.*, 1995.

[23]   M. Baglioni, D. Rengstl, D. Berti, M. Bonini, R. Giorgi, and P. Baglioni, "Removal of acrylic coatings from works of art by means of nanofluids: Understanding the mechanism at the nanoscale," *Nanoscale*, 2010, doi: 10.1039/c0nr00255k.

[24]   M. Raudino *et al.*, "Polymer films removed from solid surfaces by nanostructured fluids: Microscopic mechanism and implications for

the conservation of cultural heritage," *ACS Appl. Mater. Interfaces*, 2015, doi: 10.1021/acsami.5b00534.

[25]   M. Baglioni *et al.*, "Dewetting acrylic polymer films with water/propylene carbonate/surfactant mixtures - Implications for cultural heritage conservation," *Phys. Chem. Chem. Phys.*, 2017, doi: 10.1039/c7cp02608k.

[26]   B. Kronberg, K. Holmberg, and B. Lindman, *Surface Chemistry of Surfactants and Polymers*. 2014.

[27]   P. Baglioni *et al.*, "Micelle, microemulsions, and gels for the conservation of cultural heritage," *Advances in Colloid and Interface Science*. 2014, doi: 10.1016/j.cis.2013.09.008.

[28]   E. Carretti, B. Salvadori, P. Baglioni, and L. Dei, "Microemulsions and micellar solutions for cleaning wall painting surfaces," *Stud. Conserv.*, 2005, doi: 10.1179/sic.2005.50.2.128.

[29]   E. Carretti, E. Fratini, D. Berti, L. Dei, and P. Baglioni, "Nanoscience for art conservation: oil-in-water microemulsions embedded in a polymeric network for the cleaning of works of art," *Angew. Chemie - Int. Ed.*, 2009, doi: 10.1002/anie.200904244.

[30]   R. C. Wolbers, "Recent developments in the use of gel formulations for the cleaning of paintings.," in *Restoration '92: conservation, training, materials and techniques: latest developments. Preprints to the conference held at the RAI International Exhibition and Congress Centre, Amsterdam, 20-22 October 1992*, 1992.

[31]   A. Casoli, Z. Di Diego, and C. Isca, "Cleaning painted surfaces: evaluation of leaching phenomenon induced by solvents applied for the removal of gel residues," *Environ. Sci. Pollut. Res.*, 2014, doi: 10.1007/s11356-014-2658-5.

[32]   D. Stulik *et al.*, *Solvent Gels for the Cleaning of Works of Art: The Residue Question*. 2004.

[33]   E. Campani, A. Casoli, P. Cremonesi, I. Saccani, and E. Signorini, "L'uso di agarosio e agar per la preparazione di 'gel rigidi,'" in *Quaderni del Cesmar 7*, 2007.

[34]   C. Mazzuca *et al.*, "Cleaning of paper artworks: Development of an efficient gel-based material able to remove starch paste," *ACS Appl. Mater. Interfaces*, 2014, doi: 10.1021/am504295n.

[35]   D. Gulotta *et al.*, "Setup of a sustainable indoor cleaning methodology for the sculpted stone surfaces of the Duomo of Milan," *Herit. Sci.*,

2014, doi: 10.1186/2050-7445-2-6.

[36]   J. A. L. Domingues, N. Bonelli, R. Giorgi, E. Fratini, F. Gorel, and P. Baglioni, "Innovative hydrogels based on semi-interpenetrating p(HEMA)/PVP networks for the cleaning of water-sensitive cultural heritage artifacts," *Langmuir*, 2013, doi: 10.1021/la3048664.

[37]   N. Bonelli, G. Poggi, D. Chelazzi, R. Giorgi, and P. Baglioni, "Poly(vinyl alcohol)/poly(vinyl pyrrolidone) hydrogels for the cleaning of art," *J. Colloid Interface Sci.*, 2019, doi: 10.1016/j.jcis.2018.10.025.

[38]   M. Baglioni *et al.*, "Complex Fluids Confined into Semi-interpenetrated Chemical Hydrogels for the Cleaning of Classic Art: A Rheological and SAXS Study," *ACS Appl. Mater. Interfaces*, vol. 10, pp. 19162–19172, 2018.

[39]   E. Díaz, R. B. Valenciano, and I. A. Katime, "Study of complexes of poly(vinyl pyrrolidone) with copper and cobalt on solid state," *J. Appl. Polym. Sci.*, 2004, doi: 10.1002/app.20620.

[40]   N. Sebastian, B. George, and B. Mathew, "Metal complexes of poly(acrylic acid): Synthesis, characterization and thermogravimetric studies," *Polym. Degrad. Stab.*, 1998, doi: 10.1016/s0141-3910(97)00095-5.

[41]   A. Martell, Ed., *Critical Stability Constant - Vol. 2: Amines*. Springer US, 1975.

[42]   A. E. Comyns, "Handbook of Copper Compounds and Applications. H.W. Richardson (ed.) Marcel Dekker, New York, 1997.

[43]   E. I. Parisi, N. Bonelli, E. Carretti, R. Giorgi, G. M. Ingo, and P. Baglioni, "Film forming PVA-based cleaning systems for the removal of corrosion products from historical bronzes," *Pure Appl. Chem.*, 2018, doi: 10.1515/pac-2017-0204.

[44]   N. Sax, G. Hawley, and R. Lewis, *Hawley's condensed chemical dictionary*. 1987.

[45]   E. Carretti, L. Dei, C. Miliani, and P. Baglioni, "Oil-in-water microemulsions to solubilize acrylic copolymers: Application in cultural heritage conservation," *Prog. Colloid Polym. Sci.*, 2001, doi: 10.1007/3-540-45725-9_14.

[46]   R. Giorgi, M. Baglioni, D. Berti, and P. Baglioni, "New Methodologies for the conservation of cultural heritage: Micellar solutions, microemulsions, and hydroxide nanoparticles," *Acc. Chem. Res.*, 2010, doi: 10.1021/ar900193h.

[47]   M. Baglioni *et al.*, "Nanomaterials for the cleaning and pH adjustment of vegetable-tanned leather," *Appl. Phys. A Mater. Sci. Process.*, vol. 122, no. 114, 2016.

[48]   R. Mastrangelo, C. Montis, N. Bonelli, P. Tempesti, and P. Baglioni, "Surface cleaning of artworks: Structure and dynamics of nanostructured fluids confined in polymeric hydrogel networks," *Phys. Chem. Chem. Phys.*, 2017, doi: 10.1039/c7cp02662e.

[49]   B. Ormsby, M. Keefe, A. Phenix, and T. Learner, *A Summary of Recent Developments in Wet Surface Cleaning Systems: Unvarnished Modern and Contemporary Painted Surfaces.* Archetype Publications, 2015.

[50]   D. Gentili, G. Foschi, F. Valle, M. Cavallini, and F. Biscarini, "Applications of dewetting in micro and nanotechnology," *Chem. Soc. Rev.*, 2012, doi: 10.1039/c2cs35040h.

[51]   T. Sato, T. Akahane, K. Amano, R. Hyodo, K. Yanase, and T. Ogura, "Scattering and Spectroscopic Study on the Hydration and Phase Behavior of Aqueous Alcohol Ethoxylate and Methyl Ester Ethoxylate: Effects of Terminal Groups in Hydrophilic Chains," *J. Phys. Chem. B*, 2016, doi: 10.1021/acs.jpcb.6b04275.

[52]   M. Baglioni, D. Berti, J. Teixeira, R. Giorgi, and P. Baglioni, "Nanostructured surfactant-based systems for the removal of polymers from wall paintings: A small-angle neutron scattering study," *Langmuir*, 2012, doi: 10.1021/la303463m.

[53]   M. Baglioni *et al.*, "Nanostructured fluids from degradable nonionic surfactants for the cleaning of works of art from polymer contaminants," *Soft Matter*, 2014, doi: 10.1039/c4sm01084a.

[54]   T. Cosgrove, *Colloid Science: Principles, Methods and Applications.* 2005.

[55]   J. Estoe, "Surfactant aggregation and adsorption at the interfaces," in *Colloid Science*, T. Cosgrove, Ed. Blackwell Publishing Ltd., 2005.

[56]   P. Cremonesi, *L'uso di tensioattivi e chelanti nella pulitura di opere policrome.* Padova: Il Prato, 2001.

[57]   I. Karapanagiotis and W. W. Gerberich, "Polymer film rupturing in comparison with leveling and dewetting," *Surf. Sci.*, 2005, doi: 10.1016/j.susc.2005.07.023.

[58]   A. Sharma and E. Ruckenstein, "Energetic criteria for the breakup of liquid films on nonwetting solid surfaces," *J. Colloid Interface Sci.*, 1990, doi: 10.1016/0021-9797(90)90418-N.

[59]   A. Sharma, "Disintegration of macroscopic fluid sheets on substrates: A singular perturbation approach," *J. Colloid Interface Sci.*, 1993, doi: 10.1006/jcis.1993.1086.

[60]   G. Reiter, "Dewetting of thin polymer films," *Phys. Rev. Lett.*, 1992, doi: 10.1103/PhysRevLett.68.75.

[61]   G. Reiter, "Dewetting as a Probe of Polymer Mobility in Thin Films," *Macromolecules*, 1994, doi: 10.1021/ma00089a023.

[62]   W. J. Peppel, "Preparation and Properties of the Alkylene Carbonates," *Ind. Eng. Chem.*, 1958, doi: 10.1021/ie50581a030.

[63]   C. M. Hansen, *Hansen solubility parameters: A user's handbook: Second edition.* 2007.

[64]   M. Baglioni, C. Montis, D. Chelazzi, R. Giorgi, D. Berti, and P. Baglioni, "Polymer Film Dewetting by Water/Surfactant/Good-Solvent Mixtures: A Mechanistic Insight and Its Implications for the Conservation of Cultural Heritage," *Angew. Chemie - Int. Ed.*, 2018, doi: 10.1002/anie.201710930.

[65]   G. Genta and P. Riberi, *Technology and the Growth of Civilization.* 2019.

[66]   R. M. Organ and L. Aitchison, "A History of Metals," *Stud. Conserv.*, 1961, doi: 10.2307/1505109.

[67]   J. C. McCawley and C. Pearson, "Conservation of Marine Archaeological Objects," *Stud. Conserv.*, 1991, doi: 10.2307/1506336.

[68]   D. L. Hamilton, "Methods of conserving archaeological material from underwater sites," *Conserv. Files ANTH 605, Conserv. Cult. Resour. I. Naut. Archaeol. Program, Texas A&M Univ.*, 1999.

[69]   M. Mercalli, "Storia del concetto di patina. Riflessioni teoriche intorno al restauro dei manufatti in bronzo.," in *Monumenti in bronzo all'aperto. Esperienze a confronto*, P. Letardi, Ed. Nardini Editore, 2004, pp. 49–52.

[70]   A. Lins, "The cleaning of weathered bronze monuments: a review and comparison of current corrosion removal techniques," in *The conservation of bronze sculpture in the outdoor environment*, 1992, pp. 209–230.

[71]   S. Siano, R. Salimbeni, R. Pini, A. Giusti, and M. Matteini, "Laser cleaning methodology for the preservation of the Porta del Paradiso by Lorenzo Ghiberti," *J. Cult. Herit.*, 2003, doi: 10.1016/s1296-2074(02)01138-x.

[72]   S. Siano and R. Salimbeni, "Advances in laser cleaning of artwork and objects of historical interest: The optimized pulse duration approach,"

Acc. Chem. Res., 2010, doi: 10.1021/ar900190f.

[73]   D. A. Scott, *Copper and bronze in art*. The Getty Conservation Institute, 2002.

[74]   P. Fiorentino, M. Marabelli, M. Matteini, and A. Moles, "The condition of the 'Door of Paradise' by L. Ghiberti. Tests and proposals for cleaning," *Stud. Conserv.*, 1982, doi: 10.1179/sic.1982.27.4.145.

[75]   M. C. Ganorkar, V. Pandit Rao, P. Gayathri, and T. A. Sreenivasa Rao, "A novel method for conservation of copper-based artifacts," *Stud. Conserv.*, 1988, doi: 10.1179/sic.1988.33.2.97.

[76]   D. Chelazzi, R. Giorgi, and P. Baglioni, "Microemulsions, Micelles, and Functional Gels: How Colloids and Soft Matter Preserve Works of Art," *Angewandte Chemie - International Edition*. 2018, doi: 10.1002/anie.201710711.

[77]   P. Baglioni, D. Chelazzi, R. Giorgi, and G. Poggi, "Colloid and materials science for the conservation of cultural heritage: Cleaning, consolidation, and deacidification," *Langmuir*, 2013, doi: 10.1021/la304456n.

[78]   N. Bonelli, C. Montis, A. Mirabile, D. Berti, and P. Baglioni, "Restoration of paper artworks with microemulsions confined in hydrogels for safe and efficient removal of adhesive tapes," *Proc. Natl. Acad. Sci.*, vol. 115, no. 3, pp. 5932–5937, 2018.

[79]   N. Bonelli, D. Chelazzi, M. Baglioni, R. Giorgi, and P. Baglioni, "Confined aqueous media for the cleaning of cultural heritage: Innovative gels and amphiphile-based nanofluids," in *Nanoscience and Cultural Heritage*, 2016.

[80]   T. Guaragnone, A. Casini, D. Chelazzi, and R. Giorgi, "PVA-based peelable films loaded with tetraethylenepentamine for the removal of corrosion products from bronze," *Appl. Mater. Today*, 2020, doi: 10.1016/j.apmt.2019.100549.

[81]   J. E. Elliott, M. MacDonald, J. Nie, and C. N. Bowman, "Structure and swelling of poly(acrylic acid) hydrogels: Effect of pH, ionic strength, and dilution on the crosslinked polymer structure," *Polymer (Guildf).*, 2004, doi: 10.1016/j.polymer.2003.12.040.

[82]   G. S. Park, "Poly(vinyl alcohol) properties and applications," *Polymer (Guildf).*, 1974, doi: 10.1016/0032-3861(74)90049-4.

[83]   S. Ghoshal, P. Denner, S. Stapf, and C. Mattea, "Study of the formation of poly(vinyl alcohol) films," *Macromolecules*, 2012, doi:

10.1021/ma2023292.

[84]   G. Paradossi, F. Cavalieri, E. Chiessi, C. Spagnoli, and M. K. Cowman, "Poly(vinyl alcohol) as versatile biomaterial for potential biomedical applications," 2003, doi: 10.1023/A:1024907615244.

[85]   E. Chiellini, A. Corti, S. D'Antone, and R. Solaro, "Biodegradation of poly (vinyl alcohol) based materials," *Progress in Polymer Science (Oxford)*. 2003, doi: 10.1016/S0079-6700(02)00149-1.

[86]   I. Natali, E. Carretti, L. Angelova, P. Baglioni, R. G. Weiss, and L. Dei, "Structural and mechanical properties of 'peelable' organoaqueous dispersions with partially hydrolyzed poly(vinyl acetate)-borate networks: Applications to cleaning painted surfaces," *Langmuir*, 2011, doi: 10.1021/la2015786.

[87]   M. Abasian, V. Hooshangi, and P. N. Moghadam, "Synthesis of polyvinyl alcohol hydrogel grafted by modified Fe3O4 nanoparticles: characterization and doxorubicin delivery studies," *Iran. Polym. J. (English Ed.*, 2017, doi: 10.1007/s13726-017-0521-5.

[88]   P. Dillmann, G. Béranger, P. Piccardo, and H. Matthiesen, *Corrosion of metallic heritage artefacts*. 2007.

[89]   I. D. MacLeod and T. Stambolov, "The Corrosion and Conservation of Metallic Antiquities and Works of Art," *Stud. Conserv.*, 1987, doi: 10.2307/1506218.

[90]   A. Oddy and D. A. Scott, "Copper and Bronze in Art: Corrosion, Colorants, Conservation," *Stud. Conserv.*, 2002, doi: 10.2307/1506788.

[91]   A. M. Alfantazi, T. M. Ahmed, and D. Tromans, "Corrosion behavior of copper alloys in chloride media," *Mater. Des.*, 2009, doi: 10.1016/j.matdes.2008.10.015.

[92]   L. Robbiola, J. M. Blengino, and C. Fiaud, "Morphology and mechanisms of formation of natural patinas on archaeological Cu-Sn alloys," *Corros. Sci.*, 1998, doi: 10.1016/S0010-938X(98)00096-1.

[93]   G. Kear, B. D. Barker, and F. C. Walsh, "Electrochemical corrosion of unalloyed copper in chloride media--a critical review," *Corros. Sci.*, 2004, doi: 10.1016/S0010-938X(02)00257-3.

[94]   M. Chmielová, J. Seidlerová, and Z. Weiss, "X-ray diffraction phase analysis of crystalline copper corrosion products after treatment in different chloride solutions," *Corros. Sci.*, 2003, doi: 10.1016/S0010-938X(02)00176-2.

[95] D. A. Scott, "A review of copper chlorides and related salts in bronze corrosion and as painting pigments," *Studies in Conservation*. 2000, doi: 10.1179/sic.2000.45.1.39.

[96] F. Faraldi *et al.*, "Micro-chemical and micro-structural investigation of archaeological bronze weapons from the Ayanis fortress (lake Van, Eastern Anatolia, Turkey)," *Appl. Phys. A Mater. Sci. Process.*, 2013, doi: 10.1007/s00339-013-7772-6.

[97] G. M. Ingo *et al.*, "Large scale investigation of chemical composition, structure and corrosion mechanism of bronze archeological artefacts from Mediterranean basin," *Appl. Phys. A Mater. Sci. Process.*, 2006, doi: 10.1007/s00339-006-3550-z.

[98] E. I. Parisi, N. Bonelli, R. Giorgi, G. M. Ingo, and P. Baglioni, "Development of an innovative film-forming cleaning system for the removal of corrosion products from copper alloy artifacts."

[99] B. D. Fecchio, S. R. Valandro, M. G. Neumann, and C. C. S. Cavalheiro, "Thermal decomposition of polymer/montmorillonite nanocomposites synthesized in situ on a clay surface," *J. Braz. Chem. Soc.*, 2016, doi: 10.5935/0103-5053.20150216.

[100] F. Müller-Plathe, "Different states of water in hydrogels?," *Macromolecules*, 1998, doi: 10.1021/ma980685b.

[101] A. K. Lele, M. M. Hirve, M. V. Badiger, and R. A. Mashelkar, "Predictions of bound water content in poly(N-isopropylacrylamide) gel," *Macromolecules*, 1997, doi: 10.1021/ma950894l.

[102] P. A. Bhagwan, *A Handbook of Thermodynamics*. Mittal Publications.

[103] A. Hebeish, I. I. Abdel-Gawad, I. K. Basily, and S. El-Bazza, "Degradation of poly(vinyl alcohol) in strongly alkaline solutions of hydrogen peroxide," *J. Appl. Polym. Sci.*, 1985, doi: 10.1002/app.1985.070300605.

[104] N. A. Peppas and E. W. Merrill, "Differential scanning calorimetry of crystallized PVA hydrogels," *J. Appl. Polym. Sci.*, 1976, doi: 10.1002/app.1976.070200604.

[105] M. P. Casaletto, T. De Caro, G. M. Ingo, and C. Riccucci, "Production of reference 'ancient' Cu-based alloys and their accelerated degradation methods," *Appl. Phys. A Mater. Sci. Process.*, 2006, doi: 10.1007/s00339-006-3545-9.

[106] G. Di Carlo *et al.*, "Artificial patina formation onto copper-based alloys: Chloride and sulphate induced corrosion processes," *Appl. Surf. Sci.*,

2017, doi: 10.1016/j.apsusc.2017.01.080.

[107] G. M. Ingo, C. Riccucci, G. Guida, M. Albini, C. Giuliani, and G. Di Carlo, "Rebuilding of the Burial Environment from the Chemical Biography of Archeological Copper-Based Artifacts," *ACS Omega*, 2019, doi: 10.1021/acsomega.9b00569.

[108] T. E. Nikiforova, V. A. Kozlov, and M. K. Islyaikin, "Acid-base interactions and complex formation while recovering copper(II) ions from aqueous solutions using cellulose adsorbent in the presence of polyvinylpyrrolidone," *Russ. J. Phys. Chem. A*, 2012, doi: 10.1134/S0036024412120199.

[109] J. Cheng, G. Shan, and P. Pan, "Temperature and pH-dependent swelling and copper(ii) adsorption of poly(N-isopropylacrylamide) copolymer hydrogel," *RSC Adv.*, 2015, doi: 10.1039/c5ra09965j.

[110] K. Hara, M. Sugiyama, M. Annaka, and Y. Soejima, "Nanostructural characterization of the dehydrated (NIPA/SA + additive ion) gels," 2004, doi: 10.1016/j.colsurfb.2004.04.012.

[111] T. Canal and N. A. Peppas, "Correlation between mesh size and equilibrium degree of swelling of polymeric networks," *J. Biomed. Mater. Res.*, 1989, doi: 10.1002/jbm.820231007.

[112] W. Wang *et al.*, "Interactions among spherical poly(acrylic acid) brushes: Observation by rheology and small angle X-ray scattering," *J. Polym. Sci. Part B Polym. Phys.*, 2016, doi: 10.1002/polb.23901.

[113] K. M. Koczkur, S. Mourdikoudis, L. Polavarapu, and S. E. Skrabalak, "Polyvinylpyrrolidone (PVP) in nanoparticle synthesis," *Dalt. Trans.*, 2015, doi: 10.1039/c5dt02964c.

[114] A. Mondal and B. Mandal, "CO2 separation using thermally stable crosslinked poly(vinyl alcohol) membrane blended with polyvinylpyrrolidone/polyethyleneimine/tetraethylenepentamine," *J. Memb. Sci.*, 2014, doi: 10.1016/j.memsci.2014.02.040.

[115] M. Shahmiri, N. A. Ibrahim, F. Shayesteh, N. Asim, and N. Motallebi, "Preparation of PVP-coated copper oxide nanosheets as antibacterial and antifungal agents," *J. Mater. Res.*, 2013, doi: 10.1557/jmr.2013.316.

[116] G. E. Boyd, A. W. Adamson, and L. S. Myers, "The Exchange Adsorption of Ions from Aqueous Solutions by Organic Zeolites. II. Kinetics," *J. Am. Chem. Soc.*, 1947, doi: 10.1021/ja01203a066.

[117] J. P. Simonin and J. Bouté, "Intraparticle diffusion-adsorption model to describe liquid/solid adsorption kinetics," *Rev. Mex. Ing. Quim.*, 2016.

[118]   V. Russo, R. Tesser, E. Santacesaria, and M. Di Serio, "Chemical and technical aspects of propene oxide production via hydrogen peroxide (HPPO process)," *Industrial and Engineering Chemistry Research*. 2013, doi: 10.1021/ie3023862.

[119]   S. Azizian, "Kinetic models of sorption: A theoretical analysis," *J. Colloid Interface Sci.*, 2004, doi: 10.1016/j.jcis.2004.03.048.

[120]   W. Weber, "Kinetics of Adsorption on Carbon from Solution," *J. Sanit. Eng. Div.*, 1963.

[121]   W. Rudzinski and W. Plazinski, "Theoretical description of the kinetics of solute adsorption at heterogeneous solid/solution interfaces," *Appl. Surf. Sci.*, 2007, doi: 10.1016/j.apsusc.2006.12.038.

[122]   J. P. Simonin, "On the comparison of pseudo-first order and pseudo-second order rate laws in the modeling of adsorption kinetics," *Chem. Eng. J.*, 2016, doi: 10.1016/j.cej.2016.04.079.

[123]   H. Qiu, L. Lv, B. C. Pan, Q. J. Zhang, W. M. Zhang, and Q. X. Zhang, "Critical review in adsorption kinetic models," *Journal of Zhejiang University: Science A*. 2009, doi: 10.1631/jzus.A0820524.

[124]   J. J. Pignatello and B. Xing, "Mechanisms of slow sorption of organic chemicals to natural particles," *Environ. Sci. Technol.*, 1996, doi: 10.1021/es940683g.

[125]   S. He *et al.*, "Uptake of arsenic(V) using alumina functionalized highly ordered mesoporous SBA-15 (Alx-SBA-15) as an effective adsorbent," *J. Chem. Eng. Data*, 2015, doi: 10.1021/je500978k.

[126]   "Theories of occlusion; and the sorption of iodine by carbon," *Trans. Faraday Soc.*, 1919, doi: 10.1039/tf9191400202.

[127]   E. Carretti, C. Matarrese, E. Fratini, P. Baglioni, and L. Dei, "Physicochemical characterization of partially hydrolyzed poly(vinyl acetate)-borate aqueous dispersions," *Soft Matter*, 2014, doi: 10.1039/c4sm00355a.

[128]   L. V. Angelova, P. Terech, I. Natali, L. Dei, E. Carretti, and R. G. Weiss, "Cosolvent gel-like materials from partially hydrolyzed poly(vinyl acetate)s and borax," *Langmuir*, 2011, doi: 10.1021/la202179e.

[129]   B. Campagne, G. David, and B. Ameduri, "Recent Advances on Quasianhydrous Fuel Cell Membranes," in *Advanced Fluoride-Based Materials for Energy Conversion*, 2015.

[130] V. Goodship, D. Jacobs, and E. O. Ogur, *Polyvinyl Alcohol: Materials, Processing and Applications*. 2005.

[131] C. A. Finch, *Chemistry and Technology of Water-Soluble Polymers*. Springer US.

[132] C. M. Hassan and N. A. Peppas, "Structure and morphology of freeze/thawed PVA hydrogels," *Macromolecules*, 2000, doi: 10.1021/ma9907587.

[133] H. Burgess, "The use of chelating agents in conservation treatments," *Pap. Conserv.*, 1991, doi: 10.1080/03094227.1991.9638395.

[134] R. M. Smith, A. E. Martell, R. M. Smith, and A. E. Martell, "Aliphatic Amines," in *Critical Stability Constants*, 1975.

[135] P. K. Gallagher and Stephen Z. D. Cheng, *Handbook of Thermal Analysis and Calorimetry: Application to Polymers and Plastics*. 2002.

[136] D. Dibbern-Brunelli, T. D. Z. Atvars, I. Joekes, and V. C. Barbosa, "Mapping phases of poly(vinyl alcohol) and poly(vinyl acetate) blends by FTIR microspectroscopy and optical fluorescence microscopy," *J. Appl. Polym. Sci.*, 1998, doi: 10.1002/(SICI)1097-4628(19980725)69:4<645::AID-APP3>3.0.CO;2-J.

[137] R. L. Frost, W. Martens, J. Theo Kloprogge, and P. A. Williams, "Raman spectroscopy of the basic copper chloride minerals atacamite and paratacamite: Implications for the study of copper, brass and bronze objects of archaeological significance," *J. Raman Spectrosc.*, 2002, doi: 10.1002/jrs.921.

[138] W. Martens, R. L. Frost, and P. A. Williams, "Raman and infrared spectroscopic study of the basic copper chloride minerals - Implications for the study of the copper and brass corrosion and 'bronze disease,'" *Neues Jahrb. fur Mineral. Abhandlungen*, 2002, doi: 10.1127/0077-7757/2003/0178-0197.

[139] G. M. Ingo, G. Guida, E. Angelini, G. Di Carlo, A. Mezzi, and G. Padeletti, "Ancient mercury-based plating methods: combined use of surface analytical techniques for the study of manufacturing process and degradation phenomena," *Acc. Chem. Res.*, 2013, doi: 10.1021/ar300232e.

[140] S. Vahur, A. Teearu, P. Peets, L. Joosu, and I. Leito, "ATR-FT-IR spectral collection of conservation materials in the extended region of 4000-80 cm^{-1}," *Anal. Bioanal. Chem.*, 2016, doi: 10.1007/s00216-016-9411-5.

[141]   P. Pulkkinen *et al.*, "Poly(ethylene imine) and tetraethylenepentamine as protecting agents for metallic copper nanoparticles," *ACS Appl. Mater. Interfaces*, 2009, doi: 10.1021/am800177d.

[142]   R. Mastrangelo *et al.*, "Twin-chain polymer hydrogels based on poly(vinyl alcohol) as new advanced tool for the cleaning of modern and contemporary art," *Proc. Natl. Acad. Sci.*, vol. 117, no. 13, pp. 7011–7020, 2020.

[143]   D. D. Do, *Adsorption Analysis: Equilibria and Kinetics*. 1998.

[144]   A. Scott and C. Wild, "Transformations and r2," *Am. Stat.*, 1991, doi: 10.1080/00031305.1991.10475785.

[145]   R. Anderson-Sprecher, "Model comparisons and r2," *Am. Stat.*, 1994, doi: 10.1080/00031305.1994.10476036.

[146]   S. Agnoletti and al., "Verso il bronzo del Novecento: il restauro dell'opera Donna giacente (Militza) di Rebeca Matte Bello de Iñiguez," *OPD Restauro*, vol. 31, pp. 169–179, 2019.

[147]   B. Jegdić, S. Polić-Radovanović, S. Ristić, and A. Alil, "Corrosion stability of corrosion products on an archaeological iron artefact," *Int. J. Conserv. Sci.*, 2012.

[148]   S. Lagergren, "Zur theorie der sogenannten adsorption gelöster Stoffe. Stockholm Kongl. svenska vetenskaps-akad," *Handlinger*, 1898, doi: 10.4236/ss.2014.52008.

[149]   Y. S. Ho and G. McKay, "Pseudo-second order model for sorption processes," *Process Biochem.*, 1999, doi: 10.1016/S0032-9592(98)00112-5.

[150]   D. Robati, "Pseudo-second-order kinetic equations for modeling adsorption systems for removal of lead ions using multi-walled carbon nanotube," *J. Nanostructure Chem.*, 2013, doi: 10.1186/2193-8865-3-55.